Department of Chemistry

Early diagenetic processes associated with preservation of organic matter in concretions from the Toarcian oceanic anoxic event (Germany) and modern microbialites (Australia): A combined organic and inorganic geochemical approach

Chloé Lise Plet

This thesis is presented for the Degree of
Doctor of Philosophy
Of
Curtin University

May 2016

Declaration

To the best of my knowledge and belief this thesis contains no material previously published by any other person except where due acknowledgment has been made.

This thesis contains no material that has been accepted for the award of any other degree or diploma in any university.

Chloé Lise Plet

Perth, May 26th 2016

Abstract

Lowenstam and Weiner (1989) first described induced biomineralisation as follows, "[In aqueous environments] *even a relatively minor perturbation, such as the introduction of biologically produced metabolic end-products, the release of particular cations by the cell, or even the construction of a charged surface such as a cell wall under certain circumstances induce minerals to precipitate*". This description is the first official definition of induced biomineralisation. Such biomineralisation processes occur throughout geological time. They develop in numerous environments, as a result of the activity of different microbial ecosystems. Stromatolites are classified as induced biomineralised deposits. Stromatolites are the earliest evidence of life on our planet and are greatly represented in the rock record until 600 Ma. Stromatolites played a key role in the early life's evolution *via* the changes they triggered in the composition of the oceans and atmosphere.

Carbonate concretions are another type of microbially-induced mineralisation. They are largely present in sedimentary rocks across many geological times, but not as abundant in modern environments. Microbialites are also known to contain the oldest and/or best preserved fossils, both morphological and molecular. Consequently, the multiproxy study of fossiliferous Toarcian carbonate concretions from Germany and modern microbial mats from Shark Bay (Western Australia) provides an opportunity to gain a better understanding of the diversity of microbial communities involved in the formation of these microbialite types. Moreover, this investigation also contributes revealing the ability of these induced biomineralisation processes to preserve exceptional remains of organisms and organic (bio/geo)-molecules over extended periods of time.

An integrated investigation (geochemical and imaging techniques) bears great potential for the investigation of recent and ancient induced biomineralisation. This PhD project explored this potential and identified the advantages of using complementary organic (bulk organic matter and biomarker analyses, $\delta^{13}C$ of

biomarkers) and inorganic [$\delta^{13}C$ of carbonates, microprobe and inductively coupled plasma mass spectrometry (ICP-MS) analyses] geochemistry in association with geological (X-ray diffraction) and imaging techniques [optical microscopy, scanning electron microscopy (SEM) coupled to energy dispersive spectroscopy (EDS), X-ray fluorescence (XRF) mapping] providing a more holistic characterisation of these induced biomineralised sediments.

The main focus of this project was the characterisation of fossiliferous Toarcian carbonate concretions from the Posidonia Shale Formation (SW-Germany) in terms of i) formation processes and ii) microbial communities (**Chapter 2**) as well iii) organic matter and iv) fossil preservation as presented in **Chapters 2-4**. The secondary emphasis of this PhD project was to characterise microbial mat ecosystems along a shallow depth gradient in the most hypersaline location of the Hamelin Pool: Carbla Beach, Shark Bay (Western Australia). We applied this multiproxy approach to establish a more comprehensive understanding of these ecosystems as reported in **Chapter 5**. A more detailed synopsis of the investigation presented in this PhD thesis chapters is described below.

In **Chapter 2** of this thesis, two Toarcian carbonate concretions from the Posidonia Shale Formation were investigated using a multiproxy organic and inorganic geochemical approach. Both concretions contained a similar structure with a nucleus, a concretion body with calcite mineralogy and sedimentary bedding, as well as an outer pyrite-rich rim. The aims were three-fold: characterise i) the environment of formation and the preservation of its signal despite concretion growth, ii) the microbial communities involved in the concretion growth and iii) the concretions properties for organic matter preservation. The selection of two carbonate concretions with a nucleus of the same nature allowed a thorough comparison with minor bias due to the nature of the decaying organic matter, trigger of the concretion growth. The ^{13}C-depleted nature of the calcite and *n*-alkanes (from the concretion bodies) indicates a major role played by sulfate reducing bacteria in organic matter degradation leading to calcite precipitation. Subsequent isolation and preservation of the nucleus in a sealed calcite matrix occurs. Despite the enhanced activity of sulfate reducing bacteria around the nucleus, hydrogen index was elevated in the concretion bodies which strongly suggested that the organic matter degradation was localised at the surface of the

nucleus rather than widespread within the forming concretions. The concretion rims were marked by a ^{13}C-enrichment of calcite, a strong decrease in hydrogen index values and a major increase in pyrite content. These changes between concretion bodies and rims are attributed to a shift in the microbial community towards an enhanced iron reducing bacteria contribution coupled to a decrease in the sulfate reducing bacterial activity allowing direct precipitation of pyrite. However, no evidence of methane cycling could be inferred from biomarkers despite the overall depletion in ^{13}C. Our results contribute to the increasing evidence that carbonate concretions are not only preserving morphological fossils with the highest degree of detail but also protecting organic matter from biological and geological degradation. In addition, carbonate concretions containing sedimentary beddings also record their environment of deposition at a molecular level *via* the preservation of the host sediment signature. Therefore, even *ex-situ* carbonate concretions can bear major information on their palaeoenvironment of deposition, despite the weathering of their host rock.

Chapter 3 presents a new approach to characterise fossils encapsulated within carbonate concretions. The use of imaging techniques complemented by detailed biomarker and stable isotopic investigations are carried out on a Toarcian carbonate concretion containing a fossil ichthyosaur vertebra. The recent report of soft tissues and proteins in dinosaurs from the Late Cretaceous, showed that such labile tissues and molecules could be preserved over extended periods of geological time. The aim of this chapter was to determine if soft tissues and biomolecules could be preserved in a 182.7 Ma vertebra encapsulated in a concretion. After a light acidic treatment to remove the carbonate from the bone porosity, Scanning Electron Microscopy (SEM) revealed the presence of both collagen fibres and red-blood-cells encrusted by a fine grained fluorapatite cement. EDS showed that these structures have a higher carbon content than the bare bone in their immediate proximity. This data suggests that the source for this carbon excess is related to the original biological signal of the soft tissues. Furthermore, the occurrence of abundant sterols in the ichthyosaur bone and their dramatic decrease in the surrounding concretion support their contemporaneous origin, at the time of the ichthyosaur's death. The strong carbon stable isotopic discrepancies between cholesterol and ethylcholesterol, suggest different sources for the biolipids. The $\delta^{13}C$ value of the cholesterol, is in accordance

with a higher trophic level diet, is believed to be largely derived from the ichthyosaur bone although a minor input from zooplankton and/or algae cannot be entirely excluded.

In **Chapter 4**, the same Toarcian carbonate concretion investigated in **Chapter 3** is subject to the first molecular and isotopic investigation of maleimides within a carbonate concretion and its nucleus. The aim was to determine the likely origin of the maleimides detected in both the concretion and vertebra bone samples. A clear dominance of 2-methyl-3-ethyl maleimide (MEM) in all samples, which is commonly attributed to a chlorophyll *a*, was observed. However, the ^{13}C-enriched nature of the MEM could indicate that, in this case MEM strongly derives from bacteriochlorophylls *c*. *d* and *e*, from *Chlorobiaceae*, with a possible contribution from heme, from the ichthyosaur. Furthermore, the identification of 2-methyl-3-*iso*-butyl maleimide (MIBM) in the concretion samples is attributed to the occurrence of photic zone euxinia in the palaeo water column. Regular isoprenoids, pristane and phytane, were ^{13}C-depleted with similar values, which strongly support a common origin ascribed to the phytol side chain of chlorophyll *a*. The ichthyosaur vertebra also contained MEM as well as fossilised red-blood-cells, but no MIBM was detected. Despite the lack of δ^{13}C values due to the low abundance of the MEM in the bone, we hypothesise that the MEM is likely to have a heme source. Although, contamination of the sample *via* geochromatography cannot be entirely ruled out, an origin from weathering and/or storage for the MEM and MIBM in the concretion and bone has been rejected.

The investigation of three microbial mat types from the shallowest section of a tidal flat (Carbla Beach, Shark Bay, WA) is presented in **Chapter 5**. The approach involved microfabric characterisation, lipid and stable isotope analyses. All three mats investigated, tufted, pustular and smooth, were located in supra-, inter-, and sub-tidal environments, respectively. Lipids revealed a major cyanobacterial component in all three mat, however the type of cyanobacteria was revealed by imaging techniques. SRB lipids were present in all three mats. Abundant diatoms were observed in the pustular mat, although the $C_{25:1}$ highly branched isoprenoid (HBI), a diatom-specific biomarker, was most abundant in the smooth mat. Moreover, lipid distribution (via the use of the Paq proxy) showed that macrophytes input was greater in the smooth mat

compared to the pustular and tufted mats. This is also supported by the presence of the ^{13}C-enriched seagrass lipid C_{29} steradiene. A large eukaryotic input was revealed by both lipid distribution (sterols) and imaging techniques; eukaryotes can impact the structure of the mat and lithification processes. This eukaryotic component also complicates the comparison with Precambrian stromatolites.

This thesis present the successful application of a comprehensive analytical approach in the investigation of microbialites. It supports the need of multi-disciplinary studies of recent and ancient microbialites to better characterise their environment of formation, as well as their affinity for organic matter preservation.

References

Lowenstam, H.A., Weiner, S., 1989. On biomineralization. Oxford University Press, New York.

Acknowledgments

Firstly I would like to thanks my principal supervisor, Prof. Kliti Grice for giving me the opportunity to travel from the antipode to work on this great project. Thank you, Kliti, for your constant guidance and support, your patience, encouragement and scientific discussions throughout the three years of this PhD adventure. I am very grateful for the research freedom and initiatives you allowed me to take in building collaborations and developing my cross-disciplinary skills, and all the scientific and financial support you offered during this journey. Finally, thank you Kliti, for being kind and far-reaching when unexpected and challenging situations occurred while being so far away from family as well as for your enthused reaction when life is providing some good new surprises.

I would also like to thank my Associate supervisor, Prof. Lorenz Schwark for giving me access to such exceptional and beautiful samples. I am aware of the chance I have had to investigate such amazing samples. Lorenz, I am very grateful of your invitation to visit your lab and your hospitality. Again, thank you for offering me the opportunity to join you on this breathtaking Canadian Rockies field trip. Thank you for all the interesting scientific discussions and support along this journey.

Similarly, I would like to thank my co-supervisor A/Prof. Marco Coolen who, despite having arrived in the last year of my PhD, got involved and interested in scientific discussions and perspectives. Thank you also for your constructive comments and advice on how to write a scientific article which was definitely not a given and has progressively improved over this last year.

There are more people whose role in my PhD was of major importance. The great technical staff I have been working with for these three years, none of this PhD thesis would have been possible without your help! Thank you Geoff Chidlow and Alex Holman for making the WA-OIGC lab such a nice place to work and for your patience. Thanks also to Geoff for your sense of humour and the breaks during which

you showed me awesome photos of your trips, of a time when Curtin University was called WAIT and of course for all the knowledge you accumulated and happily shared when asked for it. Thank you Marieke, for all the work you put in analysing my samples when I was gone from Kiel already. I would also like to thank Dr Greg Skrzypek and Doug Ford (UWA) for the speed in analysing my samples and your scientific interest about isotopic measurement in fossil bones. Thanks to Derek Winchester (CSIRO) who prepared some of the best thin sections I have ever worked on.

Of course, I would like to thank my fellow students and "early career researchers" as they are called. Thank you for making this PhD journey so pleasant, with such a good and supportive atmosphere.

I would like to specially acknowledge Dr Anais Pagès, Dr Svenja Tulipani, Gemma Spaak, Dr Sebastian Naeher, Hendrik Grotheer, Jaime Cesar, Su Kose, Matt Campbell and Dr Alison Blyth with whom I have spent more time working and who assisted and helped me on a daily basis, in the lab but also sometimes at a more personal level and also made, in their own way this PhD possible. Also thanks to Dr Ines Melendez and Dr Caroline Jaraula, Dr Lyndon Berwick and Dr Rob Lockhart who were there to help me at the very beginning of my PhD and taught me all the basics. The scientific discussions and permanent support during labwork and lab experiment unknown to me, and not always without risks, will never be forgotten. I would also like to acknowledge the new PhD students, whom I have not yet spent much time with as I was isolated from them, now writing in my "cave", but whom made me realise thanks to their questions and our interactions, how much I have learned since I first stepped into the lab: Kuldeep, Nannan, Bettina and Calum.

A special thanks to the research team who made me feel so welcomed in Kiel: Lorenz, Wolfgang, Martin, Nicole, Bonnie, Ann Sophie and Thorsten. Without forgetting Marieke with whom we have become friends. Once again thanks to Lorenz who invited me on his field trip in Canada I will always remember these fantastic mountains and the great variety of their geology and of course Dr Wolfgang Ruebsam and Martin Stockhausen chopping wood to cook tonnes of hamburgers and always keep us warm!

Thank you also to various people at Curtin with whom I have crossed paths and that have left a strong impression or who supported me all along this PhD: Geol'Rob, Mongol'Rob, Jake and Malc (the twins), Amy, Milo, Seb, Eva, Laura and Julie. A special thanks also to my teaching supervisors and demonstrator buddies who each one in their own way made my little trips to the geology building not only a way to earn a bit more but such a refreshing moment providing me strength and perspective!

From the bottom of my heart I want to thank my family for their unconditional support and love even though I could barely see them once a year, they were with me on each day of this adventure. I would also like to say good bye to Michel Pi, Lina and Mamie Lapin, who have left us while I was living so far away.

Thank you Alain, my mentor, my friend who somehow became family along the way, for sparkling my scientific curiosity when I was only an undergrad student, you inspired me and you still do every day, I would never have gotten this far without you, I miss you.

Thank you my friends, from old and new, here and elsewhere, for supporting me in every way possible during this journey… For being so supportive and patient and funny and serious and … and… and… simply for being.

Finally, but certainly not least, I would like to thank Fran. No tengo palabras para decirte lo agradecida que estoy de haberte conocido. Sin ti, nada de eso hubiera sido possible, desde que te conocí siempre estuviste ahí, ayundandome y apoyandome. Me haces feliz y me tranquilizas cuando la vida me desborda. Me alegro tanto haber empezado esta nueva aventura cambia-vida contigo, te quiero, os quiero a ti y al garbanzo, nuestro pequeño sol : Thiago.

Primary publications

This thesis is assembled by publication either published, under review or in preparation which form the individual chapters and are listed below.

Chapter 2

Plet, C., Grice, K., Pagès, A., Ruebsam, W., Coolen, M., Schwark, L. 2016. Microbially-mediated fossil-bearing carbonate concretions and their significance for palaeoenvironmental reconstructions: a multi-proxy organic and inorganic geochemical appraisal. *Chemical Geology* **426**, 95-108, doi:10.1016/j.chemgeo.2016.01.026. Impact factor 3.524

Chapter 3

Plet, C., Grice, K., Pagès, A., Verrall, M., Coolen, M.J.L., Ruebsam, W., Schwark, L. 2016. Jurassic World: Palaeobiology of red blood cells, collagen and cholesterol in an ichthyosaur. *Scientific Reports*, under revision. Impact factor 5.228

Chapter 4

Plet, C., Naeher, S., Pagès, A., Ruebsam, W., Schwark, L., Grice, K. The distribution and stable carbon isotopic composition of 2-methyl-3-ethyl-maleimide (1H-pyrrole-2,5-dione) within a Toarcian (182.7 Ma) fossiliferous carbonate concretion. Organic Geochemistry, in preparation for submission. Impact factor 3.072

Chapter 5

Plet, C., Pagès, A., Holman, A. I., Madden, R. H. C., Grice, K. 2017. From supratidal to subtidal, an integrated characterisation of Carbla Beach shallow microbial mats (Hamelin Pool, Shark Bay, WA): lipid biomarkers, stable carbon isotopes and microfabrics. *Geobiology*, submitted. Impact factor 3.462

Contributions of others

The work presented in this thesis was primarily designed, experimentally executed, interpreted and the manuscripts were prepared by the first author (Chloé Plet). Contributions by co-authors are described below.

Chapter 2

Lorenz Schwark and Wolfgang Ruebsam collected and provided the samples. Chloé Plet and Kliti Grice designed the experiments. Chloé Plet performed all wet lab experiments, GC-MS and GC-iRMS analyses and processing, SEM observations. GC–MRM analyses were performed at the Institute of Geosciences, Kiel University, as well as and bulk organic matter analyses (C,N,S, analyses, Rock-Eval, $\delta^{13}C_{OM}$) which were carried out by Wolfgang Ruebsam and Chloé Plet. Anais Pagès facilitated the SEM facilities through a collaboration with CSIRO and assisted in the analyses. $\delta^{13}C_{carb}$ analyses were performed at the University of Erlangen-Nuremberg and ICP-MS analyses were performed as contract samples by Actlabs (Canada). The writing of the manuscript was carried out by Chloé Plet, with contribution of all the co-authors, whom also provided additional intellectual input. Kliti Grice and Lorenz Schwark provided the analytical facilities. Financial support was provided by an ARC Discovery grant DORA grant (Kliti Grice) as well as extra support from a European Association of Organic Geochemists (EAOG) and The Institute for Geoscience Research (TIGeR).

Chapter 3

Lorenz Schwark and Wolfgang Ruebsam collected and provided the samples. Chloé Plet, Kliti Grice and Lorenz Schwark designed the experiments. Wolfgang Ruebsam analysed TOC contents. Anais Pagès and Mike Verrall facilitated access to SEM-EDS analyses and microbeam elemental mapping (CSIRO) and participated in the interpretation. Chloé Plet, Kliti Grice and Marco Coolen and Lorenz Schwark

interpreted the data and wrote the paper. Anais Pagès and Mike Verrall also contributed in the interpretation of data and writing of the manuscript. The project was funded by and ARC discovery DORA grant (Kliti Grice) and extra financial support was provided by The Institute for Geoscience Research (TIGeR) and a European Association of Organic Geochemists (EAOG) travel grant (Plet 2014).

Chapter 4

Lorenz Schwark and Wolfgang Ruebsam collected and provided the samples. Chloé Plet, Kliti Grice and Sebastian Naeher designed the experiments. Sebastian Naeher performed the wet lab experiments. Chloé Plet performed the GC MS analyses, identification and quantification. Wolfgang Ruebsam perfomed TOC content analyses. Chloé Plet, wrote the manuscript. Kliti Grice, Sebastian Naeher and Lorenz Schwark also contributed to the writing of the manuscript. The project was funded by and ARC discovery DORA grant (Kliti Grice) and extra financial support was provided by The Institute for Geoscience Research (TIGeR).

Chapter 5

Anais Pagès performed field work and collected data, with financial support of an ARC discovery grant 2010-2013, Grice, Greenwood, Snape and Summons). Chloé Plet designed the experiments. Anais Pagès ran the SEM analyses at CSIRO. Chloé Plet performed all wet lab experiments and sample preparation as well as GC-MS measurements.GC-irMS analyses were performed by Alex Holman and Chloé Plet. Microfabric characterisations were undertaken by Robert Madden (department of Applied Geology, Curtin University). All interpretations and writing of the manuscript were carried out by Chloé Plet, with contributions and intellectual input in discussions of all co-authors. Kliti Grice provided the analytical facilities except where stated otherwise. This research was funded by ARC discovery DORA grant (Kliti Grice) and extra financial support was provided by The Institute for Geoscience Research (TIGeR).

Secondary publications

Conference abstracts based on research that was conducted during the preparation of this thesis.

*Directly related to this PhD

***Plet, C.**, Grice, K., Pagès, A., Ruebsam, W., Schwark, L. Carbonate concretions associated with fossils: snapshot of an anoxic marine environment in the Toarcian. "9th International Conference on Applications of Stable Isotope Techniques to Ecological Studies" (ISOECOL), Perth, Australia, August 2014, oral presentation.

***Plet, C.**, Grice, K., Ruebsam, W., Schwark, L. Organic and inorganic geochemical composition of a Jurassic carbonate concretion. "18th Australian Organic Geochemistry Conference" (AOGC), Adelaide, Australia, December 2014, poster presentation.

***Plet, C.**, Grice,K., Ruebsam, W., Schwark, L., Pagès, A. An integrated geochemical approach to characterise the formation of a concretion around an exceptionally preserved ichthyosaur vertebra from the Posidonia Shale Fm (SW Germany, 183 Ma). "27th International Meeting of Organic Geochemistry" (IMOG), Prague, Czech Republic, September 2015, oral presentation.

***Plet, C.**, Grice, K., Pagès, A., Ruebsam, W., Verrall, M., Coolen, M.J.L., Schwark, L. Carbonate concretions: indirect evidence for microbial life? "Astrobiology Australasia Meeting" Perth, Australia, July 2016, oral presentation.

Grice, K., **Plet, C**., Melendez, I., Lengger, S., Schwark, L. Preservation and evolution of life across oceanic anoxic events. "26th Goldschmidt Conference", Yokohama, Japan, June2016, keynote presentation.

Grice, K., **Plet, C**., Melendez, I., Lengger, S., Schwark, L. Preservation and evolution of life across oceanic anoxic events. "35th International Geological Congress" (IGC), Cape Town, South Africa, August-September 2016, oral presentation.

Table of content

Chapter 5

From supratidal to subtidal, an integrated characterisation of Carbla Beach shallow microbial mats (Hamelin Pool, Shark Bay, WA): lipid biomarkers, stable carbon isotopes and microfabrics. 128

Table of figures

Table of tables

Abbreviations

CSIA: Compound specific isotope analysis

BSTFA: Bis(trimethylsilyl)-trifluoroacetamide

DCM: Dichloromethane

DIC: Dissolved inorganic carbon

EA: Elemental analyser

EPS: Exopolymeric substances

EDS: Energy dispersive X-ray spectroscopy

FeR: Iron reducing bacteria

Fm.: Formation (geological)

Ga: *Giga annum*, (10^9 years)

GC-MS: Gas chromatography mass spectrometry

GC-irMS: Gas chromatography isotope ratio mass spectrometry

HBI: Highly branched isoprenoid

HI: Hydrogen index

HP: Hewlett Packard

irMS: Isotope ratio mass spectrometry

ka: *kilo annum* (10^3 years)

Ma: Mega annum (10^6 years)

MEM: 2-methyl-3-ethyl maleimide

MIBM: 2-methyl-3-*iso*-butyl maleimide

MTBSTFA: *N*-(*tert*-butyldimethylsilyl)-*N*-methyl trifluoroacetamide

OM: Organic matter

PDB: Pee Dee Belemnite

Ph: Phytane

Pr: Pristane

PZE: Photic zone euxinia

RBC: Red blood cells

SE: Secondary electron

SEM: Scanning electron microscopy

SRB: Sulfate reducing bacteria

TBDMS: *tert*-butyldimethylsilyl

TCA-cycle: tricarboxylic acid cycle

TIC: Total inorganic carbon

TLC: Thin layer chromatography

TLE: Total lipid extract

T-OAE: Toarcian oceanic anoxic event

TOC: Total organic carbon

VPDB: Vienna Pee Dee Belemnite

XRF: X-ray fluorescence

Chapter 1

Introduction and overview

Life throughout Earth's history

The oldest evidence of life

Unicellular organisms

New powerful analytical techniques in Geosciences (Grice, 2014; Thiel *et al.*, 2007) combined with an increasing curiosity of the scientific community, aim to unravel the mysteries of early life on Earth as well as the likely existence of extra-terrestrial life. This has led to the discovery of new evidence about the early history of our planet.

Until now, the discovery of indirect evidence for life, *e.g.* carbon preserved in a zircon, dating back to 4.1 Ga (Bell *et al.*, 2015) has been strongly debated. However, the existence of cyanobacterial fossils and stromatolites in Western Australian rocks dating back to 3.5 Ga (Archean) is now commonly accepted (Awramik, 1992) (**Figure 1-1**).

Stromatolites are biogenic sedimentary structures, which form due to micro-environmental modifications by the action of microbial communities, a process referred to as "biologically-induced mineralisation" (or "induced biomineralisation"). Stromatolite structures generally consist of layers of calcium carbonate ($CaCO_3$). The mineral forms from secondary interactions between metabolic processes and the surrounding environment. A stromatolite forms *via* precipitation of $CaCO_3$ from seawater as a result of a pH increase in microenvironments related to biological

activity in microbial mats, in addition the extracellular polymeric substance (EPS) produced by microorganisms traps and binds the particles from the surrounding environment (McNamara, 2013).

In contrast, "biologically-controlled mineralisation", or "controlled biomineralisation", consists of a direct and strict control of the organism over the mineral produced and its incorporation into biological tissues (Reitner and Thiel, 2011). In such cases, the bio-mineral produced is a metabolic product that can have some species-specific crystallo-chemical properties. These biomineralisation processes appeared and developed substantially later in the geological time, with the first occurrence reported in the mid-Neoproterozoic (811-717 Ma) consisting of phosphate biomineralisation in protists (Cohen *et al.*, 2011).

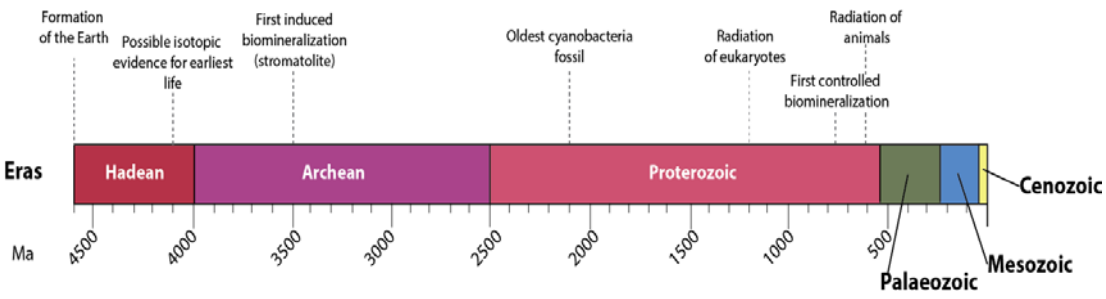

Figure 1-1. Simplified geological era with important biological events since the formation of the Earth.

Evidence of complex multicellular organisms

Controversial evidence of complex multicellular organisms as old as 2.1 Ga has been reported (El Albani *et al.*, 2010, 2014). However, the consensus amongst scientists is that even though complex organisms might have appeared multiple times throughout Earth's history (Knoll, 2011), they certainly thrived in the Ediacaran period, giving rise to the so-called Ediacaran fauna (635-541 Ma) (Narbonne, 2005). This fauna is characterised by fossils of primitive soft bodied organisms (**Figure 1-2**), which have been reported in numerous localities (>30) around the world. However, the Ediacaran biota abruptly disappeared at 542 Ma, possibly as a result of a mass extinction event and/or competition with the more complex animals that evolved during the Cambrian explosion (Narbonne, 2005). The term "Cambrian explosion" is commonly used to describe the sudden and successful development of life between 541-485 Ma, when life rapidly flourished and diversified. The first predators emerged,

followed by the evolution of external skeletons (*e.g.* teeth and horns) needed for hunting and protection (Landing *et al.*, 2010). Most phyla of multicellular organisms, showing likeness to extant flora and fauna, first evolved during the Cambrian (Landing *et al.*, 2010). This period therefore marks a pivotal stage in the history and evolution of life on Earth.

Fossil preservation

Hard and soft tissues

With the appearance of biologically controlled mineralisation, many organisms have been preserved over geological times as fossils. These are often fossils of "hard parts" (*e.g.* shells of invertebrates and/or bones and teeth of vertebrates), which are the most easily preserved tissues of any creature (**Figure 1-2**). Consequently, most of what is known at present about extinct organisms is inferred from fossilised hard parts only. The majority of fossils have lost their original mineralogical composition *via* permineralisation (*i.e.* permeation of tissue(s) by mineralising fluids).

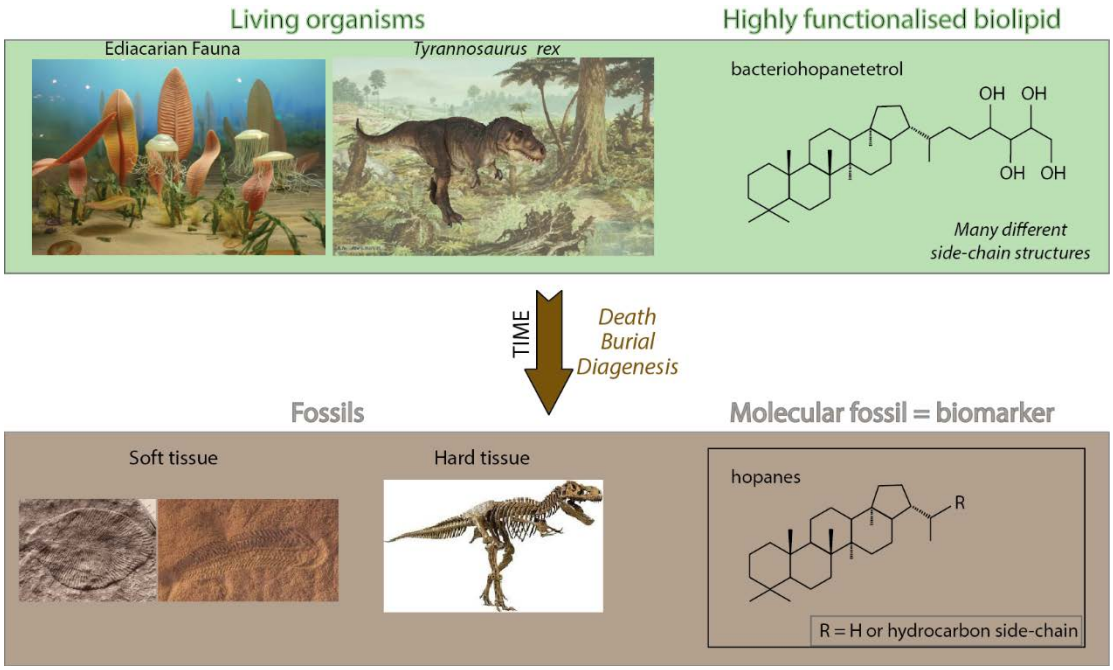

Figure 1-2. Simplified illustration of the three types of fossils. Soft bodied fossils leave an "imprint", hard tissues are preserved through mineralisation processes and biomolecules turn into biomarkers (molecular fossils) via the loss of their functionality and changes in stereochemical configurations.

However, in some cases, exceptional conditions led to the preservation of soft tissue over extended periods of geological time (Briggs, 2003; Lindgren *et al.*, 2013; Martill, 1988, 1995). In the majority of cases, the imprints of soft tissue (*e.g.* castings and mouldings) are preserved within fine-grained siliciclastic rocks. These fine-grained sediments can preserve an imprint of an organism when all the organic matter (OM) has been removed leading to a mould, which is later in-filled by fine sedimentary material that forms a cast of the original organism. Sometimes, soft bodied fossils are preserved by minerals rather than sediments. Permineralisation (explained above) and authigenic mineralisation (*i.e.* rapid *in situ* growth of minerals) are some of the processes that can occur during diagenesis. Mineralisation allows for soft bodied fossils to preserve extraordinary detail. Nonetheless, in recent years, research has also yielded some exceptional, non-mineralised, soft tissues and proteins of *e.g. Tyrannosaurs rex* from the Cretaceous (Asara *et al.*, 2007; Schweitzer *et al.*, 2007, 2005).

Diagenesis in geology and palaeontology

In geology, the term diagenesis involves physical, chemical and biological processes associated with the deposition of sedimentary material through to green-schist metamorphic facies (Marshak, 2012). Green schist metamorphism typically occurs at temperatures between 300 °C and 450 °C, and pressures between 2 and 10 Kbar. All mechanisms of diagenesis in sedimentary geology are subdivided into three stages: eogenesis, mesogenesis and telogenesis. Burley *et al.* (1985) define the three terms as follows: i) eogenesis covers the depositional environment and surface chemistry; ii) mesogenesis describes the burial and subsurface conditions and iii) telogenesis refers to the weathering or re-exposure to surface conditions.

The most important processes of diagenesis are compaction and lithification, which are inter-related to deformation, dissolution, cementation, authigenesis, replacement (including permineralisation), recrystallisation, hydration and bacterial action including the development of concretions (Southard, 2007). For example, when a sediment is deposited and bacterial activity modifies the redox conditions of its pore water, it may lead to precipitation of minerals. Meanwhile, with the increasing pressure, the primary porosity of the sediment decreases due to compaction as well as dissolution/precipitation of minerals.

Diagenesis also plays an important role in the preservation of palaeontological and archaeological objects. In most cases, such objects are not preserved over prolonged periods of time. However, when they are preserved, they are altered to some extent. In palaeontology, the term diagenesis describes the cumulative processes (chemical and biological), which affect and modify the chemical and/or structural properties of organic remains and that will govern their fate in terms of preservation or destruction. Some mineralisation processes, *e.g.* permineralisation and authigenic mineralisation, are two diagenetic mechanisms of major importance in the preservation of both hard and soft tissues as fossils (Allison, 1988a, 1988b; Briggs, 2003). The term diagenesis is also commonly used in the discipline of organic geochemistry where it has a different meaning – see section ***Geological fate of OM***.

Palaeoenvironmental settings associated with fossil preservation

The likelihood of an organism or a biomolecule to be fossilised is dependent upon a unique combination of environmental circumstances. Conditions that favour the preservation of fossils include, i) abundant supply of OM coupled to ii) a limited amount of oxygen being available in the sedimentary environment (*e.g.* dysoxic or anoxic). Such conditions limit the amount of OM oxidation and the activity of scavengers, insects and bacteria degrading the decaying organisms. Environments that have the above pre-requisites include, lakes and (semi-) enclosed marine basins with stratified waters.

Limited oxygen availability is also an important requirement for molecular fossil preservation (Peters *et al.*, 2005). However, in the case of soft tissue preservation, it appears that a rapid sedimentary burial coupled to water stagnation and the promotion of early diagenetic mineralisation processes are the pre-requisite factors for fossilisation to occur (Allison, 1988b). In contrast, in the case of soft tissue preservation oxygen availability only plays a secondary role (Allison, 1988a).

In stratified waters, animals and algae live within the upper, oxygen-rich, layer of the water column. Upon death, animals and algae are either recycled and/or sink into the deeper oxygen-depleted bottom waters before being deposited in the sediments. In these anoxic bottom waters and/or at the sediment water interface, sulfate reducing bacteria (SRB) thrive and anaerobically degrade OM.

Formation and accumulation of OM in the sediment

Oxygenic photosynthetic (**Equation 1-1**) organisms such as algae, cyanobacteria and plants (both terrestrial and aquatic), are the principal producers of OM on Earth. In anoxic settings, other organisms, *e.g.* green sulfur bacteria, can perform anoxygenic photosynthesis. In anoxygenic photosynthesis, different wavelengths of sunlight and electron donor (hydrogen sulphide; H_2S) are used to assimilate inorganic carbon into biomass, producing S_0 as a by-product (Peters *et al.*, 2005). Other autotroph organisms exist that do not need solar energy but use the energy released by chemical reactions to metabolise inorganic carbon (*i.e.* chemoautotrophs). All these autotrophs are primary producers, they are the first trophic level of the food chain, which support all higher trophic levels consisting of heterotrophic organisms (*i.e.* organisms that require organic carbon sources due to their inability to metabolise inorganic carbon).

$$2H_2S + CO_2 \xrightarrow{\text{light}} 2S_0 + CH_2O + H_2O$$

Equation 1-1. Anoxygenic photosynthesis.

Most primary OM is degraded or incorporated into the food chain. However, a minor part can be accumulated into the sediment where it is exposed to further degradation and remineralisation. Overall, a minimal proportion (>0.1 %) of the total biomass is preserved over geological times (Holser *et al.*, 1988). Typically, sediment accumulation occurs in aquatic environments both terrestrial (*e.g.* lacustrine, riverine) and marine (*e.g.* deep ocean, shallow platforms, delta, lagoons) where the associated OM displays different signals depending on its source. The best settings for accumulation and preservation of OM may change between different environments. However, OM-rich sediments are often formed in anoxic/suboxic depositional environments, where high primary productivity takes place in the shallower oxic water layer of the column while fine sediment is accumulated rapidly (Peters *et al.*, 2005).

Geological fate of OM

As mentioned above, even after OM accumulates in the sedimentary material, less than 0.1 % of the total biomass is preserved over geological time (Holser *et al.*, 1988).

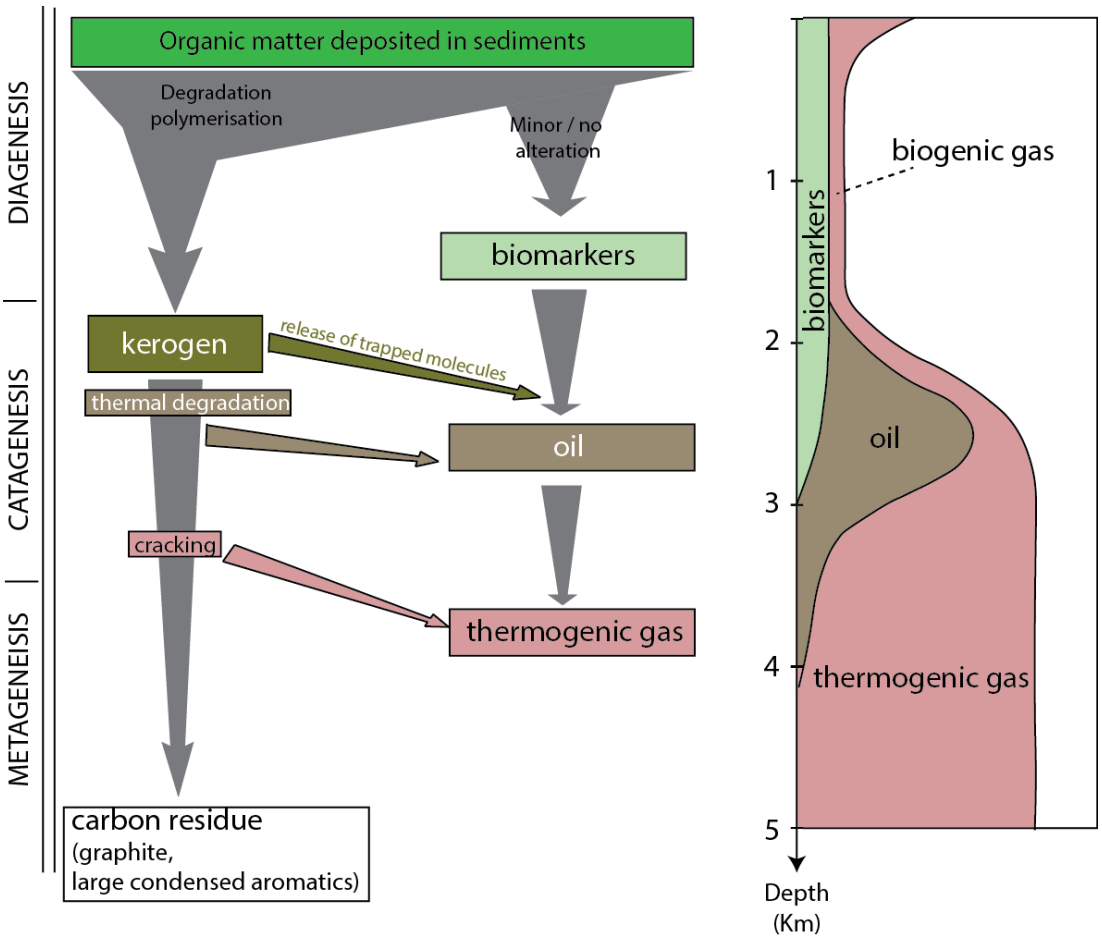

Figure 1-3. Geological fate of OM, modified after Tissot and Welte (1984).

In organic geochemistry, diagenesis describes all biological, physical and chemical processes that are involved in the degradation of OM occurring before substantial thermal alteration takes place (*i.e.* T<50°C) (**Figure 1-3**) (Peters *et al.*, 2005). By the end of diagenesis, the portion of molecules extractable using common organic solvents is referred to as bitumen (Brocks and Summons, 2003).

As an example of bitumen evolution during diagenesis, a simplified sterol evolution follows: due to their abundant asymmetric carbon atoms, sterols can have many configurations. However, all sterols present in living organism have a 5α,

14α,17α, 20R configuration (Peters *et al.*, 2005). In some organisms where C5 is saturated, as well as in the molecules resulting from early diagenesis hydrogenation of the typical C5 double bond a 5α configuration is favoured leading to stanols and steranes (**I**) with a biological ααα 20R configuration (*e.g.* Mackenzie *et al.*, 1982a, 1982b). Biolipids lose their functional groups and stereochemical configuration during diagenesis. Consequently, increasing the thermal maturity will result in an increase in more geologically stable configurations αααS, αββR and αββS stereoisomers, as well as appearance of diasteranes and aromatic steroids (*e.g.* Mackenzie *et al.*, 1982a). These modifications of stereochemical configurations have been used to develop maturity parameters to establish the thermal history of OM.

The portion of high molecular weight OM residue that is insoluble in usual organic solvents is referred to as kerogen (Tissot and Welte, 1984). Kerogen formation is commonly attributed to neogenesis (Tissot and Welte, 1984), which describe the random polymerisation and polycondensation reactions of biological residues (*e.g.* amino acids, sugars, lipids). However, selective preservation of resistant biosynthesised macromolecules that undergo only limited chemical changes during diagenesis also leads to kerogen formation (Gupta, 2015). Such preservation is particularly enhanced in sulfate-rich anaerobic environments, where sulfur can be incorporated generating complex kerogens, which are very resistant to bacteria (Briggs and Summons, 2014). As mentioned, diagenesis covers many processes. Therefore a subdivision describing the very early stages of diagenesis (*i.e.* immediately after the death of an organism) is referred to as eogenesis (Burley *et al.* (1985).

In general, with increasing burial depth and the associated temperature rise, catagenesis commences (50 °C ≤ T ≤150 °C). During catagenesis, OM present as kerogen and bitumen and contained within the sedimentary material is thermally altered (**Figure 1-3**). Remaining biolipids and molecular fossils are subject to structural changes and petroleum may eventually be expelled from rocks having petroleum potential, *i.e.* source-rock (Brocks and Summons, 2003).

When burial depth and temperature increase further (T≥150 °C), organic molecules trapped in the sedimentary rocks are cracked and expelled as gas, this process is called metagenesis (**Figure 1-3**). At this stage, molecular fossils are often entirely destroyed due to their instability under such pressure and temperature

conditions (Peters *et al.*, 2005). However, some molecules (*i.e.* diamondoids (**II**)) are thermally more stable than most hydrocarbons (Dahl *et al.*, 1999) and their concentration increase with thermal cracking of oil resulting of diamondoid-enriched condensates (Grice *et al.*, 2000).

In some rare cases, the depth of burial and associated temperatures of the sediment remain low. Therefore, under these circumstances, ancient sedimentary OM does not reach thermal maturity and is preserved from severe alteration. The occurrence of steranes with their biological configuration was reported from the Devonian (Melendez *et al.*, 2013b). Moreover, in some exceptional occasions intact biomolecules (*e.g.* sterols) were reported in sediments from the Palaeozoic (Melendez *et al.*, 2013a) and Mesozoic (Brassell *et al.*, 1987; Comet *et al.*, 1981)

Significance of molecular fossils (biomarkers) for palaeoenvironmental reconstruction

Biomarkers are defined as molecular fossils originating from biolipids in once living organisms. They typically have various functional groups and heteroatoms (N, O, S and P). In living organisms, such molecules are present with their biological stereochemical configuration.

The use of biomarkers for palaeoenvironmental reconstruction is based on the fact that life on Earth is grouped under three major domains of life: archaea, bacteria and eukaryota (**Figure 1-4**). Some biomarkers from these groups are common and ubiquitous amongst most organisms. However, others are very specific for a domain of life, for a group of organisms or sometimes for a species (Briggs and Summons, 2014; Brocks and Pearson, 2005). It is generally accepted that some lipids, steroids (**III**) and hopanoids (**IV**), are characteristic for eukaryotes and bacteria, respectively (Briggs and Summons, 2014). However, some exceptions have been reported such as ciliates (monocellular eukaryotes) that can produce tetrahymanol (**V**) and various hopanoids, or bacteria and cyanobacteria that can synthesise sterols (*e.g.* Schouten *et al.*, 2000a; Volkman, 2005, 2003).

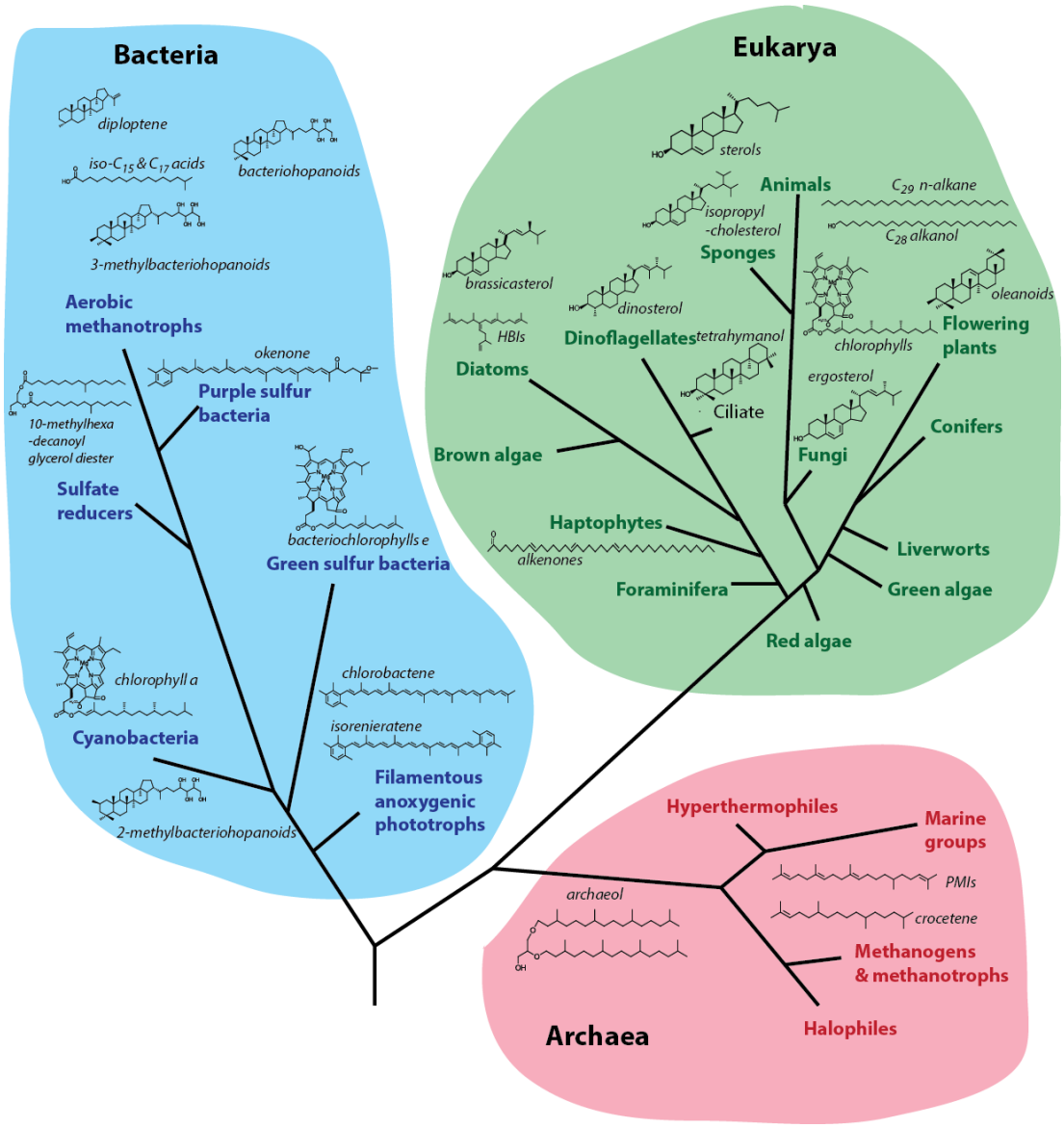

Figure 1-4. The three domains of life and their associated biomarkers (modified after Briggs and Summons, 2014).

Most organisms live in particular environmental conditions, or can produce specific molecules when subject to environmental stress. Therefore, the identification and quantification of biomarkers, as well as the development of biomarker proxies can provide information about the environment during sediment deposition. The investigation of biomarkers allows reconstructing environmental conditions across geological times, some examples such as water column stratification (*e.g.* Berndmeyer *et al.*, 2014; Sinninghe Damsté *et al.*, 1995), palaeosalinity (Barakat and Rullkötter, 1997; Sinninghe Damsté *et al.*, 1993; Ten Haven *et al.*, 1985, 1988), persistence of anoxic events (*e.g.* Schwark and Frimmel, 2004) or existence of photic zone euxinia

(PZE, Grice *et al.*, 1996; Koopmans *et al.*, 1996a; Summons and Powell, 1986) are based on biomarker presence or biomarker proxies.

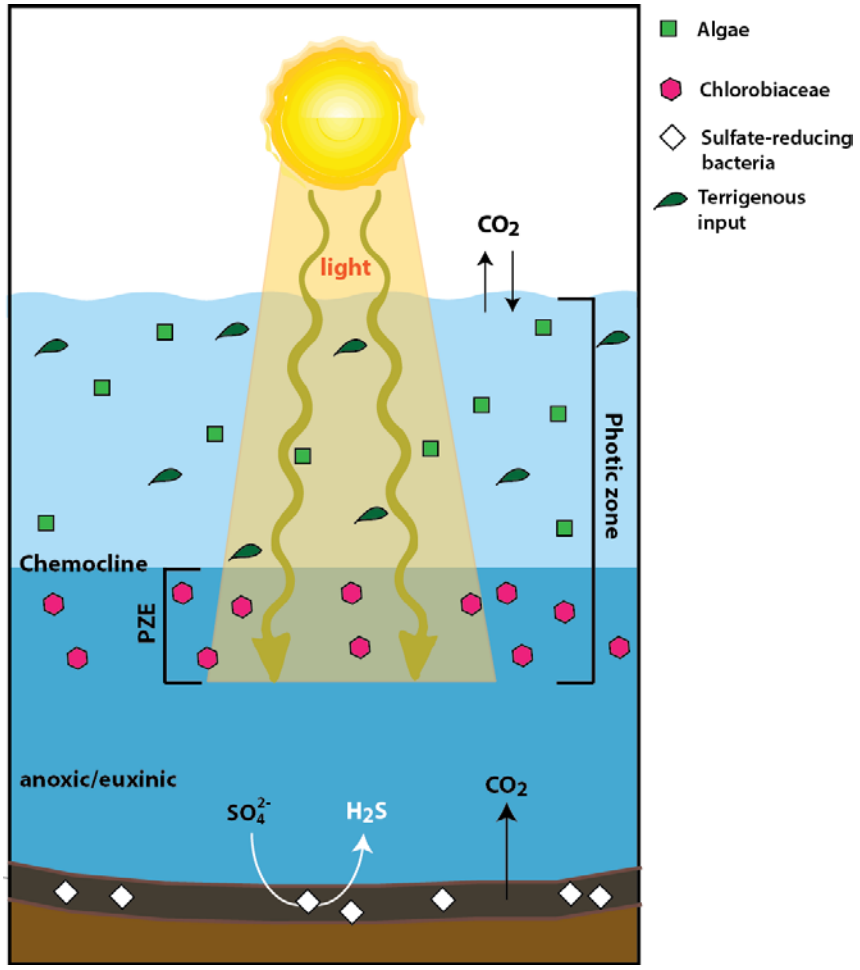

Figure 1-5: Illustration of stratified water column conditions in which the top layer is oxygenated whereas the bottom layer is anoxic/euxinic. The top of the anoxic/euxinic bottom water is overlapping with the photic zone leading to photic zone euxinia (PZE). Associated micro-organisms e.g. Chlorobiaceae in the PZE and sulfate reducing bacteria (SRB) in the sediments, modified from Whiteside and Grice (2016).

In the case of PZE, there are various source-specific biomarkers that derive from carotenoids and bacteriochlorophylls, which are characteristic of the anoxygenic phototrophic sulfur bacteria *Chlorobiaceae sp*. Some of these PZE- (**Figure 1-5**) specific biomarkers include isorenieratane (**VI**), palaeorenieratane (**VII**), chlorobactane (**VIII**), specific maleimides (**IX**) as well as a suite of 2,3,6-aryl isoprenoids (**X**) with ^{13}C-enriched isotopic signature (*e.g.* Grice *et al.*, 1996; Koopmans *et al.*, 1996a; Summons and Powell, 1986). However, depending on the environment of deposition, some of these biomarkers can have a different origin. For example, isorenieratane may originate from isorenieratene (**XI**), present in

Chlorobiaceae (Summons and Powell, 1986) in aquatic environment but also in actinomycetes in soil environment (Kohl *et al.*, 1983; Krügel *et al.*, 1999). Similarly, aryl isoprenoids may indicate PZE from *Chlorobiaceae*-derived carotenoids (*i.e.* isorenieratane) when their carbon isotopic composition is ^{13}C-enriched, but can also originate from *β*-carotene (**XII**) and would then have a more ^{13}C-depleted isotopic signature (Koopmans *et al.*, 1996b). Therefore, to address with certainty the palaeoenvironment of deposition of a sediment a combined use of biomarker identification with stable isotope analyses is recommended.

Carbon in geochemistry

The carbon cycle

The carbon cycle is essential to the evolution of Earth's climate, the preservation of life as well as the composition of both oceans and atmosphere. The carbon cycle is an interaction between the biosphere, atmosphere, hydrosphere, pedosphere and geosphere. As a result of these interconnected processes, carbon is in a constant state of flux and is continuously exchanging between storage in various sources and sinks (**Table 1-1**)

Table 1-1.Carbon reservoir sizes as a function of mass (after Falkowski et al., 2000).

CARBON RESERVOIRS	GIGATONS
Lithosphere	
Sedimentary carbonates	> 60 000 000
Kerogens	15 000 000
Fossil fuels	**4 130**
Coal	3 510
Oil	230
Gas	140
Peat	250
Atmospheric CO_2	**720**
World Ocean	**38 400**
Total inorganic	37 400
Total organic	1 000
Terrestrial biosphere	**2 000**
Living biomass	600 – 1 000
Dead biomass	1 200
Aquatic Biosphere	**1-2**

The short-term carbon cycle (Berner, 2004) influences and controls short-term climatic variations in concert with periodic changes related to astronomical

forcing. The transfer of carbon from the atmosphere (or hydrosphere) to the biosphere is driven by primary producers, largely *via* photosynthesis, absorbing carbon dioxide (CO_2) from atmosphere and/or hydrosphere to produce the essential organic compounds needed for growth (*i.e.* incorporating it into the biosphere). Upon the death of an organism, degradation of the OM will return carbon back to the environment as CO_2 or methane (CH_4). Direct gaseous exchanges can also occur between the atmosphere and the hydrosphere. These transfers between sinks and sources are constant, and they occur over relatively short periods of time (<10 Kyr) considering the age of the Earth (4.534 Ga).

Then again, the rate of flux of carbon from sources to sink varies greatly and distinctions are made between long-term and short-term cycles (Berner, 2004), which occur simultaneously (**Figure 1-6**). It is crucial to understand that over time scales of millions of years, the carbon is (in essence) permanently transferred to and from the geosphere within limestone rocks and smaller amounts in coals, shales and hydrocarbons (**Table 1-1,** Falkowski *et al.*, 2000) but also to and from some silicate rocks (Berner, 2004) this is the long term carbon cycle. Indeed, most of the carbon on Earth is contained within the geosphere (>50 000 000 Gt; **Table 1-1.** Carbon reservoir sizes as a function of mass (after Falkowski *et al.*, 2000).

Berner, 2004; Falkowski *et al.*, 2000). Carbon exchanges into/out of the geosphere can result in major modifications to the composition of the atmosphere that cannot be attained through the processes operating in the short term carbon cycle alone.

The short-term cycle cannot account for the major fluxes of carbon to and from the geosphere due principally to the far greater mass of carbon present as compared to the hydrosphere, atmosphere, pedosphere and biosphere combined (Berner, 2004). The weathering of both silicate and carbonate rocks leads to a major drawdown of CO_2 from the atmosphere to the oceans by chemical and biological processes that allow carbon to be incorporated into (primarily) calcite that trap carbon in rocks and biomineralisations. Recycling of limestones (and other rocks) in subduction zones eventually results in CO_2 release through volcanic processes associated with plate tectonics. Additionally, collapse of methane hydrates in deep sea settings and permafrosts due to global warming is a significant factor in long-term carbon cycling and can lead to a run-away greenhouse climate.

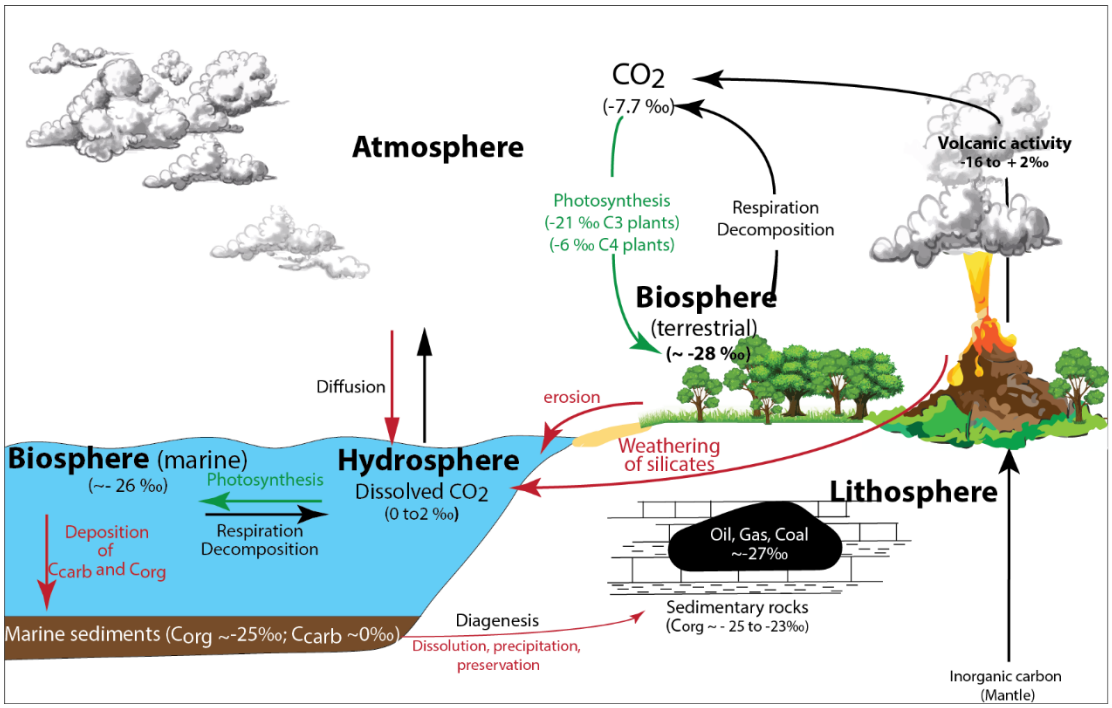

Figure 1-6. Simplified carbon cycle, combining short term and long term processes and indicative δ13C values of the different reservoirs (Hoefs, 2015; Kroopnick, 1985; Oppenheimer et al., 2014; Peterson and Fry, 2011; Schidlowski, 1988).

Stable isotopes of carbon: notation, fractionation and significance in geosciences

Carbon has three natural isotopes, amongst which only two are non-radioactive (stable) isotopes, ^{12}C and ^{13}C, at a proportion of 98.899% and 1.111%, respectively (Faure and Mensing, 2005).

Stable isotope measurements are reported as ratio of the heavier (*e.g.* ^{13}C) to the lighter isotope (*e.g.* ^{12}C) and then reported to a reference gas with a known value (**Equation 1-2**). These values are reported in per mil (‰) relative to an international standard.

$$\delta^{13}C\ (‰) = \left(\frac{R_{sample}}{R_{reference}} - 1 \right) \times 1000$$

Equation 1-2. Definition of $\delta^{13}C$.

In the case of $\delta^{13}C$, the values were originally reported against the Pee Dee Belemnite (‰ PDB), a Cretaceous belemnite from the Pee Dee Formation (North and South Carolina, USA). However, the demand for that standard exceeded its availability

and the PDB standard was eventually exhausted. Therefore it has been replaced by the Vienna Pee Dee Belemnite (VPDB) calibrated to the same ratio as the original PDB. VPDB standard is now widely used for both carbon and oxygen stable isotopes (for bulk OM, carbonate, or individual compounds).

The overall abundance of ^{13}C and ^{12}C remains constant, however most physicochemical processes (*e.g.* phase transfer and chemical reactions) and biological mechanisms (*e.g.* incorporation of inorganic carbon by primary producer *via* different metabolic pathways) result in different isotopic fractionation related to the physicochemical properties of each stable isotope. The potential energy required to break bonds with ^{12}C are lower than for ^{13}C (Kendall and Caldwell, 1998) allowing isotope fractionation.

The most significant inorganic fractionation at the Earth surface is the one taking place between the atmospheric CO_2 (CO_{2atm}) and the dissolved inorganic carbon (DIC) of the oceans. This fractionation is also temperature dependent, which leads to ^{13}C-enriched DIC in the shallow waters of the oceans ($\delta^{13}C$ up to +2 ‰ compared to deeper water) (Zhang *et al.*, 1995). Furthermore, the formation of sedimentary carbonates by isotopic equilibrium exchange reactions between the CO_{2atm}, the DIC and the inorganically precipitated carbonate lead to the formation of a ^{13}C-enriched carbonate compared to the DIC from which it precipitates (Hoefs, 2015).

The strongest carbon isotopic fractionation is occurring during kinetic isotope effects related to CO_2 incorporation *via* photosynthesis. Photosynthetic organisms overall greatly favour the assimilation of light ^{12}C over the heavy ^{13}C isotope (Hoefs, 2015). Such fractionation effects are complex as they depend on the carbon assimilation pathways of the different photosynthetic organisms. For example, most photosynthetic organisms (*e.g.* majority of terrestrial plants and phytoplankton) use the Calvin cycle metabolic pathway (C_3), which causes a depletion in ^{13}C of the OM compared to the carbon source (characteristic bulk OM values for terrestrial C_3 plant, $\delta^{13}C$ = –34‰ to –23‰). Some land plants, mainly grasses found in saltmarshes and arid environments, follow a C_4 pathway which is leads to more ^{13}C-enriched biomass ($\delta^{13}C$= –21‰ to –5‰). Other metabolic pathways exist (*e.g.* Crassulcean Acid Metabolism; CAM) for succulent plants (*e.g.* cactus) and the reversed tricarboxylic

acid (TCA)-cycle in green sulfur bacteria, which result in a less ^{13}C-depleted biomass (*e.g.* Quandt *et al.*, 1977).

Carbon isotope analyses

Stable isotopes are analysed by an isotope ratio mass spectrometer (irMS). For carbon stable isotopes analyses, the samples must be converted to a gas (CO_2) to be irMS amenable. It is on that gas that isotope ratios are measured, by monitoring the relative abundances of *m/z* 44 ($^{12}CO_2$), 45($^{13}CO_2$) and 46 ($^{12}C^{18}O^{16}O$) relative to a CO_2 reference gas of known isotopic value (calibrated to the VPDB), which is measured immediately before and after the sample. The outflow from the GC is diverted away from the irMS *via* a backflow system or heart-split valve to ensure the reference gas is measured on a clean background (*e.g.* Grice and Brocks, 2011).

Carbonate isotopes using Gas-Bench

The addition of 100% phosphoric acid to a carbonate sample at temperature between 20˚C and 90˚C (depending on the carbonate mineral being analysed) under a helium atmosphere converts the carbonate into CO_2. The by-product of the reaction (*e.g.* water) is separated and the CO_2 is diverted into the irMS for $^{13}C/^{12}C$ measurement ($\delta^{13}C_{carb}$). The organic carbon is not affected by the acid treatment, therefore the OM isotopic value does not affect the $\delta^{13}C_{carb}$ values.

Bulk organic matter isotopes analyses using Elemental Analyser (EA)-irMS

When one studies the stable carbon isotopic composition of OM in sediments ($\delta^{13}C_{org}$), the carbonate needs to be removed. To do so, the sample is subject to a hydrochloric acid (HCl) treatment to remove carbonates. The acid treatment procedure can vary for the type of carbonate present in the sample, in the case of calcium carbonate HCl (20%) at room temperature can be used. The residue of this acid digestion is then brought back to a neutral pH, dried and homogenised before being weighted into small tin capsules. The OM contained in these capsules is then oxidised into CO_2 in a combustion furnace at ~1000°C, where the tin capsules react and heat the sample up to 1800°C before the remaining oxygen, nitrate compounds and water are eliminated through various steps. The measurements give the isotopic value in delta notation of the bulk organic matter ($\delta^{13}C_{org}$) contained in the sample.

Carbon - Compound Specific Isotope Analyses (CSIA)

By contrast, CSIA allows to measure the isotopic composition of individual organic compounds within a complex organic mixture. This technique is performed with a continuous flow system that links a GC to an irMS and often results in detailed insights on the source of each compound and allows to identify the origin of many biomarkers (*e.g.* Grice *et al.*, 1996; Koopmans *et al.*, 1996b). CSIA has also been used to reconstruct changes in the carbon cycle (*e.g.* Grice *et al.*, 2005; Summons and Powell, 1985). The sample goes through a combustion furnace containing CuO (and in some system NiO) that oxidises the gases into CO_2 and H_2O at a temperature of 1000˚C. A Nafion® membrane (or in some cases liquid nitrogen maintained around –100˚C) enables the removal of H_2O, and allows CO_2 into the irMS to be analysed.

Carbonate concretions: an overview

Types of carbonate concretions

Carbonate concretions are commonly found in sediments, typically mudstone and sandstones, spanning all geological ages (*e.g.* de Craen *et al.*, 1999; Melendez *et al.*, 2013b; Mozley and Burns, 1993; Raiswell and Fisher, 2000; Wilson and Brett, 2013; Winter and Knauth, 1992). They are easily observable in outcrops where the surrounding sediment is weathered away while they protrude due to their intense cementation, which grants them a greater resistance against weathering and erosion.

Carbonate concretions are generally shaped as a ball or an ovoid, and they commonly vary from tens of cm (Melendez *et al.*, 2013b) to few meters in size (Mcbride and Milliken, 2006) (**Figure 1-7**), however smaller concretions also exist in soils for example. Carbonate concretions are common in both marine and non-marine sediments, and they are most often encountered concentrated within a particular sedimentary layer rather than dispersed in the sediment (Marshall and Pirrie, 2013).

Figure 1-7. Examples of carbonate concretions and their exceptionally preserved fossil nucleus.

The most common mineralogies for carbonate concretions are calcite ($CaCO_3$), dolomite ($MgCa(CO_3)_2$) and siderite ($FeCO_3$). They sometimes contain abundant non-carbonate minerals, such as pyrite (*e.g.* Coleman and Raiswell, 1995) and/or barite (Raiswell *et al.*, 2002).

Models of formation

Concretions are often found in OM-rich sediments, which reveals that their formation occurs within oxygen-depleted environments. Microbial degradation of OM influences the chemistry of the microenvironment that in turn triggers the precipitation of carbonate minerals (Coleman, 1993; Dale *et al.*, 2014; Marshall and Pirrie, 2013; Martill, 1989). Various features of carbonate concretions (*e.g.* shape, sedimentary bedding, and three-dimensional fossil preservation) indicate a formation at shallow depth within the sediment (Marshall and Pirrie, 2013; Seilacher, 2001; Sellés-Martínez, 1996). This would support a very early development of concretions around centres of decaying OM (*e.g.* Yoshida *et al.*, 2015). Nevertheless, the lack of modern forming analogues for carbonate concretions leads scientists to study past concretions to determine the mechanism involved in their formation. Some laboratory experiments have been performed to better understand the timing and processes of the formation of carbonate concretions (Berner, 1967, 1968), or the role of microbial mats in fossil preservation (Iniesto *et al.*, 2015).

Many studies have revealed evidence indicating that carbonate concretions formed concentrically (*e.g.* Criss *et al.*, 1988; Mozley and Burns, 1993). However, it has shown that some carbonate concretions rather form pervasively and undergo multiphase mineralisation processes (Mozley, 1989, 1996; Raiswell and Fisher, 2000). Textural and isotopic evidence in siderite and dolomite concretions support a pervasive growth (Hennessy and Knauth, 1985; Mozley, 1989), however similar observations are uncommon in calcite concretions. Raiswell and Fisher (2000) suggested that it may be the result of the smaller size of calcite minerals in concretions (typically microsparite, < 20µm). Coleman and Raiswell (1995) proposed a dynamic model for calcite concretions with a pyritic rim that involves the precipitation of the outer pyritic rim simultaneously with the precipitation of the calcite matrix of the concretion.

Concretions, fossils and preservation of OM

Concretions are known to encapsulate the most remarkable fossils of hard and soft tissues (Bertazzo *et al.*, 2015; Marshall and Pirrie, 2013; Martill, 1989; Williams *et al.*, 2015) as well as burrows (Wilson and Brett, 2013). Such fossils support a very early concretion growth after the death of an organism. Furthermore, concretions are known to preserve the three-dimensional characteristics of the encapsulated fossils, protecting them from the typical flattening related to diagenesis upon burial. Recently, studies have shown that carbonate concretions also play a pivotal role in the preservation of molecular fossils, and have confirmed the importance of microbial communities (*e.g.* sulfate reducers) in their formation (Melendez *et al.*, 2013b).

Some molecules such as sterols are very labile and are easily degraded over geologic timeframes. However, the oldest report of cholesterol was found in a 380 Ma crustacean encapsulated in a carbonate concretion. The cholesterol was present in association with a suite of transformation products and intermediates from stanols to steranes and triaromatic steroids (Melendez *et al.*, 2013a). Such findings have suggested that carbonate concretions are not only interesting in the research of morphological fossils, but that they could also contain precious information in the form of biomarkers and intact biomolecules.

Techniques of investigation

Carbonates concretions have received a lot of attention from geologists to inorganic geochemists over the previous decades. However, the interest in carbonate concretions from an organic geochemical perspective is quite recent (Kiriakoulakis *et al.*, 2000; Melendez *et al.*, 2013a, 2013b; Pearson *et al.*, 2005; Pearson and Nelson, 2005; Zatoń and Marynowski, 2004) and only very few studies of DNA of carbonate concretions exist (*e.g.* Reitner *et al.*, 2005). Furthermore, few studies use cross-disciplinary techniques to investigate such "bio-geo-sedimentary" objects. In this PhD multidisciplinary geological and geochemical techniques were involved (**Figure 1-8**) to improve our understanding of carbonate concretion formation and the preservation capabilities with regards to biomolecules.

A combination of techniques ranging from classical sedimentary geology (*e.g.* optical and scanning microscopy, X-ray diffraction) to inorganic geochemical tools (X-ray Fluorescence (XRF) mapping, inductively coupled plasma mass spectrometry, and stable isotopes of carbonates) to bulk organic geochemistry as well as biomarker analyses and CSIA were used to characterise the sedimentary environment and mechanisms in action. **Figure 1-8** illustrates the analytical approaches used in the investigation of a carbonate concretion performed during this PhD.

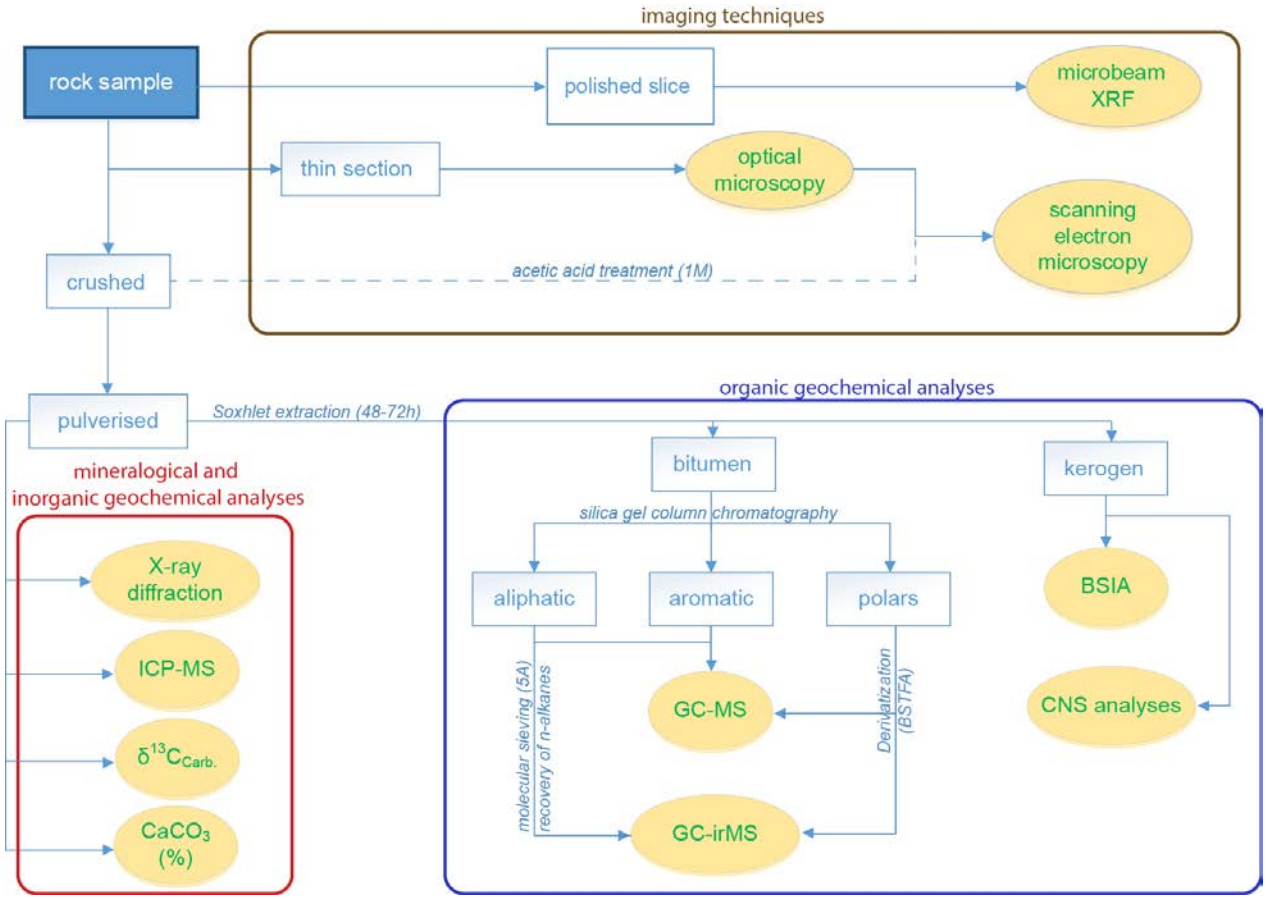

Figure 1-8. Flowchart of the cross-disciplinary methods applied to the study of carbonate concretions during this PhD project. Dashed lines represent procedures that were not applied on all concretions.

The Toarcian Oceanic Anoxic Event (T-OAE, *ca.* 183 Ma): geological settings

The Toarcian Oceanic Anoxic Event (T-OAE) lead to a 2nd order marine fauna mass extinction (Cecca and Macchioni, 2004; Macchioni and Cecca, 2002) and the widespread deposition of OM-rich sediments (Baudin *et al.*, 1990a). During this event, the carbonate production crisis led to the near disappearance of shallow carbonate platforms (Dromart *et al.*, 1996; Suan *et al.*, 2008) and the increase of more clayey sediments (Jenkyns *et al.*, 2002). Across Europe, these OM-rich shales have become one of the major source rocks for petroleum and therefore have been the focus of numerous studies.

These Early Toarcian OM-rich sediments have proven to show a very characteristic $\delta^{13}C_{org}$ trend, which consist of an increase in $\delta^{13}C_{org}$ followed by an abrupt decrease (as much as 6‰) and another increase in $\delta^{13}C_{org}$ (Jenkyns *et al.*, 2002). This characteristic carbon isotopic signatures allowed to establish stratigraphic correlations across sections within Europe (*e.g.* Cohen *et al.*, 2004; Hesselbo *et al.*, 2007; McElwain *et al.*, 2005) but also at a global scale for example in Argentina (Al-Suwaidi *et al.*, 2010) and Alaska (Magoon and Claypool, 1984). Such variations in $\delta^{13}C_{org}$ were initially attributed to local upwelling (*e.g.* Jenkyns, 1988) or variations in salinity (*e.g.* Farrimond *et al.*, 1989). Although such local fluctuations may play a role in the $\delta^{13}C_{org}$ signature of the sediments, the global nature of the event suggests that these were not the controlling factors. Furthermore, the evidence of parallel trends in $\delta^{13}C_{carb}$ and $\delta^{13}C$ analyses of biomarkers strongly support a change in the isotopic composition of the DIC (Schouten *et al.*, 2000b). Carbon isotopic analyses performed on fossil wood from different European locations (*i.e.* Denmark and Portugal) also show the existence of a negative $\delta^{13}C_{org}$ excursion, revealing that the shift in isotopic composition affects the oceanic, biospheric and atmospheric carbon reservoirs (Hesselbo *et al.*, 2000, 2007; Kemp *et al.*, 2005).

This global isotopic shift has been attributed to an intense volcanism in the Karoo-Ferrar province (McElwain *et al.*, 2005; Suan *et al.*, 2008; Svensen *et al.*, 2007) and/or to a massive methane release from the collapse of gas hydrates (Hesselbo *et al.*, 2000; Kemp *et al.*, 2005). Detailed studies showed that the release of methane occurred as three rapid pulses controlled by precession cycles (astronomical climate forcing

parameter with a frequency of 21 kyr), superimposed upon a larger global warming (Kemp *et al.*, 2005). However, Wignall *et al.* (2005) showed that mass extinction was not synchronised with the release of methane, which occurred later. The biological crisis occurred in two events that coincided with a major rise in seawater temperature and could be attributed to two major episodes of degassing of the Karoo-Ferrar volcanic province having a direct impact on the global warming (Suan *et al.*, 2008).

Study site 1: Posidonia Shale Formation (SW-Germany): the Falciferum zone

The Posidonia Shale Formation was deposited during the T-OAE. At that time, the South German sub-basin was one of several partly enclosed basins located on the structurally rich Western Tethyan shelf (Ruebsam *et al.*, 2014). These basins were connected to the Arctic *via* the Viking corridor and to the open Tethys Ocean toward the South East (**Figure 1-9**). The depositional conditions were strongly controlled by sea level changes and the monsoon driven-palaeoclimate.

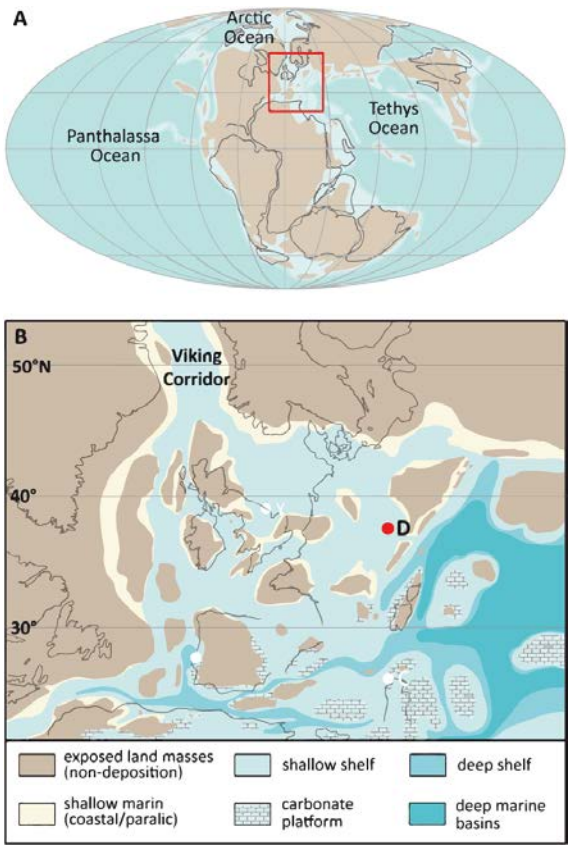

Figure 1-9. Palaeogeography of the Toarcian and localisation of the sampling site (modified after Ruebsam et al. (2014).

Most of the *Falciferum* zone was deposited during sea level low stand. The South German sub-basin was endorheic, which led to layered stagnant water conditions with oxygen-depleted bottom waters (Schmid-Röhl *et al.*, 2002). However, detailed studies of the Posidonia Shale Formation of SW-Germany indicate that these long term anoxic conditions were punctuated by short periods of oxygenated bottom water as suggested by sedimentological and bulk geochemical data (Röhl *et al.*, 2001) and supported by exhaustive biomarker studies (Frimmel *et al.*, 2004; Schwark and Frimmel, 2004). The subsequent transgression enhanced water exchange with the Tethys Ocean and improved the conditions for life at the top of the *Falciferum* zone (Röhl *et al.*, 2001).

The *Falciferum* zone is host to various carbonate rich levels and carbonate concretions. These concretions were studied during this PhD. They are the lateral equivalent of the pyritiferous calcite concretions from NE-England that have received much attention from geologist and inorganic geochemists (*e.g.* Coleman and Raiswell, 1995; Coleman, 1993; Hudson, 1982).

Study site 2: Shark Bay

Geological settings

Shark Bay is a well-known World Heritage area, located 800 Km North of Perth on the West Australian coastline. The region is renowned for its beauty and its scientific significance due to the presence of a great diversity of modern day stromatolites containing complex microbial communities. Shark Bay is subject to an arid climate characterised by limited rainfall and intense evaporation (Logan and Cebulski, 1970; Price *et al.*, 2012). The site that was investigated during this study is Carbla Beach, located in the eastern side of Hamelin Pool. The Hamelin Pool is a semi-enclosed shallow basin with a surface of approximately 1400 Km^2 (Jahnert and Collins, 2012) and is subject to high rate of evaporation. This abundant evaporation is compensated by marine inflow through the Faure Sill, a shallow sand bank that formed thousands of years ago through the trapping of sediments and organic material by seagrasses, isolating the Hamelin Pool. Through this inflow, a replacement of 70% to 200% of the Hamelin Pool water volume occurs every year (Price *et al.*, 2012).

The beach ridges of Hamelin Pool are largely dominated by the Hamelin Coquina Barrier, that resulted from an accumulation and accretion of bivalves shells (*F. erugatum*) leading to hypersaturation in $CaCO_3$ of the Hamelin Pool seawater (Jahnert *et al.*, 2012). The water is poor in dissolved nutrients (oligotrophic) with phosphorus being the limiting nutrient and nitrogen requirements are met by cyanobacterial nitrogen fixation (Smith and Atkinson, 1983). The average water temperatures are comprised between 15 ˚C and 18 ˚C in winter and 26 C-30 C in summer, but temperature at intertidal surface can be as high as 45 C-50 C (Allen, 2006; Bauld, 1984).

Jahnert and Collins (2012) established that all subtidal microbial mats overall cover approximately 300 Km^2 of the total 1400 Km^2 of Hamelin Pool. These ecosystems are prone to lithification (induced biomineralisation) and are strongly influenced by physicochemical parameters (light intensity, alkalinity, salinity, depth and wave energy) of the surrounding environment (Logan, 1974), resulting in a great variety of structures and fabrics (**Figure 1-10**).

Microbialites and biomarkers

Shark Bay microbialites have been extensively investigated as they are thought to represent robust modern day analogues of Precambrian stromatolites (*e.g.* Burns *et al.*, 2009; Goh *et al.*, 2009). Therefore, their study can help understanding and unravelling mysteries of early life on Earth. Within this context, the study of microbial communities present in modern stromatolites is also of major interest in astrobiology and the search for extra-terrestrial life.

Not all mats present the typical lamination that is observed in most ancient stromatolites. However, in laminated microbial mats, the vertical organisation of microbial communities along microscale chemical and physical gradients led to the optimisation of biogeochemical processes (Pagès *et al.*, 2015; Van Gemerden, 1993).

Shark Bay contains a variety of microbial mats presenting different morphologies. Six different types of mats were previously described in Hamelin Pool, with increasing depth these mats are: tufted, pustular, smooth, colloform, cerebroid and pavement (Jahnert and Collins, 2012). These mat types were characterised based on their i) microfabrics (*e.g.* presence or absence of laminar microstructure) (Jahnert

and Collins, 2012; Reid *et al.*, 2003), ii) presence of specific cyanobacterial species, based on taxonomy (Jahnert and Collins, 2012), iii) dominant microbial communities, based on DNA analyses (*e.g.* Allen *et al.*, 2009; Edgcomb *et al.*, 2014; Goh *et al.*, 2009) and iv) biomarkers and their isotopic composition (Pagès *et al.*, 2014a, 2014b, 2015).

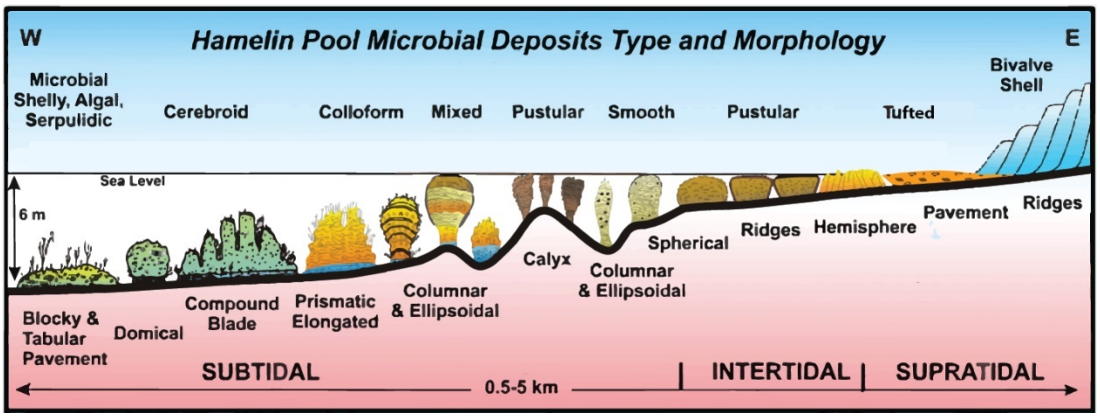

Figure 1-10. Microbial mats distribution in function of depth in Hamelin Pool (modified from Jahnert and Collins, 2012).

Modern microbial mat ecosystems are made of complex assemblage of microbial communities, commonly dominated by oxygenic phototrophic microorganisms (Atlas and Bartha, 1998). Amongst others, non strict anaerobes photsynthetic purple sulfur bacteria or strict anaerobic green sulfur bacteria were reported in microbial mats (Des Marais, 1995; Van Gemerden, 1993). Heterotrophs *e.g.* SRB and sulfur oxidising bacteria are also involved in microbial mat ecosystems. Eukaryotic input from *e.g.* foraminifers, vascular plants and protists were also reported in microbial mats.

Aims of the thesis

The main goal of the thesis was to use complementary cross disciplinary approaches such as sedimentary petrology, inorganic geochemistry and imaging and organic geochemical proxies, biomarkers and stable isotopes, to investigate OM preservation associated with different types of microbialites. This multiproxy study aims to highlight the interest of cross-disciplinary investigation to develop a better understanding of induced biomineralisation in general, and the potential they hold for early life and extra-terrestrial studies. Overall, the same techniques were applied to

concretions from ancient times that were formed within the sediment during the T-OAE and to modern stromatolites from a hypersaline tidal environment.

The purpose of the research presented in **Chapter 2** was to use a multi-proxy approach combining biomarkers, stable isotopes, imaging techniques and major, minor and trace elements distributions to investigate various Jurassic carbonate concretions. Specifically, concretion growth processes, microbial communities involved in carbonate precipitation and preservation of OM within the concretions were investigated. Organic and inorganic data were compared to those of the host euxinic shale in order to distinguish the specific signatures of the concretions and assess their potential as palaeoenvironmental recorders.

In **Chapter 3,** a Jurassic concretion containing an Ichthyosaur vertebra was studied to try to recover biological signatures from this extinct organism. A combined method using imaging techniques, biomarkers and stable isotopes was applied to the ichthyosaurs vertebra and surrounding concretion, to get further palaeobiological information about this ancient species and its evolution as well as and gain further understanding of the significance of carbonate concretion in the preservation of exceptional fossil both morphological (soft tissue) and organic (biolipids).

Chapter 4: the same concretion studied in chapter 3 was investigated using maleimides and regular isoprenoids (pristane and phytane) and their carbon stable isotopes. The purpose was to identify the origin of the maleimides detected in the concretion and bone and determine if they were i) originated in the water column, ii) derived from heme (from the ichthyosaur) or iii) resulting from contamination by geochromatography and/or iv) were artefacts from weathering or storage of the concretion.

Chapter 5 described the investigation of three microbial mats from Carbla Beach, Shark Bay. Biomarker (including aliphatic hydrocarbons, fatty acid methyl esters, alcohols, sterols and cyclic terpenoids as well as free fatty acids) and isotopic analysis were performed on the three types of mats (tufted, pustular and smooth) that live in supratidal, intertidal and shallow subtidal environments, respectively. Imaging techniques were used to characterise the microfabrics of three specimens and compare them to their biological signatures. These variations were also used to evaluate the

influence of water depth on microbial communities' distributions at shallow depth (0-1m). In addition, the potential for investigation combining lipids and microfabrics in microbial mats is highlighted.

References

Al-Suwaidi, A.H., Angelozzi, G.N., Baudin, F., Damborenea, S.E., Hesselbo, S.P., Jenkyns, H.C., Manceñido, M.O., Riccardi, A.C., 2010. First record of the Early Toarcian Oceanic Anoxic Event from Southern Hemisphere, Neuquén Basin, Argentina. *Journal of the Geological Society* **167**, 633–636.

Allen, M.A., 2006. An astrobiology focused analysis of microbial mat communities from Hamelin Pool, Shark Bay, Western Australia.

Allen, M.A., Goh, F., Burns, B.P., Neilan, B.A., 2009. Bacterial, archaeal and eukaryotic diversity of smooth and pustular microbial mat communities in the hypersaline lagoon of Shark Bay. *Geobiology* **7**, 82–96.

Allison, P.A., 1988a. Konservat-Lagerstätten : Cause and Classification. *Paleobiology* **14**, 331–344.

Allison, P.A., 1988b. The role of anoxia in the decay and mineralization of proteinaceous macro-fossils. *Paleobiology* **14**, 139–154.

Asara, J.M., Schweitzer, M.H., Freimark, L.M., Phillips, M., Cantley, L.C., 2007. Protein sequences from mastodon and Tyrannosaurus rex revealed by mass spectrometry. *Science* **316**, 280–285.

Atlas, R.M., Bartha, R., 1998. Microbial ecology: fundamentals and applications. Addison - Wiley, Reading.

Awramik, S.M., 1992. The oldest records of photosynthesis. *Photosynthesis research* **33**, 75–89.

Barakat, A.O., Rullkötter, J., 1997. A Comparative Study of Molecular Paleosalinity Indicators: Chromans, Tocopherols and C20 Isoprenoid Thiophenes in Miocene Lake Sediments (Nördlinger Ries, Southern Germany). *Aquatic Geochemistry* **3**, 169–190.

Baudin, F., Herbin, J.-P., Vandenbroucke, M., 1990. Mapping and geochemical characterization of the Toarcian organic matter in the Mediterranean Tethys and

Middle East. *Organic Geochemistry* **16**, 677–687.

Bauld, J., 1984. Microbial mats in marginal marine environments: Shark Bay, Western Australia, in: Cohen, Y., Castenholz, R.W., Halvorson, H.O. (Eds.), Microbial Mats: Stromatolites. Alan R, Liss, New York, pp. 39–58.

Bell, E.A., Boehnke, P., Harrison, T.M., Mao, W.L., 2015. Potentially biogenic carbon preserved in a 4.1 billion-year-old zircon. *Proceedings of the National Academy of Sciences of the United States of America* **112**, 14518–14521.

Berndmeyer, C., Thiel, V., Schmale, O., Wasmund, N., Blumenberg, M., 2014. Biomarkers in the stratified water column of the Landsort Deep (Baltic Sea). *Biogeosciences* **11**, 7009–7023.

Berner, R.A., 1967. Rate of concretion growth. *Geochimica et Cosmochimica Acta* **32**, 477–483.

Berner, R.A., 1968. Calcium carbonate concretions formed by the decomposition of organic matter. *Science* **159**, 195–197.

Berner, R.A., 2004. The Phanerozoic carbon cycle: O_2 and CO_2. Oxford University Press.

Bertazzo, S., Maidment, S.C.R., Kallepitis, C., Fearn, S., Stevens, M.M., Xie, H., 2015. Fibres and cellular structures preserved in 75-million–year-old dinosaur specimens. *Nature Communications* **6**, 7352.

Brassell, S.C., Eglinton, G., Howell, V.J., 1987. Palaeoenvironmental assessment of marine organic-rich sediments using molecular organic geochemistry. *Geological Society, London, Special Publications* **26**, 79–98.

Briggs, D.*E.G.*, 2003. The role of decay and mineralization in the preservation of soft-bodied fossils. *Annual Review of Earth and Planetary Sciences* **31**, 275–301.

Briggs, D.*E.G.*, Summons, R.E., 2014. Ancient biomolecules: their origins, fossilization, and role in revealing the history of life. *BioEssays : news and reviews in molecular, cellular and developmental biology* **36**, 482–90.

Brocks, J.J., Pearson, A., 2005. Building the Biomarker Tree of Life. *Reviews in Mineralogy and Geochemistry* **59**, 233–258.

Brocks, J.J., Summons, R.E., 2003. Sedimentary hydrocarbons, biomarkers for early life, in: Treatise on Geochemistry. pp. 63–115.

Burley, S., Kantorowicz, J.D., Waugh, B., 1985. Clastic diagenesis. *Geological Society, London, Special Publications* **18**, 189–226.

Burns, B.P., Anitori, R., Butterworth, P., Henneberger, R., Goh, F., Allen, M. a., Ibañez-Peral, R., Bergquist, P.L., Walter, M.R., Neilan, B. a., 2009. Modern analogues and the early history of microbial life. *Precambrian Research* **173**, 10–18.

Cecca, F., Macchioni, F., 2004. The two Early Toarcian (Early Jurassic) extinction events in ammonoids. *Lethaia* **37**, 35–56.

Cohen, A.S., Coe, A.L., Harding, S.M., Schwark, L., 2004. Osmium isotope evidence for the regulation of atmospheric CO_2 by continental weathering. *Geology* **32**, 157–160.

Cohen, P.A., Schopf, J.W., Butterfi, N.J., Kudryavtsev, A.B., Macdonald, F.A., 2011. Phosphate biomineralization in mid-Neoproterozoic protists. *Geology* **39**, 539–542.

Coleman, M.L., 1993. Microbial processes: Controls on the shape and composition of carbonate concretions. *Marine Geology* **113**, 127–140.

Coleman, M.L., Raiswell, R., 1995. Source of carbonate and origin of zonation in pyritiferous carbonate concretions: evaluation of a dynamic model. *American Journal of Science* **295**, 282–308.

Comet, P. a, McEvoy, J., Brassell, S.C., Eglinton, G., Maxwell, J.R., Thomson, I.D., 1981. Lipids of an Upper Albian limestone, Deep Sea Drilling Project Site 465. *Init. Rep. DSDP* **62**, 923–937.

Criss, R.E., Cooke, G.A., Day, S.D., 1988. An Organic Origin for the Carbonate

Concretions of the Ohio Shale. *U.S. Geological Survey Bulletin*.

Dahl, J.E., Moldowan, J.M., Peters, K.E., Claypool, G.E., Rooney, M.A., Michael, G.E., Mello, M.R., Kohnen, M.L., 1999. Diamondoid hydrocarbons as indicators of natural oil cracking. *Nature* **399**, 54–57.

Dale, A., John, C.M., Mozley, P.S., Smalley, P.C., Muggeridge, A.H., 2014. Time-capsule concretions: Unlocking burial diagenetic processes in the Mancos Shale using carbonate clumped isotopes. *Earth and Planetary Science Letters* **394**, 30–37.

de Craen, M., Swennen, R., Keppens, E.M., Macaulay, C.I., Kiriakoulakis, K., 1999. Bacterially mediated formation of carbonate concretions in the Oligocene Boom Clay of Northern Belgium.

Des Marais, D.J., 1995. The biogeochemistry of hypersaline microbial mats. *Advances in Microbial Ecology* **14**, 251–274.

Dromart, G., Allemand, P., Garcia, J.P., Robin, C., 1996. Cyclic fluctuation of carbonate production through the Jurassic along a Burgundy-Ardeche cross-section, eastern France. *Bulletin de la Societe geologique de France* **167**, 423–433.

Edgcomb, V.P., Bernhard, J.M., Summons, R.E., Orsi, W., Beaudoin, D., Visscher, P.T., 2014. Active eukaryotes in microbialites from Highborne Cay, Bahamas, and Hamelin Pool (Shark Bay), Australia. *The ISME journal* **8**, 418–29.

El Albani, A., Bengtson, S., Canfield, D.E., Bekker, A., Macchiarelli, R., Mazurier, A., Hammarlund, E.U., Boulvais, P., Dupuy, J., Fontaine, C., Fu, F.T., Riboulleau, A., Sardini, P., Vachard, D., Whitehouse, M., Meunier, A., 2010. Large colonial organisms with coordinated growth in oxygenated environments 2.1 Gyr ago. *Nature* **466**, 100–104.

El Albani, A., Bengtson, S., Canfield, D.E., Riboulleau, A., Rollion Bard, C., Macchiarelli, R., Ngombi Pemba, L., Hammarlund, E., Meunier, A.,

Moubiya Mouele, I., Benzerara, K., Bernard, S., Boulvais, P., Chaussidon, M., Cesari, C., Fontaine, C., Chi-Fru, E., Garcia Ruiz, J.-M., Gauthier-Lafaye, F., Mazurier, A., Pierson-Wickmann, A.-C., Rouxel, O., Trentesaux, A., Vecoli, M., Versteegh, G., White, L., Whitehouse, M., Bekker, A., 2014. The 2.1 Ga old Francevillian biota: biogenecity, taphonomy and biodiversity. *PloS one* **9**.

Falkowski, P.G., Scholes, R.J., Boyle, E., Canadell, J., Canfield, D., Elser, J., Gruber, N., Hibbard, K., Högberg, P., Linder, S., Mackenzie, F.T., Moore, B., Pedersen, T., Rosenthal, Y., Seitzinger, S., Smetacek, V., Steffen, W., 2000. The global carbon cycle: a test of our knowledge of earth as a system. *Science* **290**, 291–296.

Farrimond, P., Eglinton, G., Brassell, S.C., Jenkyns, H.C., 1989. Toarcian anoxic event in Europe : an organic geochemical study. *Marine and Petroleum Geology* **6**, 136–147.

Faure, G., Mensing, T.M., 2005. Isotopes, Principles and Applications, 3rd ed. John Wiley & Sons.

Frimmel, A., Oschmann, W., Schwark, L., 2004. Chemostratigraphy of the Posidonia Black Shale, SW Germany I. Influence of sea-level variation on organic facies evolution. *Chemical Geology* **206**, 199–230.

Goh, F., Allen, M. a, Leuko, S., Kawaguchi, T., Decho, A.W., Burns, B.P., Neilan, B. a, 2009. Determining the specific microbial populations and their spatial distribution within the stromatolite ecosystem of Shark Bay. *The ISME journal* **3**, 383–396.

Grice, K., 2014. Principles and practice of analytical techniques in geosciences. the Royal Society of Chemistry.

Grice, K., Alexander, R., Kagi, R.I., 2000. Diamondoid hydrocarbon ratios as indicators of biodegradation in Australian crude oils. *Organic Geochemistry* **31**, 67–73.

Grice, K., Brocks, J.J., 2011. Biomarkers (organic, compound-specific isotopes), in: Thiel, Reitner (Eds.), Encyclopaedia of Geobiology. Encyclopedia of Earth Science Series, pp. 167–182.

Grice, K., Cao, C., Love, G.D., Böttcher, M.E., Twitchett, R.J., Grosjean, E., Summons, R.E., Turgeon, S.C., Dunning, W., Jin, Y., 2005. Photic zone euxinia during the Permian-Triassic superanoxic event. *Science* **307**, 706–9.

Grice, K., Gibbison, R., Atkinson, J.E., Schwark, L., Eckardt, C.B., Maxwell, J.R., 1996. Maleimides (1H-pyrrole-2,5-diones) as Molecular Indicators of Anoxygenic Photosynthesis in Ancient Water Columns. *Geochimica et Cosmochimica Acta* **60**, 3913–3924.

Gupta, N.S., 2015. Plant biopolymer – geopolymer : organic diagenesis and kerogen formation. *Frontiers in Materials* **2**, 2007–2010.

Hennessy, J., Knauth, L.P., 1985. Isotopic variations in dolomite concretions from the Monterey Formation, California. *Journal of Sedimentary Petrology* **55**, 120–130.

Hesselbo, S., Grocke, D., Jenkyns, H.C., Bjerrum, C.J., Farrimond, P., Morgans Bell, H., Green, O., 2000. Massive dissociation of gas hydrate during a Jurassic oceanic anoxic event. *Nature* **406**, 392–395.

Hesselbo, S.P., Jenkyns, H.C., Duarte, L. V., Oliveira, L.C.V., 2007. Carbon-isotope record of the Early Jurassic (Toarcian) Oceanic Anoxic Event from fossil wood and marine carbonate (Lusitanian Basin, Portugal). *Earth and Planetary Science Letters* **253**, 455–470.

Hoefs, J., 2015. Stable isotope geochemistry, 7th ed, Geochemistry. Springer.

Holser, W., Schidlowski, M., Mackenzie, F., Maynard, J., 1988. Chemical cycles in the evolution of the Earth. Wiley Interscience.

Hudson, J.D., 1982. Pyrite in ammonite-bearing shales from the Jurassic of England and Germany. *Sedimentology* **29**, 639–667.

Iniesto, M., Zeyen, N., López-Archilla, A.I., Bernard, S., Buscalioni, Á.D., Guerrero, M.C., Benzerara, K., 2015. Preservation in microbial mats: mineralization by a talc-like phase of a fish embedded in a microbial sarcophagus. *1. Frontiers in Earth Science* **3**, 1–13.

Jahnert, R., de Paula, O., Collins, L., Strobach, E., Pevzner, R., 2012. Evolution of a coquina barrier in Shark Bay, Australia by GPR imaging: Architecture of a Holocene reservoir analog. *Sedimentary Geology* **281**, 59–74.

Jahnert, R.J., Collins, L.B., 2012. Characteristics, distribution and morphogenesis of subtidal microbial systems in Shark Bay, Australia. *Marine Geology* **303–306**, 115–136.

Jenkyns, H.C., 1988. The Early Toarcian Anoxic event: Stratigraphic, sedimentary, and geochrmical evidence. *Americal Journal of Science* **288**, 101–151.

Jenkyns, H.C., Jones, C.E., Gröcke, D.R., Hesselbo, S.P., Parkinson, D.N., 2002. Chemostratigraphy of the Jurassic System: applications, limitations and implications for palaeoceanography. *Journal of the Geological Society* **159**, 351–378.

Kemp, D.B., Coe, A.L., Cohen, A.S., Schwark, L., 2005. Astronomical pacing of methane release in the Early Jurassic period. *Nature* **437**, 396–399.

Kendall, C., Caldwell, E.A., 1998. Fundamentals of isotope geochemistry, in: Kendall, C., McDonnell, J.J. (Eds.), Isotope Tracers in Catchment Hydrology. Elsevier Science, Amsterdam, pp. 51–86.

Kiriakoulakis, K., Marshall, J.D., Wolff, G.A., 2000. Biomarkers in a Lower Jurassic concretion from Dorset (UK). *Journal of the Geological Society* **157**, 207–220.

Knoll, A.H., 2011. The multiple origins of complex multicellularity. *Annual Review of Earth and Planetary Sciences* **39**, 217–239.

Kohl, W., Achenbach, H., Reichenbach, H., 1983. The pigments of Brevibacterium linens: Aromatic carotenoids. *Phytochemistry* **22**, 207–210.

Koopmans, M.P., Köster, J., Van Kaam-Peters, H.M.E., Kenig, F., Schouten, S., Hartgers, W.A., De Leeuw, J.W., Sinninghe Damsté, J.S., 1996a. Diagenetic and catagenetic products of isorenieratene: Molecular indicators for photic zone anoxia. *Geochimica et Cosmochimica Acta* **60**, 4467–4496.

Koopmans, M.P., Schouten, S., Kohnen, M.E.L., Sinninghe Damsté, J.S., 1996b. Restricted utility of aryl isoprenoids as indicators for photic zone anoxia. *Geochimica et Cosmochimica Acta* **60**, 4873–4876.

Kroopnick, P.M., 1985. The distribution of ^{13}C of ΣCO_2 in the world oceans. *Deep Sea Research Part A, Oceanographic Research Papers* **32**, 57–84.

Krügel, H., Krubasik, P., Weber, K., Saluz, H.P., Sandmann, G., 1999. Functional analysis of genes from Streptomyces griseus involved in the synthesis of isorenieratene, a carotenoid with aromatic end groups, revealed a novel type of carotenoid desaturase. *Biochimica et Biophysica Acta - Molecular and Cell Biology of Lipids* **1439**, 57–64.

Landing, E., English, A., Keppie, J.D., 2010. Cambrian origin of all skeletalized metazoan phyla — Discovery of Earth ' s oldest bryozoans (Upper Cambrian , southern Mexico). *Geology* **38**, 547–550.

Lindgren, J., Kaddumi, H.F., Polcyn, M.J., 2013. Soft tissue preservation in a fossil marine lizard with a bilobed tail fin. *Nature communications* **4**, 2423.

Logan, B.W., 1974. Evolution and diagenesis of quaternary carbonate sequences, Shark Bay, Western Australia. *American association of petroleum geologists memoir* **22**, 195–249.

Logan, B.W., Cebulski, D.E., 1970. Sedimentary environments of Shark Bay, Western Australia. *American association of petroleum geologists memoir* **13**, 1–37.

Macchioni, F., Cecca, F., 2002. Biodiversity and biogeography of middle–late liassic ammonoids: implications for the early Toarcian mass extinction. *Geobios* **35**, 165–175.

Mackenzie, A.S., Brassel, S.C., Eglington, G., Maxwell, J.R., 1982a. Chemical fossils: the geological fate of steroids. *Science* **217**.

Mackenzie, A.S., Lamb, N.A., Maxwell, J.R., 1982b. Steroid hydrocarbons and the thermal history of sediments. *Nature* **295**, 223–226.

Magoon, L.B., Claypool, G.E., 1984. Organic Geochemical Properties and Petroleum Source Rock Quality. *Organic Geochemistry* **6**, 533–542.

Marshak, S., 2012. Essentials of Geology, 4th ed. W.W. Norton & Company.

Marshall, J.D., Pirrie, D., 2013. Carbonate concretions-explained. *Geology Today* **29**, 53–62.

Martill, D.M., 1988. Preservation of fish in the Cretaceous Santana Formation of Brazil. *Palaeontology* **31**, 1–18.

Martill, D.M., 1989. The Medusa effect: instantaneous fossilization. *Geology Today* **5**, 201–205.

Martill, D.M., 1995. Ichthyosaur with preserved soft tissue from the Sinemurian of Southern England. *Palaeontology*.

Mcbride, E.F., Milliken, K.L., 2006. Giant calcite-cemented concretions, Dakota Formation, central Kansas, USA. *Sedimentology* **53**, 1161–1179.

McElwain, J.C., Wade-Murphy, J., Hesselbo, S.P., 2005. Changes in carbon dioxide during an oceanic anoxic event linked to intrusion into Gondwana coals. *Nature* **435**, 479–482.

McNamara, K., 2013. Stromatolites. Western Australian Museum, Perth.

Melendez, I., Grice, K., Schwark, L., 2013a. Exceptional preservation of Palaeozoic steroids in a diagenetic continuum. *Scientific reports* **3**, 2768.

Melendez, I., Grice, K., Trinajstic, K., Ladjavardi, M., Greenwood, P., Thompson, K., 2013b. Biomarkers reveal the role of photic zone euxinia in exceptional fossil preservation: An organic geochemical perspective. *Geology* **41**,

123–126.

Mozley, P.S., 1989. Complex compositional zonation in concretionary siderite: implications for geochemical studies. *Journal of Sedimentary Petrology* **59**, 815–818.

Mozley, P.S., 1996. The internal structure of carbonate concretions in mudrocks: a critical evaluation of the conventional concentric model of concretion growth. *Sedimentary Geology* **103**, 85–91.

Mozley, P.S., Burns, S.J., 1993. Oxygen and carbon isotopic composition of marine carbonate concretions: an overview. *Journal of Sedimentary Petrology* **63**, 73–83.

Narbonne, G.M., 2005. The Ediacara biota: Neoproterozoic origin of animals and their ecosystems. *Annual Review of Earth and Planetary Sciences* **33**, 421–442.

Oppenheimer, C., Fischer, T.P., Scaillet, B., 2014. Volcanic degassing: processes and impact. *Treatise on Geochemistry: Second Edition* **4**, 111–179.

Pagès, A., Grice, K., Ertefai, T., Skrzypek, G., Jahnert, R., Greenwood, P., 2014a. Organic geochemical studies of modern microbial mats from Shark Bay: Part I: Influence of depth and salinity on lipid biomarkers and their isotopic signatures. *Geobiology* **12**, 469–487.

Pagès, A., Grice, K., Vacher, M., Welsh, D.T., Teasdale, P.R., Bennett, W.W., Greenwood, P., 2014b. Characterizing microbial communities and processes in a modern stromatolite (Shark Bay) using lipid biomarkers and two-dimensional distributions of porewater solutes. *Environmental microbiology* **16**, 2458–2474.

Pagès, A., Grice, K., Welsh, D.T., Teasdale, P.T., Van, M.J., Greenwood, P., 2015. Lipid Biomarker and Isotopic Study of Community Distribution and Biomarker Preservation in a LaminatedMicrobialMat from Shark Bay,Western Australia. *Environmental Microbiology* **70**, 459–472.

Pearson, M.J., Hendry, J.P., Taylor, C.W., Russell, M.A., 2005. Fatty acids in sparry calcite fracture fills and microsparite cement of septarian diagenetic

concretions. *Geochimica et Cosmochimica Acta* **69**, 1773–1786.

Pearson, M.J., Nelson, C.S., 2005. Organic geochemistry and stable isotope composition of New Zealand carbonate concretions and calcite fracture fills. *New Zealand Journal of Geology and Geophysics* **48**, 395–414.

Peters, K.E., Clifford, C.W., Moldowan, J.M., 2005. The biomarker guide, 2nd ed. Cambridge University Press, Cambridge.

Peterson, B.J., Fry, B., 2011. Stable Isotopes in Ecosystem Studies. *Source: Annual Review of Ecology and Systematics* **18**, 293–320.

Price, R., Skrzypek, G., Grierson, P.F., Swart, P.K., Fourqurean, J.W., 2012. The use of stable isotopes of oxygen and hydrogen to identify water sources in two hypersaline estuaries with different hydrologic regimes. *Marine and Freshwater Research* **63**, 952–966.

Quandt, L., Gottschalk, G., Ziegler, H., Stichler, W., 1977. Isotope discrimination by photosynthetic bacteria. *FEMS Microbiology letters* 125–128.

Raiswell, R., Bottrell, S.H., Dean, S.P., Marshall, J.D., Carr, A., Hatfield, D., 2002. Isotopic constraints on growth conditions of multiphase calcite-pyrite-barite concretions in Carboniferous mudstones. *Sedimentology* **49**, 237–254.

Raiswell, R., Fisher, Q.J., 2000. Mudrock-hosted carbonate concretions: a review of growth mechanisms and their influence on chemical and isotopic composition. *Journal of the Geological Society* **157**, 239–251.

Reid, R.P., James, N.P., Macintyre, I.G., Dupraz, C.P., Burne, R. V, Macintyre, G., 2003. Shark Bay Stromatolites : Microfabrics and Reinterpretation of Origins. *Facies* **49**, 299–324.

Reitner, J., Peckmann, J., Blumenberg, M., Michaelis, W., Reimer, A., Thiel, V., 2005. Concretionary methane-seep carbonates and associated microbial communities in Black Sea sediments. *Palaeogeography, Palaeoclimatology, Palaeoecology* **227**, 18–30.

Reitner, J., Thiel, V., 2011. Encyclopedia of Geobiology. Springer, Gottingen.

Röhl, H., Schmid-Röhl, A., Oschmann, W., Frimmel, A., Schwark, L., 2001. The Posidonia Shale (Lower Toarcian) of SW-Germany : an oxygen-depleted ecosystem controlled by sea level and palaeoclimate. *Palaeogeography, Palaeoclimatology, Palaeoecology* **165**, 27–52.

Ruebsam, W., Münzberger, P., Schwark, L., 2014. Chronology of the Early Toarcian environmental crisis in the Lorraine Sub-Basin (NE Paris Basin). *Earth and Planetary Science Letters* **404**, 273–282.

Schidlowski, M., 1988. A 3,800-million-year isotopic record of life from carbon in sedimentary rocks. *Nature* **336**, 313–318.

Schmid-Röhl, A., Röhl, H., Oschmann, W., Frimmel, A., 2002. Palaeoenvironmental reconstruction of Lower Toarcian epicontinental black shales (Posidonia Shale , SW Germany): global versus regional control. *Geobios* **35**, 13–20.

Schouten, S., Bowman, J.P., Rijpstra, W.I.C., Sinninghe Damsté, J.S., 2000a. Sterols in a psychrophilic methanotroph, Methylosphaera hansonii. *FEMS Microbiology Letters* **186**, 193–195.

Schouten, S., Van Kaam-Peters, H.M.E., Rijpstra, W.I.C., Schoell, M., Sinninghe Damste, J.S., 2000b. Effects of an oceanic anoxic event on the stable carbon isotopic composition of early Toarcian carbon. *American Journal of Science* **300**, 1–22.

Schwark, L., Frimmel, A., 2004. Chemostratigraphy of the Posidonia Black Shale, SW-Germany II. Assessment of extent and persistence of photic-zone anoxia using aryl isoprenoid distibutions. *Chemical Geology* **206**, 231–248.

Schweitzer, M.H., Suo, Z., Avci, R., Asara, J.M., Allen, M.A., Teran Arce, F., Horner, J.R., 2007. Analyses of soft tissue from Tyrannosaurus rex suggest the presence of protein. *Science* **316**, 277–280.

Schweitzer, M.H., Wittmeyer, J., Horner, J.R., Toporski, J.K., 2005. Soft-tissue

vessels and cellular preservation in *Tyrannosaurus rex*. *Science* **307**, 1952–1955.

Seilacher, A., 2001. Concretion morphologies reflecting diagenetic and epigenetic pathways. *Sedimentary ge* **143**, 41–57.

Sellés-Martínez, J., 1996. Concretion morphology, classification and genesis. *Earth-Science Reviews* **41**, 177–210.

Sinninghe Damsté, J.P., Kenig, F., Koopmans, M.P., Koster, J., Schouten, S., Hayes, J.M., De Leuuw, J.W., 1995. Evidence for gammacerane as an indicator of water column stratification. *Geochimica et Cosmochimica Acta* **59**, 1895–1900.

Sinninghe Damsté, J.S., Keely, B.J., Betts, S.E., Baas, M., Maxwell, J.R., De Leeuw, J.W., 1993. Variations in abundances and distributions of isoprenoid chromans and long-chain aikylbenzenes in sediments of the Mulhouse Basin : a molecular sedimentary record of palaeosalinity *. *Organic Geochemistry* **20**, 1201–1215.

Smith, S. V., Atkinson, M.J., 1983. Mass balance of carbon and phosphorus in Shark Bay Western Australia. *Limnology and Oceanography* **28**, 625–639.

Southard, J., 2007. Sedimentary geology : Chapter 7 Diagenesis. *Massachusetts Institute of Technology: MIT OpenCourseWare*.

Suan, G., Mattioli, E., Pittet, B., Mailliot, S., Lécuyer, C., 2008. Evidence for major environmental perturbation prior to and during the Toarcian (Early Jurassic) oceanic anoxic event from the Lusitanian Basin, Portugal. *Paleoceanography* **23**, n/a-n/a.

Summons, R.E., Powell, T.G., 1986. Chlorobiaceae in Palaeozoic seas revealed by biological markers, isotopes and geology. *Nature* **319**, 763–765.

Svensen, H., Planke, S., Chevallier, L., Malthe-Sorenssen, A., Corfu, F., Jamtveit, B., 2007. Hydrothermal venting of greenhouse gases triggering Early Jurassic global warming. *Earth and Planetary Science Letters* **256**, 554–566.

Ten Haven, H.L., De Leeuw, J.W., Schenck, P.A., 1985. Organic geochemical studies of a Messinian evaporitic basin, northern Apennines (Italy) I: Hydrocarbon biological markers for a hypersaline environment. *Geochimica et Cosmochimica Acta* **49**, 2181–2191.

Ten Haven, H.L., de Leew, J.W., Sinninghe Damsté, J.S., Schenck, P., Palmer, S.E., Zumberge, J.E., 1988. Application of biological markers in the recognition of palaeohypersaline environments. *Geological Society, London, Special Publications* **40**, 123–130.

Thiel, V., Heim, C., Arp, G., Hahmann, U., Sjövall, P., Lausmaa, J., 2007. Biomarkers at the microscopic range: ToF-SIMS molecular imaging of Archaea-derived lipids in a microbial mat. *Geobiology* **5**, 413–421.

Tissot, B.P., Welte, D.H., 1984. Petroleum Formation and Occurrence, 2nd ed. Springer-Verlag, Berlin Heidelberg New York Tokyo.

Van Gemerden, H., 1993. Microbial mats: A joint venture. *Marine Geology* **113**, 3–25.

Volkman, J.K., 2003. Sterols in microorganisms. *Applied microbiology and biotechnology* **60**, 495–506.

Volkman, J.K., 2005. Sterols and other triterpenoids: Source specificity and evolution of biosynthetic pathways. *Organic Geochemistry* **36**, 139–159.

Whiteside, J.H., Grice, K., 2016. Biomarker Records Associated with Mass Extinction Events. *Annual Review of Earth and Planetary Sciences* **44**, 581–612.

Wignall, P.B., Newton, R.J., Little, C.T.S., 2005. Cause-and-effect relationships during the Early Jurassic mass extinction in Europe. *American Journal of Science* **305**, 1014–1032.

Williams, M., Benton, M.J., Ross, A., 2015. The Strawberry Bank Lagerstätte reveals insights into Early Jurassic life. *Journal of the Geological Society* 2014–144.

Wilson, D.D., Brett, C.E., 2013. Concretions as sources of exceptional preservation,

and decay as a source of concretions: examples from the middle Devonian of New York. *Palaios* **28**, 305–316.

Winter, B.L., Knauth, L.P., 1992. Stable isotope geochemistry of early Protezozoic carbonate concretions in the Animikie group of the Lake Superior region: evidence for anaerobic bacterial processes. *Precambrian Research* **54**, 131–151.

Yoshida, H., Ujihara, A., Minami, M., Asahara, Y., Katsuta, N., Yamamoto, K., Sirono, S., Maruyama, I., Nishimoto, S., 2015. Early post-mortem formation of carbonate concretions around tusk-shells over week-month timescales. *Scientific reports* 1–7.

Zatoń, M., Marynowski, L., 2004. Konzentrat-Lagerstätte-type carbonate concretions from the uppermost Bajocian (Middle Jurassic) of the Czêstochowa area , South-Cental Poland. *Geological Quarterly* **48**, 339–350.

Zhang, J., Quay, P.D., Wilbur, D.O., 1995. Carbon isotope fractionation during gas-water exchange and dissolution of CO_2. *Geochimica et Cosmochimica Acta* **59**, 107–114.

Appendix 1

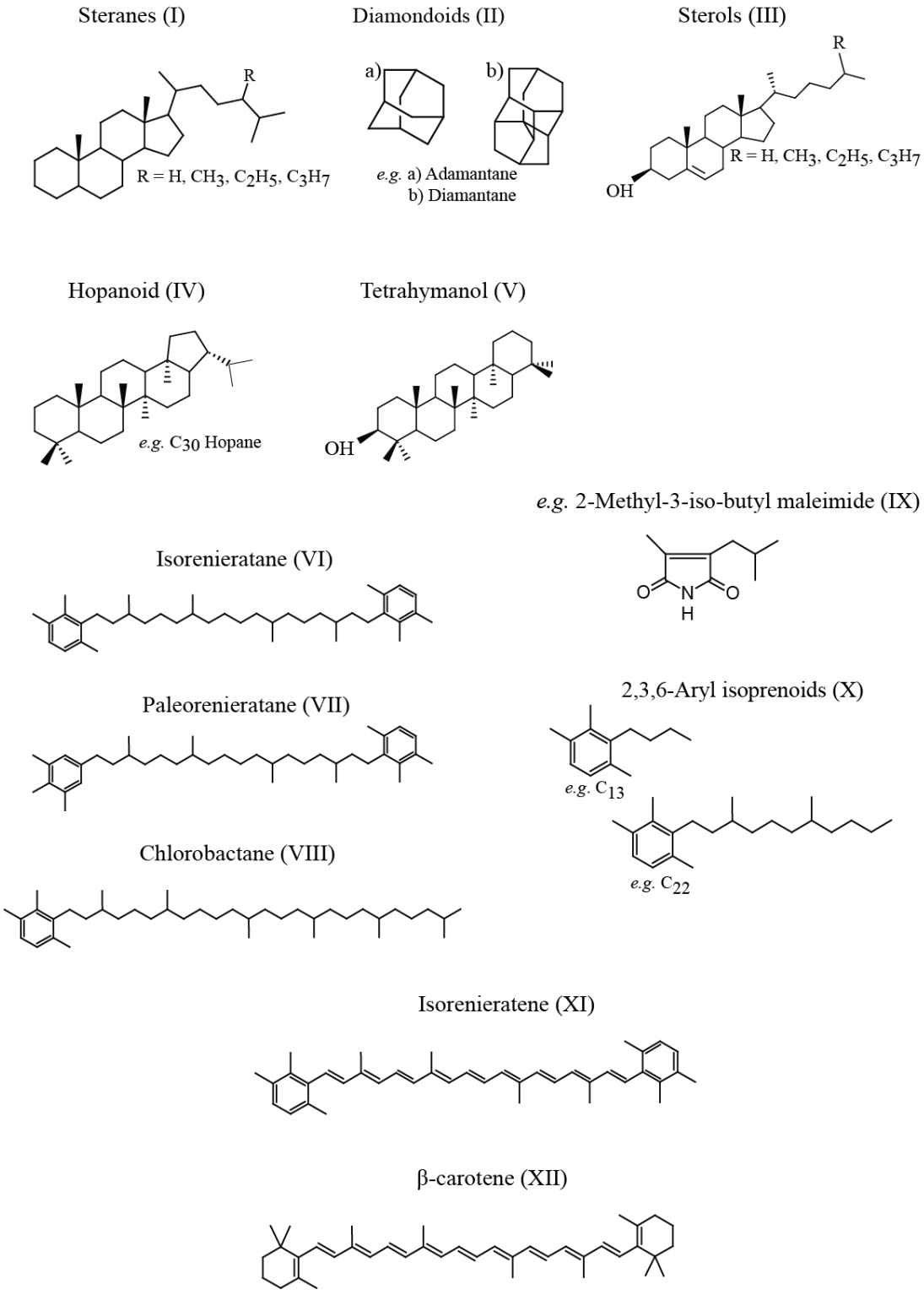

Figure A1-1. Structures referred to in the text.

Chapter 2

Microbially-mediated fossil-bearing carbonate concretions and their significance for palaeoenvironmental reconstructions: a multi-proxy organic and inorganic geochemical appraisal

Chloé Plet, Kliti Grice, Anais Pagès, Wolfgang Ruebsam, Marco J.L. Coolen, Lorenz Schwark

Chemical geology, 426, 95-108 (2016)

(Impact factor 3.524)

Abstract

Carbonate concretions are widespread within the geological record. However, the lack of recent known analogues creates a need for novel approaches to unravel the major microbial players involved in concretion formation and establish their suitability as palaeoenvironmental recorders. Here, we used a combination of geochemical and geological techniques to study two pyritiferous calcite concretions and compared the results with their host sediment (Toarcian "Posidonia Shale", 183 Ma, SW-Germany).

The ^{13}C-depleted nature of the concretion bodies, with average values of $\delta^{13}C_{carb}$ (–14.8 ‰), $\delta^{13}C_{org}$ (–32.4 ‰), and $\delta^{13}C$ *n*-alkanes (–34.9 ‰), indicates that sulfate-reducing bacteria (SRB) played a major role in the concretion growth and preservation of the nucleus *via* the rapid decomposition of organic matter (OM). However, Rock-Eval analyses from both concretions revealed elevated hydrogen indices (HI) in the body and low HI values at the rim. These values suggest that most of the microbial activity did not occur in the concretion body but rather at the rim and at the surface of the nuclei, which generally supports the exceptional preservation of OM in carbonate concretions. Furthermore, enrichment in euhedral pyrite in the concretion rims suggests they were formed through increased activities of iron reducing (FeR) bacteria coupled to a decrease of SRB activity leading towards conditions more favourable to the direct precipitation of pyrite. Despite low $\delta^{13}C$ values, the known lipid biomarkers such as acyclic extended isoprenoids or 3β-methyl-hopanes did not reveal evidence of an active methane cycling. The present study emphasises the crucial role of carbonate concretion in OM preservation and highlights their great potential as palaeoenvironmental recorders.

Keywords: Toarcian; Palaeoenvironment; Sulfate reducing bacteria (SRB); Iron reducing bacteria (FeR); $\delta^{13}C$; Lipid biomarkers

Introduction

Subsurface microbial communities decompose organic matter (OM) and trigger carbonate concretion formation in marine and lacustrine environments (Dale *et al.*, 2014; Das and Tripathi, 2009; Marshall and Pirrie, 2013; Martill, 1988, 1989; Raiswell and Fisher, 2000). Carbonate concretions are ubiquitous in the geological record, and often associated with petroleum source rocks (Kiriakoulakis *et al.*, 2000; Lash and Blood, 2004; Zatoń and Marynowski, 2004). They often encapsulate exceptionally well-preserved fossils of different ages and origins (Arua, 1991; Geraghty and Westermann, 1994; Martill, 1989; Wilson and Brett, 2013). Moreover, carbonate concretions can also contain exceptionally well-preserved molecular fossils (Kiriakoulakis *et al.*, 2000; Marynowski *et al.*, 2007a, 2007b; Melendez *et al.*, 2013b, 2013b; Pearson and Nelson, 2005; Zatoń and Marynowski, 2004).

Contemporary analogues are rare and, over the last few decades, several studies have attempted to unravel details about when, where and how carbonate concretions were formed by analysing their mineral and inorganic geochemical composition (Coleman, 1993; Coleman and Raiswell, 1995; Curtis *et al.*, 1987; Marshall and Pirrie, 2013; Woo and Khim, 2006). Field observations of *in-situ* carbonate concretions, as well as macroscopic observations of internal structures, assisted in characterising the environment of formation. Most calcium carbonate concretions are suggested to form at a very early stage of diagenesis, within the top metres of sediment accumulation (Marshall and Pirrie, 2013; Raiswell and White, 1978; Seilacher, 2001; Sellés-Martínez, 1996). Furthermore, the presence of intact three-dimensional fossils and “card house” clay fabric in many calcium carbonate concretions is concordant with their early formation and highlights the ability of carbonate concretions to resist compaction (Das and Tripathi, 2009; Geraghty and Westermann, 1994; Lash and Blood, 2004; Martill, 1988; Zatoń and Marynowski, 2004).

The association of carbonate concretions with OM-rich pelitic shales reveals a formation under anoxic environmental conditions. In such conditions, OM decays at the sediment/water interface and is controlled by anaerobic micro-organisms. Berner (1968) and Allison (1988b) established that microbial OM degradation was

responsible for local changes in porewater chemistry. These changes can lead to the formation of a Ca-rich adipocere film playing a pivotal role in the formation of carbonate concretions. Sulphate reducing bacteria (SRB) obtain energy by oxidising organic compounds while reducing sulphate (SO_4^{2-}) to hydrogen sulfide (H_2S) (**Equation 2-1**). They are believed to play major role in the formation of calcium carbonate concretions (Coleman, 1993; Coleman and Raiswell, 1980, 1995; Kiriakoulakis *et al.*, 2000; Melendez *et al.*, 2013a, 2013b) based on the following general reaction:

$$2CH_2O + SO_4^{2-} \longrightarrow 2HCO_3^- + H_2S$$

Equation 2-1. Sulfate reduction

The role of an active cycling of methane *via* the involvement, in the microbial consortium, of methanogenic archaea, anoxic methane oxidizers (**Equation 2-2**) is still poorly understood (Coleman, 1993; Coleman and Raiswell, 1995; Curtis *et al.*, 1987; Kiriakoulakis *et al.*, 2000; Woo and Khim, 2006). Such a consortium has been found in anoxic marine environments, notably gas hydrates (Boetius *et al.*, 2000; Hinrichs and Boetius, 2002), but is yet to be associated with concretions.

$$CH_4 + SO_4^{2-} \longrightarrow HCO_3^- + H_2S + HO^-$$

Equation 2-2. Anaerobic oxidation of methane

Most studies of carbonate concretions have relied on inorganic geochemistry and petrological observations. However, relatively little attention was given to organic geochemical parameters to better understand concretion growth processes (Kiriakoulakis *et al.*, 2000; Melendez *et al.*, 2013a; Pearson and Nelson, 2005; Wolff *et al.*, 1991; Zatoń and Marynowski, 2004; Zatoń *et al.*, 2011) or to establish a thorough comparison with their host rock (Marynowski *et al.*, 2007a, 2007b; Melendez *et al.*, 2013a).

The limited occurrence of known modern analogues for carbonate concretions (Reitner *et al.*, 2005) complicates the use of DNA in the identification of microbial communities. However, work on modern microbialites supports a more

complex ecosystem than originally expected (Burns *et al.*, 2009; Edgcomb *et al.*, 2014; Pagès *et al.*, 2014a, 2014b).

In order to obtain further insights into the complex ecosystems involved in subsurface diagenetic environments, multidisciplinary techniques need to be applied. Here we report the first integrative approach, using geological, organic and inorganic geochemistry, to gain a better understanding of concretion growth processes and identify the microbial communities involved in the formation of two carbonate concretions. Furthermore, a systematic comparison of the concretions with their surrounding shale was undertaken to identify geochemical variations between the concretion and the host sediment showing the concretions' potential to be used as a palaeoenvironmental recorder.

More specifically, we aim to i) characterise the timing of formation of the two concretions; ii) identify marker and footprints of microbial activity, iii) establish their significance for palaeoenvironmental reconstruction and iv) investigate the preservation properties of carbonate concretion using bulk OM proxies.

Palaeoenvironmental settings

During the Jurassic, Europe was located on a broad and shallow continental shelf that deepened towards the South-East of the Tethys Ocean (Frimmel *et al.*, 2004; Jenkyns, 2010; Röhl *et al.*, 2001; Ziegler, 2005). The shallow shelf featured several deeper sub-basins within which episodically restricted water circulation at relatively low sea level occurred (Röhl *et al.*, 2001; Schmid-Röhl *et al.*, 2002; Schwark and Frimmel, 2004). Moreover, global warming and methane release related to astronomical cycles (Cohen *et al.*, 2004; Hesselbo *et al.*, 2000; Kemp *et al.*, 2005; Ruebsam *et al.*, 2014) as well as tectonic activity (break-up of the Pangea) led to a major marine transgression during the Early Jurassic. These profound palaeoenvironmental changes led to widespread deposition of OM-rich sediments (Baudin *et al.*, 1990b).

A detailed description of the Palaeogeographical and palaeoclimatic settings associated with the deposition of the Posidonia Shale of SW-Germany during the Lower Toarcian is presented elsewhere (Cohen *et al.*, 2004; Röhl *et al.*, 2001;

Ruebsam *et al.*, 2014; Schmid-Röhl *et al.*, 2002). Here, we provide a short overview of the palaeoenvironment during the deposition of the studied section. The Posidonia Shale of SW-Germany was deposited in the SW-German Basin, a deep sub-basin of the epicontinental basin system of the Western Tethyan Shelf (Ziegler, 2005). The sediment accumulation was mostly controlled by sea-level variations. Enhanced anoxia and subsequent deposition of the OM-rich black shale occurred during intermediate sea level whereas phases of sea level highstand led to increased oxygenation of the water through a better connection to the Tethys Sea (Frimmel *et al.*, 2004; Röhl *et al.*, 2001; Schmid-Röhl *et al.*, 2002). During the deposition of the lower *H. serpentinum* zone (**Figure 2-1**), a warm and humid, monsoonal driven climate (Röhl *et al.*, 2001) was prevalent in SW-Germany. Eutrophication of the epicontinental seas (Cohen *et al.*, 2004; Ruebsam *et al.*, 2014) took place and episodic photic zone euxinia (PZE) in the sub-basins has been previously reported (Berner *et al.*, 2013; Bour *et al.*, 2007; Jenkyns, 2010; Pancost *et al.*, 2004; Röhl *et al.*, 2001; Schouten *et al.*, 2000b; Schwark and Frimmel, 2004).

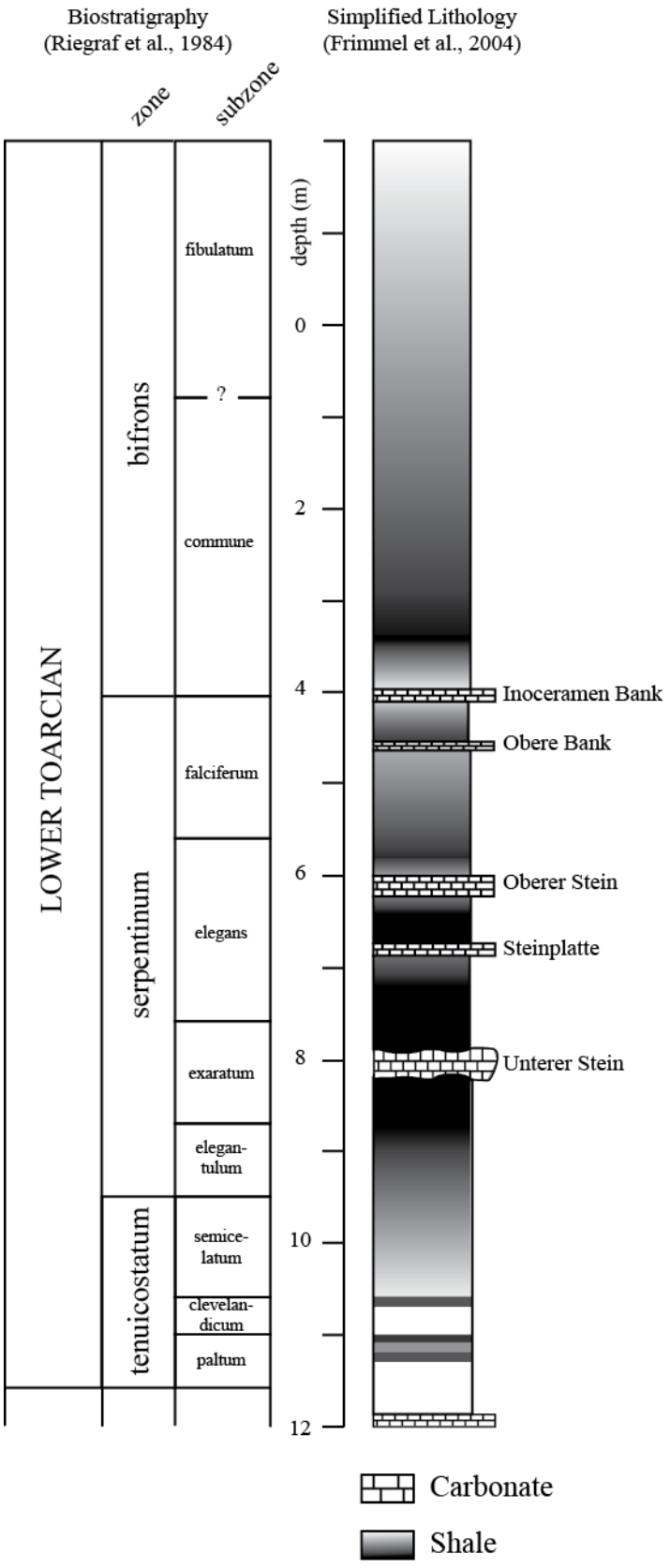

Figure 2-1. Stratigraphy of the Dotternhausen quarry, modified from Frimmel et al. (2004).

Material and methods

Study site

The concretions used for this study were collected from the Lower Toarcian Posidonia Shale Formation from the former Rohrbach now HOLCIM Cement quarry of Dotternhausen (SW-Germany) (**Figure 2-2**). Based on the comparison of microfacies, lithology and geochemical signatures with previous analyses of sediments from the same location (Frimmel *et al.*, 2004; Röhl *et al.*, 2001; Schwark and Frimmel, 2004); these concretions derive from directly above one of the major carbonate horizons (the "Unterer Stein"), within the lower *H. serpentinum* zone (Ruebsam *et al.*, 2014; Wignall *et al.*, 2005b) also known as *H. falciferum* zone (Frimmel *et al.*, 2004; Seilacher, 2001) although exact stratigraphic position could not be determined after blasting (**Figure 2-1**).

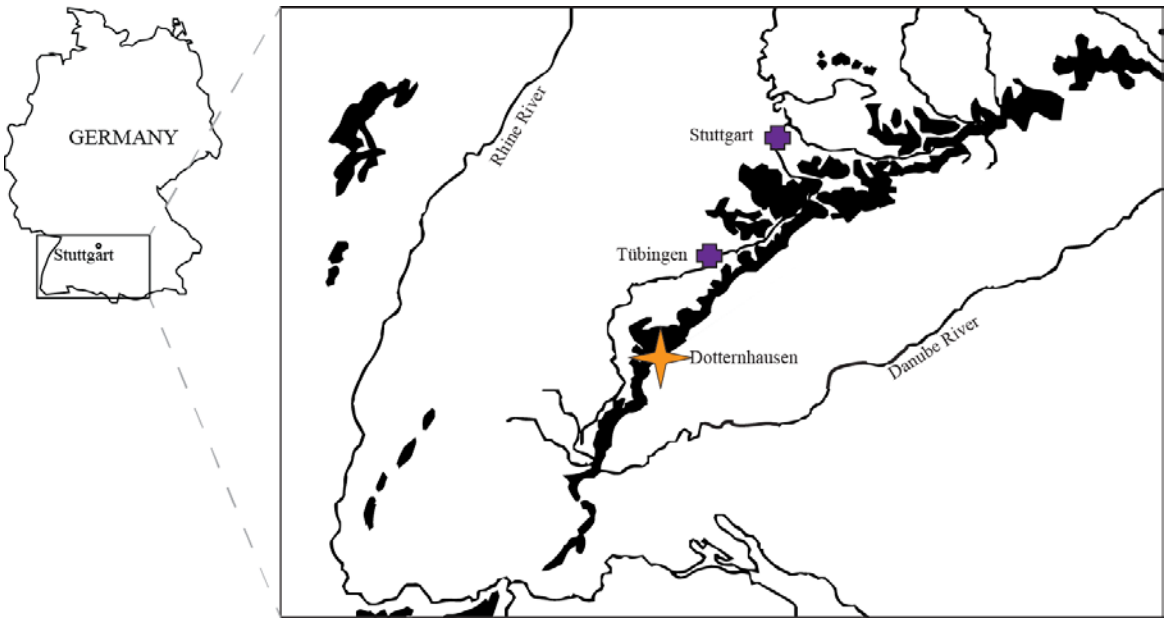

Figure 2-2. Map of SW-Germany, outcrop area of Lower Toarcian sediments (black), main cities (cross) and sampling location (yellow star). (For interpretation of the references to colour in this figure legend, the reader is referred to the online version of this article). Modified from Röhl et al. (2001).

Sample description and preparation

Two concretions (A and B) of ovoidal shape, with a longest diameter nearing the 40 cm, were selected. A slice was cut vertically through the centre of each concretion revealing a "jet" nucleus (**Figure 2-3A, B**) and the presence of sedimentary bedding (**Figure 2-3A, B, C**). Based on morphological features, the slices were further divided into three different zones referred to as i) nucleus (jet), ii) body and iii) rim (**Figure 2-3C**). Subsamples were taken radially from the concretion body to the rim. This mode of sampling was previously performed only in parallel to the bedding plane (Coleman and Raiswell, 1980; Raiswell, 1976, 1982). In this study, additional samples normal to bedding were also taken (**Figure 2-3D**) to perform a more thorough comparison. A further sample was collected from the host *H. serpentinum* zone shale for a detailed mineralogical and geochemical comparison with the two concretions. Sample blocks (5 cm^3) were sonicated three times in a mixture of dichloromethane: methanol (DCM: MeOH) at 9:1 (v:v) for 15 min to remove surficial organic contaminants. Each analysis corresponds to an average of the sampling area due to the size of each sample.

Most geochemical analyses were performed on samples from both concretions and the host sediment. A detailed description of which analysis techniques have been applied to each individual sample can be found in **Table 2-1**.

Samples for mineralogy and geochemical analyses were crushed manually and ground using a Zircon mill in a benchtop ring mill (Rocklabs) after the selection of areas for thin section preparation. Pre-annealed sand was subject to the same procedure and used as procedural blank for lipid biomarker analyses.

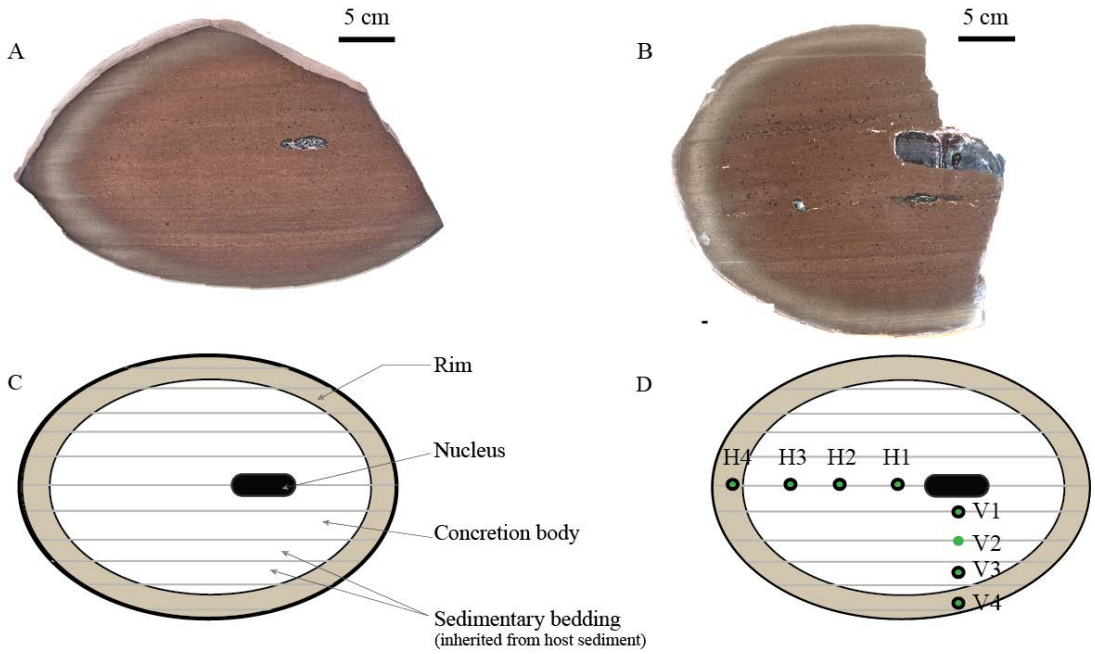

Figure 2-3. Macroscopic photo of the concretions investigated (A & B) and schematic illustration of their features (C). D displays the sampling scheme used in the text body with an additional prefix corresponding to the concretion (A & B). Concretion A was not sampled at location V2 (sample AV2)

X-ray diffraction (XRD)

Powdered XRD analyses were used to identify mineral species present in the samples. All concretion samples (**Table 2-1**) and the surrounding host-rock were measured using a Bruker-AXS D8 Advance Diffractometer with CuKα radiation and a LynxEye position sensitive detector. Data were collected from 7.5 to 90 °2Θ, with a nominal step size of 0.015 and a collection time of 0.7 s per step. Crystalline phases were identified using the Search/Match algorithm, DIFFRAC.EVA 3.1 (Bruker-AXS) to search the Powder Diffraction File.

Petrography and scanning electron microscopy (SEM)

Thin sections were studied using classical optical microscopy as well as SEM. Backscattered electron images were taken on carbon coated thin sections using a Zeiss Ultra-Plus FEG-SEM coupled with a Bruker X-Flash energy dispersive X-ray spectroscopy (EDS) detector for elemental analyses. An accelerating voltage of 20 kV in high current mode was used.

Whole rock geochemistry

Major and trace element whole rock analyses (2 g) were carried out by inductively coupled plasma mass spectrometry (ICP-MS) at ACTLABS, Ancaster, Canada. The samples were prepared following the standard procedures outlined in the protocol Ultratrace-7 (see Actlabs.com). In short, samples were fused using sodium peroxide, diluted and analysed. Blanks were fused and run in triplicates every 22 samples.

Carbonate stable isotopes

Carbon isotopic values were measured on ground samples using a Kiel III carbonate preparation line connected to a Thermo Fisher 252 isotope ratio mass spectrometer. Powdered samples were treated with 100 % phosphoric acid at 70 °C. Values for carbon and oxygen of the carbonate were given in δ-values ($\delta^{13}C_{carb}$) and reported in permil (‰) relative to Vienna PeeDee Belemnite standard (VPDB). Reproducibility of the analyses was estimated by duplicate analyses which all had standard deviations of < 0.1 ‰.

Bulk organic geochemistry

Decalcification of ground samples was achieved by using HCl (6 M) to remove calcium carbonate. Aliquots of dried residues (50 °C, 72 hr) were subject to standard organic geochemical analysis: a ROCK-EVAL II PLUS analyser (Vinci technologies) was used to determine the hydrogen index (HI); a Vario CNS-Elemental Analyser (Elementar®) was employed to estimate the total carbon content of the decarbonated samples (TOC_{cf}). The carbonate content was estimated based on the weight loss related to carbonate dissolution by HCl. Bulk organic geochemical analyses were run in duplicate or triplicate when possible and standards were run every 10 samples.

Table 2-1. Overview of the methods applied to the different samples taken from both concretions and from the Posidonia Shale (abbreviations and units are defined in section Material and Methods- Whole rock geochemistry).

	Sample	XRD	Thin sections		ICP-MS	$\delta^{13}C_{carb}$	Bulk $\delta^{13}C$ OM	Rock-Eval	Elemental analysis	GC–MS	GC–irMS	GC–MRM
			Optic	SEM-EDS								
concretion A	AH1	✓	✓	✓	✓	✓	✓	✓	✓	✓	✓	
	AH2	✓			✓	✓	✓	✓	✓	✓		
	AH3	✓			✓	✓	✓	✓	✓	✓		
	AH4	✓			✓	✓	✓	✓	✓	✓	✓	
	AV1	✓			✓	✓	✓	✓	✓	✓	✓	
	AV3	✓			✓	✓	✓	✓	✓	✓		
	AV4	✓			✓	✓	✓	✓	✓	✓	✓	
concretion B	BH1	✓	✓	✓	✓	✓	✓	✓	✓	✓	✓	✓
	BH2	✓			✓	✓	✓	✓	✓	✓		✓
	BH3	✓	✓	✓	✓	✓	✓	✓	✓	✓		✓
	BH4	✓	✓	✓	✓	✓	✓	✓	✓	✓	✓	✓
	BV1	✓			✓	✓	✓	✓	✓	✓	✓	✓
	BV2	✓			✓	✓	✓	✓	✓	✓		✓
	BV3	✓			✓	✓	✓	✓	✓	✓		✓
	BV4	✓			✓	✓	✓	✓	✓	✓		✓
Posidonia Shale	SS	✓			✓	✓	✓	✓	✓	✓		

Lipid biomarker geochemistry

Ground samples and a procedural blank were Soxhlet extracted with a mixture of (DCM: MeOH) at 9: 1 (v/v) for 72 h. Activated copper turnings were added to remove elemental sulfur. The total lipid extract (TLE) was adsorbed onto activated silica gel (at 160 C for at least 24 h). Column chromatography was performed on a large column (20 cm × 0.9 cm i.d.) filled with activated silica gel (150 °C overnight). The aliphatic fraction was eluted using 35 mL *n*-hexane, the aromatic fraction eluted using DCM in *n*-hexane (40 mL, 30 %) and the polar fraction was eluted using a mixture of DCM: MeOH (1:1).

Analyses by Gas Chromatography–Mass Spectrometry (GC–MS)

GC–MS analyses of the aliphatic and aromatic fractions were performed using a Hewlett Packard 6890 gas chromatograph (GC) with an on-column injector. The GC was fitted with a 60 m × 0.25 mm i.d. WCOT fused silica capillary column coated with a 0.25 μm film (DB-5MS, J&W Scientific). The oven was programmed at an injection temperature of 40 °C with an initial hold time of 1 min. Temperature was increased at a rate of 3 °C/min to 330 °C and kept isothermal for 35 min. Ultra-high purity helium was used as a carrier gas and maintained at a constant flow of 1.1 mL/min. An Agilent 5973 mass selective detector (MSD), interfaced with the GC, was operated at 70 eV and a source temperature of 230 °C with mass spectra acquired in full scan mode from 30 to 580 Da at about 4 scans per second.

GC–MS-MS

To determine the presence and type of methyl-hopanes, aliphatic fractions of concretion B samples were analysed on Agilent 6890 coupled to Chromtech Evolution GC – MS/MS operated in multiple reaction monitoring (MRM) mode. The GC was fitted with a 30 m DB-1 column with an internal diameter of 0.25 mm, and a film thickness of 0.25 mm (Agilent J&W); high purity Helium was used as a carrier gas at a flow of 1.1 mL/min. The oven was programmed from 180 °C to 320 °C at a rate of 2.0 °C/min. The ion source was operated at 70 eV, and 150 °C, the analyser at 230 °C. Identification of methyl-hopanes was achieved by monitoring the precursor product reactions of 440 to 205 Da, 454 to 205 Da, 468 to 205 Da and 482 to 205 Da. Data were processed using the Evolution Evo-driver software.

5 A molecular sieving

Molecular sieving and subsequent analyses were performed on the aliphatic fractions of the surrounding shale sample and representative samples of each concretion (samples AH1, AH4, AV1, AV4 and samples BH1, BH4 and BV1). Aliphatic fractions were diluted in cyclohexane (2 mL) and then transferred to a 2 mL reaction vial partially filled (3/4) with 5 A molecular sieves. Capped vials were placed in the oven at 80 °C overnight. The sieves were rinsed in a Pasteur pipette with cyclohexane (approximately 4 mL) yielding the branched/cyclic fractions. Sieves with *n*-alkanes were dried and transferred into Teflon tubes that were placed in an ice bath. *N*-hexane was added to cover the mixture, along with 20 –30 drops of hydrofluoric acid (HF). A clean Teflon covered magnetic stirrer was added to each tube until the sieves had dissolved (60 min). HF was neutralised using a saturated sodium bicarbonate solution. The *n*-hexane layer was collected and filtered through a small column (0.5 × 2 cm) containing magnesium sulfate ($MgSO_4$) to remove water and the isolated pure *n*-alkane fraction was collected.

Gas Chromatography-Isotope Ratio Mass Spectrometry (GC–irMS)

GC–irMS analyses were performed on a Thermo Scientific Trace GC Ultra interfaced to a Thermo Scientific Delta V Advantage mass spectrometer *via* a GC isolink and a Conflow IV. The reactors consisted of a combustion interface (ceramic tube lined with NiO and filled with NiO and CuO) which was held at 1000 °C for $\delta^{13}C$ analyses. GC column, carrier gas, injector conditions and oven temperature programmes were identical to the settings for GC–MS analyses. The $\delta^{13}C$ values of the compounds were determined by integrating the ion currents of masses 44, 45 and 46, and are reported in permil (‰) relative to the VPDB standard. Reported values are the average of at least two analyses with standard deviation of < 0.6 ‰. Standard solutions containing compounds with known isotopic compositions were run in duplicate every third samples to confirm accuracy of the measurements.

Results

Mineral composition and microscopic observations

XRD analyses revealed that the mineral phases present were identical for both concretions: a concretion body consisting of calcite only (**Figure 2-4A**) and a rim dominated by calcite and pyrite with small contributions of quartz (**Figure 2-4B**). The mineralogy of the rim represents a transitory composition with characteristics related to the concretion (*i.e.* abundant calcite) and to the surrounding Posidonia Shale (*i.e.* abundant pyrite, quartz) (Berner *et al.*, 2013; Röhl *et al.*, 2001). Optical microscopy revealed that calcite is present as micritic groundmass in the concretions. However, the concretion body also contains abundant foraminifera that have been recrystallised into sparite and coccoids, which had recrystallised into microspar (**Figure 2-5A**), plus some bivalve remains (**Figure 2-5B**). SEM observations revealed the presence of small (300 µm), round and very homogenous calcium carbonate objects (**Figure 2-5E**) that likely represent the sparite-recrystallised foraminifera observed in optical microscopy. In the concretions, pyrite is dominantly located in the rims as shown by XRD analyses. However, optical microscopy and SEM showed the presence of pyrite encapsulating the OM-rich nucleus and separating it from the carbonate body of the concretion (**Figure 2-5C**). The body contains few euhedral pyrite crystals (5–10 µm), in some case closely related to framboidal pyrite (**Figure 2-5D**). The rim is characterised by euhedral pyrite crystals that combine into agglomerates that can reach 150 µm in size (**Figure 2-5F**) and remnants of quartz grains.

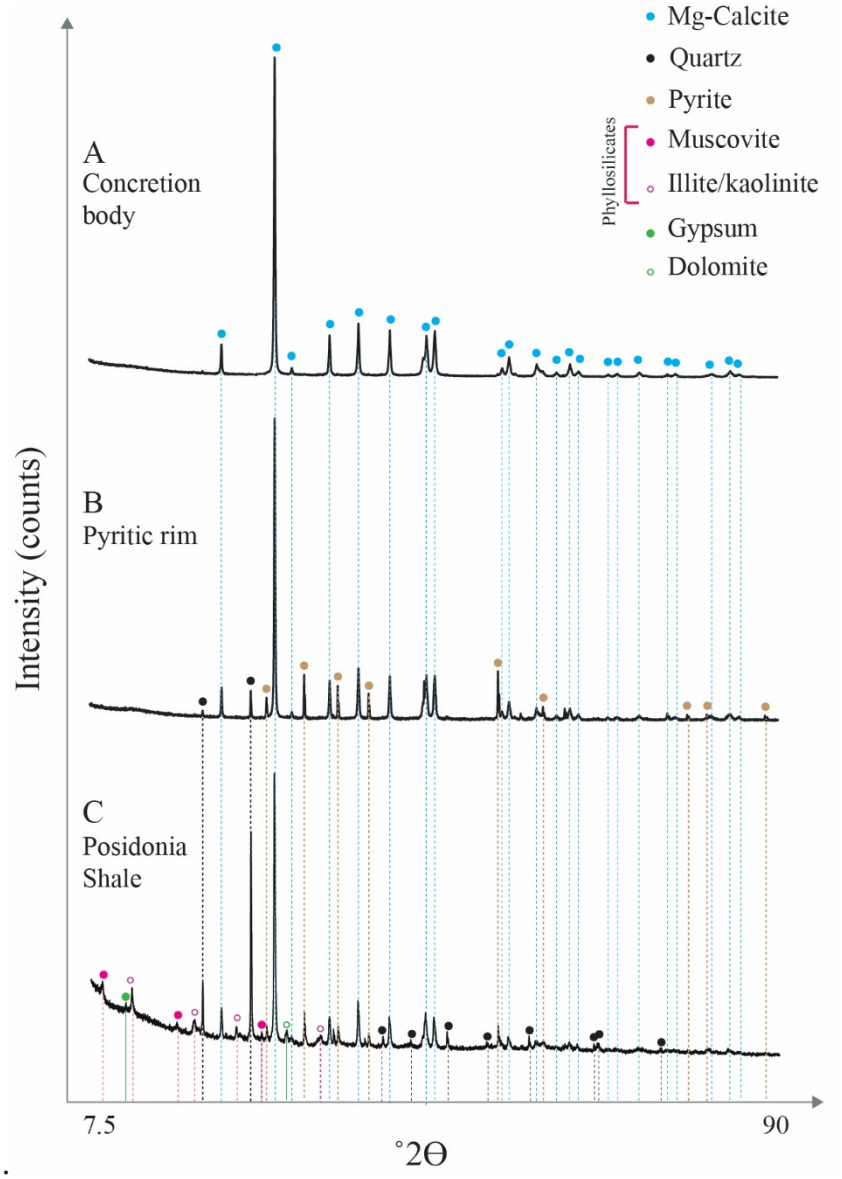

Figure 2-4. X-ray diffraction pattern for concretion A: body (A), rim (B) and surrounding Posidonia Shale (C). The mineral complexity is increasing from the body (AH1) to the rim (AH 4) and the host sediment. The Posidonia Shale contains some traces of detrital mineral (phyllosilicates) as well as dolomite and gypsum (likely a weathering by-product of pyrite). These minerals are not detected in the concretions, likely due to the calcite diluting the signal.

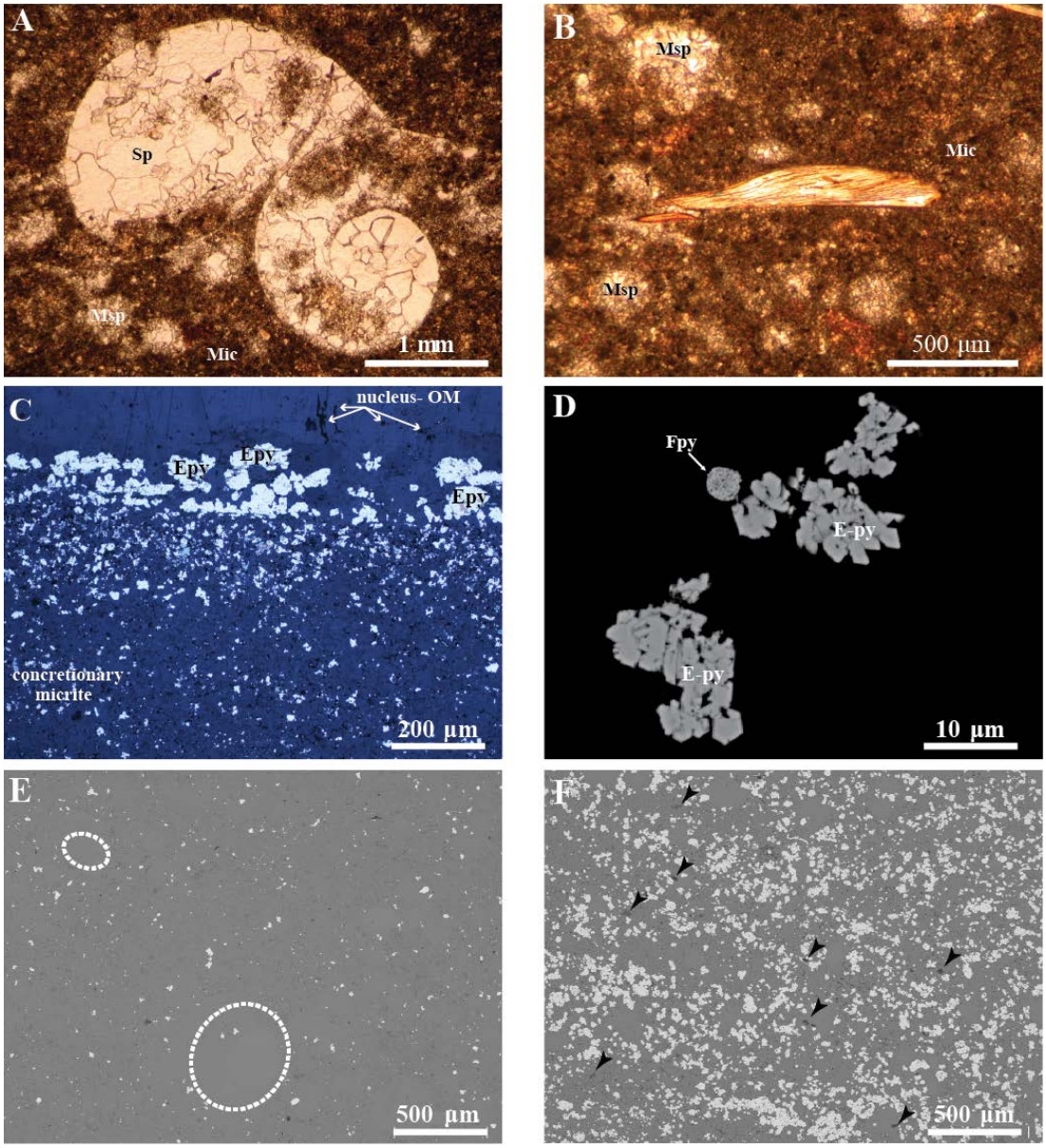

Figure 2-5. Optical and SEM imaging. A–B) optical microscopy transmitted light. A) Spar-recrystallised foraminifera (Sp) and microspar-recrystallised coccoids (Msp) in a micritic cement (Mic). B) Bivalve shell in micritic matrix. C) Optical microscopy reflected light, transition from the nucleus to the concretion body, presence of abundant and well developed pyrite microcrystals between the euhedral pyrite (Epy). D–E–F) Backscattered SEM imaging. D) Relation between two types of pyrite, Epy and framboidal pyrite (Fpy). E) Characteristic concretion body with small and sparse pyrite crystals. White-dashed-circled areas correspond to spar-recrystallised foraminifera. F) Characteristic features of the rim are the very abundant Epy (white) forming agglomerates as well as the presence of small quartz grains (arrows).

The Posidonia Shale shows a more complex mineralogy with a predominance of both calcite and quartz. It also contains abundant pyrite, described as framboidal by Berner *et al.* (2013) as well as minor amount of phyllosilicate minerals (*e.g.* muscovite and clays). Some dolomite is present and traces of gypsum are detected, likely a by-product of pyrite weathering (**Figure 2-4C**).

Major and redox sensitive element distributions

ICP-MS analyses reveal many common characteristics for both concretions, notably a very low content of most elements (often below detection limits) other than the major elements present in the formula of calcite and pyrite minerals (Ca, Fe, and S). The next most abundant element present is Mg which correlates strongly with the distribution of Ca ($r^2 > 0.9$). Other major elements (Al, K and Si), characteristic of detrital material, are present at low concentrations in the rim (**Table 2-2**) and often below detection limits in the concretion bodies. In both concretions, Fe and S show an increasing trend from the centre of the body towards the rim, associated with a decrease in Ca (detailed in **Table 2-2**). The increase in Fe and S occurs abruptly in concretion A; whereas in concretion B the increase is more progressive. The Fe/S ratios of ~ 0.5 show that in the concretion bodies, Fe and S are related to iron sulfides, presumably pyrite and an additional S-rich phase, *e.g.* elemental sulfur or aqueous FeS-clusters. However, the ratio increases in the pyrite-rich areas for both concretions (~ 0.8), suggesting that in the concretion body S is present dominantly as pyrite. Non-pyritic S is most likely present as elemental sulfur, but its occurrence in other mineral phases, below the detection threshold of XRD analyses, is also a possibility.

Table 2-2. Elemental composition from ICP-MS analyses of major and redox sensitive elements of interest and Fe/S ratio based on ICP-MS measurements.

	Al (%)	Ca (%)	Fe (%)	K (%)	Mg (%)	S (%)	Si (%)	Cu (ppm)	Mo (ppm)	Pb (ppm)	Sn (ppm)	Fe/S
AH1	0.34	39	0.25	< 0.1	1.22	0.47	0.97	6	2	< 0.8	0.7	0.5
AH2	0.35	37.8	0.26	0.1	1.11	0.45	0.97	4	2	< 0.8	< 0.5	0.6
AH3	0.33	36.7	0.34	0.1	0.97	0.57	0.97	18	19	1.8	15.6	0.5
AH4	0.69	29.4	8.61	0.2	0.61	10.5	2.41	11	19	0.8	1.4	0.8
AV1	0.36	37.7	0.43	0.1	1.01	0.67	1.01	4	< 1	< 0.8	< 0.5	0.6
AV2	0.33	37.4	0.41	0.1	0.99	0.67	1	8	2	< 0.8	< 0.5	0.6
AV3	0.36	31.2	6.14	0.1	0.71	7.65	1.02	4	14	< 0.8	< 0.5	0.8
BH1	0.29	35.9	0.62	< 0.1	1.09	1.49	0.88	14	3	< 0.8	< 0.5	0.4
BH2	0.31	39.2	0.28	0.1	1.19	0.66	0.93	< 2	< 1	< 0.8	< 0.5	0.4
BH3	0.34	35.2	2.76	< 0.1	0.95	3.63	0.95	16	6	3.1	2.5	0.8
BH4	0.74	27.2	10.2	0.2	0.54	12.5	3.18	5	22	1.8	< 0.5	0.8
BV1	0.3	36.7	0.35	< 0.1	1.14	0.68	0.84	13	2	3.9	< 0.5	0.5
BV2	0.37	37.7	0.42	0.1	1.12	0.75	1.06	3	< 1	< 0.8	< 0.5	0.6
BV3	0.38	34.6	2.35	< 0.1	0.9	3.06	1.06	< 2	5	< 0.8	1.9	0.8
BV4	0.8	25.6	9.99	0.2	0.52	12	2.51	7	18	5.2	< 0.5	0.8
Posidonia Shale	4.52	14.5	3.34	1.4	0.88	3.64	13	85	12	11.7	2.8	0.9

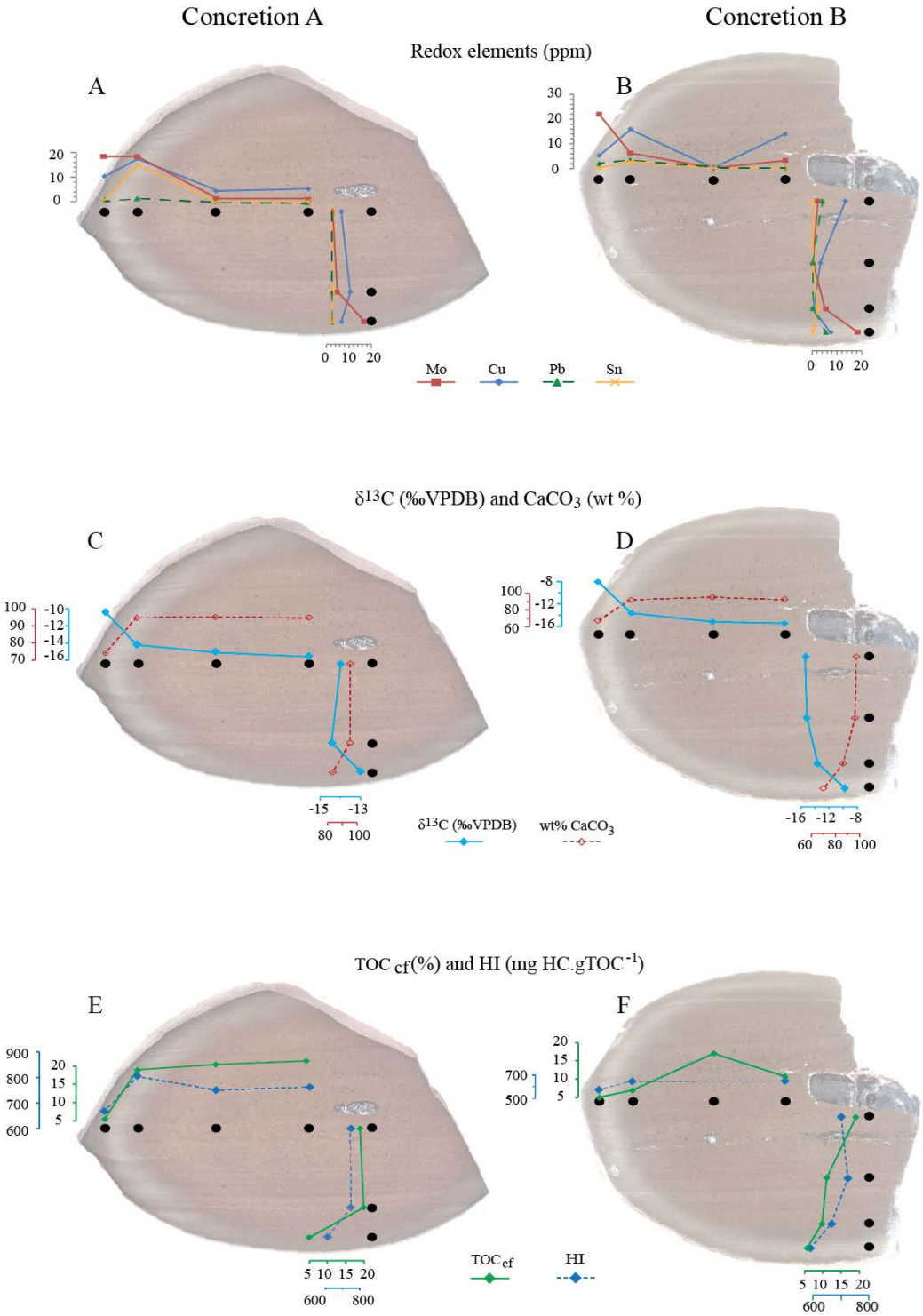

Figure 2-6. Evolution trends from the inner body to the rim for both concretions. A–B) Evolution of redox sensitive elements measured by ICP-MS showing similar overall trends for the concretions. C–D) $\delta^{13}C_{carbonates}$ and $CaCO_3$ content, showing a decrease in calcite coupled with an increase in $\delta^{13}C$ towards the rim. E-F) Bulk organic geochemical signal, obtained by Rock-Eval and CNS elemental analyses. HI and TOCcf both display decreasing trends towards the rim.

The distribution of redox sensitive elements (Cu, Mo, Pb and Sn) varies differently depending of the sampling direction (**Figure 2-6A, B**). Parallel to the bedding, a redox front is present before the rim (samples AH3, BH3) as shown by an increase in redox elements. In concretion A, this peak is followed by a decrease in association with the rim (AH4), while in concretion B, Mo increases (BH4). Normal to the bedding, Mo increases within the rims for both concretions. Different trends are otherwise observed between the concretions, which are probably influenced by the sedimentary bedding inherited from the host sediment.

In the host sediment, Ca and Si are the most abundant elements in accordance with abundant calcite and quartz minerals detected using XRD analyses. Fe and S are more abundant than in the concretion bodies but less abundant than in the rims. Fe and S distribution is related to the presence of abundant framboidal pyrite. Mg shows a slightly lower concentration than in the concretion bodies. All other elements are more abundant in the Posidonia Shale than in the concretions. Detailed data is presented in **Table 2-2**.

Carbonate composition and ^{13}C isotopes

Both concretions showed similar trends, displaying low $\delta^{13}C_{carb}$ associated with high carbonate proportion in the concretion body and enrichment in ^{13}C, coupled with a decrease in carbonate content in the rim. The details are presented in **Table 2-3** and outlined below. The inner samples of both concretions are rich in calcite (> 90 wt.%) with $\delta^{13}C_{carb}$ values of –14.6 ± 0.6 ‰ and –15.4 ± 0.3 ‰ for concretions A and B, respectively. Both concretion rims are characterised by a strong decrease in carbonate content, horizontally and vertically, down to 75 % and 65 % for concretions A and B, respectively. This decrease in carbonate is associated with an increase in $\delta^{13}C_{carb}$ values up to an average of –11.5 ‰ for concretion A (**Figure 2-6C**) and -8.9 ‰ for concretion B (**Figure 2-6D**). A difference between the two concretions is reflected by the gradual decrease in carbonate content and associated variation of $\delta^{13}C_{carb}$ values in concretion B outermost body samples (BH3 and BV3) whereas, in concretion A, such variations are abrupt and only associated with the rim.

Table 2-3. Bulk organic and inorganic parameters. TOC content and HI values, carbon isotopes of the kerogen and of the carbonates and proportion of carbonates within each sample.

	TOC_{cf} (wt %)	HI (mgHC/gTOC)	$\delta^{13}C_{org}$ (‰)	$\delta^{13}C_{carb}$ (‰)	$CaCO_3$ (wt %)
AH1	20.9	760	–32.4	–15.5	96
AH2	20.4	740	–32.5	–15.0	96
AH3	19	810	–32.5	–14.3	95
AH4	5.6	640	–32.2	–10.4	74
AV1	18.9	740	–32.5	–14.5	95
AV2	20	750	–32.4	–14.4	95
AV3	5.3	580	–32.1	–12.6	83
BH1	11.5	650	–32.2	–15.6	93
BH2	17.3	n/a	–32.5	–15.3	96
BH3	7.3	640	–32.5	–13.7	92
BH4	5	580	–32.3	–8.0	67
BV1	19.6	700	–32.7	–15.6	96
BV2	16.7	720	–32.5	–15.1	95
BV3	10.2	670	–32.5	–13.8	86
BV4	6.5	590	–32.2	–9.7	70
Posidonia Shale	15.6	820	–30.7	–1.8	40

By comparison, the Posidonia Shale sample has a carbonate content of 40 wt.% $CaCO_3$. The $\delta^{13}C_{carb}$ value of –1.8 ‰ is much enriched in ^{13}C compared to the concretions, and is within the values recorded in marine carbonates (from –2 ‰ to +3 ‰) (Tucker *et al.*, 1990).

Organic carbon content and preservation parameters

Both concretions show similar horizontal and vertical trends high TOC_{cf} and HI values in the concretion body decreasing towards the rim. Furthermore, $\delta^{13}C_{org}$ values are constant throughout both concretions with an average of $\delta^{13}C_{org} = -32.4 \pm 0.2$ ‰ (**Table 2-3**).

Concretion A shows constant TOC_{cf} values of ~ 20 wt.% in the body and an abrupt shift associated with the rim (TOC_{cf} = 5.2 wt.%). HI follows the same trend with high values associated with the concretion body (~ 760 mg HC/gTOC) and an

abrupt decrease within the rim (~ 610 mg HC/gTOC) (Fig. 6E). In concretion B, the TOC_{cf} and HI values of the body are lower (~ 14 wt% and ~ 670 mg HC/gTOC, respectively) than in concretion A. The outward decrease in TOC_{cf} and HI occurs gradually (**Figure 2-6F**) from the inner body to the rim where they reach 6 wt.% and 585 mg HC/gTOC, respectively (**Figure 2-6F**).

The TOC_{cf} content of Posidonia Shale (15.6 wt.%) was comparable to the one of the concretions, whereas HI (820 mg HC/gTOC) was higher. The Posidonia Shale showed a $\delta^{13}C_{org}$ value of –30.7 ‰, which is enriched in ^{13}C in comparison to both concretions.

Lipid biomarkers and their compound specific stable isotope signatures

Aliphatic hydrocarbons

Aliphatic hydrocarbon distributions were qualitatively similar for both concretions and the Posidonia Shale. Regular isoprenoids pristane (Pr) and phytane (Ph) predominated in all samples. The fraction is dominated by short and medium chain *n*-alkanes (*n*-C_{15}–*n*-C_{26}) and reaches a maximum at *n*-C_{17}. Long chain *n*-alkanes, as high as *n*-C_{37}, are also present in lower abundance (**Figure 2-7**). C_{27} and C_{29} ααα 20*R* are the most predominant steroids, while C_{28} and C_{30} ααα 20R are also relatively high in abundance throughout the concretions. In comparison, the ααα 20S isomers are low in abundance. In both concretions, C_{27}/C_{29} ratio is higher in the concretion body than in the rim. Biomarkers indicative of archaea *e.g.* squalene and crocetane were not detected in any of the concretions or in the host sediment. Hopanes range between C_{29} and C_{35} with the dominant analogues being C_{29} αβ and C_{30} αβ. C_{32} to C_{36} methyl-hopanes were detected in concretion B (**Figure 2-8**). 2α-methyl-hopanes are dominant in C_{32}, C_{34} and C_{36} methyl-hopanes traces. C_{33} and C_{35} traces are marked by a decline of 2α-methyl-hopanes, which enhances the relative 3β-methyl-hopanes proportion, despite 3β-methyl-hopanes remaining low in abundance (**Figure 2-8**).

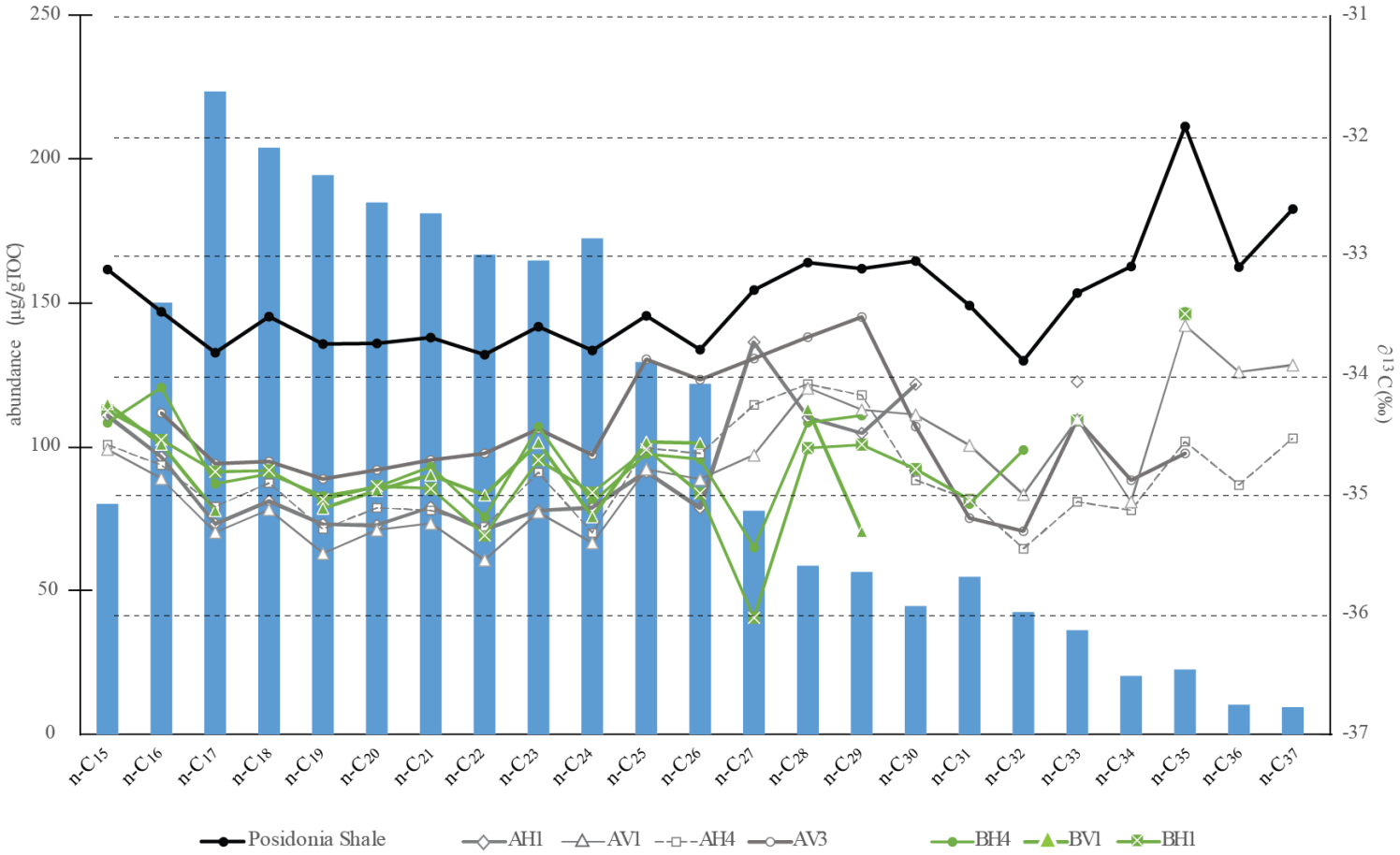

Figure 2-7. n-Alkanes abundance and stable carbon isotope compositions. Semi quantitative abundance of n-alkanes is representative of all samples. Stable isotopes analyses of carbon on n-alkanes were performed on the Posidonia Shale host sediment and on both concretions. Two samples from the concretion A body (AH1 and AV1), and two samples from the concretion A rim (AH4 and AV4) are shown in grey. Two samples from the concretion B body and one sample from the concretion B rim are represented in green. The higher $\delta^{13}C$ values noted for n-C_{35} in the host sediment are likely due to a minor co-elution with lycopane.

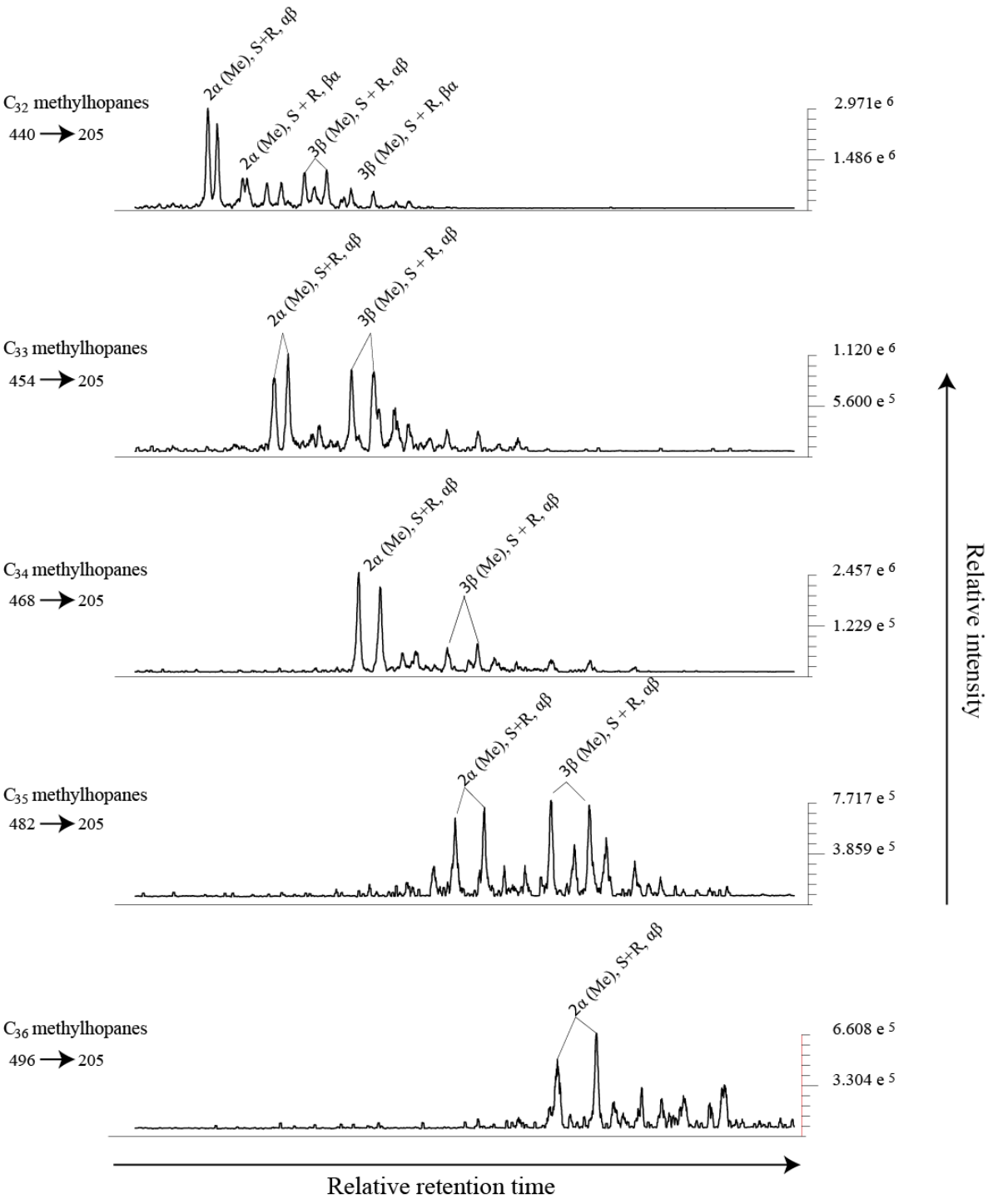

Figure 2-8. MRM chromatograms of the typical methyl-hopane distributions in concretion B. Me = methyl, S and R represent the stereochemistry at C_{22}.

Compound specific isotope analyses (CSIA) of the aliphatic fractions revealed overall similar trends for both concretions and the Posidonia Shale. Low molecular weight *n*-alkanes (LMW, ≤ *n*-C_{23}) show homogenous isotopic composition while high molecular weight *n*-alkanes (HMW, ≥ *n*-C_{24}) vary more (**Figure 2-7**). The concretions are ^{13}C-depleted, with an average $\delta^{13}C$ of –34.7 ± 0.5 ‰, compared to the Posidonia Shale ($\delta^{13}C$ = –33.4 ± 0.5 ‰). Odd HMW *n*-alkanes C_{33}, C_{35} and C_{37} are consistently more ^{13}C-enriched than their even counterpart a feature inverse to that known from plant waxes (Zhou *et al.*, 2010).

Aryl isoprenoids

Aryl isoprenoids (AI) were studied extracting the *m*/*z* 133 ion. A series of AI ranging from C_{13} to C_{23}, showing the 2,3,6-trimethylation pattern, as well as isorenieratane, were present in the Posidonia Shale. All concretion samples also contained AI and traces of isorenieratane at lower peak intensities. Both AI and isorenieratane signals were greater within the rim than in the concretion body. AI ratio (AIR), as defined by Schwark and Frimmel (2004), is plotted against the Pr/Ph ratio for all samples (**Figure 2-9**) highlighting differences between concretions A and B and the Posidonia Shale. Concretion B signal is more closely related to the Posidonia Shale and used as a reference sample in this study.

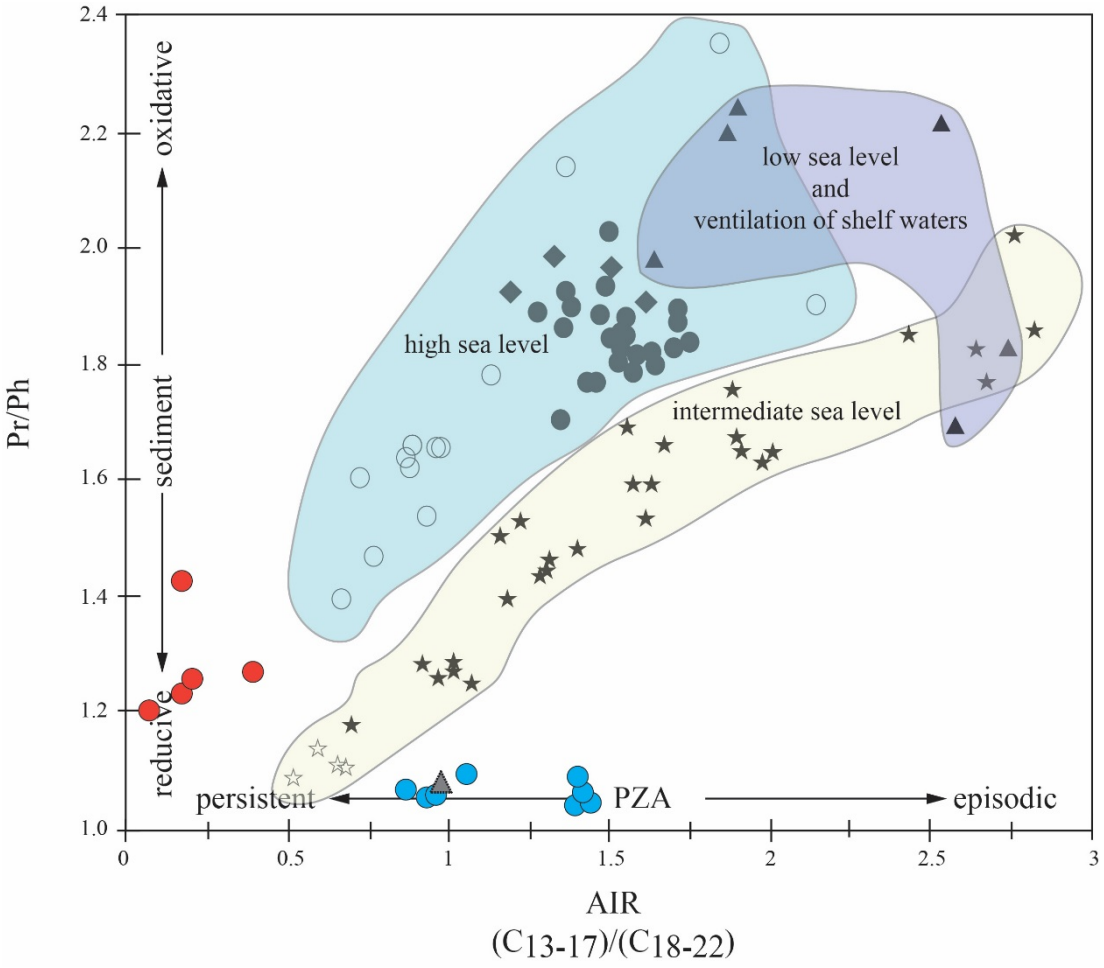

Figure 2-9. Modified From Schwark and Frimmel (2004). Crossplot of the molecular redox indicator pristane/phytane (Pr/Ph) against the aryl isoprenoid ratio (AIR). Black and white values were measured by Schwark and Frimmel (2004), red correspond to concretion A and blue reflect concretion B. The Posidonia Shale used as a reference is plotted as grey and shows stronger similarities with concretion B body.

Early diagenetic concretion formation

The most reliable indicator for early diagenetic concretion formation (*i.e.* early in the sediment evolution and consequently at shallow burial) is the three dimensional preservation of fossils within the concretion (Marshall and Pirrie, 2013; Raiswell and Fisher, 2000). This fossil played the role of concretion nucleus and triggered the concretion formation. Here, the preservation of the jet nuclei strongly suggests an early diagenetic concretion growth at shallow depth. Furthermore, the ovoidal shape of the concretions as well as the preservation of the sedimentary bedding, which showed no bending around the nucleus (**Figure 2-3**), support the general notion that concretions were formed at a shallow depth within a water-

saturated, uncompacted sediment (Marshall and Pirrie, 2013; Seilacher, 2001; Sellés-Martínez, 1996).

Microenvironmental changes related to microbial activity

Due to the absence of present/recent analogues for concretion formation, different approaches were used to identify the microorganisms involved in their formation. Coleman and Raiswell (1995) used inorganic geochemical proxies to propose a dynamic model for the formation of carbonate concretions that present a pyritic rim. The carbonate concretions that were investigated did not present any OM-rich nucleus. Their findings suggest that intense SRB activity at a centre of OM decay led to abundant production of H_2S. This resulted in an excess of H_2S relative to the Fe^{2+} available *in-situ* (supplied by siliciclastic minerals or their coatings present in the host sediment). This excess of H_2S coupled to the limited supply of Fe^{2+} led to the direct precipitation of euhedral pyrite crystals around pyrite framboids and the outward diffusion of excess H_2S. This process continued until the diminution of H_2S available matched the inward diffusion of Fe^{2+} from the sediment and led to the precipitation of abundant euhedral pyrite, defining the pyritic rim of the concretion.

In the present study, OM-rich (jet) nuclei are preserved. The decay of such OM-rich nuclei was likely the triggering factor for the concretion growth. An intense SRB activity took place around the jet nuclei, leading to the precipitation, from porewater, of abundant pyrite microcrystals at the boundary between the nucleus and the carbonate (**Figure 2-5C**). This OM decay and microbial activity resulted in complex microscale variations in the porewater microenvironment. Variations in pH and redox state are likely to occur in marine anoxic environments. Bacterial sulphate reduction (**Equation 2-1)**, methanogenesis /methanotrophy (**Equation 2-2**) and the precipitation of pyrite are as many mechanisms that can affect the redox environment of the porewater (Coleman and Raiswell, 1995). Moreover, the nature of the decaying OM (animal vs. plant) could play a significant role in the porewater chemistry and reactions involved in the formation of carbonate concretions. These changes are typically recorded by the distribution of redox sensitive elements, as shown in **Figure 2-6A, B**. These redox conditions are complex and are not discussed further in this study. A major by-product of these complex porewater chemical variations is the precipitation of minerals (calcite and pyrite), as observed herein.

In addition, the isotopic discrepancy in $\delta^{13}C_{carb}$ between the Posidonia Shale and the concretion reflect important isotopic fractionation during the formation of the carbonate concretions, and a different HCO_3^- source for the precipitation of calcite than the typical marine carbonate. This implies that the concretion formed pervasively, in relation to very intense microbial activity around the nucleus. Microbial consortia, likely dominated by SRB, decomposed the OM of the nuclei and produced abundant HCO_3^- with an isotopic signature in the range of the OM that is being used as a carbon source (^{13}C-depleted) (Pearson and Nelson, 2005). The HCO_3^- is made available for precipitation of carbonate that inherits this strongly negative $\delta^{13}C$ value which is in line with previous work on carbonate concretions (Coleman, 1993; Coleman and Raiswell, 1995; Marshall and Pirrie, 2013). This eogenetically induced precipitation of carbonate, as a cement filling the porosity of the sediment, results in the formation of the ^{13}C-depleted carbonate (**Table 2-3**) measured within the concretion. Carbonate concretions can, therefore, be identified as induced biomineralisation and consequently referred to as microbialites (*sensu latu*).

In the concretion body, the very abundant calcite (dominantly present as homogenous micritic cement) is in agreement with a very intense precipitation of carbonate by microbial activity (Flügel, 2010).

The concretion rim is marked by remaining quartz grains, as well as abundant authigenic pyrite agglomerates in the concretion rim (**Figure 2-5F**) that support a lesser micritisation. The present data show that the concretion body was formed during intense SRB activity, while the rim corresponds to a decrease in bacterial sulphate reduction. Here diminished diffusion of H_2S (Coleman and Raiswell, 1995) and/or a change in bacterial community, potentially with an enhanced Fe reduction (FeR) activity, led to a rise in Fe^{2+} concentration (Curtis *et al.*, 1986).

C_{29} steranes increase within the rim, however C_{27} steranes remain dominant. This change in the relative abundance of the two eukaryotic markers could indicate a change in the balance of the source organisms' ecosystem or possibly a preferential degradation of C_{27} over C_{29} steranes within the rim. Bulk OM ^{13}C isotopic signature of the carbonate concretion is slightly depleted in comparison to the shale (2 ‰) (**Table 2-3**), indicating input from another OM source (*e.g.* SRB and FeR bacteria, methanogens/methanotrophs).

Methanogens (and likely methanotrophs) are known to have played a major role in the formation of siderite concretions ($FeCO_3$) (Bojanowski and Clarkson, 2012; Pearson and Nelson, 2005). It is commonly suggested that they are involved as part of a bacterial consortium in the formation of calcitic concretions (Coleman, 1993; Coleman and Raiswell, 1995; Raiswell and Fisher, 2000). Recently, the investigation of modern carbonate concretions revealed abundant methanogenic archaea and methanotrophic bacteria, as well as SRB in direct association with the concretions (Reitner *et al.*, 2005).

However, compounds specific for anaerobic methane oxidation, such as crocetane (Hinrichs and Boetius, 2002; Wakeham *et al.*, 2004) are absent and 3β-methyl-hopanes (semi-specific for methanotrophic bacteria; Cvejic *et al.*, 2000) are of low abundance. This could either suggest (i) a minor involvement of these organisms in the anaerobic decay of OM and pyritiferous concretion growth, or (ii) the different methanogenic/methanotrophic organisms involved in concretion formation lacked the commonly associated biomarkers.

Concretions as palaeoenvironmental recorders?

Most studies on carbonate concretions aimed to identify the mechanisms and organisms involved in their formation (Coleman and Raiswell, 1995; Kiriakoulakis *et al.*, 2000; Melendez *et al.*, 2013a; Pearson and Nelson, 2005; Raiswell, 1976). Here, we discuss the ability of carbonate concretions to preserve the signal of the sediment within which they formed and consequently, to establish their role in palaeoenvironmental reconstruction. Often, carbonate concretions remain whereas their softer host sediment has long been eroded away. The identification of the host sediment signature at different scales and using different techniques is discussed below.

Inherited sedimentary bedding from the host Posidonia Shale is observed at a macroscopic scale (**Figure 2-3**). However, no such bedding can be distinguished at a microscopic scale, which shows a very homogenous micritic cement. Except for calcite, no other characteristic of the mineralogical composition of the Posidonia Shale could be detected in the concretion body and only quartz remains are present in the rim (**Figure 2-5F**). This observation is supported by ICP-MS analyses showing that

elements typical of detrital minerals (*i.e.* Al, K, P, Si) are commonly below detection limits in the concretion body and low abundance in the concretion rim (**Table 2-2**), most probably related to carbonate dilution of the signal.

Framboidal pyrite is forming *via* FeS and Fe_3S_4 precursors (mackinawite and greigite, respectively), and the size of the framboids is commonly used for palaeoenvironmental reconstruction (Wilkin and Barnes, 1997). During this investigation, very rare framboids could be observed in the concretions, whereas they have been described as abundant in the Posidonia Shale (Berner *et al.*, 2013). This is explained by the saturation of porewater with respect to pyrite, and the direct precipitation as euhedral pyrite nucleating and developing around the framboidal pyrite overprinting the latter (Coleman and Raiswell, 1995). The rare framboids observed are < 5 µm in diameter (**Figure 2-5D**), supporting an anoxic/euxinic environment (Wilkin and Barnes, 1997).

The stable isotope analyses of carbonate were performed on crushed samples of ~ 5 cm^3 from the concretions. Therefore, such analyses gave an averaged signal of at least two calcium carbonate phases (micrite and sparite). The values resulting from the averaged signal (**Table 2-3**) point towards a partial preservation of the sedimentary carbonate isotopic signature. SRB-derived carbonates commonly exhibit $\delta^{13}C$ values of the source OM, which in marine settings approximate –25 ‰ (Hendry *et al.*, 2006; Pearson and Nelson, 2005). Thus, the values obtained for the concretion body (–15.0 ‰, in average) and the concretion rim (–10.3 ‰, in average) indicate a mixed source for the carbonate.

The Posidonia Shale is rich in calcite with a carbonate content of 40 % and isotopic values $\delta^{13}C_{carb} = -1.8$ ‰ (**Table 2-3**). The presence of recrystallised foraminifera and coccoids (**Figure 2-5A, B**) in the carbonate concretions suggests that the ^{13}C-enriched carbonate content inherited from the Posidonia Shale was subject to dissolution and reprecipitation. The carbonate inherited from the Posidonia Shale is likely to be the second most important source of carbonate involved in concretion formation beside SRB-derived carbonate, nevertheless other sources cannot be excluded.

Aliphatic biomarker distributions showed only small differences between the concretions and the Posidonia Shale, suggesting that the biomarker signal preserved in the concretions is largely inherited from the surrounding sediment. The Posidonia Shale aliphatic hydrocarbons reflect a strong phytoplankton input, as shown by abundant Pr and Ph as well as LMW *n*-alkanes that derived from the surficial oxic zone of the stratified water column. Low abundance hopanoids reflect some limited bacterial input whereas abundant steranes indicate strong algal contribution. Very HMW *n*-alkanes (up to *n*-C_{37}) were present which can be related to bacterial sulphate reducers (Holman *et al.*, 2014; Melendez *et al.*, 2013a) and/or land plants as suggested by the relative ^{13}C-enrichment of odd ≥ *n*-C_{31} compared to the even counterparts (with the exception of *n*-C_{34}). The average values of *n*-alkanes of the Posidonia Shale ($\delta^{13}C = -33.4 \pm 0.5$ ‰) are ^{13}C-depleted in comparison with a "normal" Jurassic marine OM signature (Jenkyns *et al.*, 2002; Kemp *et al.*, 2005; Schouten *et al.*, 2000b). A negative shift in $\delta^{13}C$ values is also observed in the bulk OM $\delta^{13}C$ of the Posidonia Shale vs. concretion samples (**Table 2-3**) and was previously described in the *H. serpentinum* zone (**Figure 2-1**) (Jenkyns *et al.*, 2002; Schmid-Röhl *et al.*, 2002). This isotopic discrepancy is likely related to the well-known Toarcian negative carbon excursion (Gröcke *et al.*, 2011; Hesselbo *et al.*, 2007; Kemp *et al.*, 2005).

The aliphatic distribution in the concretion is very similar to the host rock's distribution, supporting a preservation of the biomarker signal within the concretion. However, the $\delta^{13}C$ values of *n*-alkanes show a negative shift (–1 ‰), from the Posidonia Shale to the concretion (**Figure 2-7**). This shift indicates some input from a different, ^{13}C-depleted carbon source, likely to be related to the microbial activity (*e.g.* SRB), involved in the formation of the concretions. The very HMW *n*-alkanes are showing the same trend as in the Posidonia Shale. A relative enrichment of odd chain lengths (≥ *n*-C_{31}) compared to the even counterparts can be explained by a mixed source of very ^{13}C-depleted *n*-alkanes from SRB with relatively ^{13}C-enriched odd HMW *n*-alkanes derived from land plants that were previously described in the Posidonia Shale (Frimmel *et al.*, 2004). The constantly ^{13}C-depleted values obtained for LMW *n*-alkanes can also be related to SRB or anoxygenic photo-autotrophic sulfur bacteria (Holman *et al.*, 2014; Londry *et al.*, 2004). Furthermore, the presence of AI and traces of isorenieratane, both indicative of Chlorobi (characteristic of PZE), in the concretions supports the preservation of the host sediment signal. Moreover, the plot

of the AIR vs. Pr/Ph, compared to the study published by Schwark and Frimmel (2004) (**Figure 2-9**) confirmed the origin of both concretions within the *H. serpentinum* zone and below the Oberer Stein carbonate layer (**Figure 2-1**). It appears that concretions A and B have probably not been formed simultaneously. However, the molecular composition of concretion B and Posidonia Shale reference sample show greater similarities (**Figure 2-9**), and possibly had a more immediate relation in the sediment column than with concretion A. Although isorenieratane and AI displayed low peak intensity in the concretions samples in comparison with the Posidonia Shale, concretion samples AIR vs. Pr/Ph are indicative of persistent PZE (**Figure 2-9**). Furthermore, HI indices (**Table 2-3**) show lower values and consequently poorer OM preservation in the rims where isorenieratane and AI peak intensity are greater. Hence the low peak intensity of Chlorobi-derived markers in the concretion is most likely related to a carbonate dilution effect.

Mineralogical, textural and inorganic geochemical parameters pointed to a partial to total overprinting and/or dilution of the host sediment signature by the signal associated to the cementation of the concretion. However, the compositional properties of the host sediment have been transferred at a macroscopic level (sedimentary bedding), as well as at a molecular level (biomarker distribution) to the diagenetically formed concretions. Thus, concretions might be of importance in the palaeoenvironmental reconstruction due to their resistance to compaction and diagenesis. Furthermore, the low porosity and intensive cementation allow concretions to resist weathering while often their host sediment is partially to entirely weathered out. Therefore, concretions can be of great importance as palaeoenvironmental recorders.

Carbonate concretions: importance of the nucleus and the preservation of organic matter

Carbonate concretions are known to host exceptionally well-preserved morphological fossils (Arua, 1991; Geraghty and Westermann, 1994; Wilson and Brett, 2013) as well as for preserving molecules through time (Melendez *et al.*, 2013a, 2013b). However, the preservation state of bulk OM has barely been reported (Dong *et al.*, 2008). Moreover, in the past, most studies were performed on concretions lacking any 3D nucleus (Coleman and Raiswell, 1995; Pearson and Nelson, 2005;

Wolff *et al.*, 1991). Potentially, growth of such concretions could have been triggered by any type of decaying OM, which had been entirely degraded in the process. Concretions have been reported to form around, and preserve, various types of nucleus *e.g.* wood (Marynowski *et al.*, 2007a, 2007b), fish (Martill, 1989, 1990), crustacea (Melendez *et al.*, 2013a), and burrow (Wilson and Brett, 2013). Hence a wide range of biological substrates may impact on the signal preserved in concretions.

Here, both concretions grew around a nucleus of the same nature (jet) and therefore this approach limits the potential bias that could influence the OM signal depending on the type of nucleus. The great similarities observed in all proxies, applied to the two concretions studied, are likely to be related to similar type of OM decayed.

HI index is calculated based on Rock-Eval data and TOC_{cf} measurements, and is commonly used as OM source and preservation indicator. Within the concretion bodies, high HI values were found in association with more negative $\delta^{13}C_{carb}$ (**Figure 2-6**). Highly ^{13}C-depleted carbonate of the bodies was attributed to an enhanced SRB activity. However, the high HI values in the concretion bodies support a SRB activity restricted to the nuclei surfaces. SRB did not decompose the OM trapped in the concretion body. The products of the degradation of OM by SRB (depleted HCO_3^-, and H_2S) diffused in all directions allowing for the formation of a Ca carbonate or a non-crystalline Ca precursor (Allison, 1988b; Berner, 1968) and for OM preservation. Concomitantly, lower HI values of the rims (**Figure 2-6, Table 2-3**) would indicate a higher degradation of OM. This contrast emphasises the paradox of concretion formation: OM decay initiates concretion growth. However, in parallel, the OM is exceptionally well preserved within the concretions. The explanation offered for this bias is that microbes consume a labile and easily hydrolysable fraction of OM upon anaerobic eogenesis. The lipidic fraction is preferentially preserved and subsequently protected from further degradation by encapsulation in tight carbonate cements. This implies that concretions and the OM preserved therein might hold the key for accessing the oldest bio-lipids and giving new insights on early life.

Conclusions

The present study shows how a combination of various geological and geochemical proxies could complement each other and give stronger arguments for

the identification of microbial communities involved as well as the ability of carbonate concretions record palaeoenvironments. In detail, our results highlighted that:

- Concretion formation must have occurred within the upper metres of the sedimentary accumulation.

- SRB played a crucial role in concretion formation. The very low $\delta^{13}C_{carb}$ suggest that methanotrophs could also participate in the concretion growth processes. However, no biomarker evidence of an active methane cycle was found. That finding suggests that not all methanogens/methanotrophs produce the biomarkers commonly associated with organisms involved in methane cycling.

- The concretion body did not show evidence of substantial degradation of OM, which supports an SRB activity mainly localised around the concretion nucleus while FeR bacteria may have been more abundant in the pyritic rim.

- Bulk molecular parameters such as HI can be used to address the preservation of OM in carbonate concretion and gain a better understanding of the concretion growth processes.

- Organic geochemical analyses of carbonate concretions can provide valuable insights into the palaeoenvironment at the time of deposition due to the preservation of the host sediment signal.

As the present study investigated two concretions and similar signatures were detected for most proxies, conditions of formation are likely to be similar for all pyritiferous calcite concretions on a basin-scale, and possibly for similar concretions of different ages. Finally, the common occurrence of carbonate concretions in the geological record, their significance as palaeoenvironmental recorder and their ability to preserve OM make them object of high interest for the investigation of early life.

Acknowledgements

This research was supported by a Discovery Grant from the Australian Research Council's DORA Kliti Grice (DP130100577) and ARC infrastructure grant (LE110100119).

Geoff Chidlow and Alex Holman are thanked for GC–MS and GC–IRMS technical support. Marieke Sieverding is thanked for technical support regarding Rock-Eval and CNS elemental analyses and GC–MS–MS analyses. CP thanks WA-OIG, Curtin University for a Curtin international postgraduate scholarship The Institute of Geoscience Research for a top-up scholarship and the European Association of Organic Geochemistry for a travel scholarship. A.P. acknowledges CSIRO Mineral Resources and the Science and Industry Endowment Fund (SIEF)

References

Allison, P.A., 1988. The role of anoxia in the decay and mineralization of proteinaceous macro-fossils. *Paleobiology* **14**, 139–154.

Arua, I., 1991. The trace fossil Teredolites longissimus in calcareous concretions from the Eocene Ameki formation, southeastern Nigeria. *Journal of African Earth Sciences (and the Middle East)* **12**, 605–608.

Baudin, F., Herbin, J.P., Vandenbroucke, M., 1990. Mapping and geochemical characterization of the Toarcian organic matter in the Mediterranean Tethys and Middle East. *Organic Geochemistry* **16**, 677–687.

Berner, R.A., 1968. Calcium carbonate concretions formed by the decomposition of organic matter. *Science* **159**, 195–197.

Berner, Z.A., Puchelt, H., Nöltner, T., Kramar, U., 2013. Pyrite geochemistry in the Toarcian Posidonia Shale of south-west Germany: Evidence for contrasting trace-element patterns of diagenetic and syngenetic pyrites. *Sedimentology* **60**, 548–573.

Boetius, A., Ravenschlag, K., Schubert, C.J., Rickert, D., Widdel, F., Gieseke, A., Amann, R., Jùrgensen, B.B., Witte, U., Pfannkuche, O., 2000. A marine microbial consortium apparently mediating anaerobic oxidation of methane. *Nature* **407**, 623–626.

Bojanowski, M.J., Clarkson, E.N.K., 2012. Origin of siderite concretions in microenvironments of methanogenesis developed in a sulfate reduction zone: an exception or a rule? *Journal of Sedimentary Research* **82**, 585–598.

Bour, I., Mattioli, E., Pittet, B., 2007. Nannofacies analysis as a tool to reconstruct paleoenvironmental changes during the Early Toarcian anoxic event. *Palaeogeography, Palaeoclimatology, Palaeoecology* **249**, 58–79.

Burns, B.P., Anitori, R., Butterworth, P., Henneberger, R., Goh, F., Allen, M. a., Ibañez-Peral, R., Bergquist, P.L., Walter, M.R., Neilan, B. a., 2009. Modern

analogues and the early history of microbial life. *Precambrian Research* **173**, 10–18.

Cohen, A.S., Coe, A.L., Harding, S.M., Schwark, L., 2004. Osmium isotope evidence for the regulation of atmospheric CO_2 by continental weathering. *Geology* **32**, 157–160.

Coleman, M.L., 1993. Microbial processes: Controls on the shape and composition of carbonate concretions. *Marine Geology* **113**, 127–140.

Coleman, M.L., Raiswell, R., 1980. Carbon , oxygen and sulphur isotope variations in concretions from the Upper Lias of N.E. England. *Geochimica and Cosmochimica Acta* **45**, 329–340.

Coleman, M.L., Raiswell, R., 1995. Source of carbonate and origin of zonation in pyritiferous carbonate concretions: evaluation of a dynamic model. *American Journal of Science* **295**, 282–308.

Curtis, C., Building, B., Sheffield, S., 1987. Mineralogical consequences of organic matter degradation in sediments : inorganic / organic, in: Leggett, J.K., Zuffa, G.G. (Eds.), Marine Clastic Sedimentology. pp. 108–123.

Curtis, C.D., Coleman, M.L., Love, L.G., 1986. Pore water evolution during sediment burial from isotopic and mineral chemistry of calcite , dolomite and siderite concretions. *Geochimica et Cosmochimica Acta* **50**, 2321–2334.

Cvejic, J.H., Bodrossy, L., Rohmer, M., 2000. Bacterial triterpenoids of the hopane series from the methanotrophic bacteria Methylocaldum spp.: phylogenetic implications and first evidence for an unsaturated aminobacteriohopanepolyol. *FEMS Microbiology Letters* **182**, 361–365.

Dale, A., John, C.M., Mozley, P.S., Smalley, P.C., Muggeridge, A.H., 2014. Time-capsule concretions: Unlocking burial diagenetic processes in the Mancos Shale using carbonate clumped isotopes. *Earth and Planetary Science Letters* **394**, 30–37.

Das, S.S., Tripathi, M.K., 2009. Trace fossils from Talchir carbonate concretions, Giridih basin, Jharkhand. *Journal of Earth System Science* **118**, 89–100.

Dong, J., Zhang, S., Jiang, G., Zhao, Q., Li, H., Shi, X., Liu, J., 2008. Early diagenetic growth of carbonate concretions in the upper Doushantuo Formation in South China and their significance for the assessment of hydrocarbon source rock. *Science in China Series D: Earth Sciences* **51**, 1330–1339.

Edgcomb, V.P., Bernhard, J.M., Summons, R.E., Orsi, W., Beaudoin, D., Visscher, P.T., 2014. Active eukaryotes in microbialites from Highborne Cay, Bahamas, and Hamelin Pool (Shark Bay), Australia. *The ISME journal* **8**, 418–29.

Flügel, E., 2010. Microfacies of carbonate rocks: Analysis, interpretation and application, 2nd editio. ed. Springer-Verlag Berlin Heidelberg.

Frimmel, A., Oschmann, W., Schwark, L., 2004. Chemostratigraphy of the Posidonia Black Shale, SW Germany I. Influence of sea-level variation on organic facies evolution. *Chemical Geology* **206**, 199–230.

Geraghty, M.D., Westermann, G.*E.G.*, 1994. Origin of Jurassic ammonite concretions assemblages at Alfeld, Germany: a biogenic alternative. *Palaontologische Zeitschrift* **68**, 473–490.

Gröcke, D.R., Hori, R.S., Trabucho-Alexandre, J., Kemp, D.B., Schwark, L., 2011. An open ocean record of the Toarcian oceanic anoxic event. *Solid Earth* **2**, 245–257.

Hendry, J.P., Pearson, M.J., Trewin, N.H., Fallick, A.E., 2006. Jurassic septarian concretions from NW Scotland record interdependent bacterial, physical and chemical processes of marine mudrock diagenesis. *Sedimentology* **53**, 537–565.

Hesselbo, S., Grocke, D., Jenkyns, H.C., Bjerrum, C.J., Farrimond, P., Morgans Bell, H., Green, O., 2000. Massive dissociation of gas hydrate during a Jurassic oceanic anoxic event. *Nature* **406**, 392–395.

Hesselbo, S.P., Jenkyns, H.C., Duarte, L. V., Oliveira, L.C.V., 2007. Carbon-isotope record of the Early Jurassic (Toarcian) Oceanic Anoxic Event from fossil

wood and marine carbonate (Lusitanian Basin, Portugal). *Earth and Planetary Science Letters* **253**, 455–470.

Hinrichs, K., Boetius, A., 2002. The anaerobic oxidation of methane : new insights in microbial ecology and biogeochemistry, in: Van Weering, T. (Ed.), Ocean Margin Systems. Springer, berlin Heidelberg, pp. 457–477.

Holman, A.I., Grice, K., Jaraula, C.M.B., Schimmelmann, A., 2014. Bitumen II from the Paleoproterozoic Here's Your Chance Pb/Zn/Ag deposit: Implications for the analysis of depositional environment and thermal maturity of hydrothermally-altered sediments. *Geochimica et Cosmochimica Acta* **139**, 98–109.

Jenkyns, H.C., 2010. Geochemistry of oceanic anoxic events. *Geochemistry, Geophysics, Geosystems* **11**, Q03004.

Jenkyns, H.C., Jones, C.E., Gröcke, D.R., Hesselbo, S.P., Parkinson, D.N., 2002. Chemostratigraphy of the Jurassic System: applications, limitations and implications for palaeoceanography. *Journal of the Geological Society* **159**, 351–378.

Kemp, D.B., Coe, A.L., Cohen, A.S., Schwark, L., 2005. Astronomical pacing of methane release in the Early Jurassic period. *Nature* **437**, 396–399.

Kiriakoulakis, K., Marshall, J.D., Wolff, G.A., 2000. Biomarkers in a Lower Jurassic concretion from Dorset (UK). *Journal of the Geological Society* **157**, 207–220.

Lash, G.G., Blood, D., 2004. Geochemical and textural evidence for early (shallow) diagenetic growth of stratigraphically confined carbonate concretions, Upper Devonian Rhinestreet black shale, western New York. *Chemical Geology* **206**, 407–424.

Londry, K.L., Jahnke, L.L., Des Marais, D.J., 2004. Stable carbon isotope ratios of lipid biomarkers of sulfate-reducing bacteria. *Applied and Environmental Microbiology* **70**, 745–751.

Marshall, J.D., Pirrie, D., 2013. Carbonate concretions-explained. *Geology Today* **29**, 53–62.

Martill, D.M., 1988. Preservation of fish in the Cretaceous Santana Formation of Brazil. *Palaeontology* **31**, 1–18.

Martill, D.M., 1989. The Medusa effect: instantaneous fossilization. *Geology Today* **5**, 201–205.

Martill, D.M., 1990. Macromolecular resolution of fossilized muscle tissue from an elopomorph fish. *Nature* **346**, 171–172.

Marynowski, L., Otto, A., Zatoń, M., Philippe, M., Simoneit, B.R.T., 2007a. Biomolecules preserved in ca. 168 million year old fossil conifer wood. *Die Naturwissenschaften* **94**, 228–236.

Marynowski, L., Zatoń, M., Simoneit, B.R.T., Otto, A., Jedrysek, M., Grelowski, C., Kurkiewics, S., 2007b. Compositions , sources and depositional environments of organic matter from the Middle Jurassic clays of Poland. *Applied Geochemistry* **22**, 2456–2485.

Melendez, I., Grice, K., Schwark, L., 2013a. Exceptional preservation of Palaeozoic steroids in a diagenetic continuum. *Scientific reports* **3**, 2768.

Melendez, I., Grice, K., Trinajstic, K., Ladjavardi, M., Greenwood, P., Thompson, K., 2013b. Biomarkers reveal the role of photic zone euxinia in exceptional fossil preservation: An organic geochemical perspective. *Geology* **41**, 123–126.

Pagès, A., Grice, K., Ertefai, T., Skrzypek, G., Jahnert, R., Greenwood, P., 2014a. Organic geochemical studies of modern microbial mats from Shark Bay: Part I: Influence of depth and salinity on lipid biomarkers and their isotopic signatures. *Geobiology* **12**, 469–487.

Pagès, A., Grice, K., Vacher, M., Welsh, D.T., Teasdale, P.R., Bennett, W.W., Greenwood, P., 2014b. Characterizing microbial communities and processes in a

modern stromatolite (Shark Bay) using lipid biomarkers and two-dimensional distributions of porewater solutes. *Environmental microbiology* **16**, 2458–2474.

Pancost, R.D., Crawford, N., Magness, S., Turner, A., Jenkyns, H.C., Maxwell, J.R., 2004. Further evidence for the development of photic-zone euxinic conditions during Mesozoic oceanic anoxic events. *Journal of the Geological Society* **161**, 353–364.

Pearson, M.J., Nelson, C.S., 2005. Organic geochemistry and stable isotope composition of New Zealand carbonate concretions and calcite fracture fills. *New Zealand Journal of Geology and Geophysics* **48**, 395–414.

Raiswell, R., 1976. The microbiological formation of carbonate concretions in the Upper Lias of the NE England. *Chemical Geology* **18**, 227–244.

Raiswell, R., 1982. Pyrite texture isotopic composition and the availability of iron. *American Journal of Science* **282**, 1244–1263.

Raiswell, R., Fisher, Q.J., 2000. Mudrock-hosted carbonate concretions: a review of growth mechanisms and their influence on chemical and isotopic composition. *Journal of the Geological Society* **157**, 239–251.

Raiswell, R., White, N.J.M., 1978. Spatial aspects of concretionary growth in the Upper Lias of Northeast England. *Sedimentary Geology* **20**, 291–300.

Reitner, J., Peckmann, J., Blumenberg, M., Michaelis, W., Reimer, A., Thiel, V., 2005. Concretionary methane-seep carbonates and associated microbial communities in Black Sea sediments. *Palaeogeography, Palaeoclimatology, Palaeoecology* **227**, 18–30.

Röhl, H., Schmid-Röhl, A., Oschmann, W., Frimmel, A., Schwark, L., 2001. The Posidonia Shale (Lower Toarcian) of SW-Germany : an oxygen-depleted ecosystem controlled by sea level and palaeoclimate. *Palaeogeography, Palaeoclimatology, Palaeoecology* **165**, 27–52.

Ruebsam, W., Münzberger, P., Schwark, L., 2014. Chronology of the Early Toarcian environmental crisis in the Lorraine Sub-Basin (NE Paris Basin). *Earth and Planetary Science Letters* **404**, 273–282.

Schmid-Röhl, A., Röhl, H., Oschmann, W., Frimmel, A., 2002. Palaeoenvironmental reconstruction of Lower Toarcian epicontinental black shales (Posidonia Shale , SW Germany): global versus regional control. *Geobios* **35**, 13–20.

Schouten, S., Van Kaam-Peters, H.M.E., Rijpstra, W.I.C., Schoell, M., Sinninghe Damste, J.S., 2000. Effects of an oceanic anoxic event on the stable carbon isotopic composition of early Toarcian carbon. *American Journal of Science* **300**, 1–22.

Schwark, L., Frimmel, A., 2004. Chemostratigraphy of the Posidonia Black Shale, SW-Germany II. Assessment of extent and persistence of photic-zone anoxia using aryl isoprenoid distibutions. *Chemical Geology* **206**, 231–248.

Seilacher, A., 2001. Concretion morphologies reflecting diagenetic and epigenetic pathways. *Sedimentary ge* **143**, 41–57.

Sellés-Martínez, J., 1996. Concretion morphology, classification and genesis. *Earth-Science Reviews* **41**, 177–210.

Tucker, M., Wright, V.P., Dickson, J.A.D., 1990. Carbonate sedimentology. Blackwell Scientific Publication, Oxford.

Wakeham, S.G., Hopmans, E.C., Schouten, S., Sinninghe Damsté, J.S., 2004. Archaeal lipids and anaerobic oxidation of methane in euxinic water columns: a comparative study of the Black Sea and Cariaco Basin. *Chemical Geology* **205**, 427–442.

Wignall, P.B., Newton, R.J., Little, C.T.S., 2005. The timing of paleoenvironmental change and cause-and-effect relationships during the Early Jurassic mass extinction in Europe. *American Journal of Science* **305**, 1014–1032.

Wilkin, R.T., Barnes, H.L., 1997. Formation processes of framboidal pyrite. *Geochemica et Cosmochimica Acta* **61**, 323–339.

Wilson, D.D., Brett, C.E., 2013. Concretions as sources of exceptional preservation, and decay as a source of concretions: examples from the middle Devonian of New York. *Palaios* **28**, 305–316.

Wolff, G.A., Rukin, N., Marshall, J.D., 1991. Geochemistry of an early diagenetic concretion from the Birchi Bed (L. Lias, W. Dorset, U.K.). *Organic Geochemistry* **19**, 431–444.

Woo, K.S., Khim, B.K., 2006. Stable oxygen and carbon isotopes of carbonate concretions of the Miocene Yeonil Group in the Pohang Basin, Korea: Types of concretions and formation condition. *Sedimentary Geology* **183**, 15–30.

Zatoń, M., Kremer, B., Marynowski, L., Wilson, M.A., Krawczyński, W., 2011. Middle Jurassic (Bathonian) encrusted oncoids from the Polish Jura, southern Poland. *Facies* **58**, 57–77.

Zatoń, M., Marynowski, L., 2004. Konzentrat-Lagerstätte-type carbonate concretions from the uppermost Bajocian (Middle Jurassic) of the Czêstochowa area , South-Cental Poland. *Geological Quarterly* **48**, 339–350.

Zhou, Y., Grice, K., Stuart-williams, H., Farquhar, G.D., Hocart, C.H., Lu, H., Liu, W., 2010. Biosynthetic origin of the saw-toothed profile in $\delta^{13}C$ and $\delta^{2}H$ of *n*-alkanes and systematic isotopic differences between *n*-, *iso*-, and *anteiso*-alkanes in leaf waxes of land plants. *Phytochemistry* **71**, 388–403.

Ziegler, P.A., 2005. EUROPE : Permian to Recent Evolution: Jurassic, in: Selley, R.C., Cocks, L.R.M., Plimer, I.R. (Eds.), Encyclopedia of Geology. Elsevier, pp. 106–112..

Chapter 3

Jurassic World: Palaeobiology of red blood cell-like structures, collagen and cholesterol in an ichthyosaur bone

Chloé Plet, Kliti Grice, Anais Pagès, Michael Verrall, Marco J.L. Coolen, Wolfgang Ruebsam, Lorenz Schwark

Submitted to Scientific Reports

(Impact factor: 5.228)

Abstract

Carbonate concretions are known to contain well-preserved fossils and soft tissue. Recently, biomolecules (*e.g.* cholesterol) and molecular fossils (biomarkers) were also discovered in a 380 million-year-old concretion revealing their importance in exceptional preservation. Here, we used a range of techniques (XRF mapping, electron microscopy imaging, biomarkers and compound specific isotopes analyses) to report the presence of red blood cell-like structures, collagen and cholesterol in an ichthyosaur bone encapsulated in a carbonate concretion from the Early Jurassic (~182.7 Ma). The red blood cell-like structures are 4 to 5 times smaller than those identified in modern birds and reptiles. This could result from an evolutionary adaptation to the prolonged low oxygen atmospheric levels during the 70 Ma when ichthyosaur thrived. The cholesterol and collagen detected here are the second oldest occurrence in fossils. The $\delta^{13}C$ of the ichthyosaur bone cholesterol indicates that it largely derives from a higher level in the food chain and confirms a fish and cephalopod diet. The combined findings above demonstrate that carbonate concretions create isolated environments that allow exceptional preservation of fragile tissues and biomolecules and open up a hitherto underexploited archive of palaeobiological information across geological ages providing further insight into preservational pathways and evolution of life.

Introduction

Dinosaur fossils, even with the most beautifully preserved anatomy, generally lack soft tissues such as fibrous or cellular remains as well as biomolecules or molecular fossils. However, over the last three decades several studies have shown that fragile tissues and molecules can be preserved over surprisingly long periods of time (tens of millions of years) 1–8.

Heme-derived porphyrins were detected in a blood engorged mosquito from the Middle Eocene (Greenwalt *et al.*, 2013). More recently, red blood cell (RBC)-like structures, along with amino acids associated with collagen-like fibres, were also found in 75 million-year-old dinosaur bones (Bertazzo *et al.*, 2015). The latter finding was remarkable considering the fact that the bone fragments were not particularly well preserved, which is in agreement with models suggesting that preservation of biomolecules and soft tissues in the fossil record is more common than previously thought (Bertazzo *et al.*, 2015; Briggs, 2003; Briggs and Kear, 1993; Schweitzer *et al.*, 2014). Collagen fibres were also reported in-situ in a 195 million-year-old dinosaur (Lee *et al.*, 2017).

Here, we investigated an ichthyosaur vertebra bone of Lower Toarcian age (~ 182.7 Ma), which has been exceptionally well-preserved through encapsulation in a carbonate concretion (**Figure 3-1**). The sample was collected from the renowned Posidonia Shale Konservat Fossil Lagerstätte in SW-Germany. Ichthyosaurs thrived in the Mesozoic era; they evolved following the largest mass extinction event of our planet (near to the Permian/Triassic boundary event, ca. 252 Ma; Motani, 2005) and became extinct at the end-Cenomanian (93.9 Ma; Fischer *et al.*, 2016).

Generally, Jurassic shallow-water ichthyosaur falls have low preservation potential for tissues and biomolecules due to the presence of a specialised consortia of degraders (Danise *et al.*, 2014). However, in the Lower Toarcian, when the *H. falciferum* zone was deposited, the preservational environment in epicontinental seas was excellent due to water column stratification and strong euxinic conditions in the bottom waters (Berner *et al.*, 2013; Schwark and Frimmel, 2004). Under these euxinic conditions, organic matter-rich mudstones (black shales) deposited and the diagenetic formation of carbonate concretions was common (Marshall and Pirrie, 2013). Such

carbonate concretions often contain morphological fossils of striking preservation(Martill, 1988, 1990) or in some exceptional cases even intact biomolecules (Melendez *et al.*, 2013a, 2013b).

The aim of this study was to investigate the potential of carbonate concretions to preserve microscopic soft tissue (*i.e.* collagen and RBC-like structures) and biomolecules (*e.g.* cholesterol) from a vertebra bone of the ichthyosaur Stenopterygius. A combined approach using in-situ imaging techniques and molecular investigations was employed to emphasise the capacity of carbonate concretions in preserving soft tissue and biomolecules. Here, we report the oldest RBC-like structures (> 100 Myr older than in a previous report by Bertazzo *et al.*, 2015), the second oldest occurrences of collagen fibres and ancient cholesterol. Furthermore, important insights about the palaeoenvironment and evolutionary adaptation of this extinct genus are discussed.

Results and discussion

Geological settings and sampling

The investigated sample was recovered from the Toarcian Posidonia Shale Formation at the HOLCIM Cement quarry of Dotternhausen (SW-Germany). The concretion was collected shortly after blasting within the quarry and stored in the dark at room temperature before transverse slices were cut in its centre, shortly before analyses.

Following the global Toarcian transgression, the black shale host sediment was deposited in the SW-German sub-basin, on the epicontinental Western Tethyan Shelf (Röhl *et al.*, 2001; Schmid-Röhl *et al.*, 2002; Ziegler, 2005). The sub-basin experienced high algal productivity coupled with restrictions in water circulation leading to stratification of the water column and development of anoxic to euxinic bottom waters, which favoured the deposition of organic matter-rich black shales (Röhl *et al.*, 2001; Schmid-Röhl *et al.*, 2002; Schwark and Frimmel, 2004).

Encapsulation of an ichthyosaur vertebra in a concretion

A range of imaging techniques was applied to a polished transverse section of the encapsulated vertebra, a selection of three-dimensional samples from the vertebra cortical and trabecular bones were taken. Both cortical and trabecular bones displayed a homogenous structure. Early mineralisation of concretions around the decaying organic matter may occur within weeks or months (Yoshida *et al.*, 2015). During this early encapsulation, the formation of a tight carbonate cement prevented the bone from further microbial degradation (**Figure 3-1A**) and inhibited exchange of fluids with the surrounding environment. The concretion body, enclosing the vertebra, also contains abundant coccoids and foraminifera that are recrystallised in sparry calcite, as well as small (~ 10 µm) dispersed euhedral crystals of pyrite within a microspar carbonate matrix. The outer rim of the concretion is rich in pyrite. No septaria were observed within the concretion, which further supports the absence of post depositional exchange with the diagenetic environment. Therefore, early post mortem encapsulation led to excellent preservation of the bone tissue in the concretion.

Bone structure and elemental mapping

Microbeam XRF mapping of phosphorus (P), only located in the bone fragments within the concretion (**Figure 3-1B**), distinguished the cortical (*i.e.* compact) bone from the trabecular (*i.e.* spongy) bone. The high primary porosity (*e.g.* up to 65 %) of vertebra bones has been reported previously in ichthyosaurs (Lopuchowycz and Massare, 2002). We calculated a porosity of the same range (estimated at ~ 60 %) in the trabecular bone (**Figure 3-1B**), where pores have been predominantly cemented by calcite (**Figure 3-1C**). Elemental mapping (Ba, S) (**Figure 3-2**) and optical imaging (**Figure 3-1D***)* revealed a bone compartment cemented with trace element-enriched barite (BaSO4), a feature often observed in bones deposited under anoxic conditions where trace elements may be mobilised from a black shale (Leduc, 2012).

Examination of the internal bone structure of the ichthyosaur, using backscattered electron imaging, revealed remarkable morphological preservation of fossilised 250 µm-diameter secondary osteons (Haversian system), known to be involved in mature bone remodelling and renewal. Within the osteons, a number of osteocytes and lamellae are visible (**Figure 3-1E**). Osteocytes play a predominant role

in the synthesis of collagen and regulate osteoblast function as well as biomineralisation of bones (*e.g.* Sanchez *et al.*, 2014)).

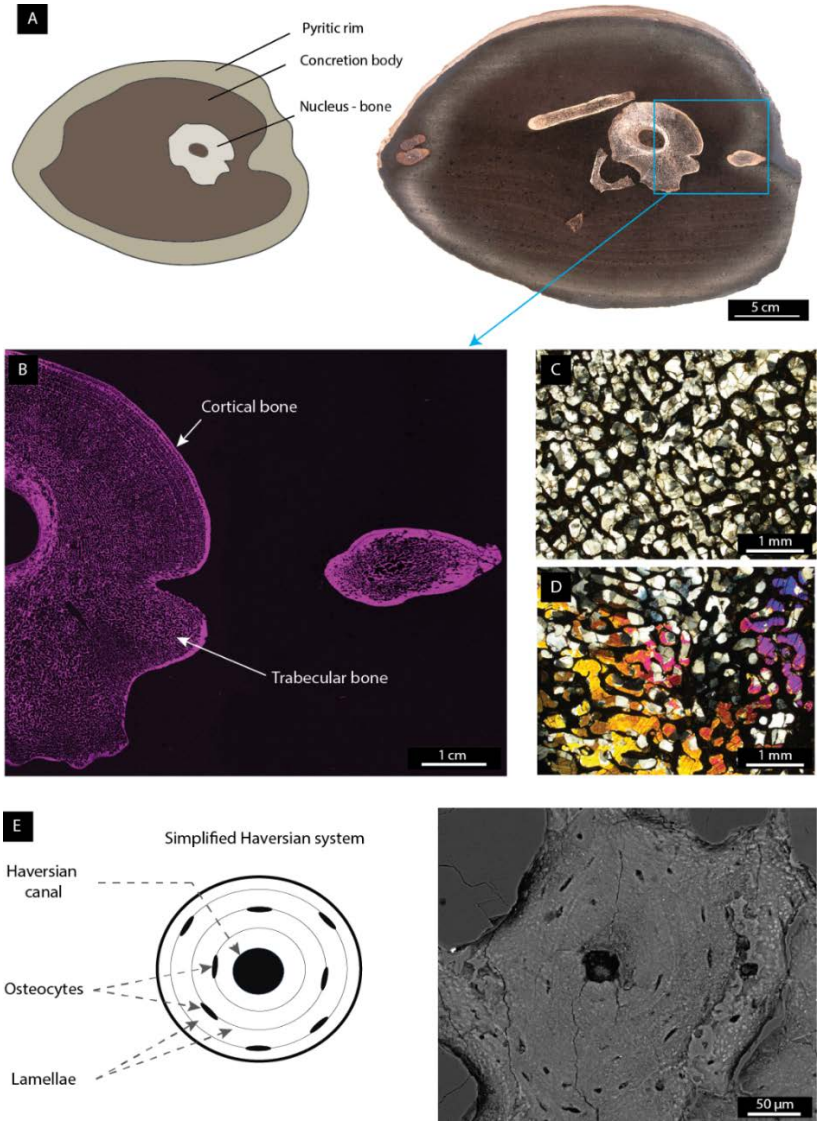

Figure 3-1. Morphology, mineralogy and chemical composition of ichthyosaur bones within a carbonate concretion. A) Photographic image and schematic drawing (with named features) of a polished section of the bone containing concretion. The vertebra served as a nucleus which triggered the microbial degradation processes leading to the concretion. The rim contains a high amount of pyrite (observed by XRD, optical microscopy and SEM) in contrast to the concretion body. B) Microbeam XRF elemental mapping of phosphorus (magenta) showing that phosphorus is only present in the bones. C) and D) Optical imaging on a thin section using cross polarised light microscopy showing the minerals filling the porosity of the bone C) equant calcite spar (CaCO3) and D) barite (BaSO4). Barite was identified by its mineral properties (clear colour and 90° cleavages) and high birefringence as well as by elemental distribution using microbeam XRF (Figure 3-2). E) Backscattered electron photomicrograph and simplified sketch of a Haversian system, including Haversian canal, osteocytes and lamellae

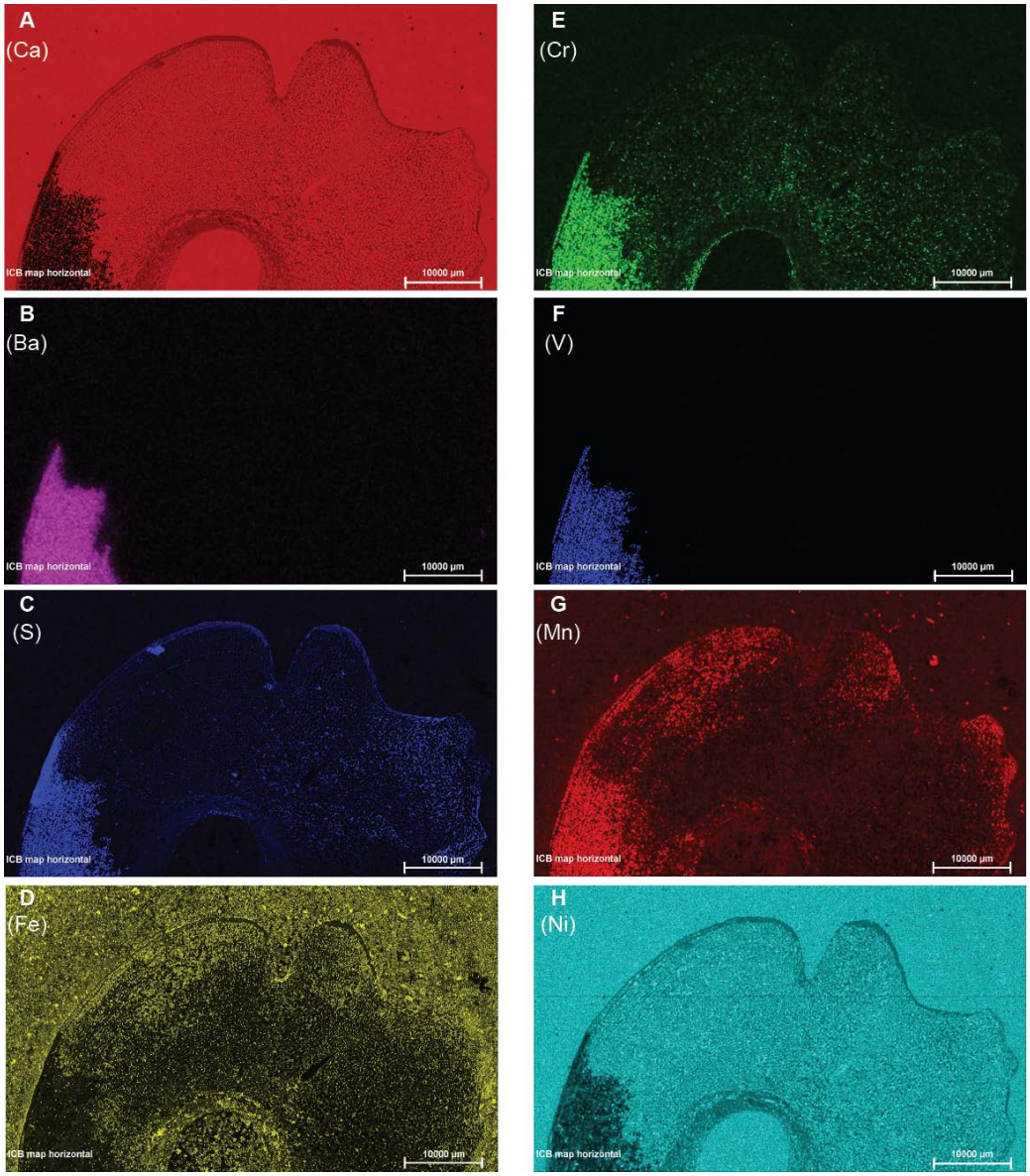

Figure 3-2. Microbeam XRF elemental mapping of a polished section of the concretion. A) Calcium (Ca) distribution map, showing high abundance of Ca in the concretion and bone porosity (related to calcite) and in the bone (related to apatite). Locally, Ca is virtually absent from the porosity suggesting the presence of another mineral. B) Barium (Ba) distribution map. Ba signal is strong only located in the porosity of the bone, where Ca is absent, which emphasises a different crystalline phase filling the porosity of the bone. C) Sulfur (S) distribution. The distribution of S correlates with Ba suggesting that the mineral phase is barite ($BaSO_4$). D) Iron (Fe) elemental distribution. Fe is widespread within the concretion but does not match the S distribution suggesting it is incorporated within the calcite. (E) to (H) distribution of various redox sensitive elements such as E) Chromium (Cr), F) Vanadium (V), G) Manganese (Mn), and H) Nickel (Ni) clearly demonstrating the presence of different redox micro-environments within the bone porosity itself during the early stages of concretion precipitation.

.

Red blood cells and collagen fibres in an ichthyosaur

Three-dimensional samples studied by SEM analyses were taken from an area within the trabecular and cortical bones where the porosity was filled by calcite. SEM imaging of fossilised soft tissue in the trabecular bone (**Figure 3-3**) revealed intertwined elongated fibres (average width of 160 ± 1 nm; n = 88). These show curved geometries and bundled groupings (**Figure 3-3A-C**), which in size and alignment resemble modern crocodile collagen fibres (**Figure A3-** 1) and fossil fibrous structures previously identified as collagen in Late Cretaceous dinosaurs (Bertazzo *et al.*, 2015; Schweitzer *et al.*, 2007b). In close proximity to these collagen fibres, clusters of concave disks with an average size of 1.95 ± 0.21 µm (n = 75), closely resembling RBC-like structures reported from dinosaurs (Bertazzo *et al.*, 2015), were observed (**Figure 3-3D-E**). However, the RBC-like structures in both cases are 4 to 5 times smaller than those identified in modern birds and reptiles.

Furthermore, both structures resembling fossil RBCs and collagen fibres differ from their modern analogues by displaying a granular superficial texture (**Figure 3-3**). This irregular texture is likely due to the formation of ultrafine fluorapatite crystals (~ 100 nm; Ca5(PO4)3F) (**Figure 3-4** & **Figure 3-5**). Microcrystalline fluorapatite is well-known to preserve soft-bodied fossils with the highest and most exceptional degree of detail and resolution (Briggs, 2003; Martill, 1989; Martill, 1990). In this closed anoxic system, fluorapatite most likely derived from the tissue of the decaying organism and/or from dissolution of bone hydroxyapatite (Briggs, 2003; Briggs and Kear, 1993). Fossilised RBC-like structures displayed enhanced carbon preservation (**Figure 3-4**) compared to the recrystallised bone (**Figure 3-4**), suggesting that besides the formation of a fluorapatite sheath, remnants of original biomolecules may still be present in the fossil RBC-like structures. The fluorapatite crystals formed a crust over the fragile organic structures, isolating and protecting them from the surrounding environment. By contrast, collagen-like fibres show a less intense carbon peak in their EDS signal (**Figure 3-5**), only slightly higher than the signal in the bone background, which suggests that the fossil collagen underwent a more extensive replacement by fluorapatite.

Two different explanations are proposed to account for the small size of these RBC-like structures, (i) post mortem alteration and/or (ii) evolutionary adaptation to environmental conditions.

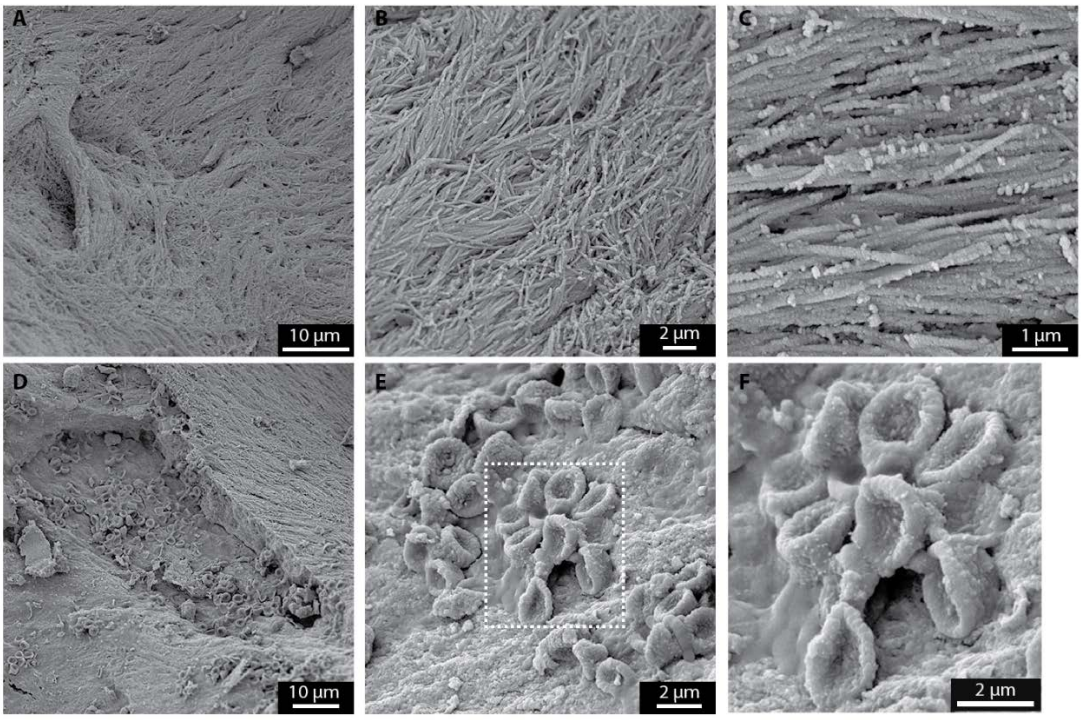

Figure 3-3. Secondary electron photomicrographs of the trabecular bone following the removal of sparry calcite by light acetic acid treatment revealing exceptionally well-preserved soft tissues. A) to C) represent collagen fibres (Bertazzo et al., 2015) with increasing magnification. The highest magnification image C) shows the presence of fluorapatite crystals (~100 nm width) on the collagen fibrils identified by energy dispersive spectroscopy (EDS; Figure 3-5). D) to F) represent RBCs with increasing magnification. The surface of these structures display a granular texture identified by EDS as fluorapatite (Figure 3-4)

Post mortem alteration

We propose that morphological changes of the RBC-like structures are related to the early formation of a relatively thin fluorapatite crust surrounding the cells shortly after death of the ichthyosaur. The three dimensional bowl-like shape of the RBC-like structures suggests they represent stomatocytes which could result from post-mortem modifications (*e.g.* reduced blood pH (Donaldson and Lamont, 2013)). Post mortem osmotic shrinkage is considered insufficient to explain the small cell size since a shrinkage of 80 % would have created significant space between the RBC-like structures. On the contrary, the RBC-like structures observed are closely distributed as

clusters, often packed and in contact with each other (**Figure 3-3D-F**), arguing against substantial osmotic shrinkage.

Evolutionary adaptation to environmental conditions

Ichthyosaurs evolved during an episode typified by low atmospheric oxygen levels, lasting over 70 million years from the Permian/Triassic boundary to the Lower Jurassic (Berner *et al.*, 2007). We suggest that under the prolonged low oxygen levels in the atmosphere (Berner, 2004, 2006; Poulsen *et al.*, 2015), small RBCs could have been favoured because the surface to volume ratio provides a more efficient oxygen transport and diffusion. The "bowl-like" shape of the cells resembling RBCs (*i.e.* stomatocytes) has been widely reported in disease-related studies of mammalian species with anucleated RBCs (Reagan *et al.*, 2008; Stewart, 2003). However, the study of blood in reptiles is limited, which makes the interpretation of reptilian hematologic data challenging (Claver and Quaglia, 2009; Nardini *et al.*, 2013).

We hypothesise that the fossil occurrence of small RBC-like structures in ichthyosaurs could be consistent with an oxygen-depleted marine palaeoenvironment and evolutionary adaptation. This adaptation is supported by the occurrence of RBC-like structures of similar size in terrestrial dinosaurs (Bertazzo *et al.*, 2015). Although oxygen concentrations reached today's levels during the Late Cretaceous (Tappert *et al.*, 2013), most of dinosaurs' evolution took place during prolonged periods of low oxygen levels and they lived under the same atmospheric conditions as the ichthyosaurs. With respect to adaption, we emphasize that Stenopterygius is considered to have been one of the fastest marine predators of its time (Motani, 2002), its cruising speed equivalent to that of modern day dolphin and with a similar morphology (Bernard *et al.*, 2010). The clustering of RBC-like structures in this Stenopterygius is consistent with a high degree of RBC aggregation reported in modern higher athletic species (Popel *et al.*, 1994). In order to sustain the metabolism required for high-speed pursuit predators, the muscular tissue must have been highly effective and have been supported by a complex blood circulation system, adapted to low-oxygen environment, to provide sufficient oxygen to the lungs of the breathing ichthyosaurs. Given that the bone studied is a medullary bone (*i.e.* vertebra), it would yield sufficient bone marrow (see below) to synthesise RBCs. Based on their small size, the fossilised RBC-like structures indicate a fast and efficient oxygen diffusion

into the cells, allowing for high pursuit speed and thus providing competitive advantage over slower moving prey.

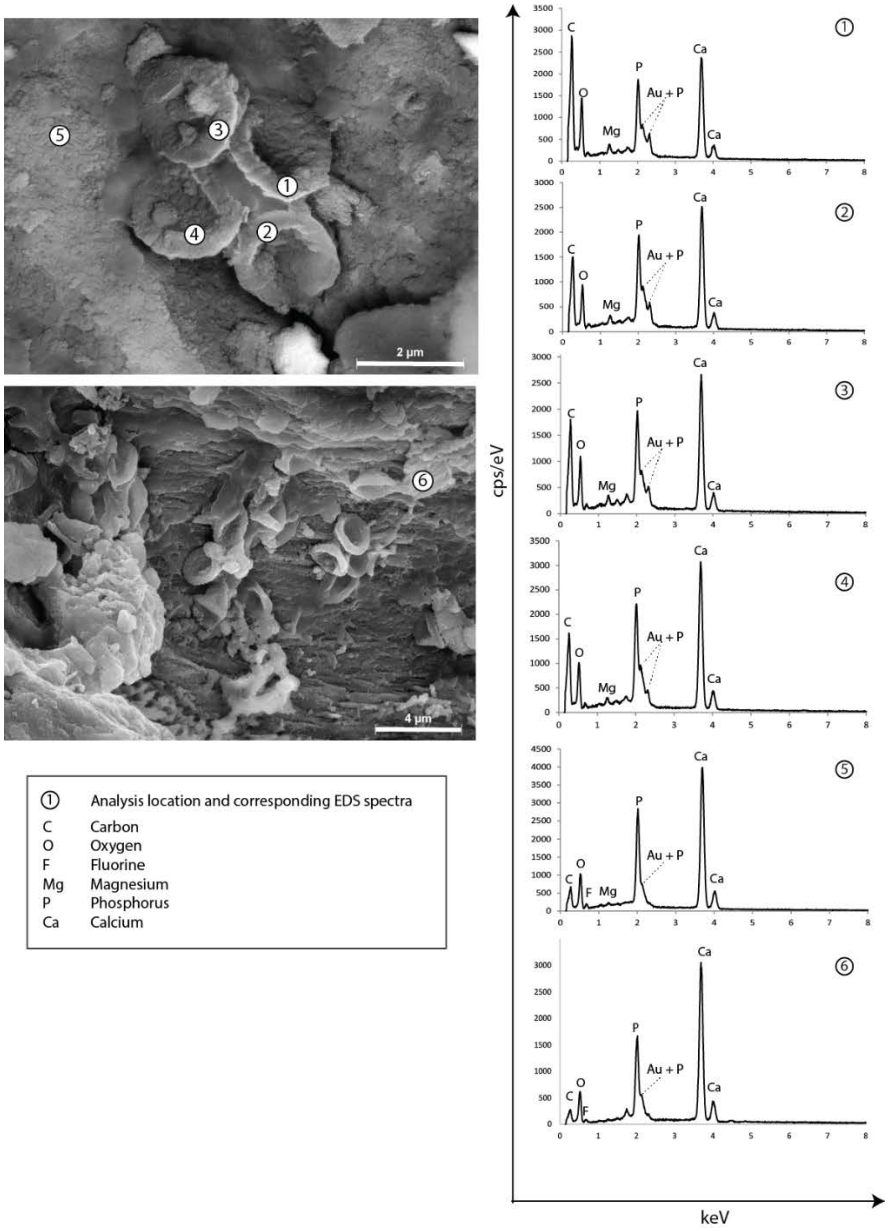

Figure 3-4. SEM images of RBCs with analysis locations of associated EDS spectra. Analyses 1 to 4 correspond to RBCs, and show a strong enrichment in C with a C-peak intensity 3 to 6 times greater than measured in analyses 5 and 6, performed on the bone background. Fluorapatite does not contain C in its structure and consequently the C signal present in analyses 5 and 6 is related to the C coating of the sample (signal of 300-600 cps/eV). These background bone analyses are reproducible on different areas of the bone. Therefore the high C peak of the RBCs is autochthonous. Not all RBCs display a strong C increase; however, the C signal of the bone is always low corresponding to the initial C coating of the sample. Gold (Au) corresponds to the sample coating.

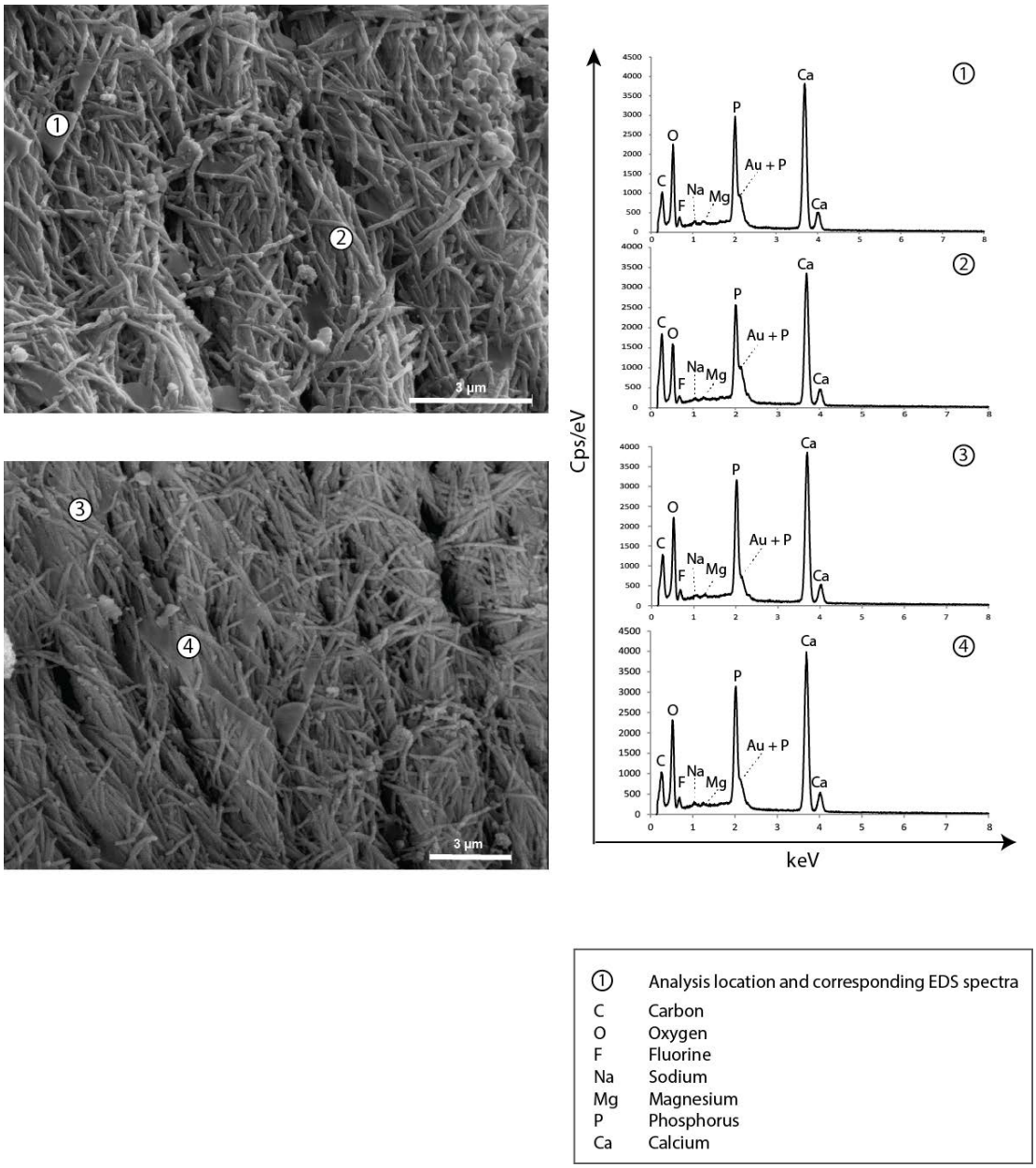

Figure 3-5. Scanning electron microphotographs of collagen fibre structures with analysis locations for associated EDS spectra. A) and B) SEM images with the location of four EDS spectra measured. C) to F) EDS spectra corresponding to the different points analysed. Gold (Au) corresponds to the sample coating.

Cholesterol in an ichthyosaur

Besides fossilised RBC-like structures, the ichthyosaur bone would have contained adipocytes, which have not been preserved morphologically. Their presence within the ichthyosaur bone and the preservation of biological material over ~ 182.7 Ma is documented by elevated concentrations of the intact biomolecule cholesterol (565 µg/g TOC, **Figure 3-** 6 & **Table A3-1**). It was previously reported that free cholesterol is relatively abundant in the bone marrow (Aigueperse *et al.*,

1978) supporting the high amount of neutrally extracted free bone cholesterol in our sample. The bone cholesterol differed significantly in its isotopic carbon composition (– 28.9 ‰ VPDB) compared to ethylcholesterol (– 34.6 ‰ VPDB; **Figure 3-** 6). The isotopic discrepancy between these two sterols supports different origin(s). The ^{13}C enrichment of the cholesterol by 4.5 ‰ VPDB indicates that it largely derives from a higher level in the food chain and corroborates a fish and cephalopod diet of the ichthyosaur (Druckenmiller *et al.*, 2014; Fröbisch *et al.*, 2013). The ^{13}C isotopic composition of the ethylcholesterol is consistent with a source from phytoplankton in the ancient water column. Recently, soft tissue of a crustacean inside a Devonian concretion from the Gogo Formation (Canning Basin, Western Australia) was reported to contain an entire diagenetic continuum of organic molecules with the remarkable co-occurrence of biomolecules and geomolecules, from sterols to triaromatic steroids (including sterenes and diasterenes) (Melendez *et al.*, 2013a). The exceptional preservation of these compounds was attributed to rapid encapsulation by microbially-mediated and eogenetic processes. In our study, steroid end-products of diagenesis were also identified in association with the vertebra (**Figure 3- 6C**). However, the absence of sterenes and diasterenes suggests the formation of the concretion within the sediments (corroborated by the preservation of slightly disturbed sedimentary bedding) and not in the water column (Melendez *et al.*, 2013a, 2013b). The Posidonia Shale Formation and the Gogo Formation concretions were both formed under similar euxinic (H_2S-rich) conditions and are well known Fossil Lagerstätten.

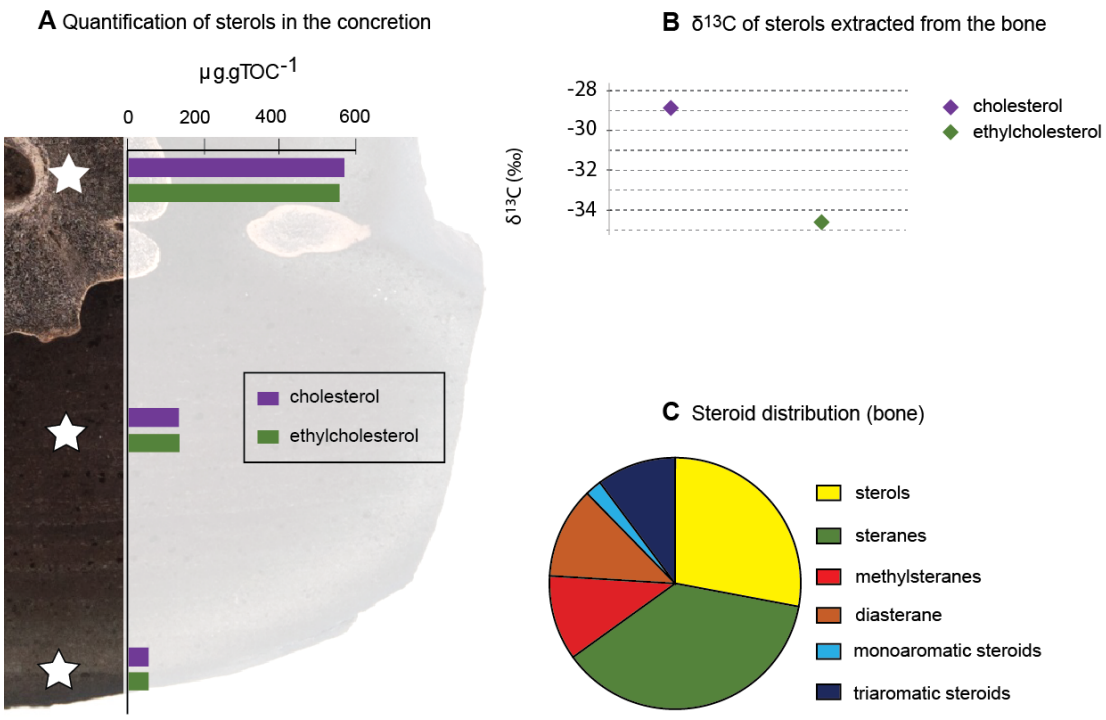

Figure 3- 6. Steroid distribution and compound specific $\delta^{13}C$ values. A) Sterol distribution within the bone and concretion, showing high concentrations of cholesterol (565 µg/g TOC) and ethylcholesterol (523 µg/g TOC) and negligible concentrations in the concretion body and rim. B) $\delta^{13}C$ values (‰ VPDB) of sterols associated with the bone (cholesterol: –28.9 ± 0.4 ‰ VPDB; ethylcholesterol: – 34.6± 0.4 ‰ VPDB. from the concretion. The error bars are contained within the symbol. C) Relative proportion of compound classes within the fossil, dominated by sterols and steranes representing the end-members of the diagenetic sequence.

Tight encapsulation of a Jurassic ichthyosaur bone in a diagenetically formed carbonate concretion allowed for the fossilisation of structures showing great resemblance to modern day bone collagen and RBCs with a high level of detail. It also led to the preservation of cholesterol, largely derived from the vertebra bone, over a period of ~ 182.7 million years. These observations highlight the development of a closed environment within carbonate concretions. In such cases, carbonate concretions preserve morphological (structural and cellular) and biomolecules as well as molecular fossils with an excellent level of detail, without significant diagenetic alteration. This outstandingly well-preserved primary biomaterial suggests that carbonate concretions could play a major role in the investigation of the palaeobiology of extinct species and in understanding the evolution of life. Based on the small size of the RBCs and their associated high oxygen diffusion capacity, we hypothesise that ichthyosaur must have followed a high-energy life style as a pursuit predator. This would distinguish its hunting strategy from that of an ambush predator life style as assumed for plesiosaurs.

Material and methods

Sample preparation

Three 1 cm-slices were cut from the central area of the lens shaped concretion, perpendicular to horizontal bedding. One slice was polished for microbeam X-Ray Fluorescence (XRF) (Bruker M4 TORNADO^{TM}) elemental mapping. A thin section of the vertebra was prepared from the second slice. From the third slice, three samples were taken from i) vertebra, ii) concretion body presenting sedimentary bedding and iii) concretion rim for organic geochemical and compound specific isotope analyses (CSIA). Each sample was cleaned in an ultrasonic bath using a mixture of dichloromethane: methanol (DCM: MeOH) at 9:1 (v/v) (3 x 20 min) to remove any surface contaminants. Fossil bone samples were crushed and mm-sized pieces of bone were collected and treated with 1 M acetic acid solution prior to SEM imaging. The remainder of the samples was pulverized using a Rocklabs benchtop ring mill (BTRM) in a pre-annealed zircon mill. Pre-annealed quartz sand was pulverised and analysed as a procedural blank for organic geochemical techniques. Mineralogy was determined using aliquots of pulverised samples for X-ray diffraction (XRD).

A modern crocodile leg sample was obtained from Mahogany Creek Distributors (Perth, Australia). The bones were cut and isolated from the flesh. A sample was then left to dry in the oven for 24 h (50°C, below the denaturation threshold of native hydrated collagen fibrils (Bozec and Odlyha, 2011)) and treated with concentrated H_2O_2 (48 h). The oxidised flesh and bone marrow were removed using tweezers and the bone was left to dry at room temperature.

Mineralogy

XRD analyses on powdered samples were performed using a Bruker-AXS D8 Advance Diffractometer with CuKα radiation and a LynxEye position sensitive detector. The data were collected from 7.5 to 90° 2Θ, with a nominal step size of 0.015° and a collection time of 0.7 seconds per step. Crystalline phases were identified using the Search/Match algorithm, DIFFRAC.EVA 3.1 (Bruker-AXS) to search the Powder Diffraction File.

Imaging methods

Porosity estimation

The estimation of the trabecular porosity of the ichthyosaur vertebra has been determined through digital point counting on a recursive grid to two times 200 points and stabilisation of the point count distribution plot. The overall trabecular porosity evaluated was estimated at 59.5 %.

Microbeam XRF mapping

A Bruker M4 TORNADO™ Micro-XRF equipped with a rhodium target X-ray tube operating at 50 kV and 500 nA and an XFlash® silicon drift X-ray detector was used for elemental mapping of the polished slice of the Toarcian concretion samples. Maps were created using a 25 µm spot size on a 25 µm raster with dwell time of 5 ms per pixel.

Scanning Electron Microscopy

Both modern crocodile and fossil ichthyosaur bone samples were coated using a Quorum Q150T ES coating unit. A carbon layer of approximately 25 nm was applied and as samples were charging, an additional thin coating of gold (3-5 nm) was applied.

The bone samples were examined using a Tescan Mira-3 Field Emission Scanning Electron Microscope (FESEM). The instrument was operated with an accelerating voltage 5 kV and a beam current of approximately 200 pA. The images acquired were collected with using an Everhart-Thornley Secondary Electron (SE) detector.

Lipid biomarker analyses.

Toarcian samples were subject to Soxhlet extraction with a mixture of DCM: MeOH (9:1, 72 hrs). Activated copper turnings were added to remove elemental sulfur. An aliquot of each total lipid extract was adsorbed onto activated silica gel (160 °C, > 24 hrs). Each aliquot was then separated using column chromatography with a small column containing activated silica gel (5 cm x 0.5 cm i.d.) into five fractions. i) The aliphatic hydrocarbon fraction was eluted using 2 mL of *n*-hexane; ii) the aromatic hydrocarbon fraction was eluted with 2 mL *n*-hexane: DCM (4:1); iii) the ketone and

fatty acid methyl esters fraction was eluted with 2 mL DCM; iv) the alcohol fraction was eluted with 2 mL DCM: ethyl acetate (4:1) and v) the polar fraction was eluted using DCM: MeOH (7:3).

Alcohols were derivatised using bis(trimethylsilyl)-trifluoroacetamide (BSTFA) and anhydrous pyridine (for 100 µg, 60 µL BSTFA, 40 µL pyridine) heated at 70 °C for 30 min and dried under a nitrogen purge. The fractions were dissolved in *n*-hexane and analysed using gas chromatography-mass spectrometry (GC-MS). Semi quantitative analyses of the aliphatic hydrocarbon and aromatic fractions were performed after spiking the fractions with a known amound of internal standard. On the alcohol fraction, semi quantitative analyses were carried out using external calibration with a derivatised cholesterol standard. Procedural blanks were performed throughout.

GC-MS analyses were performed using a Hewlett Packard 6890 gas chromatograph (GC) interfaced with a Hewlett Packard 5973 mass selective detector. The GC was equipped with a split/splitless injector and a DB-5 capillary column (60 m x 0.25 mm i.d. coated with a 0.25 µm film thickness). The initial oven temperature (50 ˚C) was increased at a rate of 6 ˚C/min until reaching the final temperature (320 ˚C), initial and final hold times were 1 minute and 24 minutes, respectively. Ultra-high purity helium was used as a carrier gas at a constant flow (1.1 mL/min). The MS detector was operated at 70 eV (full scan) from 35 - 650 Da.

CSIA was performed on a Thermo Finnigan Delta V mass spectrometer coupled to an Isolink GC. A pure cholesterol standard (underivatised and derivatised) was analysed in order to calculate the $\delta^{13}C$ of the additional methyl-groups from BSTFA (Jones *et al.*, 1991). Samples were run as triplicates and the $\delta^{13}C$ values of the parent compounds were corrected for the isotopic composition from the methyl-groups of the BSTFA. A CO_2 reference gas standard with a known $\delta^{13}C$ value was introduced during CSIA to determine the $\delta^{13}C$ values of the sterols. The $\delta^{13}C$ are reported in per mil (‰) relative to the international Vienna Peedee Belemnite standard (VPDB).

Acknowledgements

The authors thank Geoff Chidlow, Alex Holman and Marieke Sieverding for their technical support with GC-MS, GC-irMS and GC-MS-MS analyses. Robert Madden is thanked for his assistance with optical imaging and porosity estimation. Sebastian's Butchers (Kalamunda, WA) is thanked for cutting and de-fleshing the crocodile bones. Grice and Plet thank the Australian Research Council (ARC) for an ARC-DORA grant (awarded to Grice: DP130100577) and for Plet's PhD stipend. Plet acknowledges Curtin University for a fee waiver and The Institute of Geoscience Research (TIGeR) for a top-up scholarship, as well as the European Association of Organic Geochemist (EAOG) for a travel award to the organic geochemistry workgroup at Christian Albrecht University (Germany). Schwark acknowledges support by DFG-grant (Schw554/23-1,2) as well as permission to conduct and assistance with field work by M. Jaeger, who identified the *Stenopterygius sp.* and A. Schmidt-Roehl, HOLCIM, Dotternhausen. The species was identified by comparison with other curated specimens of *Stenopterygius*.

References

Aigueperse, J., Remy, J., Chevallier, F., 1978. Sterols in various organs of adult female swine. *Annales de biologie animale, biochimie, biophysique* **18**, 1317–1324.

Asara, J.M., Schweitzer, M.H., Freimark, L.M., Phillips, M., Cantley, L.C., 2007. Protein sequences from mastodon and Tyrannosaurus rex revealed by mass spectrometry. *Science* **316**, 280–285.

Bernard, A., Lécuyer, C., Vincent, P., Amiot, R., Bardet, N., Buffetaut, E., Cuny, G., Fourel, F., Martineau, F., Mazin, J.-M., Prieur, A., 2010. Regulation of body temperature by some Mesozoic marine reptiles. *Science* **328**, 1379–1382.

Berner, R.A., 2004. The Phanerozoic carbon cycle: O_2 and CO_2. Oxford University Press.

Berner, R.A., 2006. GEOCARBSULF: A combined model for Phanerozoic atmospheric O_2 and CO_2. *Geochimica et Cosmochimica Acta* **70**, 5653–5664.

Berner, R.A., Vandenbrooks, J.M., Ward, P.D., 2007. Oxygen and Evolution. *Science* **316**, 557–559.

Berner, Z.A., Puchelt, H., Nöltner, T., Kramar, U., 2013. Pyrite geochemistry in the Toarcian Posidonia Shale of south-west Germany: Evidence for contrasting trace-element patterns of diagenetic and syngenetic pyrites. *Sedimentology* **60**, 548–573.

Bertazzo, S., Maidment, S.C.R., Kallepitis, C., Fearn, S., Stevens, M.M., Xie, H., 2015. Fibres and cellular structures preserved in 75-million–year-old dinosaur specimens. *Nature Communications* **6**, 7352.

Bozec, L., Odlyha, M., 2011. Thermal denaturation studies of collagen by microthermal analysis and atomic force microscopy. *Biophysical Journal* **101**, 228–236.

Briggs, D.*E.G.*, 2003. The role of decay and mineralization in the preservation of soft-bodied fossils. *Annual Review of Earth and Planetary Sciences* **31**, 275–301.

Briggs, D.*E.G.*, Kear, A.J., 1993. Fossilization of soft tissue in the laboratory. *Science* **259**, 1439–1442.

Claver, J.A., Quaglia, A.*I.E.*, 2009. Comparative Morphology, Development, and Function of Blood Cells in Nonmammalian Vertebrates. *Journal of Exotic Pet Medicine* **18**, 87–97.

Danise, S., Twitchett, R.J., Matts, K., 2014. Ecological succession of a Jurassic shallow-water ichthyosaur fall. *Nature communications* **5**, 4789.

Donaldson, A.E., Lamont, I.L., 2013. Biochemistry changes that occur after death: Potential markers for determining post-mortem interval. *PLoS ONE* **8**, 1–10.

Druckenmiller, P.S., Kelley, N., Whalen, M.T., McRoberts, C., Carter, J.G., 2014. An Upper Triassic (Norian) ichthyosaur (Reptilia, Ichthyopterygia) from northern Alaska and dietary insight based on gut contents. *Journal of Vertebrate Paleontology* **34**, 1460–1465.

Fischer, V., Bardet, N., Benson, R.B.J., Arkhangelsky, M.S., Friedman, M., 2016. Extinction of fish-shaped marine reptiles associated with reduced evolutionary rates and global environmental volatility. *Nature communications* **7**, 1–11.

Fröbisch, N.B., Fröbisch, J., Sander, P.M., Schmitz, L., Rieppel, O., 2013. Macropredatory ichthyosaur from the Middle Triassic and the origin of modern trophic networks. *Proceedings of the National Academy of Sciences of the United States of America* **110**, 1393–7.

Greenwalt, D.E., Goreva, Y.S., Siljeström, S.M., Rose, T., Harbach, R.E., 2013. Hemoglobin-derived porphyrins preserved in a Middle Eocene blood-engorged mosquito. *Proceedings of the National Academy of Sciences of the United States of America* **110**, 18496–18500.

Jones, D.M., Carter, J.F., Eglington, G., Jumeau, E.J., Fenwick, C.S., 1991. Determination of $\delta^{13}C$ values of sedimentary straight chain and cyclic alcohols by

gas chromatography/isotope ratio mass spectrometry. *Journal of mass spectrometry* **20**, 641–646.

Leduc, T., 2012. Diagenesis of the fossil bones of Iguanodon bernissartensis from the Iguanodon sinkhole, in: Godefroit, P. (Ed.), Bernissart Dinosaurs and Early Cretaceous Terrestrial Ecosystems. Indiana University Press, pp. 111–136.

Lee, Y.-C., Chiang, C.-C., Huang, P.-Y., Chung, C.-Y., Huang, T.D., Wang, C.-C., Chen, C.-I., Chang, R.-S., Liao, C.-H., Reisz, R.R., 2017. Evidence of preserved collagen in an Early Jurassic sauropodomorph dinosaur revealed by synchrotron FTIR microspectroscopy. *Nature Communications* **8**, 14220.

Lopuchowycz, V.B., Massare, J.A., 2002. Bone Microstructure of a Cretaceous Ichtyosaur. *Paludicola* **3**, 139–147.

Marshall, J.D., Pirrie, D., 2013. Carbonate concretions-explained. *Geology Today* **29**, 53–62.

Martill, D.M., 1988. Preservation of fish in the Cretaceous Santana Formation of Brazil. *Palaeontology* **31**, 1–18.

Martill, D.M., 1989. The Medusa effect: instantaneous fossilization. *Geology Today* **5**, 201–205.

Martill, D.M., 1990. Macromolecular resolution of fossilized muscle tissue from an elopomorph fish. *Nature* **346**, 171–172.

Melendez, I., Grice, K., Schwark, L., 2013a. Exceptional preservation of Palaeozoic steroids in a diagenetic continuum. *Scientific reports* **3**, 2768.

Melendez, I., Grice, K., Trinajstic, K., Ladjavardi, M., Greenwood, P., Thompson, K., 2013b. Biomarkers reveal the role of photic zone euxinia in exceptional fossil preservation: An organic geochemical perspective. *Geology* **41**, 123–126.

Motani, R., 2002. Scaling effects in caudal propulsion and the speed of ichthyosaurs. *Nature* **415**, 309–312.

Motani, R., 2005. Evolution of Fish-Shaped Reptiles (Reptilia: Ichthyopterygia) in Their Physical Environments and Constraints. *Annual Review of Earth and Planetary Sciences* **33**, 395–420.

Nardini, G., Leopardi, S., Bielli, M., 2013. Clinical hematology in reptilian species. *Veterinary Clinics of North America: Exotic Animal Practice* **16**, 1–30.

Popel, A.S., Johnson, P.C., Kameneva, M. V, Wild, M.A., 1994. Capacity for red blood cell aggregation is higher in athletic mammalian species than in sedentary species. *Journal of applied physiology (Bethesda, Md. : 1985)* **77**, 1790–4.

Poulsen, C.J., Tabor, C., White, J.D., 2015. Long-term climate forcing by atmospheric oxygen concentrations. *Science* **348**, 1238–1242.

Reagan, W.J., Irizarry Rovira, A.R., DeNicola, D.B., 2008. Veterinary hematology. Atlas of common domestic and non domestic species, 2nd ed. Wiley-Blackwell.

Röhl, H., Schmid-Röhl, A., Oschmann, W., Frimmel, A., Schwark, L., 2001. The Posidonia Shale (Lower Toarcian) of SW-Germany : an oxygen-depleted ecosystem controlled by sea level and palaeoclimate. *Palaeogeography, Palaeoclimatology, Palaeoecology* **165**, 27–52.

Sanchez, S., Tafforeau, P., Ahlberg, P.E., 2014. The humerus of Eusthenopteron: a puzzling organization presaging the establishment of tetrapod limb bone marrow. *Proceedings. Biological sciences / The Royal Society* **281**, 20140299.

Schmid-Röhl, A., Röhl, H., Oschmann, W., Frimmel, A., 2002. Palaeoenvironmental reconstruction of Lower Toarcian epicontinental black shales (Posidonia Shale , SW Germany): global versus regional control. *Geobios* **35**, 13–20.

Schwark, L., Frimmel, A., 2004. Chemostratigraphy of the Posidonia Black Shale, SW-Germany II. Assessment of extent and persistence of photic-zone anoxia using aryl isoprenoid distibutions. *Chemical Geology* **206**, 231–248.

Schweitzer, M.H., Johnson, C., Zocco, T.G., Horner, J.R., Starkey, J.R., 1997. Preservation of biomolecules in cancellous bone of Tyrannosaurus rex. *Journal of Vertebrate Paleontology* **17**, 349–359.

Schweitzer, M.H., Suo, Z., Avci, R., Asara, J.M., Allen, M.A., Teran Arce, F., Horner, J.R., 2007a. Analyses of soft tissue from Tyrannosaurus rex suggest the presence of protein. *Science* **316**, 277–280.

Schweitzer, M.H., Wittmeyer, J., Horner, J.R., Toporski, J.K., 2005. Soft-tissue vessels and cellular preservation in *Tyrannosaurus rex*. *Science* **307**, 1952–1955.

Schweitzer, M.H., Wittmeyer, J.L., Horner, J.R., 2007b. Soft tissue and cellular preservation in vertebrate skeletal elements from the Cretaceous to the present. *Proceedings. Biological sciences / The Royal Society* **274**, 183–197.

Schweitzer, M.H., Zheng, W., Cleland, T.P., Goodwin, M., Boatman, E., Theil, E., Marcus, M.A., Fakra, S.C., 2014. A role for iron and oxygen chemistry in preserving soft tissues, cells and molecules from deep time. *Proceedings. Biological sciences / The Royal Society* **281**, 20132741.

Stewart, G.W., 2003. The hereditary stomatocytosis and allied conditions': inherited disorders Na+ and K+ transport, in: Ingolf, B., Clive, E.J. (Eds.), Red Cell Membrane Transport in Health and Disease. Springer Berlin Heidelberg, pp. 511–523.

Tappert, R., McKellar, R.C., Wolfe, A.P., Tappert, M.C., Ortega-Blanco, J., Muehlenbachs, K., 2013. Stable carbon isotopes of C_3 plant resins and ambers record changes in atmospheric oxygen since the Triassic. *Geochimica et Cosmochimica Acta* **121**, 240–262.

Yoshida, H., Ujihara, A., Minami, M., Asahara, Y., Katsuta, N., Yamamoto, K., Sirono, S., Maruyama, I., Nishimoto, S., 2015. Early post-mortem formation of carbonate concretions around tusk-shells over week-month timescales. *Scientific reports* 1–7.

Ziegler, P.A., 2005. EUROPE : Permian to Recent Evolution: Jurassic, in: Selley, R.C., Cocks, L.R.M., Plimer, I.R. (Eds.), Encyclopedia of Geology. Elsevier, pp. 106–112.

Appendix 3

Table A3-1. Shows the total organic and inorganic carbon contents of the samples studied and the proportion of CaCO3 inferred from weight loss after acid treatment and from the total inorganic carbon (TIC) contents, assuming TIC is present as calcite only. The minor shift in values between the two methods is attributed to the higher uncertainty of the weight loss measurement; however, values strongly suggest TIC is contained in the calcite.

	TOC (%)	TIC (%)	$CaCO_3$ (wt.%) (by weight loss)	$CaCO_3$ (wt.%) (measured based on TIC)
Bone	0.23	7.1	55.6	59.1
Concretion body	1.13	10.5	90.4	87.5
Concretion rim	2.01	7.9	68.2	65.8

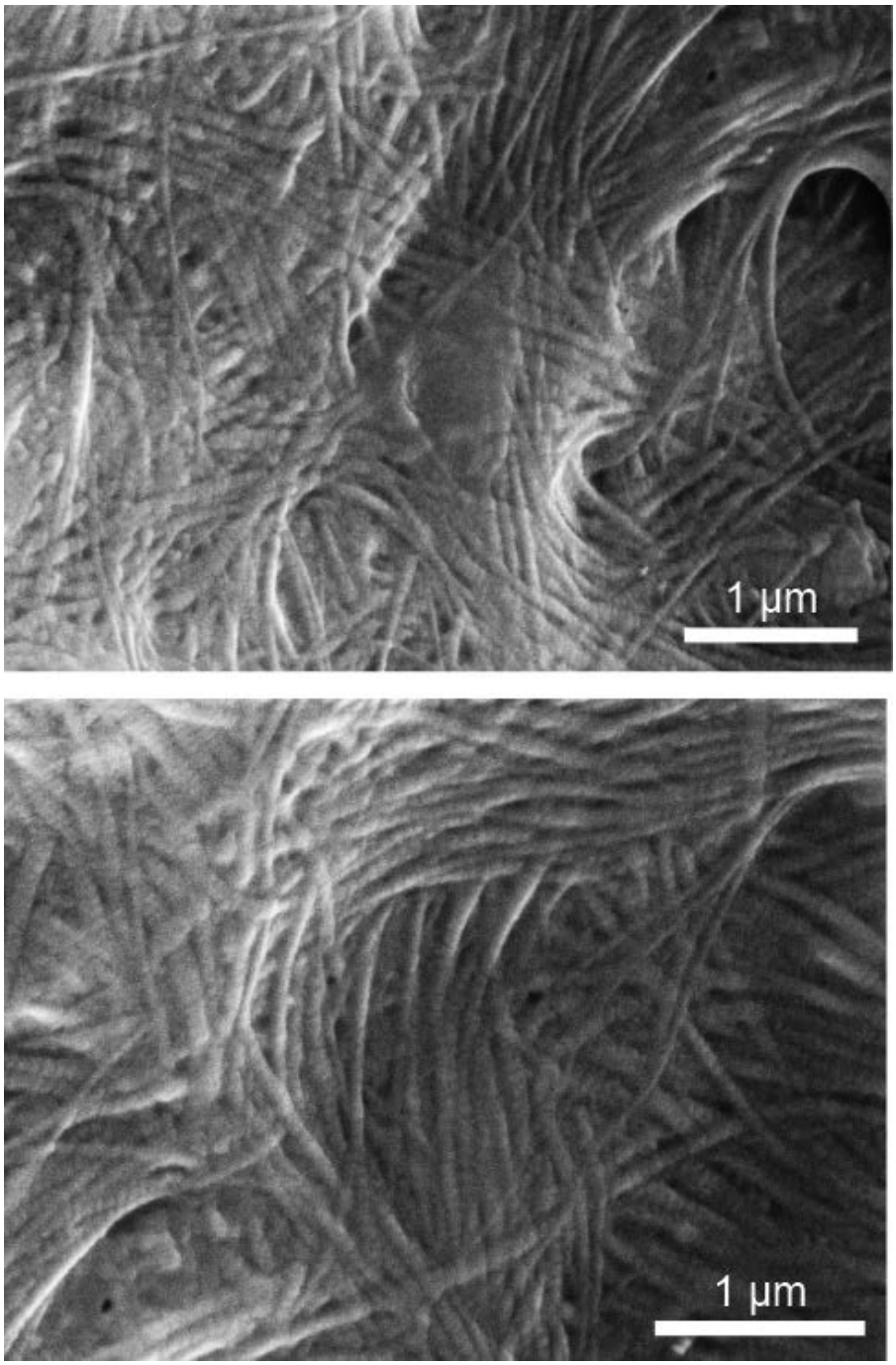

Figure A3- 1. SEM images of collagen fibres in a modern crocodile bone. Abundant flexible fibres that show darker banding, characteristic of collagen, were observed. These images display strong morphological similarities (shape and size) with the collagen-like fibres identified in the fossil ichthyosaur bone (Figure 3-3).

Chapter 4

The distribution and stable carbon isotopic composition of 2-methyl-3-ethyl-maleimide (1*H*-pyrrole-2,5-dione) within a Toarcian (182.7Ma) fossiliferous carbonate concretion

Chloé Plet, Naeher Sebastian, Anais Pagès, Wolfgang Ruebsam, Lorenz Schwark, Kliti Grice

Organic geochemistry, in preparation

(Impact factor: 3.072)

Abstract

The identification of 2-methyl-3-ethyl-maleimide (MEM) and its ^{13}C signature, coupled with the identification of 2-methyl-3-*iso*-butyl-maleimide (MIBM) in a carbonate concretion support the existence of photic zone euxinia in the ancient water column at the time of formation of the concretion. Regular isoprenoids (pristane and phytane) were ^{13}C-depleted, however both showed $\delta^{13}C$ values within a similar range, supporting a common origin from oxygenic phototrophs (*e.g.* algae and cyanobacteria). The co-occurrence of ^{13}C-depleted pristane and phytane with relatively ^{13}C-enriched MEM corroborate the occurrence of a stratified water column at the time of concretion formation.

The nucleus of the concretion, a vertebra bone that was encapsulated in the carbonate matrix, show the presence of MEM, whereas MIBM not detected. The low relative abundance of MEM in the vertebra bone did not allow for $\delta^{13}C$ analyses. However, the occurrence of the oldest fossilised red blood cells in this vertebra associated with the absence of MIBM suggest a possible origin from heme for the MEM. To confirm or invalidate this hypothesis, further investigation on greater amount of sample is required. Although impregnation of maleimides into the concretion matrix from the surrounding sediment cannot be entirely ruled out, the formation of maleimides during weathering and/or storage of the sample is highly unlikely.

Introduction

Maleimides (1*H*-pyrrole-2,5-diones) are oxidation products of tetrapyrrole pigments (*e.g.* intact chlorophylls, bacteriochlorophylls, chlorins and porphyrins) and have been reported in marine and lacustrine sediments, sedimentary rocks and crude oils (*e.g.* Grice *et al.*, 1997, 1996; Naeher *et al.*, 2013; Quirke *et al.*, 1980). The most common and abundant maleimide is 2-methyl-3-ethyl-maleimide (methyl ethyl maleimide: MEM), which can originate from all tetrapyrrole pigments (*e.g.* Grice *et al.*, 1996; Naeher *et al.*, 2013) including heme (Ellsworth, 1970). However, the main source of MEM is usually chlorophyll *a* (and its derivatives), which is present in most oxygenic photosynthetic organisms. MEM and its stable isotopic signature can be a

useful indicator for establishing its source organism (*e.g.* chlorophyll *a* of algae and cyanobacteria and/or bacteriochlorophylls *c*, *d*, *e* of *Chlorobiaceae*) and the depositional environment for recent (Naeher *et al.*, 2013) and ancient sediments (Grice *et al.*, 1996, 1997). In contrast, it has been shown (based on structural and isotopic grounds) that 2-methyl-3-*iso*-butyl-maleimide (methyl *iso*-butyl maleimide: MIBM) is ultimately derived from bacteriochlorophylls *c, d, e* of *Chlorobiaceae* (Grice *et al.*, 1996). Therefore. MIBM is considered a strong proxy for photic zone euxinia.

Carbonate concretions are known for their exceptional preservation of morphological fossils (*e.g.* Marshall and Pirrie, 2013), and more recently examples of exceptional lipid and OM preservation have been reported (Melendez *et al.*, 2013a, 2013b; Plet *et al.*, 2016). In this study, we investigate the distribution of two maleimides (MEM and MIBM) as well as the carbon isotopic composition of MEM and regular isoprenoids within a freshly sampled carbonate concretion from the Lower Toarcian (182.7 Ma) and containing fossil bones. The overall aim is to identify the potential source(s) of the maleimides detected in the bone and the carbonate matrix.

Materials and methods

Study site and sample preparation.

The concretion studied was sampled from the Lower Toarcian Posidonia Shale Formation outcrop of the HOLCIM cement quarry of Dotternhausen (SW-Germany), a detailed description of the sampling site is reported in Plet *et al.* (2016). The concretion was taken soon after blasting preventing major weathering. However, it was *ex-situ* released from its surrounding sediment and its exact stratigraphic position was lost. The concretion was sliced vertically shortly before organic geochemical analyses and revealed the presence of fossil bones (**Figure 4-1A**), including a vertebra, that were attributed to an ichthyosaur (M. Jaeger, *pers. comm.*).

Local preservation of sedimentary bedding was observed within the concretion. The vertebra was encapsulated within a calcite matrix (**Figure 4-1A**) surrounded by a pyrite-rich rim (Plet *et al.*, 2016 and references therein). Samples were taken along a vertical transect including the vertebra (**Figure 4-1B**). Each sample (ca.

3 cm^3) was cleaned and prepared following the same procedure reported in Plet *et al.* (2016).

Maleimide analysis

The detailed procedure used for maleimide purification is reported in Naeher *et al.* (2013). In short, polar fractions were purified by thin layer chromatography (TLC) using DCM: ethyl acetate (EtOAc) (4:1, v:v), along with a reference compound (H,H maleimide; Sigma Aldrich) used as a retention standard. The band between retention factor (Rf) 0.6 and 0.9 (containing the maleimides) was recovered by elution with EtOAc over a small silica gel column.

Derivatisation with *N*-(*tert*-butyldimethylsilyl)-*N*-methyl trifluoroacetamide (MTBSTFA) in pyridine was performed to obtain *tert*-butyldimethylsilyl (TBDMS) derivatives of maleimides (*e.g.* Grice *et al.*, 1996; Naeher *et al.*, 2013). TBDMS derivatives of maleimides in *n*-hexane were analysed by gas chromatography-mass spectrometry (GC-MS) using an Agilent HP 6890 GC system equipped with an Agilent DB-5MS column [60 m x 0.25 mm i.d. x 0.25 µm f.t.] coupled to an Agilent 5973 Mass Selective Detector operated at 70 *eV*. The temperature program for both instruments was 40 °C (1 min isothermal), 40 °C to 100 °C at 10 °C min^{-1}, 100 °C to 320 °C at 4 °C min^{-1}, isothermal at 320 °C for 30 min. Helium was used as carrier gas (1.2 mL min^{-1}). Quantification of MEM was performed *via* co-injection of phthalimide (as TBDMS derivative) of a known concentration and comparing the peak area of *m/z* 196, 224 and 204, base peaks for MEM, MIBM and phthalimide, respectively. The maleimides were identified based on their mass spectra, retention times and elution order based on the comparison with other published work (*e.g.* Grice *et al.*, 1996; Naeher *et al.*, 2016).

Carbon compound specific isotope analyses (C-CSIA) of maleimides

C-CSIA were performed on a Thermo Scientific Trace GC Ultra, interfaced to a Thermo Scientific Delta V Advantage mass spectrometer via a GC isolink and a Conflow IV. The combustion interface (ceramic tube lined with NiO and filled with NiO and CuO) was maintained at 1000 °C for analyses. The GC column used was a 60 m x 0.25 mm i.d. WCOT fused silica capillary column coated with a 0.25 µm film (DB-5MS), helium was used as carrier gas at a constant flow rate of 1.1 mL/min, and

samples were injected at 280 °C. The oven temperature was programmed from 40 °C to 325 °C at a rate of 3 °C/min with initial and final hold times of 1 and 30 minutes, respectively.

In order to determine the $\delta^{13}C$ values of the MEM corrected for derivatisation, a pure phthalimide standard was measured both underivatised and as TBDMS derivative. The $\delta^{13}C$ value for TBDMS group was calculated using **Equation 4-1** according to Jones *et al.* (1991). The $\delta^{13}C$ values for MEM (analysed as TBDMS derivatives) were measured and then corrected for the TBDMS group using **Equation 4-2**.

$$\delta^{13}C_{deriv} = \frac{\delta^{13}C_{derivatised\ standard} \times n_{derivatised\ standard} - \delta^{13}C_{standard} \times n_{standard}}{n_{deriv}}$$

Equation 4-1: Calculation of the $\delta^{13}C$ for a derivatisation group.

$$\delta^{13}C_{compound} = \frac{\delta^{13}C_{derivatised\ compound} \times n_{derivatised\ compound} - \delta^{13}C_{deriv} \times n_{deriv}}{n_{compound}}$$

Equation 4-2: Correction of the $\delta^{13}C$ value of a compound for a group added by derivatisation.

where "$n_{derivatised\ standard}$" is the number of carbon atoms in the phthalimide as TBDMS derivative (=14 carbon atoms), "$n_{standard}$" is the number of carbon atoms in non-derivatised phthalimide (=8 carbon atoms), "$n_{derivatised\ compound}$" is the number of carbon atom in MEM as TBDMS derivative (=13 carbon atoms), "$n_{compound}$" is the number of carbon atoms in underivatised MEM (=7 carbon atoms) and "n_{deriv}" is the number of carbon atoms added by derivatisation, here a TBDMS group (=6 carbon atoms).

All $\delta^{13}C$ values are reported in per mil (‰) relative to the Vienna Pee Dee Belemnite (VPDB) international standard. Each sample was run in triplicate and the standard deviation for all $\delta^{13}C$ of samples reported here is below 0.4 ‰.

Scanning Electron Microscopy (SEM)

Samples were coated using a Quorum Q150T ES coating unit. A carbon layer of approximately 25 nm was applied and where charging was still an issue an additional thin, approximately 3-5 nm, coating of gold was applied. The samples were examined using a Tescan Mira-3 Field Emission Scanning Electron Microscope (FESEM). The instrument was operated with an accelerating voltage 5 kV and a beam current of approximately 200 pA. The image was collected with using an Everhart-Thornley Secondary Electron (SE) detector.

Results and discussion

Source of maleimides and isoprenoids in a concretion

The sources of maleimides in the concretion and bone studied herein probably arise from different natural precursors (*i.e.* chlorophylls vs. bacteriochlorophylls vs. heme). As maleimides can form by i) primary natural oxidation processes or ii) during sample storage (Grosjean *et al.*, 2004), their distributions should mainly be governed by degradation process. However, the concentrations of maleimides could also be affected by iii) geochromatography, *i.e.* the different rate of migration of compounds and biomarkers within a mineral matrix, upon which more polar molecules such as maleimides are retained more strongly on mineral surfaces (*e.g.* Larter *et al.*, 2000; Li *et al.*, 1995, 1994). Each of these possibilities are discussed below together with limited $\delta^{13}C$ analyses of MEM, pristane (Pr) and phytane (Ph).

All isolated maleimide fractions were dominated by MEM (**Figure 4-2**, **Table 4-1**). For two samples (CV4 and CV5), $\delta^{13}C$ values were measured for both MEM, Pr and Ph. In these samples, $\delta^{13}C$ values for MEM were similar (CV4 = –25.3 ‰ and CV5 = –25.9 ‰). The $\delta^{13}C$ values for the regular isoprenoids Pr and Ph were also comparable to each other. Pr showed $\delta^{13}C$ values of –34.7 ‰ and –34.4 ‰ for CV4 and CV5, respectively and $\delta^{13}C$ of Ph was measured at –34 ‰ and –34.2 ‰ for CV4 and CV5, respectively (**Table 4-1**).

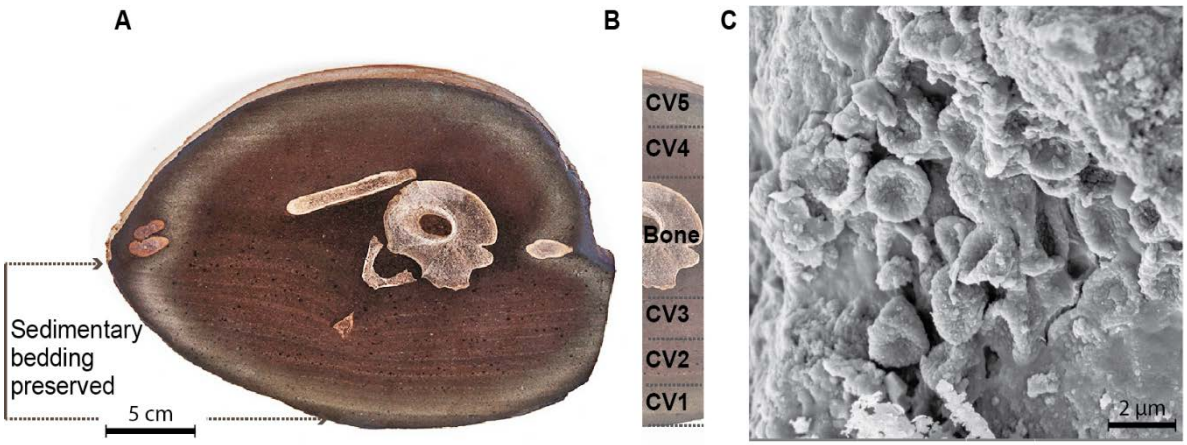

Figure 4-1. A) Slice of the concretion investigated showing the presence of an encapsulated vertebra bone and locally some slightly disturbed sedimentary bedding. B) Illustration of the vertical transect sampled with sample names. C) SEM imaging of the oldest fossilised red blood cells in association with the vertebra bone.

The similar low $\delta^{13}C$ values measured for Pr and Ph support a common origin for the regular isoprenoids in these samples ascribed largely to the phytol side of chlorophyll *a* (Bogacheva and Galimov, 1979; Galimov, 1977). Nonetheless, bacteriochlorophylls *a* and *b* of purple sulfur bacteria (*Chromatiaceae*), or tocopherol for Pr, cannot be fully excluded (Madigan *et al.*, 1989).

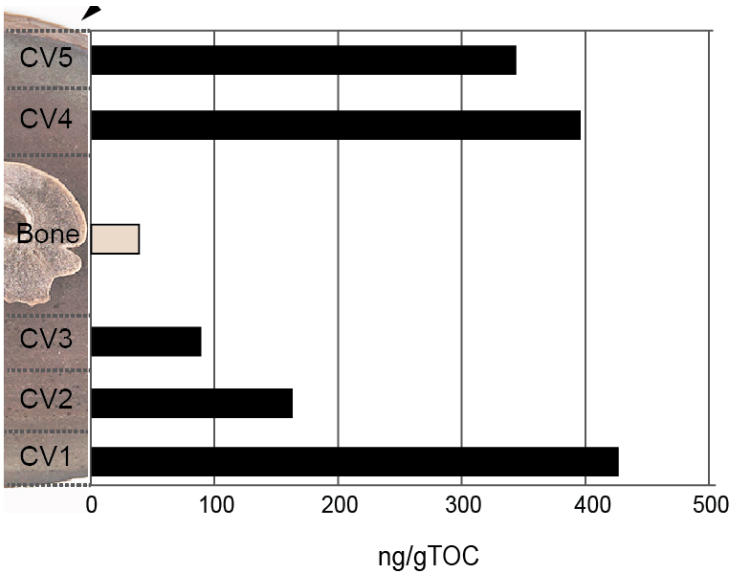

Figure 4-2: Distribution of MEM along a vertical transect through the concretion and the bone nucleus.

For example, Bogacheva and Galimov (1979) and Galimov (1977) showed that the phytol of side chain of both chlorophylls *a* and *b* from extant plants is about 4 ‰ more ^{13}C-depleted relative to their tetrapyrrole nucleus, which is due to their separate biosynthetic pathways. In this study, the $\delta^{13}C$ value of MEM is more than 8‰

^{13}C-enriched compared to that of Ph, and significantly greater (ca. 4 ‰) than expected for a common chlorophyll *a* origin (*i.e.* phytoplankton using a C_3 pathway for photosynthesis; Grice *et al.*, 1996). The ^{13}C-enrichment of MEM is attributed to the contribution of *Chlorobiaceae* (Quandt *et al.*, 1977) that is known to use the reverse tricarboxylic acid cycle (or reverse Krebs cycle) (Grice *et al.*, 1996).

The overall ^{13}C-enriched MEM supports a mixed source from chlorophyll *a* derived from algae and/or cyanobacteria, chlorophyll *b* from green algae and bacteriochlorophylls *c*, *d*, and *e* from *Chlorobiaceae*. Based on the relative abundances and the δ^{13}C values measured for MEM, it is unlikely that heme is a source of MEM in the concretion matrix.

Table 4-1. Characteristics of the samples analysed. When possible maleimide ratios and carbon isotopic values are reported. n.d. = not detected or too low to obtain a reliable value.

	TOC (wt. %)	MEM (ng/gTOC)	MIBM (ng/gTOC)	MIBM/MEM	$\delta^{13}C_{Pr}$ (‰VPDB)	$\delta^{13}C_{Ph}$ (‰VPDB)	$\delta^{13}C_{MEM}$ (‰VPDB)
CV1	2.01	427	3.5	$1.15x10^{-3}$	n.d.	n.d.	n.d.
CV2	1.39	163	1.8	$1.512x10^{-3}$	n.d.	n.d.	n.d.
CV3	0.8	89	nd	n.d.	n.d.	n.d.	n.d.
Bone	0.23	38	nd	n.d.	n.d.	n.d.	n.d.
CV4	1.13	396	3	$16.02x10^{-3}$	–34.7	–34.2	–25.3
CV5	1.47	344	3	$0.959x10^{-3}$	–34.4	–34	–25.9

MIBM is also detected (at low abundances) in all the matrix samples, concordant with a contribution of bacteriochlorophylls *c*, *d*, *e* source from *Chlorobiaceae* (MIBM/MEM ratios range between $0.959x10^{-3}$ and $16.02x10^{-3}$; **Table 4-1**). Considering the formation of the carbonate concretion within the sediments, as indicated by the presence of sedimentary bedding, maleimides and regular isoprenoids are likely derived from primary producers in the ancient water column. The presence of MIBM also corroborates the existence of a stratified water column (Röhl *et al.*, 2001; Schwark and Frimmel, 2004) and supports the existence of photic zone euxinia in the water column at the time of sedimentary accumulation.

Maleimides can also be oxidative artefacts formed during storage or weathering (Grice *et al.*, 1996; Grosjean *et al.*, 2004). However, this concretion was

collected fresh, which prevented major weathering and was analysed by organic geochemical methods shortly after the sample was sub-divided. Therefore, we exclude that the maleimides identified in this concretion are artefacts formed during storage or weathering.

Due to the formation of the concretion within an organic-rich black shale, the presence of maleimides in the concretion may potentially result in part from migration. Lipids, including maleimides, could impregnate the carbonate matrix by diffusion from the surrounding sediment and maleimides could migrate. Although, due to the exposed pyrrole functionality of maleimide, they would migrate at a lower rate than less polar hydrocarbons, leading to geochromatographic effects (Krooss *et al.*, 1991; Larter *et al.*, 2000; Li *et al.*, 1995, 1994). In this study, however, the carbonate matrix is well cemented presenting minor porosity and lacking septaria and cracks, which strongly supports that the vertebrae is isolated from potential environmental and diagenetic contaminants (**Chapter 3**). Furthermore, other compounds were found in the vertebra bone, such as cholesterol that has a $\delta^{13}C$ value largely consistent with the ichthyosaur's diet (**Chapter 3**). Because of the above facts, the impregnation of polar compounds by geochromatography seems highly unlikely.

Significance of MEM in a vertebra fossil

As mentioned above, MEM in the concretion is predominantly derived from chlorophyll *a* of phytoplankton with some contributions from and bacteriochlorophylls *c, d, e* of *Chlorobiaceae*. It is however possible that the lower relative abundance of MEM in the bone could be derived from heme as proposed by Ellsworth (1970) and also suggested by Boreham *et al.* (1989) who studied stable carbon isotopic composition of C_{32} etioporphyrin.

MIBM was not detected in the bone, which could indicate that MEM present in the bone is largely derived from heme rather than from the water column. Unfortunately, we were not able to measure the $\delta^{13}C$ of MEM in the bone due to low concentrations (**Table 4-1**). Further $\delta^{13}C$ analyses would need to be performed on a significantly larger sample to confirm the hypothesis of a heme origin. Interestingly, this ichthyosaur vertebra has revealed the presence of the oldest fossilised red blood

cells (see **Chapter 3**) and **Figure 4-1C**, which indirectly points to the possibility that MEM inside the bone could be derived from heme.

Conclusions and future work

The MEM present in the concretion matrix is largely derived from tetrapyrroles present in the water column and their $\delta^{13}C$ values indicate a mixed origin from algae and cyanobacteria, but also from *Chlorobiaceae*, which is supported by the presence of MIBM in the samples. This reveals the presence of photic zone euxinia in the ancient water column at the time of organic matter accumulation in the sediment. A secondary origin from weathering and storage for the maleimides has been ruled out. Moreover an impregnation from the surrounding sediments also seem highly unlikely.

In theory, the MEM present in the vertebra could also be the result of geochromatography. However, the presence of the oldest red blood cells identified in the sample and the low relative abundance of MEM strongly suggest that, in the vertebra bone, MEM could be derived from heme. Further analyses are to be performed on greater amounts of vertebra to measure the $\delta^{13}C$ of MEM and possibly investigate more biomarkers such as porphyrins, in particular C_{32} Fe-etioporphyrin that is believed to be derived from heme.

Acknowledgments

The authors thank Geoff Chidlow for his technical support with GC-MS analyses, as well as Alex Holman for GC-irMS analyses. Michael Verrall is thanked for his support and expertise in sample preparation and acquisition of SEM images. Grice and Plet thank the Australian Research Council for an ARC-DORA grant (DP130100577) and for Plet's PhD stipend. Plet acknowledges Curtin University for a fee waiver and The Institute of Geoscience Research for a top-up scholarship. Naeher acknowledges DFG Research Fellowship (NA 1172/1-1). Schwark acknowledges support by DFG grant (Schw554/23-1,2) as well as permission to conduct field work and assistance by M. Jaeger, who also identified the ichthyosaur remains.

References

Bogacheva, M.P., Galimov, E.M., 1979. Intramolecular distribution of carbon isotopes in chlorophyll and hemin. *Geokhimiya* **7**, 1166–1172.

Boreham, C.J., Fookes, C.J.R., Popp, B.N., Hayes, J.M., 1989. Origins of etioporphyrins in sediments: Evidence from stable carbon isotopes. *Geochimica et Cosmochimica Acta* **53**, 2451–2455.

Ellsworth, R.K., 1970. Gas chromatographic determination of some maleimides produced by the oxidation of heme and chlorophyll a. *Journal of Chromatography A* **50**, 131–134.

Galimov, E.M., 1977. Investigation of the distribution of carbon isotopes in biogenic compounds, in: Proceedings of the VIII International Congress on Organic Geochemistry. Nauka.

Grice, K., Gibbison, R., Atkinson, J.E., Schwark, L., Eckardt, C.B., Maxwell, J.R., 1996. Maleimides (1H-pyrrole-2,5-diones) as Molecular Indicators of Anoxygenic Photosynthesis in Ancient Water Columns. *Geochimica et Cosmochimica Acta* **60**, 3913–3924.

Grice, K., Schaeffer, P., Schwark, L., Maxwell, J.R., 1997. Changes in palaeoenvironmental conditions during deposition of the Permian Kupferschiefer (Lower Rhine Basin , northwest Germany) inferred from molecular and isotopic compositions of biomarker components. *Organic geochemistry* **26**, 677–690.

Grosjean, E., Adam, P., Connan, J., Albrecht, P., 2004. Effects of weathering on nickel and vanadyl porphyrins of a Lower Toarcian shale of the Paris basin. *Geochemica et Cosmochimica Acta* **68**, 789–804.

Krooss, B.M., Brothers, L., Engel, M.H., 1991. Geochromatography in petroleum migration: a review. *Geological Society, London, Special Publications* **59**, 149–163.

Larter, S.R., Bowler, B.F.J., Clarke, E., Wilson, C., Moffatt, B., Bennett, B., Yardley, G., Carruthers, D., 2000. An experimental investigation of

geochromatography during secondary migration of petroleum performed under subsurface conditions with a real rock. *Geochemical Transactions* **1**, 54.

Li, M., Larter, S.R., Stoddart, D., Bjorøy, M., 1995. Fractionation of pyrrolic nitrogen compounds in petroleum during migration: derivation of migration-related geochemical parameters. *Geological Society, London, Special Publications* **86**, 103–123.

Li, M.W., Larter, S.R., Frolov, Y.B., Bjoroy, M., 1994. Adsorptive Interaction between Nitrogen-Compounds and Organic and/or Mineral Phases in Subsurface Rocks - Models for Compositional Fractionation of Pyrrolic Nitrogen-Compounds in Petroleum During Petroleum Migration. *Journal of high resolution chromatography* **17**, 230–236.

Madigan, M.T., Takigiku, R., Lee, R.G., Gest, H., Hayes, J.M., 1989. Carbon isotope fractionation by thermophilic phototrophic sulfur bacteria : evidence for autotrophic growth in natural populations. *Applied and environmental microbiology* **55**, 639–644.

Marshall, J.D., Pirrie, D., 2013. Carbonate concretions-explained. *Geology Today* **29**, 53–62.

Melendez, I., Grice, K., Schwark, L., 2013a. Exceptional preservation of Palaeozoic steroids in a diagenetic continuum. *Scientific reports* **3**, 2768.

Melendez, I., Grice, K., Trinajstic, K., Ladjavardi, M., Greenwood, P., Thompson, K., 2013b. Biomarkers reveal the role of photic zone euxinia in exceptional fossil preservation: An organic geochemical perspective. *Geology* **41**, 123–126.

Naeher, S., Lengger, S.K., Grice, K., 2016. A new method for the rapid analysis of 1 H -Pyrrole-2 , 5-diones (maleimides) in environmental samples by two-dimensional gas chromatography time-of-flight mass spectrometry. *Journal of Chromatography A* **1435**, 125–135.

Naeher, S., Schaeffer, P., Adam, P., Schubert, C.J., 2013. Maleimides in recent sediments – Using chlorophyll degradation products for palaeoenvironmental reconstructions. *Geochimica et Cosmochimica Acta* **119**, 248–263.

Plet, C., Grice, K., Pagès, A., Ruebsam, W., Coolen, M.J., Schwark, L., 2016. Microbially-mediated fossil-bearing carbonate concretions and their significance for palaeoenvironmental reconstructions: A multi-proxy organic and inorganic geochemical appraisal. *Chemical Geology* **426**, 95–108.

Quandt, L., Gottschalk, G., Ziegler, H., Stichler, W., 1977. Isotope discrimination by photosynthetic bacteria. *FEMS Microbiology letters* 125–128.

Quirke, J., Shaw, G.J., Super, P.D., Maxwell, J.R., 1980. The presence of porphyrins with extended alkyl substituents. *Tetrahedron* **36**, 3261–3267.

Röhl, H., Schmid-Röhl, A., Oschmann, W., Frimmel, A., Schwark, L., 2001. The Posidonia Shale (Lower Toarcian) of SW-Germany : an oxygen-depleted ecosystem controlled by sea level and palaeoclimate. *Palaeogeography, Palaeoclimatology, Palaeoecology* **165**, 27–52.

Schwark, L., Frimmel, A., 2004. Chemostratigraphy of the Posidonia Black Shale, SW-Germany II. Assessment of extent and persistence of photic-zone anoxia using aryl isoprenoid distibutions. *Chemical Geology* **206**, 231–248.

Chapter 5

From supratidal to subtidal, an integrated characterisation of Carbla Beach shallow microbial mats (Hamelin Pool, Shark Bay, WA): lipid biomarkers, stable carbon isotopes and microfabrics.

Chloé Plet, Anais Pagès, Alex I. Holman, Robert H.C. Madden, Kliti Grice

Submitted to Geobiology

(Impact factor: 3.462)

Abstract

Modern microbial mats from Shark Bay are commonly regarded as robust analogues for Precambrian stromatolites. These microbial mats are complex ecosystems that exhibit intense biogeochemical recycling. In this study, a multi-proxy approach (including lipids, compound specific carbon isotope analysis and petrography) is used to characterise microbial communities in three different types of mats (tufted, pustular and smooth) along the shallowest section of a tidal flat gradient.

Cyanobacterial lipids were present in all three mats; yet, the cyanobacterial variability was only revealed by imaging techniques (filamentous cyanobacteria dominant in the tufted and smooth mats *vs.* coccoid cyanobacteria in the pustular mat). Petrographical (Scanning Electron Microscopy) investigations also revealed abundant ooids in the tufted mat, which decreased in size and abundance in the pustular and smooth mats. Biomarkers specific to sulfate reducing bacteria were detected in all mats. The diatom-specific $C_{25:1}$ highly branched isoprenoid alkene was most abundant in the smooth mat. However, it revealed that the smooth mat only contained rare diatoms of small size (~10 µm) whereas the pustular mat contained abundant and large diatoms (~50 µm). The $C_{25:1}$ HBI alkene marker is only produced by four diatom genera, which were most likely dominant in the smooth mat. Additionally, the smooth mat contained a greater input of aquatic macrophytes (Paq=0.38) compared to the shallower mats, which is corroborated by the presence of ^{13}C-enriched seagrass lipids.

In all the mats, a major eukaryotic input was revealed *via* imaging techniques and supported by a high sterol content. This eukaryotic component can impact the cohesive structure of the mats, the lithification processes and the lipid distribution, potentially leading to a challenging comparison with Precambrian microbialites that were not affected by eukaryotic activity. This study reemphasizes the complexity of microbial ecosystems and therefore, highlights the benefit of multi-proxy approaches to characterise these biological systems.

.

Introduction

Stromatolites are biological laminated structures that have been detected in the rock record up to 3.5 Ga and are recognised as the earliest evidence of life on Earth (Hoffman, 2000). Although stromatolites are widespread in the geological record, nowadays the distribution of microbial ecosystems building stromatolites is limited (Reid, 2011). Amongst these locations, Shark Bay, Western Australia is host to a diversity of microbial mats and stromatolite-forming microbial communities. These microbial ecosystems are regarded as robust analogues of ancient stromatolites and can potentially provide an exceptional insight into ancient biogeochemical cycling and the evolution of life (Riding, 2000).

The littoral zone of the Shark Bay tidal flats is host to five different types of microbial mats. This classification is based on the distinctive morphology of each microbial mat type (Jahnert and Collins, 2012; 2013), and further supported by the complex internal microfabrics (*e.g.* laminated, sub-laminar, scalloped, irregular or clotted; Logan, 1974; Reid *et al.*, 2003), characteristic of the different mat types. The precipitation of carbonates within these mats depends on the fragile balance between the processes increasing the alkalinity (*e.g.* cyanobacterial photosynthesis, anoxygenic phototrophy and sulfate reduction) and those leading to a decrease in alkalinity (*e.g.* aerobic heterotrophy, sulfide oxidation and fermentation; Visscher and Stolz, 2005; Dupraz *et al.*, 2009). The lithification also depends on the trapping and binding of carbonate by ExoPolymeric Substances (EPS), largely produced by cyanobacteria (Stal, 2000; Richert *et al.*, 2005) and sulfate reducing bacteria (SRB) (Bosak and Newman, 2005; Braissant *et al.*, 2007).

DNA analyses (*e.g.* genomic DNA, 16S rDNA; rRNA) performed on the Hamelin Pool microbial mats have revealed that complex micro-ecosystems and high biological diversity are found within a single microbial mat type, including great bacterial diversity as well as numerous archaea and eukaryotes (Burns *et al.*, 2004; Papineau *et al.*, 2005; Allen *et al.*, 2009; Edgcomb *et al.*, 2014). Although DNA carries the most information on a phylogenetic and taxonomic level, it does not survive over geological timescales (Briggs and Summons, 2014), and therefore cannot be used for comparison with ancient stromatolites. In contrast, lipids are biomolecules that have

greater preservation potential and therefore are more easily preserved over geological timescales (even as free sterols; Melendez *et al.*, 2013). Lipids, combined with their stable isotopic composition, are often specific for a microbial group (sometimes species) thus can give some valuable insights into microbial ecosystems. Lipids of microbial mat communities have been previously characterised from a variety of localities and environmental settings (Bühring *et al.*, 2009; Jahnke *et al.*, 2004; Pagès *et al.*, 2014b, 2015).

The characterisation of parameters that have a good preservation potential over time (*e.g.* biomineralisation, textures preserved in the microfabrics, and biolipids) to study modern microbial mats is therefore of great interest to establish comparison with ancient stromatolites. In the present study, we investigate three shallow microbial mat types from Carbla Beach, located on the eastern part of Hamelin Pool (**Figure 5-1**) and characterised by an abrupt depth gradient compared to other Hamelin Pool localities (Jahnert and Collins, 2012). Carbla Beach is also characterised by a high abundance of ooids (Summons *et al.*, 2013). Although biosignatures from the Carbla Beach ooids have been investigated in detail (Summons *et al.*, 2013), lipids and isotopic signatures from the nearby microbial mats have not been reported to date. The aim of this study is to provide a combined characterisation of the microfabrics, the lipid distribution and their compound-specific carbon isotopic signatures within three microbial mat types found along the shallowest section of the littoral gradient: (i) supratidal tufted mat, (ii) intertidal pustular mat and (iii) shallow subtidal smooth mat.

Materials and methods

Study site

Shark Bay is located in Western Australia, 800 km north of Perth (**Figure 5-1**). Hamelin Pool, the eastern embayment of Shark Bay, is a semi-enclosed shallow marine system with a semi-arid climate. These environmental conditions favour high evaporation rates leading to hypersaline marine conditions (56-70 psu, Logan and Cebulski (1970)).

Samples of microbialites were collected near Carbla Station (**Figure 5-1**) during a field excursion to Shark Bay in June 2011. At that time, the highest salinity

measured at this sampling site reached 90 psu, which is in the upper range of hypersaline environments. In contrast, the measured pH of the seawater was within average marine values and ranged between 8.3 and 8.4.

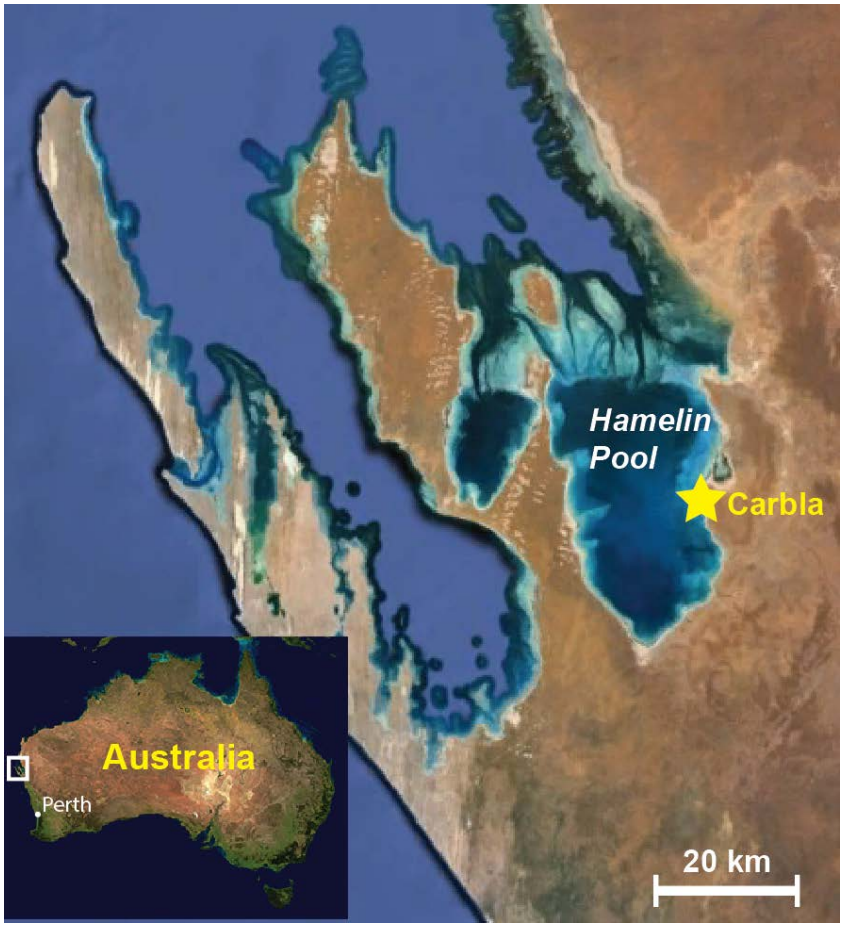

Figure 5-1. Google Earth image of Shark Bay showing the location of Hamelin Pool. The yellow star represents the Carbla sampling site in Shark Bay, Western Australia.

Carbla Beach is characterised by a steep littoral gradient and microbial mats with striking morphological differences at a macroscopic level, which allow for clear identification of the different types of microbial mats (**Figure 5-2**). Three shallow microbial mats from supratidal, intertidal and shallow subtidal environments (tufted mat, pustular mat and smooth mat, respectively) were sampled. Details on the assemblages and macroscopic features of these mats are reported elsewhere (Jahnert and Collins, 2011; 2012).

The tufted mat was sampled at a water depth of 10 cm. It shows an accumulation of grains at its surface that are attributed to prevailing winds and tides.

The pustular mat sample was collected at a depth of 40 cm and is characterised by an irregular clotted fabric covered by a brown-coloured mucilage. The laminated smooth mat was sampled at 70 cm water depth and is characterised by a flat and smooth surface (**Figure 5-2**).

Tufted, pustular and smooth mats (**Figure 5-2**) were sampled with a stainless steel spatula, transferred into pre-annealed glass jars (450 °C for 5 hr) and were immediately frozen at – 18 °C on site. Samples were then freeze-dried before analyses.

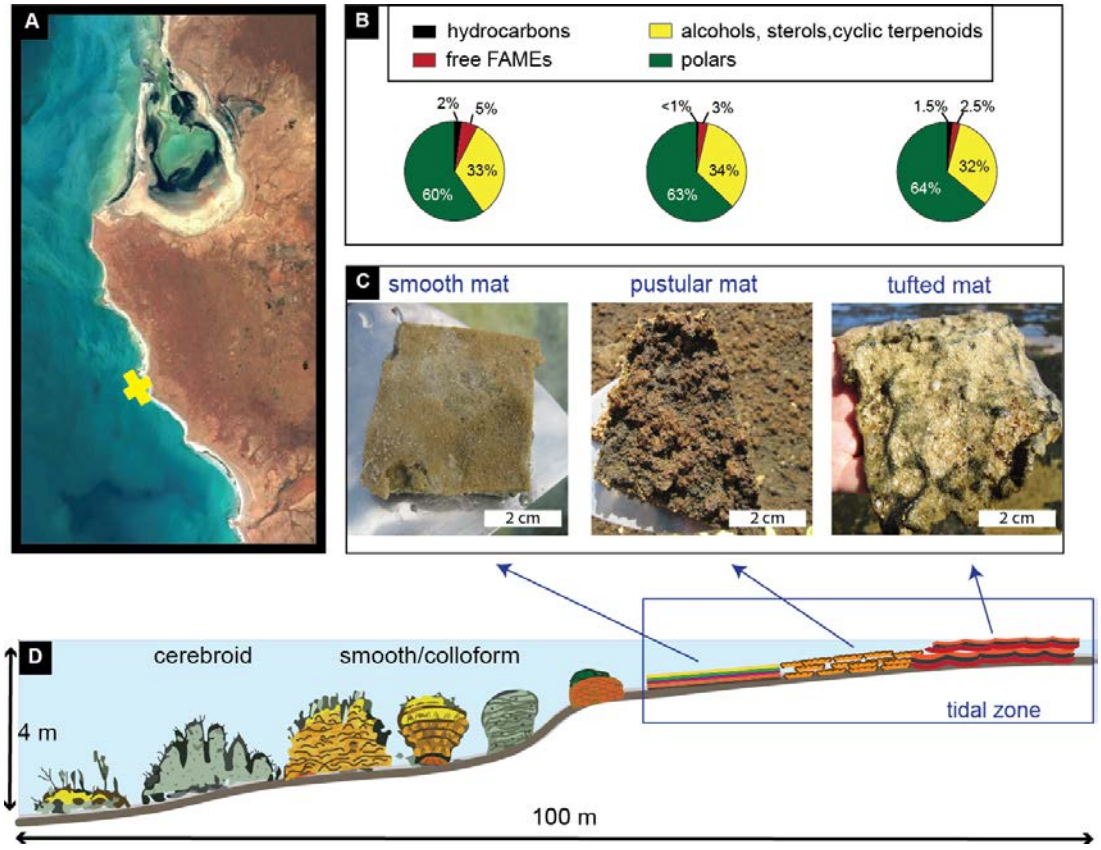

Figure 5-2. Characterisation of the Carbla Beach area and mats sampled (modified from Jahnert and Collins, 2012). A) Map with sampling location (google earth), B) proportion of the four lipid fractions investigated in the three mat types. C) Macroscopic morphology of the three mat types and D) Facies model of the Carbla beach microbial mats.

$\delta^{13}C$ of Carbonates

Carbonate samples were analysed for $\delta^{18}O$ and $\delta^{13}C$ using a GasBench II coupled with a Delta XL Mass Spectrometre (Thermo-Fisher, Scientific), reaction at 50C over 24 hours.

Imaging techniques

Aliquots of the three dried mats were used for thin section preparation. Thin sections were studied using standard optical microscopy. Scanning electron microscopy (SEM) images using secondary electrons were obtained during the investigation of Au-coated (3-5 nm) three-dimensional pieces of mats. Analyses were performed using a Zeiss Ultra-Plus FEG-SEM coupled with a Bruker X-Flash energy dispersive X-ray spectroscopy (EDS) detector for elemental analyses. An accelerating voltage of 20kV in high current mode was used.

Clasts, cements and micrite estimation.

The relative abundance of components was determined quantitatively through point counting. Point counting was continued to a minimum of 200 points and until percentages of components had reached equilibrium (c.f. Madden *et al.*, 2017).

Lipid analyses

Extraction

Aliquots of the three mat types (8-10 g) were crushed and ground manually using pestle and mortar. Lipid biomarkers were extracted with a mixture 9:1 (v/v) dichloromethane: methanol (DCM: MeOH) for 1 hr (20 mins, x 3) in an ultrasonic bath. The total lipid extracts (TLEs) were reduced to 3 mL under a purge of nitrogen at room temperature (25 °C). The TLEs were filtered through pre-extracted (DCM: MeOH, 9:1) cotton wool to remove particles and filtered through annealed anhydrous magnesium sulfate ($MgSO_4$) powder to remove any residual water from the samples. Activated copper turnings were added to each TLE and stirred (72 hr) to remove elemental sulfur.

Column chromatography

An aliquot of each TLE was adsorbed onto activated silica (160 °C, 8 hr) and placed onto the top of a small silica column (*ca*. 5 cm, Pasteur pipette). Five fractions were obtained as follows. (1) Aliphatic hydrocarbons were eluted using *n*-hexane (2 mL), followed by (2) aromatic hydrocarbons in 4:1 hexane: DCM (2 mL), then (3) free fatty acid methyl esters (FAME) and ketones in DCM (2 mL), (4) alcohols in 4:1 DCM: ethyl acetate (2 mL) and (5) the polar fraction in 7:3 DCM: MeOH (2 mL). Excess solvent from each fraction was removed by a nitrogen purge before analyses.

Derivatisation

Alcohols and polar fractions were derivatised using bis(trimethylsilyl)-trifluoroacetamide (BSTFA) and anhydrous pyridine (150 µL and 100µL, respectively per 0.25 mg of sample) and heated (70 °C for 1 hr). Once cooled, the alcohol and polar fractions were dried under a nitrogen purge and dissolved in *n*-hexane. They were analysed using gas chromatography mass spectrometry (GC-MS) and gas chromatography – isotope ratio mass spectrometry (GC-irMS) for compound specific isotope analyses (CSIA).

GC-MS analyses

Samples were analysed using a Hewlett Packard (HP) 6890 GC interfaced to a HP 5973 mass selective detector (MSD). The fractions were dissolved in *n*-hexane and introduced by a split/splitless injector operated in a pulsed splitless mode. The GC was fitted with a 60 m x 0.25 mm i.d. WCOT fused silica capillary column coated with a 0.25 µm film DB-5MS). The initial temperature of the oven (40 °C) was held for 1 min and heated at a rate of 3 °C/min up to 325 °C (isothermal for 30 min). Ultra-high purity helium was used as the carrier gas and maintained at a constant flow of 1.1 mL/min. The mass scan range acquired was 50 Da to 600 Da.

Compound identification and semi-quantitative analyses were performed on the separated fractions and derivatised aliquots. Each fraction was spiked with a known amount of internal standard (squalane) and analysed by GC-MS.

CSIA

CSIA was performed on the aliphatic and free FAME fractions as well as on derivatised alcohol and polar fractions using a Thermo Delta V Advantage isotope ratio mass spectrometer (irMS) coupled to a Thermo Trace GC Ultra *via* a GC Isolink and Conflo IV. GC conditions were the same as (GC-MS section). GC column outflow passed through the GC Isolink combustion reactor (copper oxide / nickel oxide, 1000 °C) to combust hydrocarbons to CO_2. $\delta^{13}C$ values were determined by integrating the ion currents of masses 44, 45 and 46 using Thermo Isodat software, and calibrated to the international Vienna Peedee Belemnite (VPDB) scale by comparison with a mixture of *n*-alkane standards of known isotopic composition. Samples were run in duplicate, and standards were run in duplicate every third sample to confirm consistency of the measurements. A pure cholesterol standard (underivatised and derivatised) was analysed in order to calculate the $\delta^{13}C$ of the additional methyl-groups from BSTFA (Jones *et al.*, 1991). All values reported in this study have a maximum standard deviation of 0.4 ‰ VPDB from at least two analyses.

Results

Carbonate isotopes and microfabrics: optical microscopy and SEM

The Shark Bay microbialites have microfabrics that can vary significantly, depending on the water depth, salinity and corresponding microbial ecosystem involved in the mat formation (Reid *et al.*, 2003; Jahnert and Collins, 2012; 2013). The carbonate fractions of all three mats shows enriched $\delta^{18}O_{carb}$ and $\delta^{13}C_{carb}$ values. $\delta^{18}O_{carb}$ values are comprised between +3.07‰ and +3.50‰, whereas $\delta^{13}C_{carb}$ vary between +4.67‰ and +5.36‰. A qualitative description of the internal fabrics of the three mat types investigated here is presented below.

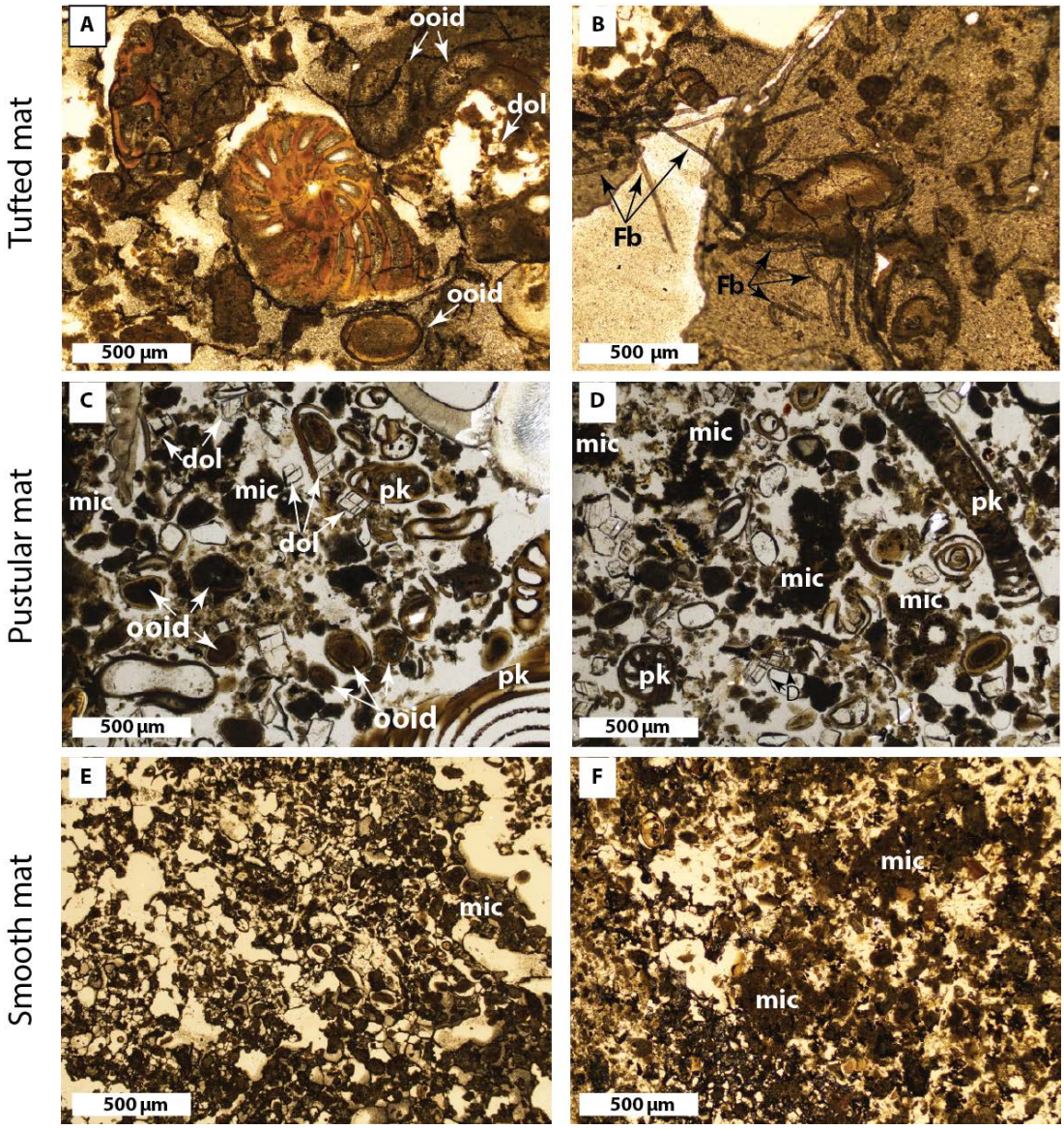

Figure 5-3. Photographs of the characteristic internal microfabrics observed in the three microbial mats: A & B = Tufted mat, The tufted mat shows a high degree of porosity and (A) contains planktonic remains (pk) as well as <100 micron euhedral dolomite crystals (dol) and superficial micritic ooids at various stages of preservation plus (B) abundant filamentous cyanobacteria (Fb). (C and D) The pustular mat shows abundant dolomite crystals and smaller concentric ooids. Abundant planktonic remains and clotted micrite patches (mic) are also present. (E and F) The smooth mat shows the lowest porosity of the three mat types and contains less dolomite crystals. It also contains the smallest ooids (E). Micrite patches are significantly more abundant and larger than in the other two mat types.

Tufted mat

Figure 5-3A-B shows clotted to slightly dense micritic material accounts for 39% of the sample. This mat also shows high porosity (36%) dominated by three main types: interparticular, growth-framework and vuggy porosity Imperforate larger benthic foraminifera with a high degree of preservation and robust forms (low length

to width ratios) are common and present their original mineralogy. In addition, fragmented bivalves account for 9% of the sample. Miliolid foraminifera are rare (<2%) and are well preserved. Bivalve fragments often display intense micritisation and show pervasive thick rims (up to <100 µm). Superficial micritic ooids are present (5%) at sizes up to 500 µm. A fine (100-250 µm) quartz content is additionally present (3%). Calcite cements account for <6% of the sample. Cements include (1) fine (40 µm) micritic to granular calcite infilling primary porosity within the micritic matrix and (2) rarer fine (40-50 µm) acicular calcite infilling original intraparticular porosity of bioclasts.

SEM observations of mat aliquots revealed a greater abundance of ooids (~ 200 µm diameter) than observed on thin section and confirmed a low degree of cementation (**Figure 5-4A-C**). The outer layer of the ooids appears smooth and homogenous, however abundant EPS is observed around the ooids and aids in binding them together (**Figure 5-4**). Small euhedral crystals, identified mostly as dolomite ($Ca,Mg(CO_3)_2$) and halite (NaCl), were observed in association with the ooids (**Figure 5-4A-C**). Most of the halite crystals are covered by EPS, corroborating their authigenic origin from the highly evaporitic environment in supratidal settings of Carbla Beach, rather than from precipitation during sample preparation. Very few detrital grains were detected.

Pustular mat

The pustular mat sample (**Figure 5-3C-D**) is dominated by dense to slightly clotted micrite (38%) and growth-framework as well as interparticular porosity (31%). Superficial ooids and concentric to composite ooids are the dominant allochem (9%) together with common bioclasts (8%). Ooids have both pelitic and mature quartz grain nuclei and demonstrate reworking into ‘grapestone’ style composite ooids. Bioclasts include: (i) fragmented bivalves (<500 µm) that have been replaced by granular-blocky (anhedral to euhedral mosaic; terminology of Flügel, 2010) to fibrous calcite and (ii) heterostegina and peneropolis forms of larger benthic foraminifera. Locally, bioclasts show micro-perforations typical of endolithic microborers. Bioclasts do not typically show micritic rims. Microdolomite rhombs (50-80 µm) are common (6%) together with clean micritic to granular (~100 µm) calcite (7%). Additionally, authigenic evaporate crystals are also seen (<2%). The presence of ‘ghost fabrics’ and relict

structures in the larger bivalve fragments indicates that the cement (granular mosaic to fibrous calcite) is of neomorphic, and likely early marine, origin. The clean, inclusion free miciritc cement, is indicative of primary cement rather than neomorphism of the clay rich clotted micritic fabric.

SEM imaging also shows that ooids are extensively coated by partially mineralised EPS (**Figure 5-4D-F**). Numerous diatoms of relatively large size (up to 50 µm), characteristic of this mat, were revealed. The highly diverse morphology of the diatoms suggests that numerous diatom species are present, most of them deposited onto or trapped within the EPS. Carbonate spherules (<1 µm) are also present and, when associated with the micritic texture of the mat (**Figure 5-4D-F**), represent the biologically-induced mineralisation surrounding coccoid cyanobacteria (Jahnert and Collins, 2012; 2013).

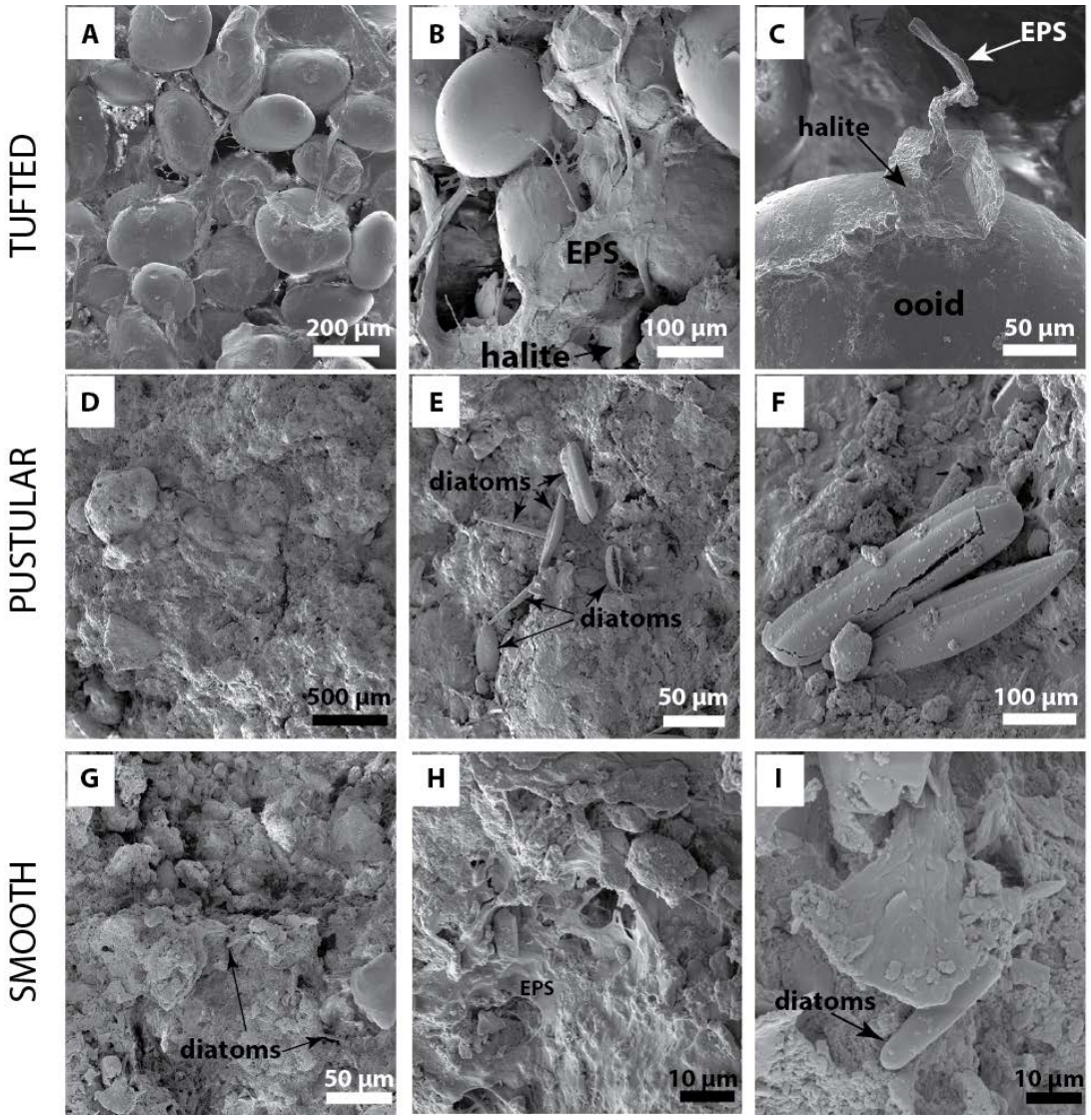

Figure 5-4. SEM images of the three microbial mats A – C= Tufted mat, D – F = Pustular mat and G – I = Smooth mat. The tufted mat is characterised by abundant ooids either showing a smooth surface or surrounded by EPS. The presence of halite (NaCl) crystals encrusted by EPS suggests that the highly evaporitic environment does not prevent the formation of EPS. The pustular mat displays a granular type texture at a microscopic scale, covered by EPS. Abundant diatoms of various morphologies are observed in this mat type. The smooth mat displays a more compact structure almost entirely coated by EPS. Few diatoms, which are smaller compared to the pustular mat, are observed.

Smooth mat

A clotted to slightly diffuse micritic fabric (53%) dominates the sample (**Figure 5-3E-F**), which also shows a lower interparticular and growth porosity (27%) than the two shallower mats. The dark brown colour in plane-polarised light (PPL) is suggestive of a high organic or clay fraction. The presence of terrigenous material is supported by a common (9%), fine sub-rounded to rounded quartz fraction (150-250 µm). Carbonate allochems include common finely comminuted (100-300 µm)

molluscan fragments (likely bivalves) and relatively well preserved larger benthic foraminifera (peneropolis, heterostegina and miliolid forms) and account for ~2% of the sample. Additionally, micritic surficial ooids are present (3%).

Early alteration of bioclasts is present as thin (20 µm) constructive micritic envelopes (micritic rims) but also as bivalve shells that have typically been replaced by neomorphic calcite. Larger benthic foraminifera typically show less pervasive micritic rims. Inclusion free, (clean) micritic calcite is present as a cementing phase but in low abundance (<5%). Rare (<1%) microdolomite rhombs (50-70 µm) are found within the clotted micritic matrix that rarely show erosional surfaces. SEM confirms a more intense micritisation (**Figure 5-4G-I**) and EDS analyses of the EPS highlight a mineralogy dominated by calcium carbonate. Few diatoms of reduced size were observed (15 µm, **Figure 5-4G-I**), however no variation in their morphologies was identifiable.

Aliphatic hydrocarbons

Aliphatic hydrocarbons were the least abundant lipids of the three mats (**Figure 5-2**). They were analysed to assess the contributions of bacterial communities, higher plant/aquatic plants, and other eukaryotic inputs (**Figure 5-5**). All three mats contain *n*-alkanes ranging from *n*-C_{15} to *n*-C_{34} maximising at *n*-C_{17} or $C_{17:1}$ alkene. In the tufted mat type, *n*-C_{17} alkane is largely dominant (8.63 µg/gsed) whereas the pustular mat is characterised by comparable abundance of *n*-C_{17} and $C_{17:1}$ alkene (~3.6 µg/gsed), and the smooth mat shows a greater contribution of $C_{17:1}$ alkene (6.73 µg/gsed). All mats also show an odd-over-even carbon preference in the long chain *n*-alkanes (C_{23} to C_{34}). Phytene isomers are more abundant than phytane in both the tufted mat (4.74 µg/gsed *vs.* 0.93 µg/gsed, respectively) and smooth mat (4.21 µg/gsed *vs.* 0.45 µg/gsed, respectively). However, in the pustular mat only phytane is present (0.37 µg/gsed). The $C_{25:1}$ highly branched isoprenoid ($C_{25:1}$ HBI) is present in trace amounts in the pustular mat (0.40 µg/gsed), abundant in the smooth mat (2.81 µg/gsed) and absent in the tufted mat.

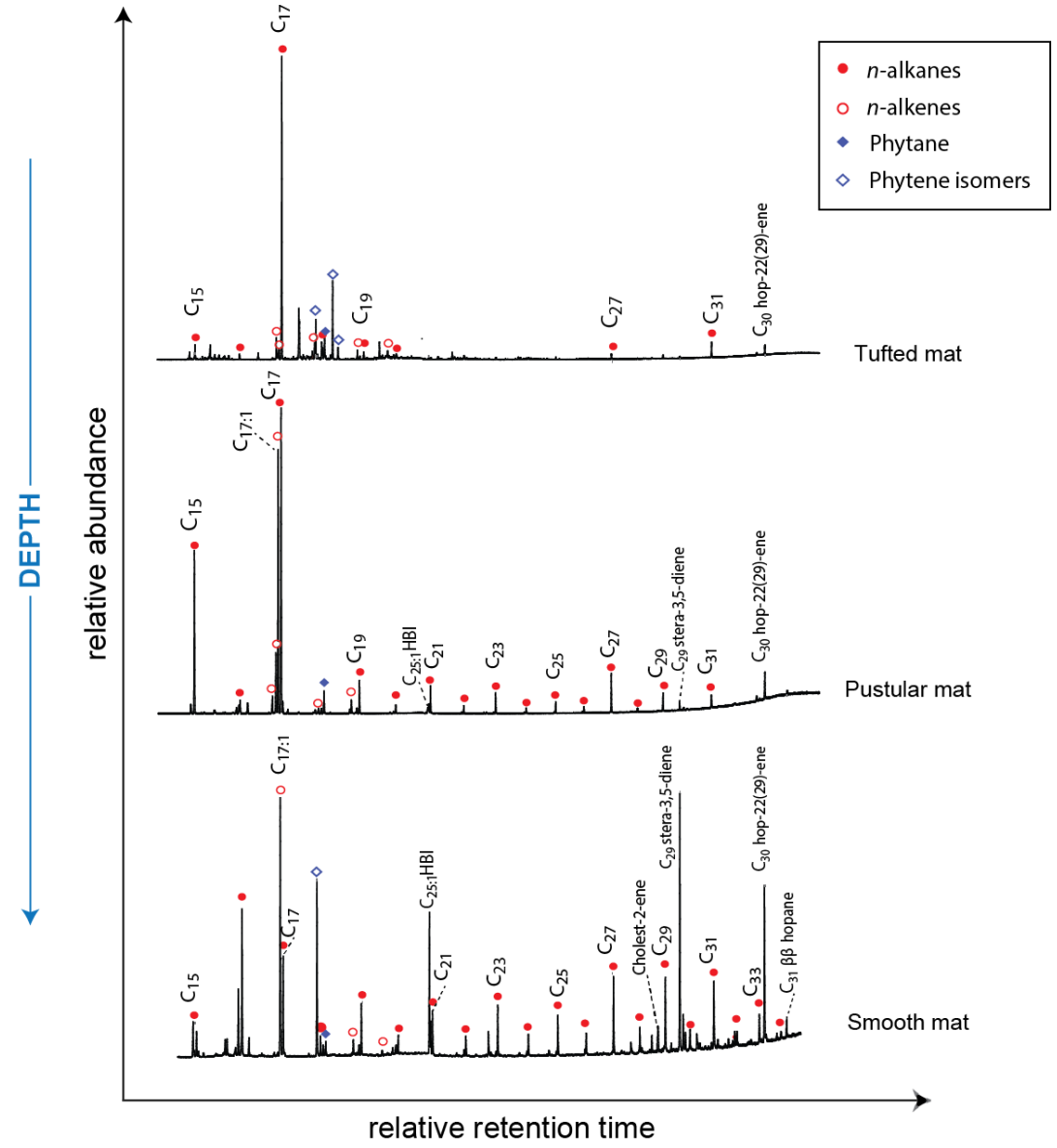

Figure 5-5. Total ion chromatograms from GC-MS analyses of the aliphatic hydrocarbon fractions from the three mats.

All mats show the presence of C_{30}-hop-22(29)-ene with the lowest abundance in the tufted mat (0.21 µg/gsed) and a maximum of 0.52 µg/gsed in the smooth mat. The abundance of this compound therefore increases with depth. Both the pustular and smooth mats contain C_{29}-stera-3,5-diene (0.18 and 2.45 µg/gsed, respectively). The smooth mat shows a greater abundance of C_{30}-hop-22(29)-ene and C_{29}-stera-3,5-diene and minor contribution of a C_{31}-ββ-hopane and cholest-2-ene. Overall, the smooth mat differs in hydrocarbon distributions compared to the two shallower mat types.

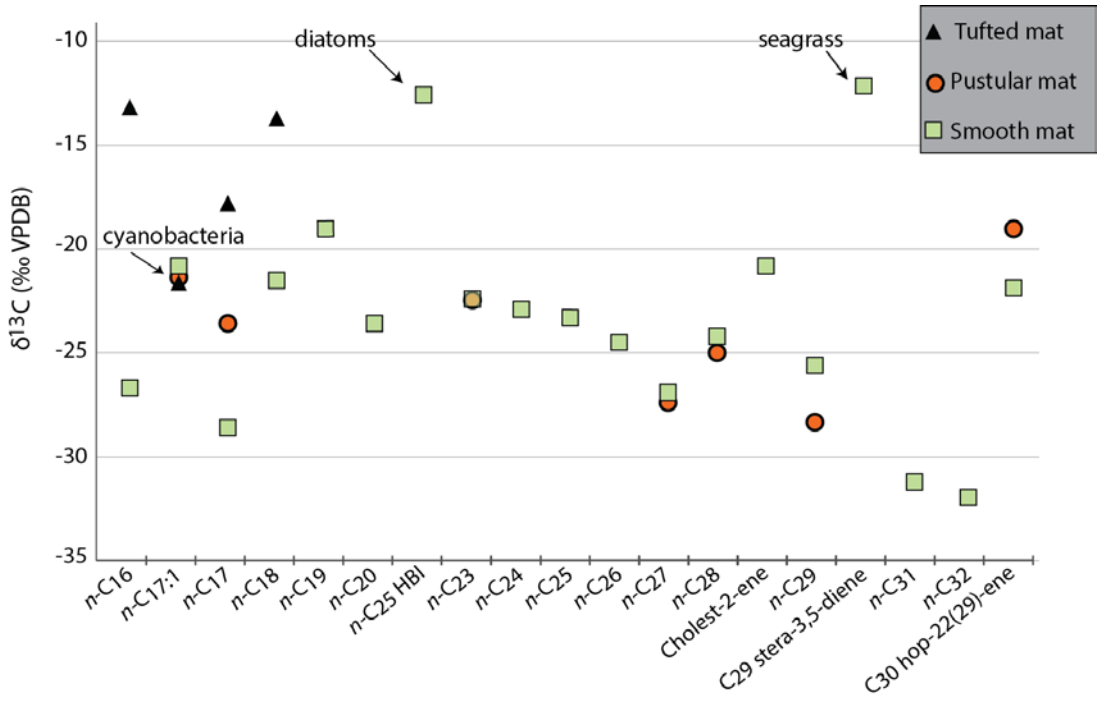

Figure 5-6. The $\delta^{13}C$ values of the aliphatic hydrocarbon fractions of the three mats.

The carbon isotopic compositions of the aliphatic hydrocarbon fraction from each mat type are shown in **Figure 5-6**. The $\delta^{13}C$ values of the short chain *n*-alkanes (*n*-C_{16} – *n*-C_{20}) show major isotopic discrepancies between mat types with isotopically heavier *n*-C_{16}, *n*-C_{17} and *n*-C_{18} alkanes (with values up to –13.2 ‰) in the tufted mat. However, the $\delta^{13}C$ value of $C_{17:1}$ alkene is similar for the three mats (~– 21.2 ± 0.4 ‰).

The $\delta^{13}C$ values of the long chain *n*-alkanes (C_{23}-C_{32}) for both the pustular and smooth mats are similar (except for the *n*-C_{29} alkane) and show that higher molecular weight *n*-alkanes are more ^{13}C-depleted than medium chain *n*-alkanes. In the pustular mat, the *n*-C_{29} alkane is ^{13}C-depleted by ca. 3 ‰ compared to the smooth mat.

The C_{30} hop-22(29)-ene shows a more ^{13}C-enriched signal in the pustular mat than in the smooth mat (by up to ca. 3 ‰). In the smooth mat, the $C_{25:1}$ HBI and C_{29} stera-3,5-diene have $\delta^{13}C$ values of –12.6 ‰, and –12.1 ‰, respectively. The cholest-2-ene, detected in the smooth mat only, shows a $\delta^{13}C$ value of –20.8 ‰.

Free Fatty acid methyl esters (FAMEs)

The free FAMEs distribution and carbon isotope compositions are presented in **Figure 5-7**. The free FAMEs fraction shows low relative abundance compared to

more polar compounds (**Figure 5-2**) with absolute concentrations of 11.9 µg/gsed in the smooth mat, 7.9 µg/gsed in the pustular mat and only 4.7 µg/gsed in the tufted mat. The tufted mat is characterised by a small diversity of compounds and low concentrations of free FAMEs. The most abundant compounds in the tufted mat (*i*-C_{15}, *n*-$C_{16:1}$, *n*-C_{16}, *n*-C_{18}) show similar concentrations with a maximum of 580 ng/gsed for *n*-$C_{16:1}$.The pustular mat is dominated by *n*-C_{16} (2710 ng/gsed) and *n*-C_{18} (508 ng/gsed) and their unsaturated homologues. The smooth mat free FAMEs distribution shows more diversity, although two compounds are clearly dominant; *n*-C_{16} (1815 ng/gsed) and compound **II** (1840 ng/gsed).

All three mat types contain short chain saturated FAMEs ranging from *n*-$C_{14:0}$ to *n*-$C_{18:0}$; unsaturated homologues and traces of 10-methyl-$C_{16:0}$ are also present. The medium/long chain saturated FAMEs from *n*-C_{22} to *n*-C_{28}; which display an even-over-odd predominance, are more abundant in the smooth mat and pustular mat types, with total concentrations of 141.4 ng/gsed and 663.9 ng/gsed, respectively. Lipids characteristic of sulfate reducing bacteria (*e.g.* *i*C_{15}, *ai*C_{15}, *i*$C_{17:1\omega9}$, *i*C_{17}, *ai*C_{17} and 10MeC_{16}, Londry *et al.*, 2004; Taylor and Parkes, 1983, 1985) are present in the three mat types. These markers are most abundant in the tufted mat where their total concentration reaches 1191 ng/gsed. Their abundances decrease with depth with concentrations of 524 ng/gsed in the pustular mat and 432 ng/gsed in the smooth mat.

A series of lipids, tentatively identified based on mass spectra comparison with the NIST library and retention times, as *n*-alkyl-*n*-decanoates (**I, II, III, V**, **VI**, **VII,** mass spectra in **Figure A5-1**) is dominant in the smooth mat. In this mat, the total abundance of these compounds is 6557 ng/gsed. Although the whole series is not present in the other mats, the tufted mat also contains compounds **IV**, **V**, **VI**, **VII** and compound **VI** is detected in the pustular mat.

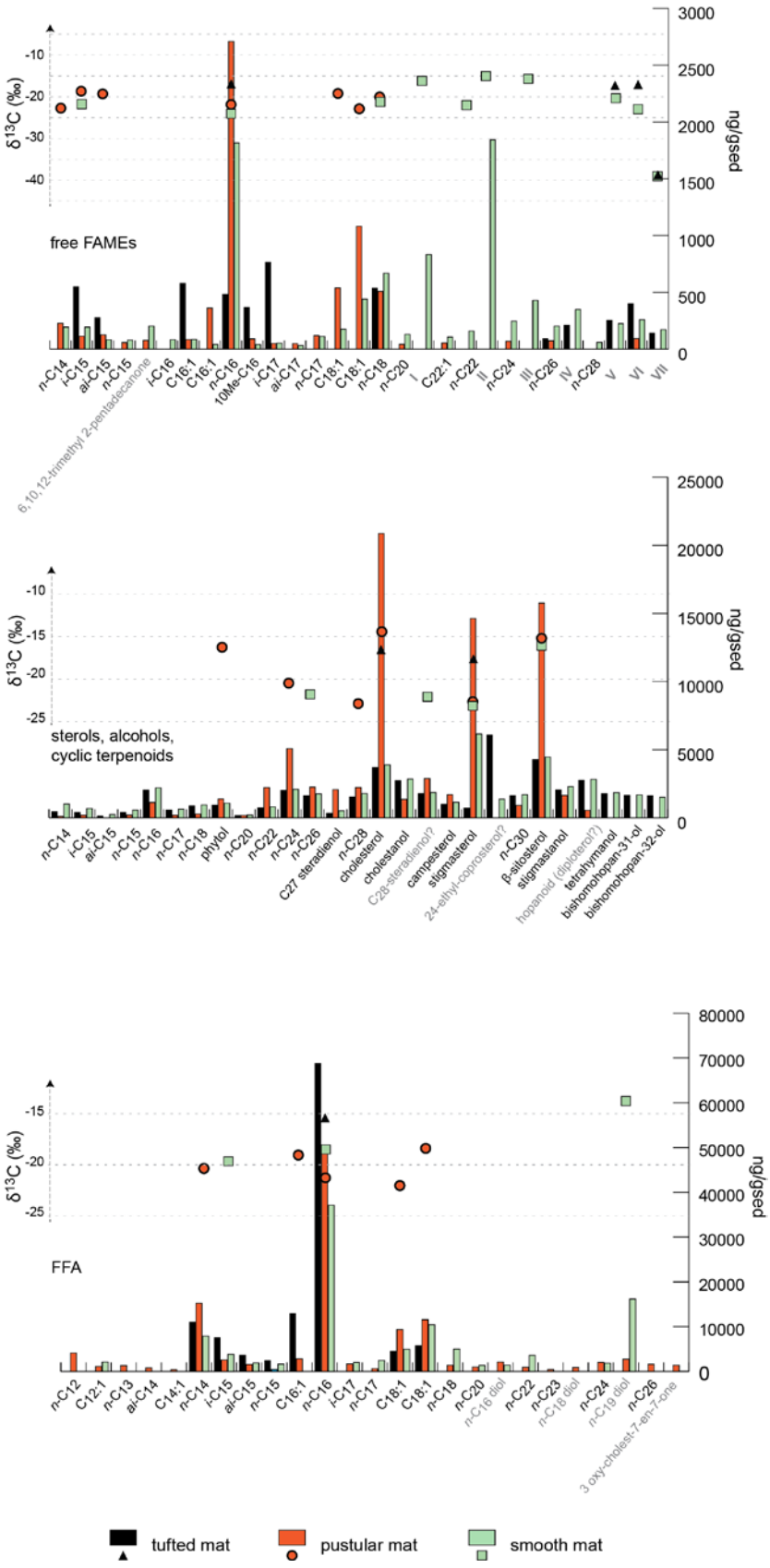

Figure 5-7. Chart representing the lipid distribution (in ng/gsed) and their $\delta^{13}C$ values in the free FAMEs fraction, the alcohols, sterols, cyclic terpenoids fraction and the FFA fraction. Compounds I, II, III, IV, V, VI, VII have their mass spectra included in Figure A5-1.

CSIA of individual FAMEs revealed a depletion in ^{13}C in the deeper mats. The saturated *n*-C_{16} becomes more ^{13}C-depleted, with $\delta^{13}C$ values of –16.9 ‰ in the tufted mat, –21.8 ‰ in the pustular mat and –24.0 ‰ in the smooth mat. A similar ^{13}C-depletion with depth is also observed for the other compounds, with the smooth mat being systematically more ^{13}C-depleted than the shallower tufted and pustular mats (**Figure 5-7**).

The short to medium chain FAMEs in the pustular and smooth mats have average $\delta^{13}C$ values of –20.7 ‰ and –22.2 ‰, respectively. The *n*-alkyl-*n*-decanoates **V** and **VI** display a similar trend of depletion with increasing water depth. In the tufted, mat *n*-alkyl-*n*-decanoates **V** and **VI** display values of –17.0 ‰ and –17.2 ‰, respectively; whereas they are more depleted in the smooth mat (–20.3 ‰ and –22.9 ‰, respectively). In contrast, *n*-alkyl-*n*-decanoate **VII** displays depleted $\delta^{13}C$ values for the tufted (–38.6 ‰) and the smooth (–39.0 ‰) mats.

Sterols, fatty alcohols and cyclic terpenoids

The fraction containing sterols, fatty alcohols and cyclic terpenoids was the second most abundant after the polar fraction in all three mats (**Figure 5-2**). However, only part of it is GC-amenable allowing for absolute concentrations estimations of 65.7 µg/gsed in the tufted mat, 85.7 µg/gsed in the pustular mat and a maximum of 72.5 µg/gsed in the smooth mat (**Figure 5-7**). The three mats show a variety of compounds from straight chain and methylated fatty alcohols to steroids and pentacyclic terpenoids.

Straight short chain fatty alcohols from C_{14} to C_{18} are present in the three mats. In the tufted and smooth mats, C_{16} reaches ~2200 ng/gsed; however, it is less concentrated in the pustular mat (1123 ng/gsed). Straight medium and long chain fatty alcohols (C_{20} to C_{30}) are observed in all three mats and present strong even-over-odd predominance. Phytol is present in the three mats with concentrations varying between 925 ng/gsed (tufted mat) and 1384 ng/gsed (pustular mat). The C_{27} and C_{29} sterols are dominant in each mat, particularly in the pustular mat where the cholesterol, stigmasterol and β-sitosterol reach their maximum concentrations (20867 ng/gsed, 14634 ng/gsed and 15755 ng/gsed, respectively). In contrast, pentacyclic terpenoids (diplopterol, tetrahymanol, bishomohopanol) show similar concentrations in the tufted

and smooth mats but were not detected in the pustular mat where only diplopterol was identified.

Cholesterol, β-sitosterol and phytol show an overall enrichment in ^{13}C with values between –15.3 ‰ and –16.7 ‰ (**Figure 5-7**). Stigmasterol is also ^{13}C-enriched in the tufted mat with a $\delta^{13}C$ value of –17.6 ‰ in the tufted mat and is more ^{13}C-depleted in the pustular and smooth mats (–22.7 ‰ and –23.1 ‰, respectively). The $\delta^{13}C$ values of medium and long chain *n*-alcohols were measured in the pustular and smooth mats, where they range between –20.5 ‰ and –22.9 ‰.

Free Fatty acids (FFA) and diols

In all three mat types, the polar fraction is the most abundant (**Figure 5-2**) and is composed of straight chain fatty acids, diols, and branched short-chain FFA. The fractions are dominated by C_{16} which varies between a maximum of 68800 ng/gsed in the tufted mat and a minimum of 37130 ng/gsed in the smooth mat. All mat types contain *i*-C_{15} and *ai*-C_{15}, whereas *i*-C_{17} is only present in trace amounts in the tufted mat. Although the short-chain compounds from C_{14} to C_{18} are dominant in all three mat types, compounds between C_{12} and C_{14}, as well as straight-chain compounds from C_{20} to C_{26} and straight chain C_{16}, C_{18} and C_{19} diols are present in the pustular and smooth mat types only (**Figure 5-7**).

The $\delta^{13}C$ value of the saturated C_{16} FFA ranges between –15.5 ‰ in the tufted mat and –21.3 ‰ in the pustular mat. In the smooth mat, the saturated C_{16} FFA has an intermediate $\delta^{13}C$ value of –18.5 ‰. In the pustular mat, $\delta^{13}C$ values of C_{14} and unsaturated C_{16} and C_{18} FFA vary between –18.4 ‰ and –22 ‰. In the smooth mat, *i*-C_{15} and *n*-C_{19} diol have $\delta^{13}C$ values of –19.7 ‰ and –13.5 ‰, respectively.

Discussion

Both imaging techniques and lipid biomarker distributions have previously proven to be useful in characterising microbial communities in modern mats from Shark Bay (Reid *et al.*, 2003; Jahnert and Collins, 2011; 2012; 2013; Pagès *et al.*, 2015). In the present study, a multiproxy approach combining lipid biomarker analyses, microfabrics and stable isotope analyses, was used to characterise the

environment of formation as well as dominant microbial groups present in each mat type.

Mat type and environment of formation

The positive $\delta^{18}O$ values of carbonates are characteristic of highly evaporitic enclosed systems; the enriched $\delta^{13}C$ values reflect extensive microbial activity consistent with previous reports (*e.g.* Jahnert and Collins, 2012).

Microfabric characterisation of the tufted mat has shown the co-occurrence of both bioclasts showing original mineralogy with others displaying intense micritisation of the margins. The presence of robust foraminifera forms is commensurate with the supratidal nature of this mat (*e.g.* Perry, 1999; Perry and Hepburn, 2008; Madden *et al.*, 2013). Granular calcite cements are not exclusively inclusion free and therefore may indicate some neomorphic replacement of micritic matrix and early marine diagenesis.

In the pustular mat, the early alteration of bioclasts by endolithic microborers was observed with optical microscopy, although it is localised and overall uncommon. Together with coarse fragmented bivalves and abundant concentric, superficial and composite ooids indicates higher energies. The reworking of bioclasts and abundant diatoms observed in this mat is consistent with intertidal settings.

The clotted micritic fabric characteristic of the smooth mat indicates shallow marine settings and is common for low energy environments. The generation of constructive micritic envelopes and cortoids is consistent with endolithic microborers being most active in a moderate to low energy shallow-photic environment. Some of these envelopes may be representative of biofilm calcification (*e.g.* Perry, 1999). Generally, bioclasts with non-pervasive rims are compatible with nutrient reduced conditions although a transport from higher energy environments (and therefore reduced micritisation) cannot be excluded.

Comparison: microfabrics and biomarkers

Cyanobacteria

Cyanobacteria were observed in all three mat types (**Figure 5-3**). Imaging techniques applied on the three mats provided information about the type of cyanobacteria present. The tufted and smooth mats show a predominance of filamentous cyanobacteria, in agreement with previous studies (*e.g.* Bauld, 1984; Jahnert and Collins, 2012; Logan, 1974). In contrast the pustular mat shows abundant mineralised coccoids, typical of encrusted coccoid cyanobacteria, as previously reported at other localities in Shark Bay (Jahnert and Collins, 2012).

The type of cement present in each mat can also serve as indicator of cyanobacteria. For example, in the tufted mat, the presence of acicular calcite could be related to cyanobacterial precipitates or cement nucleation on bacterial cells (Guo and Riding, 1992). Similarly, the smooth mat displays a clotted micritic fabric, which is typical for EPS calcification and is commonly associated with filamentous cyanobacteria (Guo and Riding, 1992).

Lipids also reflect a large contribution of cyanobacteria. Hydrocarbon fractions of all three mat types are generally dominated by *n*-C_{17} alkane and *n*-$C_{17:1}$ alkene. These hydrocarbons were previously reported as the main hydrocarbons extracted from cultured filamentous cyanobacteria (Paoletti *et al.*, 1976), as well as microbial mats from hot springs, freshwater and hypersaline environments (Fourçans *et al.*, 2004; Grimalt *et al.*, 1991, 1992; Robinson and Eglinton, 1990; Rontani and Volkman, 2005; Thiel *et al.*, 1997). In Hamelin Pool microbial mats, *n*-C_{17} and *n*-$C_{17:1}$ alkene hydrocarbons were largely attributed to cyanobacteria (Allen *et al.*, 2010; Pagès *et al.*, 2015), although some degree of contribution from eukaryotic algae is also possible(Paoletti *et al.*, 1976). In our study, all three mats show similar $\delta^{13}C$ values for *n*-$C_{17:1}$ (–21.3 ‰ on average), consistent with a common source. In contrast, *n*-C_{17} shows large isotopic differences in $\delta^{13}C$ values between the three mats studied, likely reflecting a varying input from cyanobacteria and eukaryotic algae between the different mat types.

Diatoms

Diatoms are present in both the pustular and smooth mat types. SEM imaging shows abundant diatoms (~50 µm) deposited onto (or trapped in) the EPS within the pustular mat. Most of these diatoms present a symmetrical biraphid morphology (Spaulding *et al.*, 2010). By contrast, SEM observations of the smooth mat revealed diatoms that are relatively less abundant and of a smaller size (<10 µm).

In contrast, the $C_{25:1}$ HBI, a diatom-specific marker (Grossi *et al.*, 2004; Summons *et al.*, 1993; Volkman *et al.*, 1998), shows the opposite trend: low in the pustular mat and approximately five times more abundant in the smooth mat type. Previous studies suggest that environmental conditions (*e.g.* salinity) can interfere with the biosynthesis of C_{25} HBI alkenes in diatoms (Wraige *et al.*, 1997). However, the occurrence of authigenic evaporitic minerals (*e.g.* calcite, dolomite, and halite) in both pustular and smooth mat suggests similar salinities for both mat types. An alternative explanation comes from the work of Sinninghe Damsté *et al.* (2004), which highlighted that only four diatom genera are capable of HBI alkene synthesis (*Navicula, Haslea, Pleurosigna* and *Rhizosolenia*). Based on the latter study, our data suggests that diatoms present in the smooth mat most likely belong to one of these four genera, therefore producing abundant $C_{25:1}$ HBI, whereas the diatoms observed in the pustular mat belong to another genera not able to synthesise C_{25} HBI alkenes.

In the smooth mat, this diatom marker is ^{13}C-enriched (–12.6 ‰). Such ^{13}C-enriched signatures are common for diatom markers from a range of environments such as lagoonal (McKirdy *et al.*, 2010), hypersaline (Summons *et al.*, 1993) and estuarine (Canuel *et al.*, 1997) settings. This characteristic ^{13}C signature is generally explained by the tendency of diatoms to grow in blooms, which leads to a localised depletion of CO_2, and therefore decreases the discrimination against ^{13}C during photosynthesis (Freeman *et al.*, 1994; McKirdy *et al.*, 2010), although the capacity of some diatoms to assimilate HCO_3^- can also explain such an enrichment in ^{13}C (Freeman *et al.*, 1994). Diatoms are able to synthesise some sterols (*e.g.* cholesta-5,22-dien-3β-ol, 24 methylcholesta-5,22-dien-3β-ol, β-sitosterol); however these sterols are non-specific and can also derive from micro-algae and/or higher plants (Volkman, 2003). Our ^{13}C data suggest that most sterols present in the mats have a mixed origin.

Sulfate-reducing bacteria

Markers of SRB were also detected in all mats. The 10-methylhexadecanoic acid has been detected from cultures of *Desulfobacula*, *Desulfotignum* and *Desulfobacter* (Taylor and Parkes, 1983; Kuever *et al.*, 2001). This fatty acid is present in all three mat types, although in a greater abundance in the tufted mat. These results contrast with the mats from Nilemah, Shark Bay where the 10-methylhexadecanoic acid was most abundant in the deepest microbial mat (Pagès *et al.*, 2014a).

Other SRB markers such as *iso*- and *anteiso*-15:0 and 17:0, previously identified in *Desulfobulbus* and *Desulfobacter sp,* were measured in the three mat types. However, *iso*- and *anteiso*-15:0 were present in both in the free FAME and FFA fractions whereas 10-methylhexadecanoic acid methyl ester as well as *iso*-17:0 and *anteiso*-17:0 were abundant in the free FAME but only present as traces in the FFA fraction of the tufted mat.

Higher plants

Shark Bay contains one of the largest seagrass meadows reported worldwide (Walker *et al.*, 1988). C_{29} steradiene, also reported in ooids from Carbla Beach (Summons *et al.*, 2013), was previously identified in the rhizomes of seagrass from mangrove environments (Florida, USA, Killops and Frewin, 1994). C_{29} steradiene is abundant in the smooth mat and is also detected at a lower relative abundance in the pustular mat. This suggests a greater input from submerged aquatic macrophytes into the deepest microbial mat. In the smooth mat, both C_{29} steradiene (–12.1 ‰) and β-sitosterol (–16.6 ‰) have heavy $\delta^{13}C$ values. It has been recently suggested that seagrasses have an intermediate C_3-C_4 pathway where the C_4 metabolism could be induced by local environmental conditions (McKirdy *et al.*, 2010; Touchette and Burkholder, 2000; Tulipani *et al.*, 2014). Here, the high salinity could be triggering a switch to C_4 metabolism in seagrasses. The ^{13}C-enriched composition of C_{29} steradiene supports a C_4 metabolic pathway, although some epiphytic contribution is not excluded (Belicka *et al.*, 2012). However, β-sitosterol is more depleted by 4.5 ‰ suggesting a contribution from another source.

In general, higher plant inputs can often be characterised by long chain *n*-alkanes with an odd-over-even predominance (OEP) and a depleted ^{13}C signature

(between –31 ‰ and –39 ‰ for C_3 plants) and a wide range of ^{13}C (between –19 ‰ and –34 ‰) for some species of macrophytes (Collister *et al.*, 1994; Canuel *et al.*, 1997). In Carbla Beach, long-chain *n*-alkanes with an odd-over-even carbon predominance are present in the three mat types. The long-chain *n*-alkanes (C_{24}-C_{33}) in the pustular and smooth mat types were on average more depleted than *n*-C_{17} (**Figure 5-6**) while abundances of long-chain *n*-alkanes in the tufted mat were too low for CSIA. The presence of ^{13}C-depleted long-chain *n*-alkanes in the mats is consistent with an origin from terrestrial plant and/or submerged macrophytes. The use of Paq, a molecular proxy based on relative abundances of long-chain *n*-alkanes (**Equation 5-1**), provides an estimation of the input from aquatic macrophytes relative to the input from emergent and terrestrial plants to the total biomass. It has been successfully applied to sediments from lakes (Ficken *et al.*, 2000), lagoons, estuaries (Xu *et al.*, 2006; McKirdy *et al.*, 2010) and has also previously been applied to Shark Bay mats (Pagès *et al.*, 2014a). Paq is calculated as follows:

$$Paq = \frac{C_{23} + C_{25}}{C_{23} + C_{25} + C_{27} + C_{29}}$$

Equation 5-1. Paq formula, proxy for aquaticmacrophytes/terrestrial input.

Values ranging between 0.1 and 0.4 are characteristic of a mixture of inputs from terrestrial plants and aquatic macrophytes while values between 0.4 and 1, represent a greater contribution from submerged macrophytes (Ficken *et al.*, 2000). In the present study, Paq of 0.32 (pustular mat) and 0.37 (smooth mat) indicate a mixed contribution for both mat types with a slightly greater contribution from aquatic macrophytes to the deeper smooth mat, which is concordant with an increase of macrophyte contribution with depth reported by Pages *et al* (2014a) (Pagès *et al.*, 2014a). In addition, the increase in relative abundance of both C_{29} sterols in the smooth mat also indicates a higher vascular plant contribution compared to the other mats investigated.

Other organisms

Observation of thin sections for the three mats clearly highlights the presence of a great variety of eukaryotic organisms such as benthic foraminifera (*e.g.* heterostegina, peneropolis, miliolids) and bioclasts (fragments of bivalve shell, likely

the endemic bivalve *Fragum erugatum*), which is concordant with previous DNA work on Carbla Beach microbial mats (Edgcomb *et al.*, 2014). In addition, tetrahymanol, found in the tufted and smooth mats, is largely derived from heterotrophic ciliates (*e.g.* Grice *et al.*, 1998b; Harvey and McManus, 1991; Sinninghe Damsté *et al.*, 1995). However, no ciliates were observed microscopically, highlighting the need for complementary lipid biomarker studies.

The $\delta^{13}C$ values of compounds **I**, **II**, and **III** were measured in the smooth mat only and ranged between –24 ‰ and –15 ‰. The exclusive presence of these *n*-alkyl *n*-decanoates in the smooth mat type may indicate that it harbours some microorganisms that are not as abundant in the other mats. Microbial mats are known to contain high sulfur cycling microbial activity, which could be a potential source for these compounds.

The role of microbial communities in carbonate precipitation

Carbonate precipitation in microbial mats strongly depends on alkalinity production, which represents a fine balance between the processes favouring a rise in alkalinity (*e.g.* cyanobacterial photosynthesis, anoxygenic phototrophy and sulfate reduction) and those decreasing the alkalinity (*e.g.* aerobic heterotrophy, sulfide oxidation and fermentation) (Visscher and Stolz, 2005; Dupraz *et al.*, 2009). SRB activity (**Equation 5-2**) leads to an increase in HCO_3^- concentration, promoting an increase in alkalinity (Abd-el Malek and Rizk, 1963) through the following reaction:

$$SO_4^{2-} + 2(CH_2O) + OH^- \rightarrow HS^- + 2HCO_3^- + H_2O$$

Equation 5-2. Equation for sulfate reduction.

HCO_3^- can further react with Ca^{2+} ions to precipitate carbonate minerals in microbial mats (Baumgartner *et al.*, 2006; Dupraz and Visscher, 2005; Visscher *et al.*, 2000). In Bahamian stromatolites, specific zones characterised by enhanced sulfate reduction (Visscher *et al.*, 2000) and highest SRB abundance (Baumgartner *et al.*, 2006) were shown to correlate with areas of maximum $CaCO_3$ precipitation. Therefore, sulfate reduction is regarded as a major contributor to carbonate precipitation in microbial mats. However, a rise in alkalinity is not the only factor necessary for the precipitation of $CaCO_3$. The presence of a nucleation site is also

required. In microbial mats, EPS plays the role of nucleation site, allowing for $CaCO_3$ mineral precipitation (Dupraz *et al.*, 2004; Dupraz and Visscher, 2005; Reid *et al.*, 2000). Cyanobacteria are the most common producers of EPS in microbial mats (Richert *et al.*, 2005; Stal, 2000), but SRB are also known to be involved in EPS production (Bosak and Newman, 2005; Braissant *et al.*, 2007).

A recent study on microbial mats from Hamelin Pool by Suosaari *et al.* (2016) suggested that the micrite, which forms the framework and cement, presents strong similarities with microstructures identified in Precambrian stromatolites. Thus, could potentially provide a window into Precambrian environments. Suosaari *et al.*, (2016) also revealed that lithified, well laminated buildups in Hamelin Pool usually derive from coccoid cyanobacterial mats whereas mats dominated by filamentous cyanobacteria result in poorly lithified sheets. In the present study, the smooth mat contains the highest proportion of micrite (~53%) *versus* ~38% for the pustular mat and ~39% for the tufted mat. This observation was also supported by SEM imaging that highlighted the more cohesive nature of the smooth mat compared to the two shallower mat types investigated here.

Suosaari *et al.* (2016) have suggested that the lithification of modern Shark Bay microbial differs depending on the location of the mats. In seaward mats, lithification potential was related to the dominant cyanobacterial type in the mat. They showed that mats dominated by coccoid cyanobacteria are more prone to lithification than mats where filamentous cyanobacteria were dominant. However, in shoreward mats, such a distinction is not apparent (Suosaari *et al.*, 2016). Our data from intertidal settings, comparable to Suosaari *et al.* (2016) "shoreward" mats, shows that the smooth mat type investigated here is the most lithified (micrite 53%) of the three mats investigated here. Pustular and tufted mats both show a comparable and lower degree of lithification (micrite ~38.5%). Both tufted and smooth mats are dominated by filamentous cyanobacterial communities whereas the pustular mat is dominated by coccoid cyanobacteria; This indicates that, within tidal settings, the type of cyanobacteria dominating the mat does not exclusively determine the lithification potential and that additional parameters should therefore be considered when investigating the processes involved in biologically-induced and influenced

lithification in modern mats. This comparison further demonstrates the complexity of these microbial systems.

Shark bay mats as analogues of Precambrian mats?

Modern microbial mats found in Shark Bay are regarded as potential analogues of Precambrian stromatolites (*e.g.* Walter, 1994). Therefore, the characterisation of microbial communities and isotopic signatures in modern mats from Shark Bay is believed to provide further insight into Precambrian ecosystems. Suosaari *et al.* (2016) suggested that well-laminated buildups in Hamelin Pool derive from coccoid cyanobacterial mats and that *Entophysalis*, which is common in most lithifying mats of Hamelin Pool, is related to the *Eoentophysalis sp*. which has been reported in early and middle Proterozoic stromatolite assemblages. In addition, internal fabrics of Neoproterozoic stromatolites from the Pilbara have shown strong similarities with clotted peloidal textures of the micrite detected in Hamelin microbial mats, suggesting that these modern mats indeed offer a window into Precambrian environments (Suosaari *et al.*, 2016).

Nonetheless, the present study highlights slight variations in terms of microbial communities, isotopic signatures and microfabrics that could potentially be related to the different water depths at which the microbial mats are thriving. The lipid distribution and CSIA show that SRB and seagrass contribution vary with depth. Moreover, the combination of lipid and imaging techniques suggests that diatom genera vary in the different mats. In addition, a previous study by Jahnke *et al.* (2004) on two microbial mats from similar environments (*e.g.* similar temperature, pH, $\delta^{13}C_{DIC}$) presented differences in $\delta^{13}C_{biomass}$ values (6.4‰ discrepancy), that were associated with the different macroscopic structures of the mats, highlighting the need for multi-proxy studies including isotopic signatures and microfabric characterisation.

Then again, despite the many resemblances highlighted above, a key difference between the modern microbial mats from Hamelin Pool and the Precambrian stromatolites is the high abundance of eukaryotes (foraminifers, bivalve shells, diatoms), also highlighted by the evidence of eukaryotic activity (*e.g.* microboring) and eukaryotic lipids (*e.g.* C_{25} HBI and steroids) in the modern mats. These results are in accordance with the previous study by Edgcomb *et al.* (2014) that

revealed a high eukaryotic diversity in Shark Bay mats including stramenopiles (diatoms; 10-30%), Alveolata (ciliates and dinoflagellates; 10-50%) and unclassified eukaryotes (5-45%).

This eukaryotic activity (*e.g.* bioturbation) is likely to play a role in the formation of clotted structures observed in several modern microbial mat types. Moreover, eukaryotes can actively consume the EPS, which would affect the cohesive structure of the mats and the mat lithification processes (Edgcomb *et al.*, 2014). Therefore, eukaryotic organisms present in the modern Carbla mats most probably impact their microstructure, potentially causing difficulties in the comparison with Precambrian mats that were not affected by eukaryotic activity.

Conclusions

The present comparison of microfossils, bioclast remains and the micritic content of the mats with lipid distribution and their stable carbon isotopic signatures highlighted the importance of combined investigations to characterise modern microbial mats. Our main results are described as follows:

- This complimentary study allowed a more detailed characterisation of mat communities. While cyanobacteria, for instance, were detected by both imaging techniques and lipid analyses, the presence of specific diatoms, ciliates or higher plant input was revealed by lipid analyses only.

- The contribution of aquatic macrophytes increases with rising water depth suggesting a greater contribution from the seagrass meadows to the deepest mat, whereas SRB markers are most abundant in the shallowest tufted mat.

- In tidal settings, the dominant type of cyanobacteria of each mat type does not appear to be the main controlling factor for lithification potential.

- All mats investigated show a major eukaryotic input, revealed by imaging techniques as well as lipid analyses. These eukaryotes have impacted the microstructure, lipid composition and stable isotopic signatures of modern

mats, potentially complicating the comparison between modern mats and Precambrian mats.

This study highlights the benefit of using a multiproxy approach when investigating such complex modern ecosystems. Cross-disciplinary studies can therefore allow for a more holistic understanding of the processes involved in the lithification of microbial mats and formation of stromatolites. In addition, as numerous factors (*e.g.* environmental conditions, carbon uptake physiologies, presence of bioturbators) can affect isotopic signatures and microfabrics, the investigation of recent and fossil stromatolites need to be regarded with caution and should be complemented by biological, sedimentological and geochemical data.

Acknowledgments

Field work was supported by an ARC discovery grant (Grice, Greenwood, Snape and Summons – 2010-2013). Geoff Chidlow and Peter Hopper are thanked for GC-MS technical support. Greg Skrzypek is acknowledged for carbonate stable isotopes analyses and Michael Verrall for his technical support regarding SEM analyses. This research was supported by an ARC DORA Discovery Grant (Grice, 2013-2016; DP130100577) and an ARC infrastructure grant (LE110100119). CP thanks WA-OIG, Curtin University for a PhD stipend and the Institute of Geoscience Research (TIGeR) for a top up scholarship.

References

Abd-el Malek, Y., Rizk, S.G., 1963. Bacterial sulphate reduction and the development of alkalinity. III. Experiments under natura conditions in the Wadi Natriin. *Journal of applied bacteriology* **26**, 20–26.

Allen, M.A., Goh, F., Burns, B.P., Neilan, B.A., 2009. Bacterial, archaeal and eukaryotic diversity of smooth and pustular microbial mat communities in the hypersaline lagoon of Shark Bay. *Geobiology* **7**, 82–96.

Bauld, J., 1984. Microbial mats in marginal marine environments: Shark Bay, Western Australia, in: Cohen, Y., Castenholz, R.W., Halvorson, H.O. (Eds.), Microbial Mats: Stromatolites. Alan R, Liss, New York, pp. 39–58.

Baumgartner, L.K., Reid, R.P., Dupraz, C.P., Decho, A.W., Buckly, D.H., Spear, J.R., Przekop, K.M., Visscher, P.T., 2006. Sulfate reducing bacteria in microbial mats: Changing paradigms, new discoveries. *Sedimentary Geology* **185**, 131–145.

Belicka, L.L., Burkholder, D., Fourqurean, J.W., Heithaus, M.R., MacKo, S.A., Jaffé, R., 2012. Stable isotope and fatty acid biomarkers of seagrass, epiphytic, and algal organic matter to consumers in a pristine seagrass ecosystem. *Marine and Freshwater Research* **63**, 1085–1097.

Bosak, T., Newman, D.K., 2005. Microbial kinetic controls on calcite morphology in supersaturated solutions. *Journal of Sedimentary Research* **75**, 190–199.

Braissant, O., Decho, A.W., Dupraz, C.P., Glunk, C., Przekop, K.M., Visscher, P.T., 2007. Exopolymeric substances of sulfate-reducing bacteria: Interactions with calcium at alkaline pH and implication for formation of carbonate minerals. *Geobiology* **5**, 401–411.

Briggs, D.*E.G.*, Summons, R.E., 2014. Ancient biomolecules: their origins, fossilization, and role in revealing the history of life. *BioEssays : news and reviews in molecular, cellular and developmental biology* **36**, 482–90.

Bühring, S.I., Smittenberg, R.H., Sachse, D., Lipp, J.S., Golubic, S., Sachs, J.P., Hinrichs, K.U., Summons, R.E., 2009. A hypersaline microbial mat from the Pacific Atoll Kiritimati: Insights into composition and carbon fixation using biomarker analyses and a ^{13}C-labeling approach. *Geobiology* **7**, 308–323.

Burns, B.P., Goh, F., Allen, M., Neilan, B.A., 2004. Microbial diversity of extant stromatolites in the hypersaline marine environment of Shark Bay, Australia. *Environmental Microbiology* **6**, 1096–1101.

Canuel, E.A., Freeman, K.H., Wakeham, S.G., 1997. Isotopic compositions of lipid biomarker compounds in estuarine plants and surface sediments. *Limnology and Oceanography* **42**, 1570–1583.

Dupraz, C.P., Visscher, P.T., 2005. Microbial lithification in marine stromatolites and hypersaline mats. *Trends in microbiology* **13**, 429–438.

Dupraz, C.P., Visscher, P.T., Baumgartner, L.K., Reid, R.P., 2004. Microbe-mineral interactions: early carbonate precipitation in a hypersaline lake (Eleuthera Island, Bahamas). *Sedimentology* **51**, 745–765.

Edgcomb, V.P., Bernhard, J.M., Summons, R.E., Orsi, W., Beaudoin, D., Visscher, P.T., 2014. Active eukaryotes in microbialites from Highborne Cay, Bahamas, and Hamelin Pool (Shark Bay), Australia. *The ISME journal* **8**, 418–29.

Flügel, E., 2010. Microfacies of carbonate rocks: Analysis, interpretation and application, 2nd editio. ed. Springer-Verlag Berlin Heidelberg.

Fourçans, A., De Oteyza, T.G., Wieland, A., Solé, A., Diestra, E., Van Bleijswijk, J., Grimalt, J.O., Kühl, M., Esteve, I., Muyzer, G., Caumette, P., Duran, R., 2004. Characterization of functional bacterial groups in a hypersaline microbial mat community (Salins-de-Giraud, Camargue, France). *FEMS Microbiology Ecology* **51**, 55–70.

Freeman, K.H., Wakeham, S.G., Hayes, J.M., 1994. Predictive isotopic biogeochemistry of lipids from marine anoxic basins. *Organic Geochemistry* **21**, 629–644.

Grice, K., Schouten, S., Peters, K.E., Sinninghe Damsté, J.S., 1998. Molecular isotopic characterisation of hydrocarbon biomarkers in Palaeocene-Eocene evaporitic, lacustrine source rocks from the Jianghan Basin, China. *Organic Geochemistry* **29**, 1745–1764.

Grimalt, J.O., de Wit, R., Teixidor, P., Albaigés, J., 1992. Lipid biogeochemistry of Phormidium and Microcoleus mats. *Organic Geochemistry* **19**, 509–530.

Grimalt, J.O., Yruela, I., Saiz-Jimenez, C., Toja, J., de Leeuw, J.W., Albaigés, J., 1991. Sedimentary lipid biogeochemistry of an hypereutrophic alkaline lagoon. *Geochimica et Cosmochimica Acta* **55**, 2555–2577.

Grossi, V., Beker, B., Geenevasen, J.A.J., Schouten, S., Raphel, D., Fontaine, M.F., Sinninghe Damsté, J.S., 2004. C 25 highly branched isoprenoid alkenes from the marine benthic diatom Pleurosigma strigosum. *Phytochemistry* **65**, 3049–3055.

Guo, L., Riding, R., 1992. Aragonite laminae in hot water travertine crusts, Rapolano Terme, Italy. *Sedimentology* **39**, 1067–1079.

Harvey, H.R., McManus, G.B., 1991. Marine ciliates as a widespread source of tetrahymanol and hopan-3β-ol in sediments. *Geochimica et Cosmochimica Acta* **55**, 3387–3390.

Hoffman, H.J., 2000. Archean stromatolites as microbial archives, in: Riding, R.E., Awramik, S.M. (Eds.), Microbial Sediments. Springer, Berlin, pp. 315–327.

Jahnert, R.J., Collins, L.B., 2011. Significance of subtidal microbial deposits in Shark Bay, Australia. *Marine Geology* **286**, 106–111.

Jahnert, R.J., Collins, L.B., 2012. Characteristics, distribution and morphogenesis of subtidal microbial systems in Shark Bay, Australia. *Marine Geology* **303–306**, 115–136.

Jahnert, R.J., Collins, L.B., 2013. Controls on microbial activity and tidal flat evolution in Shark Bay, Western Australia. *Sedimentology* **60**, 1071–1099.

Jahnke, L., Embaye, T., Hope, J., Turk, K.A., Van Zuilen, M., Des Marais, D.J., Farmer, J.D., Summons, R.E., 2004. Lipid biomarker and carbon isotopic signatures for stromatolite-forming, microbial mat communities and Phormidium cultures from Yellowstone National Park. *Geobiology* **2**, 31–47.

Jones, D.M., Carter, J.F., Eglington, G., Jumeau, E.J., Fenwick, C.S., 1991. Determination of $\delta^{13}C$ values of sedimentary straight chain and cyclic alcohols by gas chromatography/isotope ratio mass spectrometry. *Journal of mass spectrometry* **20**, 641–646.

Killops, S.D., Frewin, N.L., 1994. Triterpenoid diagenesis and cuticular preservation. *Organic Geochemistry* **21**, 1193–1209.

Logan, B.W., 1974. Evolution and diagenesis of quaternary carbonate sequences, Shark Bay, Western Australia. *American association of petroleum geologists memoir* **22**, 195–249.

Logan, B.W., Cebulski, D.E., 1970. Sedimentary environments of Shark Bay, Western Australia. *American association of petroleum geologists memoir* **13**, 1–37.

Londry, K.L., Jahnke, L.L., Des Marais, D.J., 2004. Stable carbon isotope ratios of lipid biomarkers of sulfate-reducing bacteria. *Applied and Environmental Microbiology* **70**, 745–751.

Madden, R.H.C., Wilson, M.E.J., O'Shea, M., 2013. Modern fringing reef carbonates from equatorial SE Asia: An integrated environmental, sediment and satellite characterisation study. *Marine Geology* **344**, 163–185.

McKirdy, D.M., Thorpe, C.S., Haynes, D.E., Grice, K., Krull, E.S., Halverson, G.P., Webster, L.J., 2010. The biogeochemical evolution of the Coorong during the mid- to late Holocene: An elemental, isotopic and biomarker perspective. *Organic Geochemistry* **41**, 96–110.

Melendez, I., Grice, K., Schwark, L., 2013. Exceptional preservation of Palaeozoic steroids in a diagenetic continuum. *Scientific reports* **3**, 2768.

Pagès, A., Grice, K., Ertefai, T., Skrzypek, G., Jahnert, R., Greenwood, P., 2014a. Organic geochemical studies of modern microbial mats from Shark Bay: Part I: Influence of depth and salinity on lipid biomarkers and their isotopic signatures. *Geobiology* **12**, 469–487.

Pagès, A., Grice, K., Vacher, M., Welsh, D.T., Teasdale, P.R., Bennett, W.W., Greenwood, P., 2014b. Characterizing microbial communities and processes in a modern stromatolite (Shark Bay) using lipid biomarkers and two-dimensional distributions of porewater solutes. *Environmental microbiology* **16**, 2458–2474.

Pagès, A., Grice, K., Welsh, D.T., Teasdale, P.T., Van, M.J., Greenwood, P., 2015. Lipid Biomarker and Isotopic Study of Community Distribution and Biomarker Preservation in a LaminatedMicrobialMat from Shark Bay,Western Australia. *Environmental Microbiology* **70**, 459–472.

Paoletti, C., Pushparaj, B., Florenzano, G., Capella, P., Lercker, G., 1976. Unsaponifiable matter of green and blue-green algal lipids as a factor of biochemical differentiation of their biomasses: I. Total unsaponifiable and hydrocarbon fraction. *Lipids* **11**, 258–265.

Papineau, D., Walker, J.J., Mojzsis, S.J., Pace, N.R., 2005. Composition and Structure of Microbial Communities from Stromatolites of Hamelin Pool in Shark Bay , Western Australia Composition and Structure of Microbial Communities from Stromatolites of Hamelin Pool in Shark Bay , Western Australia. *Applied and environmental microbiology* **71**, 4822–4832.

Perry, C.T., 1999. Biofilm-related calcification, sediment trapping and constructive micrite envelopes: A criterion for the recognition of ancient grass-bed environments? *Sedimentology* **46**, 33–45.

Perry, C.T., Hepburn, L.J., 2008. Syn-depositional alteration of coral reef framework through bioerosion, encrustation and cementation: Taphonomic signatures of reef accretion and reef depositional events. *Earth-Science Reviews* **86**, 106–144.

Reid, R.P., 2011. Stromatolites, in: Hopley, D. (Ed.), Encyclopedia of Modern Coral Reefs: Structure, Form and Process. Springer Netherlands, Dordrecht, pp. 1045–1051.

Reid, R.P., James, N.P., Macintyre, I.G., Dupraz, C.P., Burne, R. V, Macintyre, G., 2003. Shark Bay Stromatolites : Microfabrics and Reinterpretation of Origins. *Facies* **49**, 299–324.

Reid, R.P., Visscher, P.T., Decho, A.W., Stolz, J.F., Bebout, B.M., 2000. The role of microbes in accretion, lamination and early lithification of modern marine stromatolites. *Nature* **406**, 989–992.

Richert, L., Golubic, S., Le Guédès, R., Ratiskol, J., Payri, C., Guezennec, J., 2005. Characterization of exopolysaccharides produced by cyanobacteria isolated from Polynesian microbial mats. *Current microbiology* **51**, 379–384.

Riding, R., 2000. Microbial carbonates: the geological record of calcified bacterial-algal mats and biofilms. *Sedimentology* **47**, 179–214.

Robinson, N., Eglinton, G., 1990. Lipid chemistry of Icelandic hot spring microbial mats. *Organic Geochemistry* **15**, 291–298.

Rontani, J.F., Volkman, J.K., 2005. Lipid characterization of coastal hypersaline cyanobacterial mats from the Camargue (France). *Organic Geochemistry* **36**, 251–272.

Sinninghe Damsté, J.P., Kenig, F., Koopmans, M.P., Koster, J., Schouten, S., Hayes, J.M., De Leuuw, J.W., 1995. Evidence for gammacerane as an indicator of water column stratification. *Geochimica et Cosmochimica Acta* **59**, 1895–1900.

Sinninghe Damsté, J.S., Muyzer, G., Abbas, B., Rampen, S.W., Massé, G., Allard, W.G., Belt, S.T., Robert, J.-M., Rowland, S.J., Moldowan, J.M., Barbanti, S.M., Fago, F.J., Denisevich, P., Dahl, J., Trindade, L.A.F., Schouten, S., 2004. The Rise of the Rhizosolenid Diatoms. *Science* **304**, 584–587.

Spaulding, S.A., Lubinski, D.J., Potapova, M., 2010. Diatoms of the United States [WWW Document].

Stal, L.J., 2000. Cyanobacterial mats and stromatolites, in: Whitton, B.A., Potts, M. (Eds.), The Ecology of Cyanobacteria. Their Diversity in Time and Space. Kluwer Academic Publishers, Dordrecht, pp. 61–120.

Summons, R., Barrow, R., Capon, R., Hope, J., Stranger, C., 1993. The Structure of a New C_{25} Isoprenoid Alkene Biomarker from Diatomaceous Microbial Communities. *Aust. J. Chem.* **46**, 907–915.

Summons, R.E., Bird, L.R., Gillespie, A. L., Pruss, S.B., Roberts, M., Sessions, A. L., 2013. Lipid biomarkers in ooids from different locations and ages: Evidence for a common bacterial flora. *Geobiology* **11**, 420–436.

Suosaari, E.P., Reid, R.P., Playford, P.E., Foster, J.S., Stolz, J.F., Casaburi, G., Hagan, P.D., Chirayath, V., Macintyre, I.G., Planavsky, N.J., Eberli, G.P., 2016. New multi-scale perspectives on the stromatolites of Shark Bay, Western Australia. *Scientific Reports* **6**, 20557.

Taylor, J., Parkes, R., 1983. The Cellular Fatty Acids of the Sulphate-reducing Bacteria, *Desulfobacter sp*., *Desulfobulbus sp*. and *Desulfovibrio desulfuricans*. *Journal of General Microbiology* **129**, 3303–3309.

Taylor, J., Parkes, R.J., 1985. Identifying Different Populations of Sulfate-Reducing Bacteria within Marine Sediment Systems, Using Fatty-Acid Biomarkers. *Journal of General Microbiology* **131**, 631–642.

Thiel, V., Merz-Preiß, M., Reitner, J., Michaelis, W., 1997. Biomarker studies on microbial carbonates: Extractable lipids of a Calcifying Cyanobacterial mat (Everglades, USA). *Facies* **36**, 163–172.

Touchette, B.W., Burkholder, J.M., 2000. Overview of the physiological ecology of carbon metabolism in seagrasses. *Journal of Experimental Marine Biology and Ecology* **250**, 169–205.

Tulipani, S., Grice, K., Krull, E., Greenwood, P., Revill, A.T., 2014. Salinity variations in the northern Coorong Lagoon, South Australia: Significant changes

in the ecosystem following human alteration to the natural water regime. *Organic Geochemistry* **75**, 74–86.

Visscher, P.T., Reid, R.P., Bebout, B.M., 2000. Microscale observations of sulfate reduction : Correlation of microbial activity with lithified micritic laminae in modern marine stromatolites. *Geology* 919–922.

Volkman, J.K., Barrett, S.M., Blackburn, S.I., Mansour, M.P., Sikes, E.L., Gelin, F., 1998. Microalgal biomarkers: A review of recent research developments. *Organic Geochemistry* **29**, 1163–1179.

Walker, D.I., Kendrick, G.A., McComb, A.J., 1988. The distribution of seagrass species in Shark Bay, Western Australia, with notes on their ecology. *Aquatic Botany* **30**, 305–317.

Wraige, E.J., Belt, S.T., Lewis, C.A., Cooke, D.A., Robert, J., 1997. Variations in structures and distributions of C_{25} highly branched isoprenoid (HBI) alkenes in cultures of the diatom , Haslea ostrearia (Simonsen). *Organic Geochemistry* **27**, 497–505.

Appendix 5

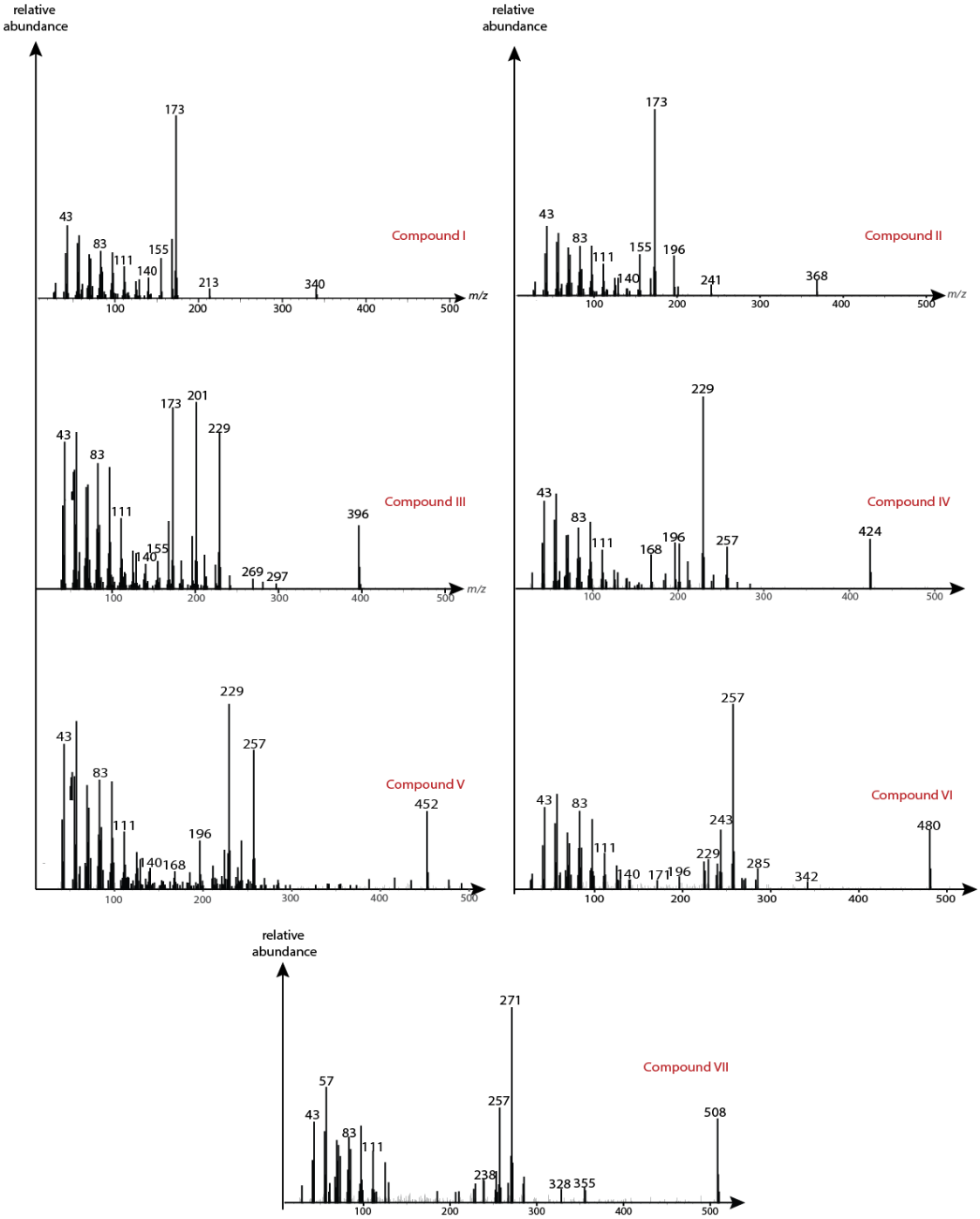

Figure A5-1. Mass spectra of the compounds tentatively identified as n-alkyl-n-decanoates.

Chapter 6

Conclusions and Outlook

This PhD project explored and introduced the use of complementary techniques (combined organic, inorganic and stable isotope geochemistry with imaging tools) to investigate induced carbonate biomineralisations. These techniques were applied to concretions associated with the Toarcian Oceanic Anoxic Event and to modern stromatolites from a hypersaline tidal environment (Shark Bay, Western Australia). The three main outcomes from the thesis are described under the sub-headings below i) Preservation of complex palaeoenvironmental signals in carbonate concretions, ii) Exceptional organic matter (OM) and soft tissue preservation in carbonate concretions and, iii) Integrated investigation of tidal microbialites at Carbla Beach, Hamelin Pool, Shark Bay.

Carbonate concretions are microbialites widely present in sedimentary rocks (*i.e.* OM-rich shales and sandstones) covering all geological ages. However, analogues are rare in modern environments, which limits the use of readily degradable biomarkers (*e.g.* DNA) to assess the natural environment of formation and the microbial communities involved in the formation of carbonate concretions. In earlier studies, the processes and environments of concretion formation have been modelled based on morphological and inorganic geochemical proxies. However, an increasing interest in carbonate concretions has recently developed due to the research potential they hold for finding evidence of early life.

Another type of microbialites, the stromatolites, are also widespread in sedimentary rocks, particularly in Archean and Proterozoic marine sediments, whereas their modern microbial mats homologues only occur in a few localities, often under hypersaline marine conditions (*e.g.* Shark Bay (WA), Bahamas (US)). Over time, modern and ancient stromatolites have been widely studied because of their potential as reservoir rocks for petroleum. This led to detailed characterisation of stromatolite morphologies, structures and microfabrics. However, the rising interest for early life over the past two decades, has generated a whole new interest for microbial ecosystems and the role they play(ed) in elemental cycling.

In this PhD project, various parameters (such as microscopy techniques, elemental distribution, lipid biomarkers and stable isotopes) have been applied to two distinct microbialite types (carbonate concretions and microbial mats) formed under contrasting settings and age.

Preservation of complex palaeoenvironmental signals in carbonate concretions

The role of microbial ecosystems in the formation of carbonate concretions is well-established, primarily based on inorganic, structural and mineralogical data (*e.g.* stable isotopes of carbonate, and texture, different phases of crystal growth, and the common occurrence of pyrite). Similarly, the depth at which concretions form within sediments has been previously addressed based on concretion morphology. However, little was known about OM composition and preservation within carbonate concretions. The data obtained based on mineralogy, texture as well as inorganic geochemical parameters (*i.e.:* elemental distribution, $\delta^{13}C$ values of carbonates) clearly records concretion growth signals (**Chapter 2**). Combined, these proxies support the major role played by sulfate reducing bacteria (SRB) in calcium carbonate concretion formation, as well as the likely role of iron reducing bacteria (FeR) in the development of an outer pyrite-rich rim. Furthermore, elemental analyses have suggested the existence of a redox front shortly before the pyritic rim that supports a change in microenvironmental conditions and/or microbial communities.

In contrast, lipid biomarker distributions reflect the sedimentary signal of the environment within which the concretion formed. In **Chapter 2**, aliphatic hydrocarbon distributions (within all sub-samples of the concretion) showed to be identical to the biomarkers found in the surrounding shale. However, the corresponding stable carbon isotopes were more negative in the concretion, which was attributed to the enhanced SRB activity. Other biomarkers, such as aryl isoprenoids (**Chapter 2**) and maleimides (**Chapter 4**), also provide information about the palaeoenvironmental conditions in the ancient water column.

Due to their greater cementation, concretions are often found *ex-situ*, with their host rock being weathered or eroded away. Up until recently only a few biomarker and biolipid studies have been found to be useful to characterise palaeoenvironmental conditions. For example, biomarkers derived from *Chlorobiaceae* demonstrate photic zone euxinia was prevalent in a Devonian water column playing a pivotal role in soft tissue preservation.

Exceptional organic matter and soft tissue preservation in carbonate concretions

Not only do carbonate concretions record both concretion growth and palaeoenvironmental signals, they are also well-known for their capacity to preserve beautiful morphological fossils. Although not all carbonate concretions contain a fossil, when a fossil is encapsulated it often shows a high degree of detail. These exceptionally-preserved fossils serve as nuclei for anaerobic OM degradation, often by SRB. This SRB activity is localised at the surface of the nuclei (**Chapter 2**). Thus, bulk OM parameters, such as the hydrogen indices (HI) that can reflect the state of preservation of the OM, were surprisingly high within the concretion body compared to the rim. These elevated HI values indicate that the OM is well-preserved in the body of the concretion whereas it is subjected to enhanced degradation within the pyritic rim.

Studies involving molecular geochemistry, stable isotopes and microstructure of concretions' nuclei are rare due to the destructive nature of the techniques involved. In **Chapter 3** of this thesis, an ichthyosaur vertebra encapsulated in a carbonate

concretion was subjected to lipid biomarker and elemental distribution as well as imaging. It was established that the oldest remains of red blood cells, collagen fibres encrusted in fluorapatite were identified, pushing back the occurrence of red blood cells and collagen by 108 Ma. The very small size of the red blood cells were attributed to the low oxygen levels in the oceans and atmosphere when the ichthyosaur lived.

The oldest original biolipids were previously reported in a Devonian concretion. In this PhD thesis (**Chapter 3**), the second oldest sterols (and a number of diagenetic products) were identified in the ichthyosaur vertebra. In particular abundant cholesterol and its stable carbon isotopic composition, is attributed to the ichthyosaur's diet (with minor planktonic contribution) from the ancient water column.

This research opens up an underexploited area of palaeobiological information across geological ages. It is possible for example that highly labile molecules such as proteins, or DNA fragments much older than presently known might be extracted from concretions containing fossils.

Integrated investigation of tidal microbialites at Carbla Beach, Hamelin Pool, Shark Bay

Modern microbial mat ecosystems are often investigated using DNA assessments. They have revealed a great complexity and diversity within modern microbial mat ecosystems. However, this approach cannot be used to investigate microbial communities in ancient mat types (*e.g.* Precambrian and Phanerozoic) as DNA is readily degraded. Integrated techniques, similar to the ones employed in **Chapter 3,** were applied to modern microbial mats from Shark Bay (**Chapter 5**). They highlighted the efficiency of using complementary approach (microfabrics characterisation with lipid biomarker and stable isotopic analyses) to characterise modern microbial mats.

Three different types of mats (tufted, pustular and smooth) along a tidal flat gradient were investigated. All mats were dominated by cyanobacteria and imaging techniques revealed the preferential occurrence of filamentous cyanobacteria for the tufted and smooth mats; and coccoid cyanobacteria for the pustular mat. Imaging and biomarker analyses of diatoms showed contrasting results, where diatoms were

abundant and diverse in the pustular mat the $C_{25:1}$ HBI (attributed to diatom) was low. In contrast, the smooth mat showed high relative abundance of $C_{25:1}$ HBI but only few diatoms of other species. Major eukaryotic input was highlighted in all mats, which could potentially make the comparison of Shark Bay microbial mats with Precambrian mats challenging.

Chapter 5 allowed a detailed appraisal of the microbial mat ecosystems and environments based on long lasting markers. Furthermore, these observations were in agreement with previous DNA studies of the microbial mats from the same location, confirming the strength of a complementary approach. Such a comparison with previous DNA studies is only possible for modern or recent microbialites; whereas the combined study of lipid biomarkers and stable isotopes with imaging techniques can also be employed on more ancient microbialites, as demonstrated in **Chapters 2-4**.

Future perspectives

The exceptionally preserved biomolecules and soft tissues present in the ichthyosaur bone presented in Chapter 3, strongly suggest that proteins and DNA (although partly degraded) could be preserved as well in that sample. This microbiological approach is likely to be the next step in the investigation of such an exceptional sample and is currently underway.

Chapter 4 of this thesis demonstrated the need of further geochemical analyses in the investigation of the source for 2-methyl-3-ethyl-maleimide (MEM) in the vertebra of the ichthyosaur. Future work will include the extraction of lipid biomarkers from a larger quantity of bone to try to obtain stable carbon isotopic measurement for the MEM. Furthermore investigation of the iron porphyrin content would also aid to determine if the MEM from the vertebra has a heme origin.

Furthermore, the development of biomarker and stable isotopes work on carbonate concretions would be very useful to better understand past environments. The overall establishment of a systematic application of combined organic, inorganic and imaging techniques on a much larger set of induced biomineralisations, from different ages, types and environments of formation would be very useful in determining more thoroughly the limits of such an approach (*e.g.* time limits, sample

sizes). This type of multiproxy investigation is likely to retain key information for the understanding of the evolution of life over extended periods of geological time, and the first microbial ecosystems on Earth.

Bibliography

"Every reasonable effort has been made to acknowledge the owners of copyright material. I would be pleased to hear from any copyright owner who has been omitted or incorrectly acknowledged"

Abd-el Malek, Y., Rizk, S.G., 1963. Bacterial sulphate reduction and the development of alkalinity. III. Experiments under natura conditions in the Wadi Natriin. *Journal of applied bacteriology* **26**, 20–26.

Aigueperse, J., Remy, J., Chevallier, F., 1978. Sterols in various organs of adult female swine. *Annales de biologie animale, biochimie, biophysique* **18**, 1317–1324.

Al-Suwaidi, A.H., Angelozzi, G.N., Baudin, F., Damborenea, S.E., Hesselbo, S.P., Jenkyns, H.C., Manceñido, M.O., Riccardi, A.C., 2010. First record of the Early Toarcian Oceanic Anoxic Event from Southern Hemisphere, Neuquén Basin, Argentina. *Journal of the Geological Society* **167**, 633–636.

Allen, M.A., 2006. An astrobiology focused analysis of microbial mat communities from Hamelin Pool, Shark Bay, Western Australia.

Allen, M.A., Goh, F., Burns, B.P., Neilan, B.A., 2009. Bacterial, archaeal and eukaryotic diversity of smooth and pustular microbial mat communities in the hypersaline lagoon of Shark Bay. *Geobiology* **7**, 82–96.

Allison, P.A., 1988a. Konservat-Lagerstätten : Cause and Classification. *Paleobiology* **14**, 331–344.

Allison, P.A., 1988b. The role of anoxia in the decay and mineralization of proteinaceous macro-fossils. *Paleobiology* **14**, 139–154.

Arua, I., 1991. The trace fossil Teredolites longissimus in calcareous concretions from the Eocene Ameki formation, southeastern Nigeria. *Journal of African Earth Sciences (and the Middle East)* **12**, 605–608.

Asara, J.M., Schweitzer, M.H., Freimark, L.M., Phillips, M., Cantley, L.C., 2007. Protein sequences from mastodon and Tyrannosaurus rex revealed by mass spectrometry. *Science* **316**, 280–285.

Atlas, R.M., Bartha, R., 1998. Microbial ecology: fundamentals and applications. Addison - Wiley, Reading.

Awramik, S.M., 1992. The oldest records of photosynthesis. *Photosynthesis research* **33**, 75–89.

Barakat, A.O., Rullkötter, J., 1997. A Comparative Study of Molecular Paleosalinity Indicators: Chromans, Tocopherols and C_{20} Isoprenoid Thiophenes in Miocene Lake Sediments (Nördlinger Ries, Southern Germany). *Aquatic Geochemistry* **3**, 169–190.

Baudin, F., Herbin, J.-P., Vandenbroucke, M., 1990a. Mapping and geochemical characterization of the Toarcian organic matter in the Mediterranean Tethys and Middle East. *Organic Geochemistry* **16**, 677–687.

Baudin, F., Herbin, J.P., Vandenbroucke, M., 1990b. Mapping and geochemical characterization of the Toarcian organic matter in the Mediterranean Tethys and Middle East. *Organic Geochemistry* **16**, 677–687.

Bauld, J., 1984. Microbial mats in marginal marine environments: Shark Bay, Western Australia, in: Cohen, Y., Castenholz, R.W., Halvorson, H.O. (Eds.), Microbial Mats: Stromatolites. Alan R, Liss, New York, pp. 39–58.

Baumgartner, L.K., Reid, R.P., Dupraz, C.P., Decho, A.W., Buckly, D.H., Spear, J.R., Przekop, K.M., Visscher, P.T., 2006. Sulfate reducing bacteria in microbial mats: Changing paradigms, new discoveries. *Sedimentary Geology* **185**, 131–145.

Belicka, L.L., Burkholder, D., Fourqurean, J.W., Heithaus, M.R., MacKo, S.A.,

Jaffé, R., 2012. Stable isotope and fatty acid biomarkers of seagrass, epiphytic, and algal organic matter to consumers in a pristine seagrass ecosystem. *Marine and Freshwater Research* **63**, 1085–1097.

Bell, E.A., Boehnke, P., Harrison, T.M., Mao, W.L., 2015. Potentially biogenic carbon preserved in a 4.1 billion-year-old zircon. *Proceedings of the National Academy of Sciences of the United States of America* **112**, 14518–14521.

Bernard, A., Lécuyer, C., Vincent, P., Amiot, R., Bardet, N., Buffetaut, E., Cuny, G., Fourel, F., Martineau, F., Mazin, J.-M., Prieur, A., 2010. Regulation of body temperature by some Mesozoic marine reptiles. *Science* **328**, 1379–1382.

Berndmeyer, C., Thiel, V., Schmale, O., Wasmund, N., Blumenberg, M., 2014. Biomarkers in the stratified water column of the Landsort Deep (Baltic Sea). *Biogeosciences* **11**, 7009–7023.

Berner, R.A., 1967. Rate of concretion growth. *Geochimica et Cosmochimica Acta* **32**, 477–483.

Berner, R.A., 1968. Calcium carbonate concretions formed by the decomposition of organic matter. *Science* **159**, 195–197.

Berner, R.A., 2004. The Phanerozoic carbon cycle: O_2 and CO_2. Oxford University Press.

Berner, R.A., 2006. GEOCARBSULF: A combined model for Phanerozoic atmospheric O_2 and CO_2. *Geochimica et Cosmochimica Acta* **70**, 5653–5664.

Berner, R.A., Vandenbrooks, J.M., Ward, P.D., 2007. Oxygen and Evolution. *Science* **316**, 557–559.

Berner, Z.A., Puchelt, H., Nöltner, T., Kramar, U., 2013. Pyrite geochemistry in the Toarcian Posidonia Shale of south-west Germany: Evidence for contrasting trace-element patterns of diagenetic and syngenetic pyrites. *Sedimentology* **60**, 548–573.

Bertazzo, S., Maidment, S.C.R., Kallepitis, C., Fearn, S., Stevens, M.M., Xie, H.,

2015. Fibres and cellular structures preserved in 75-million–year-old dinosaur specimens. *Nature Communications* **6**, 7352.

Boetius, A., Ravenschlag, K., Schubert, C.J., Rickert, D., Widdel, F., Gieseke, A., Amann, R., Jùrgensen, B.B., Witte, U., Pfannkuche, O., 2000. A marine microbial consortium apparently mediating anaerobic oxidation of methane. *Nature* **407**, 623–626.

Bogacheva, M.P., Galimov, E.M., 1979. Intramolecular distribution of carbon isotopes in chlorophyll and hemin. *Geokhimiya* **7**, 1166–1172.

Bojanowski, M.J., Clarkson, E.N.K., 2012. Origin of siderite concretions in microenvironments of methanogenesis developed in a sulfate reduction zone: an exception or a rule? *Journal of Sedimentary Research* **82**, 585–598.

Boreham, C.J., Fookes, C.J.R., Popp, B.N., Hayes, J.M., 1989. Origins of etioporphyrins in sediments: Evidence from stable carbon isotopes. *Geochimica et Cosmochimica Acta* **53**, 2451–2455.

Bosak, T., Newman, D.K., 2005. Microbial kinetic controls on calcite morphology in supersaturated solutions. *Journal of Sedimentary Research* **75**, 190–199.

Bour, I., Mattioli, E., Pittet, B., 2007. Nannofacies analysis as a tool to reconstruct paleoenvironmental changes during the Early Toarcian anoxic event. *Palaeogeography, Palaeoclimatology, Palaeoecology* **249**, 58–79.

Bozec, L., Odlyha, M., 2011. Thermal denaturation studies of collagen by microthermal analysis and atomic force microscopy. *Biophysical Journal* **101**, 228–236.

Braissant, O., Decho, A.W., Dupraz, C.P., Glunk, C., Przekop, K.M., Visscher, P.T., 2007. Exopolymeric substances of sulfate-reducing bacteria: Interactions with calcium at alkaline pH and implication for formation of carbonate minerals. *Geobiology* **5**, 401–411.

Brassell, S.C., Eglinton, G., Howell, V.J., 1987. Palaeoenvironmental assessment of marine organic-rich sediments using molecular organic geochemistry. *Geological*

Society, London, Special Publications **26**, 79–98.

Briggs, D.*E.G.*, 2003. The role of decay and mineralization in the preservation of soft-bodied fossils. *Annual Review of Earth and Planetary Sciences* **31**, 275–301.

Briggs, D.*E.G.*, Kear, A.J., 1993. Fossilization of soft tissue in the laboratory. *Science* **259**, 1439–1442.

Briggs, D.*E.G.*, Summons, R.E., 2014. Ancient biomolecules: their origins, fossilization, and role in revealing the history of life. *BioEssays : news and reviews in molecular, cellular and developmental biology* **36**, 482–90.

Brocks, J.J., Pearson, A., 2005. Building the Biomarker Tree of Life. *Reviews in Mineralogy and Geochemistry* **59**, 233–258.

Brocks, J.J., Summons, R.E., 2003. Sedimentary hydrocarbons, biomarkers for early life, in: Treatise on Geochemistry. pp. 63–115.

Bühring, S.I., Smittenberg, R.H., Sachse, D., Lipp, J.S., Golubic, S., Sachs, J.P., Hinrichs, K.U., Summons, R.E., 2009. A hypersaline microbial mat from the Pacific Atoll Kiritimati: Insights into composition and carbon fixation using biomarker analyses and a ^{13}C-labeling approach. *Geobiology* **7**, 308–323.

Burley, S., Kantorowicz, J.D., Waugh, B., 1985. Clastic diagenesis. *Geological Society, London, Special Publications* **18**, 189–226.

Burns, B.P., Anitori, R., Butterworth, P., Henneberger, R., Goh, F., Allen, M. a., Ibañez-Peral, R., Bergquist, P.L., Walter, M.R., Neilan, B. a., 2009. Modern analogues and the early history of microbial life. *Precambrian Research* **173**, 10–18.

Burns, B.P., Goh, F., Allen, M., Neilan, B.A., 2004. Microbial diversity of extant stromatolites in the hypersaline marine environment of Shark Bay, Australia. *Environmental Microbiology* **6**, 1096–1101.

Canuel, E.A., Freeman, K.H., Wakeham, S.G., 1997. Isotopic compositions of lipid biomarker compounds in estuarine plants and surface sediments. *Limnology and*

Oceanography **42**, 1570–1583.

Cecca, F., Macchioni, F., 2004. The two Early Toarcian (Early Jurassic) extinction events in ammonoids. *Lethaia* **37**, 35–56.

Claver, J.A., Quaglia, A.*I.E.*, 2009. Comparative Morphology, Development, and Function of Blood Cells in Nonmammalian Vertebrates. *Journal of Exotic Pet Medicine* **18**, 87–97.

Cohen, A.S., Coe, A.L., Harding, S.M., Schwark, L., 2004. Osmium isotope evidence for the regulation of atmospheric CO_2 by continental weathering. *Geology* **32**, 157–160.

Cohen, P.A., Schopf, J.W., Butterfi, N.J., Kudryavtsev, A.B., Macdonald, F.A., 2011. Phosphate biomineralization in mid-Neoproterozoic protists. *Geology* **39**, 539–542.

Coleman, M.L., 1993. Microbial processes: Controls on the shape and composition of carbonate concretions. *Marine Geology* **113**, 127–140.

Coleman, M.L., Raiswell, R., 1980. Carbon , oxygen and sulphur isotope variations in concretions from the Upper Lias of N.E. England. *Geochimica and Cosmochimica Acta* **45**, 329–340.

Coleman, M.L., Raiswell, R., 1995. Source of carbonate and origin of zonation in pyritiferous carbonate concretions: evaluation of a dynamic model. *American Journal of Science* **295**, 282–308.

Comet, P. a, McEvoy, J., Brassell, S.C., Eglinton, G., Maxwell, J.R., Thomson, I.D., 1981. Lipids of an Upper Albian limestone, Deep Sea Drilling Project Site 465. *Init. Rep. DSDP* **62**, 923–937.

Criss, R.E., Cooke, G.A., Day, S.D., 1988. An Organic Origin for the Carbonate Concretions of the Ohio Shale. *U.S. Geological Survey Bulletin*.

Curtis, C., Building, B., Sheffield, S., 1987. Mineralogical consequences of organic matter degradation in sediments : inorganic / organic, in: Leggett, J.K., Zuffa,

G.G. (Eds.), Marine Clastic Sedimentology. pp. 108–123.

Curtis, C.D., Coleman, M.L., Love, L.G., 1986. Pore water evolution during sediment burial from isotopic and mineral chemistry of calcite , dolomite and siderite concretions. *Geochimica et Cosmochimica Acta* **50**, 2321–2334.

Cvejic, J.H., Bodrossy, L., Rohmer, M., 2000. Bacterial triterpenoids of the hopane series from the methanotrophic bacteria *Methylocaldum sp*.: phylogenetic implications and first evidence for an unsaturated aminobacteriohopanepolyol. *FEMS Microbiology Letters* **182**, 361–365.

Dahl, J.E., Moldowan, J.M., Peters, K.E., Claypool, G.E., Rooney, M.A., Michael, G.E., Mello, M.R., Kohnen, M.L., 1999. Diamondoid hydrocarbons as indicators of natural oil cracking. *Nature* **399**, 54–57.

Dale, A., John, C.M., Mozley, P.S., Smalley, P.C., Muggeridge, A.H., 2014. Time-capsule concretions: Unlocking burial diagenetic processes in the Mancos Shale using carbonate clumped isotopes. *Earth and Planetary Science Letters* **394**, 30–37.

Danise, S., Twitchett, R.J., Matts, K., 2014. Ecological succession of a Jurassic shallow-water ichthyosaur fall. *Nature communications* **5**, 4789.

Das, S.S., Tripathi, M.K., 2009. Trace fossils from Talchir carbonate concretions, Giridih basin, Jharkhand. *Journal of Earth System Science* **118**, 89–100.

de Craen, M., Swennen, R., Keppens, E.M., Macaulay, C.I., Kiriakoulakis, K., 1999. Bacterially mediated formation of carbonate concretions in the Oligocene Boom Clay of Northern Belgium.

Des Marais, D.J., 1995. The biogeochemistry of hypersaline microbial mats. *Advances in Microbial Ecology* **14**, 251–274.

Donaldson, A.E., Lamont, I.L., 2013. Biochemistry changes that occur after death: Potential markers for determining post-mortem interval. *PLoS ONE* **8**, 1–10.

Dong, J., Zhang, S., Jiang, G., Zhao, Q., Li, H., Shi, X., Liu, J., 2008. Early

diagenetic growth of carbonate concretions in the upper Doushantuo Formation in South China and their significance for the assessment of hydrocarbon source rock. *Science in China Series D: Earth Sciences* **51**, 1330–1339.

Dromart, G., Allemand, P., Garcia, J.P., Robin, C., 1996. Cyclic fluctuation of carbonate production through the Jurassic along a Burgundy-Ardeche cross-section, eastern France. *Bulletin de la Societe geologique de France* **167**, 423–433.

Druckenmiller, P.S., Kelley, N., Whalen, M.T., McRoberts, C., Carter, J.G., 2014. An Upper Triassic (Norian) ichthyosaur (*Reptilia, Ichthyopterygia*) from northern Alaska and dietary insight based on gut contents. *Journal of Vertebrate Paleontology* **34**, 1460–1465.

Dupraz, C.P., Visscher, P.T., 2005. Microbial lithification in marine stromatolites and hypersaline mats. *Trends in microbiology* **13**, 429–438.

Dupraz, C.P., Visscher, P.T., Baumgartner, L.K., Reid, R.P., 2004. Microbe-mineral interactions: early carbonate precipitation in a hypersaline lake (Eleuthera Island, Bahamas). *Sedimentology* **51**, 745–765.

Edgcomb, V.P., Bernhard, J.M., Summons, R.E., Orsi, W., Beaudoin, D., Visscher, P.T., 2014. Active eukaryotes in microbialites from Highborne Cay, Bahamas, and Hamelin Pool (Shark Bay), Australia. *The ISME journal* **8**, 418–29.

El Albani, A., Bengtson, S., Canfield, D.E., Bekker, A., Macchiarelli, R., Mazurier, A., Hammarlund, E.U., Boulvais, P., Dupuy, J., Fontaine, C., Fu, F.T., Riboulleau, A., Sardini, P., Vachard, D., Whitehouse, M., Meunier, A., 2010. Large colonial organisms with coordinated growth in oxygenated environments 2.1 Gyr ago. *Nature* **466**, 100–104.

El Albani, A., Bengtson, S., Canfield, D.E., Riboulleau, A., Rollion Bard, C., Macchiarelli, R., Ngombi Pemba, L., Hammarlund, E., Meunier, A., Moubiya Mouele, I., Benzerara, K., Bernard, S., Boulvais, P., Chaussidon, M., Cesari, C., Fontaine, C., Chi-Fru, E., Garcia Ruiz, J.-M., Gauthier-

Lafaye, F., Mazurier, A., Pierson-Wickmann, A.-C., Rouxel, O., Trentesaux, A., Vecoli, M., Versteegh, G., White, L., Whitehouse, M., Bekker, A., 2014. The 2.1 Ga old Francevillian biota: biogenecity, taphonomy and biodiversity. *PloS one* **9**.

Ellsworth, R.K., 1970. Gas chromatographic determination of some maleimides produced by the oxidation of heme and chlorophyll a. *Journal of Chromatography A* **50**, 131–134.

Falkowski, P.G., Scholes, R.J., Boyle, E., Canadell, J., Canfield, D., Elser, J., Gruber, N., Hibbard, K., Högberg, P., Linder, S., Mackenzie, F.T., Moore, B., Pedersen, T., Rosenthal, Y., Seitzinger, S., Smetacek, V., Steffen, W., 2000. The global carbon cycle: a test of our knowledge of earth as a system. *Science* **290**, 291–296.

Farrimond, P., Eglinton, G., Brassell, S.C., Jenkyns, H.C., 1989. Toarcian anoxic event in Europe : an organic geochemical study. *Marine and Petroleum Geology* **6**, 136–147.

Faure, G., Mensing, T.M., 2005. Isotopes, Principles and Applications, 3rd ed. John Wiley & Sons.

Fischer, V., Bardet, N., Benson, R.B.J., Arkhangelsky, M.S., Friedman, M., 2016. Extinction of fish-shaped marine reptiles associated with reduced evolutionary rates and global environmental volatility. *Nature communications* **7**, 1–11.

Flügel, E., 2010. Microfacies of carbonate rocks: Analysis, interpretation and application, 2nd editio. ed. Springer-Verlag Berlin Heidelberg.

Fourçans, A., De Oteyza, T.G., Wieland, A., Solé, A., Diestra, E., Van Bleijswijk, J., Grimalt, J.O., Kühl, M., Esteve, I., Muyzer, G., Caumette, P., Duran, R., 2004. Characterization of functional bacterial groups in a hypersaline microbial mat community (Salins-de-Giraud, Camargue, France). *FEMS Microbiology Ecology* **51**, 55–70.

Freeman, K.H., Wakeham, S.G., Hayes, J.M., 1994. Predictive isotopic

biogeochemistry of lipids from marine anoxic basins. *Organic Geochemistry* **21**, 629–644.

Frimmel, A., Oschmann, W., Schwark, L., 2004. Chemostratigraphy of the Posidonia Black Shale, SW Germany I. Influence of sea-level variation on organic facies evolution. *Chemical Geology* **206**, 199–230.

Fröbisch, N.B., Fröbisch, J., Sander, P.M., Schmitz, L., Rieppel, O., 2013. Macropredatory ichthyosaur from the Middle Triassic and the origin of modern trophic networks. *Proceedings of the National Academy of Sciences of the United States of America* **110**, 1393–7.

Galimov, E.M., 1977. Investigation of the distribution of carbon isotopes in biogenic compounds, in: Proceedings of the VIII International Congress on Organic Geochemistry. Nauka.

Geraghty, M.D., Westermann, G.*E.G.*, 1994. Origin of Jurassic ammonite concretions assemblages at Alfeld, Germany: a biogenic alternative. *Palaontologische Zeitschrift* **68**, 473–490.

Goh, F., Allen, M. a, Leuko, S., Kawaguchi, T., Decho, A.W., Burns, B.P., Neilan, B. a, 2009. Determining the specific microbial populations and their spatial distribution within the stromatolite ecosystem of Shark Bay. *The ISME journal* **3**, 383–396.

Greenwalt, D.E., Goreva, Y.S., Siljeström, S.M., Rose, T., Harbach, R.E., 2013. Hemoglobin-derived porphyrins preserved in a Middle Eocene blood-engorged mosquito. *Proceedings of the National Academy of Sciences of the United States of America* **110**, 18496–18500.

Grice, K., 2014. Principles and practice of analytical techniques in geosciences. the Royal Society of Chemistry.

Grice, K., Alexander, R., Kagi, R.I., 2000. Diamondoid hydrocarbon ratios as indicators of biodegradation in Australian crude oils. *Organic Geochemistry* **31**, 67–73.

Grice, K., Brocks, J.J., 2011. Biomarkers (organic, compound-specific isotopes), in: Thiel, Reitner (Eds.), Encyclopaedia of Geobiology. Encyclopedia of Earth Science Series, pp. 167–182.

Grice, K., Cao, C., Love, G.D., Böttcher, M.E., Twitchett, R.J., Grosjean, E., Summons, R.E., Turgeon, S.C., Dunning, W., Jin, Y., 2005. Photic zone euxinia during the Permian-Triassic superanoxic event. *Science* **307**, 706–9.

Grice, K., Gibbison, R., Atkinson, J.E., Schwark, L., Eckardt, C.B., Maxwell, J.R., 1996. Maleimides (1H-pyrrole-2,5-diones) as Molecular Indicators of Anoxygenic Photosynthesis in Ancient Water Columns. *Geochimica et Cosmochimica Acta* **60**, 3913–3924.

Grice, K., Schaeffer, P., Schwark, L., Maxwell, J.R., 1997. Changes in palaeoenvironmental conditions during deposition of the Permian Kupferschiefer (Lower Rhine Basin , northwest Germany) inferred from molecular and isotopic compositions of biomarker components. *Organic geochemistry* **26**, 677–690.

Grice, K., Schouten, S., Peters, K.E., Sinninghe Damsté, J.S., 1998. Molecular isotopic characterisation of hydrocarbon biomarkers in Palaeocene-Eocene evaporitic, lacustrine source rocks from the Jianghan Basin, China. *Organic Geochemistry* **29**, 1745–1764.

Grimalt, J.O., de Wit, R., Teixidor, P., Albaigés, J., 1992. Lipid biogeochemistry of Phormidium and Microcoleus mats. *Organic Geochemistry* **19**, 509–530.

Grimalt, J.O., Yruela, I., Saiz-Jimenez, C., Toja, J., de Leeuw, J.W., Albaigés, J., 1991. Sedimentary lipid biogeochemistry of an hypereutrophic alkaline lagoon. *Geochimica et Cosmochimica Acta* **55**, 2555–2577.

Gröcke, D.R., Hori, R.S., Trabucho-Alexandre, J., Kemp, D.B., Schwark, L., 2011. An open ocean record of the Toarcian oceanic anoxic event. *Solid Earth* **2**, 245–257.

Grosjean, E., Adam, P., Connan, J., Albrecht, P., 2004. Effects of weathering on nickel and vanadyl porphyrins of a Lower Toarcian shale of the Paris basin.

Geochemica et Cosmochimica Acta **68**, 789–804.

Grossi, V., Beker, B., Geenevasen, J.A.J., Schouten, S., Raphel, D., Fontaine, M.F., Sinninghe Damsté, J.S., 2004. C_{25} highly branched isoprenoid alkenes from the marine benthic diatom Pleurosigma strigosum. *Phytochemistry* **65**, 3049–3055.

Guo, L., Riding, R., 1992. Aragonite laminae in hot water travertine crusts, Rapolano Terme, Italy. *Sedimentology* **39**, 1067–1079.

Gupta, N.S., 2015. Plant biopolymer – geopolymer : organic diagenesis and kerogen formation. *Frontiers in Materials* **2**, 2007–2010.

Harvey, H.R., McManus, G.B., 1991. Marine ciliates as a widespread source of tetrahymanol and hopan-3β-ol in sediments. *Geochimica et Cosmochimica Acta* **55**, 3387–3390.

Hendry, J.P., Pearson, M.J., Trewin, N.H., Fallick, A.E., 2006. Jurassic septarian concretions from NW Scotland record interdependent bacterial, physical and chemical processes of marine mudrock diagenesis. *Sedimentology* **53**, 537–565.

Hennessy, J., Knauth, L.P., 1985. Isotopic variations in dolomite concretions from the Monterey Formation, California. *Journal of Sedimentary Petrology* **55**, 120–130.

Hesselbo, S., Grocke, D., Jenkyns, H.C., Bjerrum, C.J., Farrimond, P., Morgans Bell, H., Green, O., 2000. Massive dissociation of gas hydrate during a Jurassic oceanic anoxic event. *Nature* **406**, 392–395.

Hesselbo, S.P., Jenkyns, H.C., Duarte, L. V., Oliveira, L.C.V., 2007. Carbon-isotope record of the Early Jurassic (Toarcian) Oceanic Anoxic Event from fossil wood and marine carbonate (Lusitanian Basin, Portugal). *Earth and Planetary Science Letters* **253**, 455–470.

Hinrichs, K., Boetius, A., 2002. The anaerobic oxidation of methane : new insights in microbial ecology and biogeochemistry, in: Van Weering, T. (Ed.), Ocean Margin Systems. Springer, berlin Heidelberg, pp. 457–477.

Hoefs, J., 2015. Stable isotope geochemistry, 7th ed, Geochemistry. Springer.

Hoffman, H.J., 2000. Archean stromatolites as microbial archives, in: Riding, R.E., Awramik, S.M. (Eds.), Microbial Sediments. Springer, Berlin, pp. 315–327.

Holman, A.I., Grice, K., Jaraula, C.M.B., Schimmelmann, A., 2014. Bitumen II from the Paleoproterozoic Here's Your Chance Pb/Zn/Ag deposit: Implications for the analysis of depositional environment and thermal maturity of hydrothermally-altered sediments. *Geochimica et Cosmochimica Acta* **139**, 98–109.

Holser, W., Schidlowski, M., Mackenzie, F., Maynard, J., 1988. Chemical cycles in the evolution of the Earth. Wiley Interscience.

Hudson, J.D., 1982. Pyrite in ammonite-bearing shales from the Jurassic of England and Germany. *Sedimentology* **29**, 639–667.

Iniesto, M., Zeyen, N., López-Archilla, A.I., Bernard, S., Buscalioni, Á.D., Guerrero, M.C., Benzerara, K., 2015. Preservation in microbial mats: mineralization by a talc-like phase of a fish embedded in a microbial sarcophagus. *1. Frontiers in Earth Science* **3**, 1–13.

Jahnert, R., de Paula, O., Collins, L., Strobach, E., Pevzner, R., 2012. Evolution of a coquina barrier in Shark Bay, Australia by GPR imaging: Architecture of a Holocene reservoir analog. *Sedimentary Geology* **281**, 59–74.

Jahnert, R.J., Collins, L.B., 2011. Significance of subtidal microbial deposits in Shark Bay, Australia. *Marine Geology* **286**, 106–111.

Jahnert, R.J., Collins, L.B., 2012. Characteristics, distribution and morphogenesis of subtidal microbial systems in Shark Bay, Australia. *Marine Geology* **303–306**, 115–136.

Jahnert, R.J., Collins, L.B., 2013. Controls on microbial activity and tidal flat evolution in Shark Bay, Western Australia. *Sedimentology* **60**, 1071–1099.

Jahnke, L., Embaye, T., Hope, J., Turk, K.A., Van Zuilen, M., Des Marais, D.J.,

Farmer, J.D., Summons, R.E., 2004. Lipid biomarker and carbon isotopic signatures for stromatolite-forming, microbial mat communities and Phormidium cultures from Yellowstone National Park. *Geobiology* **2**, 31–47.

Jenkyns, H.C., 1988. The Early Toarcian Anoxic event: Stratigraphic, sedimentary, and geochrmical evidence. *Americal Journal of Science* **288**, 101–151.

Jenkyns, H.C., 2010. Geochemistry of oceanic anoxic events. *Geochemistry, Geophysics, Geosystems* **11**, Q03004.

Jenkyns, H.C., Jones, C.E., Gröcke, D.R., Hesselbo, S.P., Parkinson, D.N., 2002. Chemostratigraphy of the Jurassic System: applications, limitations and implications for palaeoceanography. *Journal of the Geological Society* **159**, 351–378.

Jones, D.M., Carter, J.F., Eglington, G., Jumeau, E.J., Fenwick, C.S., 1991. Determination of $\delta^{13}C$ values of sedimentary straight chain and cyclic alcohols by gas chromatography/isotope ratio mass spectrometry. *Journal of mass spectrometry* **20**, 641–646.

Kemp, D.B., Coe, A.L., Cohen, A.S., Schwark, L., 2005. Astronomical pacing of methane release in the Early Jurassic period. *Nature* **437**, 396–399.

Kendall, C., Caldwell, E.A., 1998. Fundamentals of isotope geochemistry, in: Kendall, C., McDonnell, J.J. (Eds.), Isotope Tracers in Catchment Hydrology. Elsevier Science, Amsterdam, pp. 51–86.

Killops, S.D., Frewin, N.L., 1994. Triterpenoid diagenesis and cuticular preservation. *Organic Geochemistry* **21**, 1193–1209.

Kiriakoulakis, K., Marshall, J.D., Wolff, G.A., 2000. Biomarkers in a Lower Jurassic concretion from Dorset (UK). *Journal of the Geological Society* **157**, 207–220.

Knoll, A.H., 2011. The multiple origins of complex multicellularity. *Annual Review of Earth and Planetary Sciences* **39**, 217–239.

Kohl, W., Achenbach, H., Reichenbach, H., 1983. The pigments of Brevibacterium linens: Aromatic carotenoids. *Phytochemistry* **22**, 207–210.

Koopmans, M.P., Köster, J., Van Kaam-Peters, H.M.E., Kenig, F., Schouten, S., Hartgers, W.A., De Leeuw, J.W., Sinninghe Damsté, J.S., 1996a. Diagenetic and catagenetic products of isorenieratene: Molecular indicators for photic zone anoxia. *Geochimica et Cosmochimica Acta* **60**, 4467–4496.

Koopmans, M.P., Schouten, S., Kohnen, M.E.L., Sinninghe Damsté, J.S., 1996b. Restricted utility of aryl isoprenoids as indicators for photic zone anoxia. *Geochimica et Cosmochimica Acta* **60**, 4873–4876.

Kroopnick, P.M., 1985. The distribution of ^{13}C of ΣCO_2 in the world oceans. *Deep Sea Research Part A, Oceanographic Research Papers* **32**, 57–84.

Krooss, B.M., Brothers, L., Engel, M.H., 1991. Geochromatography in petroleum migration: a review. *Geological Society, London, Special Publications* **59**, 149–163.

Krügel, H., Krubasik, P., Weber, K., Saluz, H.P., Sandmann, G., 1999. Functional analysis of genes from Streptomyces griseus involved in the synthesis of isorenieratene, a carotenoid with aromatic end groups, revealed a novel type of carotenoid desaturase. *Biochimica et Biophysica Acta - Molecular and Cell Biology of Lipids* **1439**, 57–64.

Landing, E., English, A., Keppie, J.D., 2010. Cambrian origin of all skeletalized metazoan phyla — Discovery of Earth ’ s oldest bryozoans (Upper Cambrian , southern Mexico). *Geology* **38**, 547–550.

Larter, S.R., Bowler, B.F.J., Clarke, E., Wilson, C., Moffatt, B., Bennett, B., Yardley, G., Carruthers, D., 2000. An experimental investigation of geochromatography during secondary migration of petroleum performed under subsurface conditions with a real rock. *Geochemical Transactions* **1**, 54.

Lash, G.G., Blood, D., 2004. Geochemical and textural evidence for early (shallow) diagenetic growth of stratigraphically confined carbonate concretions, Upper

Devonian Rhinestreet black shale, western New York. *Chemical Geology* **206**, 407–424.

Leduc, T., 2012. Diagenesis of the fossil bones of Iguanodon bernissartensis from the Iguanodon sinkhole, in: Godefroit, P. (Ed.), Bernissart Dinosaurs and Early Cretaceous Terrestrial Ecosystems. Indiana University Press, pp. 111–136.

Lee, Y.-C., Chiang, C.-C., Huang, P.-Y., Chung, C.-Y., Huang, T.D., Wang, C.-C., Chen, C.-I., Chang, R.-S., Liao, C.-H., Reisz, R.R., 2017. Evidence of preserved collagen in an Early Jurassic sauropodomorph dinosaur revealed by synchrotron FTIR microspectroscopy. *Nature Communications* **8**, 14220.

Li, M., Larter, S.R., Stoddart, D., Bjorøy, M., 1995. Fractionation of pyrrolic nitrogen compounds in petroleum during migration: derivation of migration-related geochemical parameters. *Geological Society, London, Special Publications* **86**, 103–123.

Li, M.W., Larter, S.R., Frolov, Y.B., Bjoroy, M., 1994. Adsorptive Interaction between Nitrogen-Compounds and Organic and/or Mineral Phases in Subsurface Rocks - Models for Compositional Fractionation of Pyrrolic Nitrogen-Compounds in Petroleum During Petroleum Migration. *Journal of high resolution chromatography* **17**, 230–236.

Lindgren, J., Kaddumi, H.F., Polcyn, M.J., 2013. Soft tissue preservation in a fossil marine lizard with a bilobed tail fin. *Nature communications* **4**, 2423.

Logan, B.W., 1974. Evolution and diagenesis of quaternary carbonate sequences, Shark Bay, Western Australia. *American association of petroleum geologists memoir* **22**, 195–249.

Logan, B.W., Cebulski, D.E., 1970. Sedimentary environments of Shark Bay, Western Australia. *American association of petroleum geologists memoir* **13**, 1–37.

Londry, K.L., Jahnke, L.L., Des Marais, D.J., 2004. Stable carbon isotope ratios of lipid biomarkers of sulfate-reducing bacteria. *Applied and Environmental*

Microbiology **70**, 745–751.

Lopuchowycz, V.B., Massare, J.A., 2002. Bone Microstructure of a Cretaceous Ichtyosaur. *Paludicola* **3**, 139–147.

Lowenstam, H.A., Weiner, S., 1989. On biomineralization. Oxford University Press, New York.

Macchioni, F., Cecca, F., 2002. Biodiversity and biogeography of middle–late liassic ammonoids: implications for the early Toarcian mass extinction. *Geobios* **35**, 165–175.

Mackenzie, A.S., Brassel, S.C., Eglington, G., Maxwell, J.R., 1982a. Chemical fossils: the geological fate of steroids. *Science* **217**.

Mackenzie, A.S., Lamb, N.A., Maxwell, J.R., 1982b. Steroid hydrocarbons and the thermal history of sediments. *Nature* **295**, 223–226.

Madden, R.H.C., Wilson, M.E.J., O'Shea, M., 2013. Modern fringing reef carbonates from equatorial SE Asia: An integrated environmental, sediment and satellite characterisation study. *Marine Geology* **344**, 163–185.

Madigan, M.T., Takigiku, R., Lee, R.G., Gest, H., Hayes, J.M., 1989. Carbon isotope fractionation by thermophilic phototrophic sulfur bacteria : evidence for autotrophic growth in natural populations. *Applied and environmental microbiology* **55**, 639–644.

Magoon, L.B., Claypool, G.E., 1984. Organic Geochemical Properties and Petroleum Source Rock Quality. *Organic Geochemistry* **6**, 533–542.

Marshak, S., 2012. Essentials of Geology, 4th ed. W.W. Norton & Company.

Marshall, J.D., Pirrie, D., 2013. Carbonate concretions-explained. *Geology Today* **29**, 53–62.

Martill, D.M., 1988. Preservation of fish in the Cretaceous Santana Formation of Brazil. *Palaeontology* **31**, 1–18.

Martill, D.M., 1989. The Medusa effect: instantaneous fossilization. *Geology Today* **5**, 201–205.

Martill, D.M., 1990. Macromolecular resolution of fossilized muscle tissue from an elopomorph fish. *Nature* **346**, 171–172.

Martill, D.M., 1995. Ichthyosaur with preserved soft tissue from the Sinemurian of Southern England. *Palaeontology*.

Marynowski, L., Otto, A., Zatoń, M., Philippe, M., Simoneit, B.R.T., 2007a. Biomolecules preserved in ca. 168 million year old fossil conifer wood. *Die Naturwissenschaften* **94**, 228–236.

Marynowski, L., Zatoń, M., Simoneit, B.R.T., Otto, A., Jedrysek, M., Grelowski, C., Kurkiewics, S., 2007b. Compositions , sources and depositional environments of organic matter from the Middle Jurassic clays of Poland. *Applied Geochemistry* **22**, 2456–2485.

Mcbride, E.F., Milliken, K.L., 2006. Giant calcite-cemented concretions, Dakota Formation, central Kansas, USA. *Sedimentology* **53**, 1161–1179.

McElwain, J.C., Wade-Murphy, J., Hesselbo, S.P., 2005. Changes in carbon dioxide during an oceanic anoxic event linked to intrusion into Gondwana coals. *Nature* **435**, 479–482.

McKirdy, D.M., Thorpe, C.S., Haynes, D.E., Grice, K., Krull, E.S., Halverson, G.P., Webster, L.J., 2010. The biogeochemical evolution of the Coorong during the mid- to late Holocene: An elemental, isotopic and biomarker perspective. *Organic Geochemistry* **41**, 96–110.

McNamara, K., 2013. Stromatolites. Western Australian Museum, Perth.

Melendez, I., Grice, K., Schwark, L., 2013a. Exceptional preservation of Palaeozoic steroids in a diagenetic continuum. *Scientific reports* **3**, 2768.

Melendez, I., Grice, K., Trinajstic, K., Ladjavardi, M., Greenwood, P., Thompson, K., 2013b. Biomarkers reveal the role of photic zone euxinia in

exceptional fossil preservation: An organic geochemical perspective. *Geology* **41**, 123–126.

Motani, R., 2002. Scaling effects in caudal propulsion and the speed of ichthyosaurs. *Nature* **415**, 309–312.

Motani, R., 2005. Evolution of Fish-Shaped Reptiles (*Reptilia: Ichthyopterygia*) in Their Physical Environments and Constraints. *Annual Review of Earth and Planetary Sciences* **33**, 395–420.

Mozley, P.S., 1989. Complex compositional zonation in concretionary siderite: implications for geochemical studies. *Journal of Sedimentary Petrology* **59**, 815–818.

Mozley, P.S., 1996. The internal structure of carbonate concretions in mudrocks: a critical evaluation of the conventional concentric model of concretion growth. *Sedimentary Geology* **103**, 85–91.

Mozley, P.S., Burns, S.J., 1993. Oxygen and carbon isotopic composition of marine carbonate concretions: an overview. *Journal of Sedimentary Petrology* **63**, 73–83.

Naeher, S., Lengger, S.K., Grice, K., 2016. A new method for the rapid analysis of 1H-Pyrrole-2,5-diones (maleimides) in environmental samples by two-dimensional gas chromatography time-of-flight mass spectrometry. *Journal of Chromatography A* **1435**, 125–135.

Naeher, S., Schaeffer, P., Adam, P., Schubert, C.J., 2013. Maleimides in recent sediments – Using chlorophyll degradation products for palaeoenvironmental reconstructions. *Geochimica et Cosmochimica Acta* **119**, 248–263.

Narbonne, G.M., 2005. The Ediacara biota: Neoproterozoic origin of animals and their ecosystems. *Annual Review of Earth and Planetary Sciences* **33**, 421–442.

Nardini, G., Leopardi, S., Bielli, M., 2013. Clinical hematology in reptilian species. *Veterinary Clinics of North America: Exotic Animal Practice* **16**, 1–30.

Oppenheimer, C., Fischer, T.P., Scaillet, B., 2014. Volcanic degassing: processes and impact. *Treatise on Geochemistry: Second Edition* **4**, 111–179.

Pagès, A., Grice, K., Ertefai, T., Skrzypek, G., Jahnert, R., Greenwood, P., 2014a. Organic geochemical studies of modern microbial mats from Shark Bay: Part I: Influence of depth and salinity on lipid biomarkers and their isotopic signatures. *Geobiology* **12**, 469–487.

Pagès, A., Grice, K., Vacher, M., Welsh, D.T., Teasdale, P.R., Bennett, W.W., Greenwood, P., 2014b. Characterizing microbial communities and processes in a modern stromatolite (Shark Bay) using lipid biomarkers and two-dimensional distributions of porewater solutes. *Environmental microbiology* **16**, 2458–2474.

Pagès, A., Grice, K., Welsh, D.T., Teasdale, P.T., Van, M.J., Greenwood, P., 2015. Lipid Biomarker and Isotopic Study of Community Distribution and Biomarker Preservation in a LaminatedMicrobialMat from Shark Bay,Western Australia. *Environmental Microbiology* **70**, 459–472.

Pancost, R.D., Crawford, N., Magness, S., Turner, A., Jenkyns, H.C., Maxwell, J.R., 2004. Further evidence for the development of photic-zone euxinic conditions during Mesozoic oceanic anoxic events. *Journal of the Geological Society* **161**, 353–364.

Paoletti, C., Pushparaj, B., Florenzano, G., Capella, P., Lercker, G., 1976. Unsaponifiable matter of green and blue-green algal lipids as a factor of biochemical differentiation of their biomasses: I. Total unsaponifiable and hydrocarbon fraction. *Lipids* **11**, 258–265.

Papineau, D., Walker, J.J., Mojzsis, S.J., Pace, N.R., 2005. Composition and Structure of Microbial Communities from Stromatolites of Hamelin Pool in Shark Bay , Western Australia Composition and Structure of Microbial Communities from Stromatolites of Hamelin Pool in Shark Bay , Western Australia. *Applied and environmental microbiology* **71**, 4822–4832.

Pearson, M.J., Hendry, J.P., Taylor, C.W., Russell, M.A., 2005. Fatty acids in sparry calcite fracture fills and microsparite cement of septarian diagenetic

concretions. *Geochimica et Cosmochimica Acta* **69**, 1773–1786.

Pearson, M.J., Nelson, C.S., 2005. Organic geochemistry and stable isotope composition of New Zealand carbonate concretions and calcite fracture fills. *New Zealand Journal of Geology and Geophysics* **48**, 395–414.

Perry, C.T., 1999. Biofilm-related calcification, sediment trapping and constructive micrite envelopes: A criterion for the recognition of ancient grass-bed environments? *Sedimentology* **46**, 33–45.

Perry, C.T., Hepburn, L.J., 2008. Syn-depositional alteration of coral reef framework through bioerosion, encrustation and cementation: Taphonomic signatures of reef accretion and reef depositional events. *Earth-Science Reviews* **86**, 106–144.

Peters, K.E., Clifford, C.W., Moldowan, J.M., 2005. The biomarker guide, 2nd ed. Cambridge University Press, Cambridge.

Peterson, B.J., Fry, B., 2011. Stable Isotopes in Ecosystem Studies. *Source: Annual Review of Ecology and Systematics* **18**, 293–320.

Plet, C., Grice, K., Pagès, A., Ruebsam, W., Coolen, M.J., Schwark, L., 2016. Microbially-mediated fossil-bearing carbonate concretions and their significance for palaeoenvironmental reconstructions: A multi-proxy organic and inorganic geochemical appraisal. *Chemical Geology* **426**, 95–108.

Popel, A.S., Johnson, P.C., Kameneva, M. V, Wild, M.A., 1994. Capacity for red blood cell aggregation is higher in athletic mammalian species than in sedentary species. *Journal of applied physiology (Bethesda, Md. : 1985)* **77**, 1790–4.

Poulsen, C.J., Tabor, C., White, J.D., 2015. Long-term climate forcing by atmospheric oxygen concentrations. *Science* **348**, 1238–1242.

Price, R., Skrzypek, G., Grierson, P.F., Swart, P.K., Fourqurean, J.W., 2012. The use of stable isotopes of oxygen and hydrogen to identify water sources in two hypersaline estuaries with different hydrologic regimes. *Marine and Freshwater Research* **63**, 952–966.

Quandt, L., Gottschalk, G., Ziegler, H., Stichler, W., 1977. Isotope discrimination by photosynthetic bacteria. *FEMS Microbiology letters* 125–128.

Quirke, J., Shaw, G.J., Super, P.D., Maxwell, J.R., 1980. The presence of porphyrins with extended alkyl substituents. *Tetrahedron* **36**, 3261–3267.

Raiswell, R., 1976. The microbiological formation of carbonate concretions in the Upper Lias of the NE England. *Chemical Geology* **18**, 227–244.

Raiswell, R., 1982. Pyrite texture isotopic composition and the availability of iron. *American Journal of Science* **282**, 1244–1263.

Raiswell, R., Bottrell, S.H., Dean, S.P., Marshall, J.D., Carr, A., Hatfield, D., 2002. Isotopic constraints on growth conditions of multiphase calcite-pyrite-barite concretions in Carboniferous mudstones. *Sedimentology* **49**, 237–254.

Raiswell, R., Fisher, Q.J., 2000. Mudrock-hosted carbonate concretions: a review of growth mechanisms and their influence on chemical and isotopic composition. *Journal of the Geological Society* **157**, 239–251.

Raiswell, R., White, N.J.M., 1978. Spatial aspects of concretionary growth in the Upper Lias of Northeast England. *Sedimentary Geology* **20**, 291–300.

Reagan, W.J., Irizarry Rovira, A.R., DeNicola, D.B., 2008. Veterinary hematology. Atlas of common domestic and non domestic species, 2nd ed. Wiley-Blackwell.

Reid, R.P., 2011. Stromatolites, in: Hopley, D. (Ed.), Encyclopedia of Modern Coral Reefs: Structure, Form and Process. Springer Netherlands, Dordrecht, pp. 1045–1051.

Reid, R.P., James, N.P., Macintyre, I.G., Dupraz, C.P., Burne, R. V, Macintyre, G., 2003. Shark Bay Stromatolites : Microfabrics and Reinterpretation of Origins. *Facies* **49**, 299–324.

Reid, R.P., Visscher, P.T., Decho, A.W., Stolz, J.F., Bebout, B.M., 2000. The role of microbes in accretion, lamination and early lithification of modern marine stromatolites. *Nature* **406**, 989–992.

Reitner, J., Peckmann, J., Blumenberg, M., Michaelis, W., Reimer, A., Thiel, V., 2005. Concretionary methane-seep carbonates and associated microbial communities in Black Sea sediments. *Palaeogeography, Palaeoclimatology, Palaeoecology* **227**, 18–30.

Reitner, J., Thiel, V., 2011. Encyclopedia of Geobiology. Springer, Gottingen.

Richert, L., Golubic, S., Le Guédès, R., Ratiskol, J., Payri, C., Guezennec, J., 2005. Characterization of exopolysaccharides produced by cyanobacteria isolated from Polynesian microbial mats. *Current microbiology* **51**, 379–384.

Riding, R., 2000. Microbial carbonates: the geological record of calcified bacterial-algal mats and biofilms. *Sedimentology* **47**, 179–214.

Robinson, N., Eglinton, G., 1990. Lipid chemistry of Icelandic hot spring microbial mats. *Organic Geochemistry* **15**, 291–298.

Röhl, H., Schmid-Röhl, A., Oschmann, W., Frimmel, A., Schwark, L., 2001. The Posidonia Shale (Lower Toarcian) of SW-Germany : an oxygen-depleted ecosystem controlled by sea level and palaeoclimate. *Palaeogeography, Palaeoclimatology, Palaeoecology* **165**, 27–52.

Rontani, J.F., Volkman, J.K., 2005. Lipid characterization of coastal hypersaline cyanobacterial mats from the Camargue (France). *Organic Geochemistry* **36**, 251–272.

Ruebsam, W., Münzberger, P., Schwark, L., 2014. Chronology of the Early Toarcian environmental crisis in the Lorraine Sub-Basin (NE Paris Basin). *Earth and Planetary Science Letters* **404**, 273–282.

Sanchez, S., Tafforeau, P., Ahlberg, P.E., 2014. The humerus of Eusthenopteron: a puzzling organization presaging the establishment of tetrapod limb bone marrow. *Proceedings. Biological sciences / The Royal Society* **281**, 20140299.

Schidlowski, M., 1988. A 3,800-million-year isotopic record of life from carbon in sedimentary rocks. *Nature* **336**, 313–318.

Schmid-Röhl, A., Röhl, H., Oschmann, W., Frimmel, A., 2002. Palaeoenvironmental reconstruction of Lower Toarcian epicontinental black shales (Posidonia Shale , SW Germany): global versus regional control. *Geobios* **35**, 13–20.

Schouten, S., Bowman, J.P., Rijpstra, W.I.C., Sinninghe Damsté, J.S., 2000a. Sterols in a psychrophilic methanotroph, Methylosphaera hansonii. *FEMS Microbiology Letters* **186**, 193–195.

Schouten, S., Van Kaam-Peters, H.M.E., Rijpstra, W.I.C., Schoell, M., Sinninghe Damste, J.S., 2000b. Effects of an oceanic anoxic event on the stable carbon isotopic composition of early Toarcian carbon. *American Journal of Science* **300**, 1–22.

Schwark, L., Frimmel, A., 2004. Chemostratigraphy of the Posidonia Black Shale, SW-Germany II. Assessment of extent and persistence of photic-zone anoxia using aryl isoprenoid distibutions. *Chemical Geology* **206**, 231–248.

Schweitzer, M.H., Johnson, C., Zocco, T.G., Horner, J.R., Starkey, J.R., 1997. Preservation of biomolecules in cancellous bone of Tyrannosaurus rex. *Journal of Vertebrate Paleontology* **17**, 349–359.

Schweitzer, M.H., Suo, Z., Avci, R., Asara, J.M., Allen, M.A., Teran Arce, F., Horner, J.R., 2007a. Analyses of soft tissue from *Tyrannosaurus rex* suggest the presence of protein. *Science* **316**, 277–280.

Schweitzer, M.H., Wittmeyer, J., Horner, J.R., Toporski, J.K., 2005. Soft-tissue vessels and cellular preservation in *Tyrannosaurus rex*. *Science* **307**, 1952–1955.

Schweitzer, M.H., Wittmeyer, J.L., Horner, J.R., 2007b. Soft tissue and cellular preservation in vertebrate skeletal elements from the Cretaceous to the present. *Proceedings. Biological sciences / The Royal Society* **274**, 183–197.

Schweitzer, M.H., Zheng, W., Cleland, T.P., Goodwin, M., Boatman, E., Theil, E., Marcus, M.A., Fakra, S.C., 2014. A role for iron and oxygen chemistry in preserving soft tissues, cells and molecules from deep time. *Proceedings.*

Biological sciences / The Royal Society **281**, 20132741.

Seilacher, A., 2001. Concretion morphologies reflecting diagenetic and epigenetic pathways. *Sedimentary ge* **143**, 41–57.

Sellés-Martínez, J., 1996. Concretion morphology, classification and genesis. *Earth-Science Reviews* **41**, 177–210.

Sinninghe Damsté, J.P., Kenig, F., Koopmans, M.P., Koster, J., Schouten, S., Hayes, J.M., De Leuuw, J.W., 1995. Evidence for gammacerane as an indicator of water column stratification. *Geochimica et Cosmochimica Acta* **59**, 1895–1900.

Sinninghe Damsté, J.S., Keely, B.J., Betts, S.E., Baas, M., Maxwell, J.R., De Leeuw, J.W., 1993. Variations in abundances and distributions of isoprenoid chromans and long-chain aikylbenzenes in sediments of the Mulhouse Basin : a molecular sedimentary record of palaeosalinity. *Organic Geochemistry* **20**, 1201–1215.

Sinninghe Damsté, J.S., Muyzer, G., Abbas, B., Rampen, S.W., Massé, G., Allard, W.G., Belt, S.T., Robert, J.-M., Rowland, S.J., Moldowan, J.M., Barbanti, S.M., Fago, F.J., Denisevich, P., Dahl, J., Trindade, L.A.F., Schouten, S., 2004. The Rise of the Rhizosolenid Diatoms. *Science* **304**, 584–587.

Smith, S. V., Atkinson, M.J., 1983. Mass balance of carbon and phosphorus in Shark Bay Western Australia. *Limnology and Oceanography* **28**, 625–639.

Southard, J., 2007. Sedimentary geology : Chapter 7 Diagenesis. *Massachusetts Institute of Technology: MIT OpenCourseWare*.

Spaulding, S.A., Lubinski, D.J., Potapova, M., 2010. Diatoms of the United States [WWW Document].

Stal, L.J., 2000. Cyanobacterial mats and stromatolites, in: Whitton, B.A., Potts, M. (Eds.), The Ecology of Cyanobacteria. Their Diversity in Time and Space. Kluwer Academic Publishers, Dordrecht, pp. 61–120.

Stewart, G.W., 2003. The hereditary stomatocytosis and allied conditions': inherited disorders Na^+ and K^+ transport, in: Ingolf, B., Clive, E.J. (Eds.), Red Cell Membrane Transport in Health and Disease. Springer Berlin Heidelberg, pp. 511–523.

Suan, G., Mattioli, E., Pittet, B., Mailliot, S., Lécuyer, C., 2008. Evidence for major environmental perturbation prior to and during the Toarcian (Early Jurassic) oceanic anoxic event from the Lusitanian Basin, Portugal. *Paleoceanography* **23**, n/a-n/a.

Summons, R., Barrow, R., Capon, R., Hope, J., Stranger, C., 1993. The Structure of a New C_{25} Isoprenoid Alkene Biomarker from Diatomaceous Microbial Communities. *Aust. J. Chem.* **46**, 907–915.

Summons, R.E., Bird, L.R., Gillespie, A. L., Pruss, S.B., Roberts, M., Sessions, A. L., 2013. Lipid biomarkers in ooids from different locations and ages: Evidence for a common bacterial flora. *Geobiology* **11**, 420–436.

Summons, R.E., Powell, T.G., 1986. Chlorobiaceae in Palaeozoic seas revealed by biological markers, isotopes and geology. *Nature* **319**, 763–765.

Suosaari, E.P., Reid, R.P., Playford, P.E., Foster, J.S., Stolz, J.F., Casaburi, G., Hagan, P.D., Chirayath, V., Macintyre, I.G., Planavsky, N.J., Eberli, G.P., 2016. New multi-scale perspectives on the stromatolites of Shark Bay, Western Australia. *Scientific Reports* **6**, 20557.

Svensen, H., Planke, S., Chevallier, L., Malthe-Sorenssen, A., Corfu, F., Jamtveit, B., 2007. Hydrothermal venting of greenhouse gases triggering Early Jurassic global warming. *Earth and Planetary Science Letters* **256**, 554–566.

Tappert, R., McKellar, R.C., Wolfe, A.P., Tappert, M.C., Ortega-Blanco, J., Muehlenbachs, K., 2013. Stable carbon isotopes of C_3 plant resins and ambers record changes in atmospheric oxygen since the Triassic. *Geochimica et Cosmochimica Acta* **121**, 240–262.

Taylor, J., Parkes, R., 1983. The Cellular Fatty Acids of the Sulphate-reducing

Bacteria, *Desulfobacter sp*., *Desulfobulbus sp*. and *Desulfovibrio desulfuricans*. *Journal of General Microbiology* **129**, 3303–3309.

Taylor, J., Parkes, R.J., 1985. Identifying Different Populations of Sulfate-Reducing Bacteria within Marine Sediment Systems, Using Fatty-Acid Biomarkers. *Journal of General Microbiology* **131**, 631–642.

Ten Haven, H.L., De Leeuw, J.W., Schenck, P.A., 1985. Organic geochemical studies of a Messinian evaporitic basin, northern Apennines (Italy) I: Hydrocarbon biological markers for a hypersaline environment. *Geochimica et Cosmochimica Acta* **49**, 2181–2191.

Ten Haven, H.L., de Leew, J.W., Sinninghe Damsté, J.S., Schenck, P., Palmer, S.E., Zumberge, J.E., 1988. Application of biological markers in the recognition of palaeohypersaline environments. *Geological Society, London, Special Publications* **40**, 123–130.

Thiel, V., Heim, C., Arp, G., Hahmann, U., Sjövall, P., Lausmaa, J., 2007. Biomarkers at the microscopic range: ToF-SIMS molecular imaging of Archaea-derived lipids in a microbial mat. *Geobiology* **5**, 413–421.

Thiel, V., Merz-Preiß, M., Reitner, J., Michaelis, W., 1997. Biomarker studies on microbial carbonates: Extractable lipids of a Calcifying Cyanobacterial mat (Everglades, USA). *Facies* **36**, 163–172.

Tissot, B.P., Welte, D.H., 1984. Petroleum Formation and Occurrence, 2nd ed. Springer-Verlag, Berlin Heidelberg New York Tokyo.

Touchette, B.W., Burkholder, J.M., 2000. Overview of the physiological ecology of carbon metabolism in seagrasses. *Journal of Experimental Marine Biology and Ecology* **250**, 169–205.

Tucker, M., Wright, V.P., Dickson, J.A.D., 1990. Carbonate sedimentology. Blackwell Scientific Publication, Oxford.

Tulipani, S., Grice, K., Krull, E., Greenwood, P., Revill, A.T., 2014. Salinity variations in the northern Coorong Lagoon, South Australia: Significant changes

in the ecosystem following human alteration to the natural water regime. *Organic Geochemistry* **75**, 74–86.

Van Gemerden, H., 1993. Microbial mats: A joint venture. *Marine Geology* **113**, 3–25.

Visscher, P.T., Reid, R.P., Bebout, B.M., 2000. Microscale observations of sulfate reduction : Correlation of microbial activity with lithified micritic laminae in modern marine stromatolites. *Geology* 919–922.

Volkman, J.K., 2003. Sterols in microorganisms. *Applied microbiology and biotechnology* **60**, 495–506.

Volkman, J.K., 2005. Sterols and other triterpenoids: Source specificity and evolution of biosynthetic pathways. *Organic Geochemistry* **36**, 139–159.

Volkman, J.K., Barrett, S.M., Blackburn, S.I., Mansour, M.P., Sikes, E.L., Gelin, F., 1998. Microalgal biomarkers: A review of recent research developments. *Organic Geochemistry* **29**, 1163–1179.

Wakeham, S.G., Hopmans, E.C., Schouten, S., Sinninghe Damsté, J.S., 2004. Archaeal lipids and anaerobic oxidation of methane in euxinic water columns: a comparative study of the Black Sea and Cariaco Basin. *Chemical Geology* **205**, 427–442.

Walker, D.I., Kendrick, G.A., McComb, A.J., 1988. The distribution of seagrass species in Shark Bay, Western Australia, with notes on their ecology. *Aquatic Botany* **30**, 305–317.

Whiteside, J.H., Grice, K., 2016. Biomarker Records Associated with Mass Extinction Events. *Annual Review of Earth and Planetary Sciences* **44**, 581–612.

Wignall, P.B., Newton, R.J., Little, C.T.S., 2005a. Cause-and-effect relationships during the Early Jurassic mass extinction in Europe. *American Journal of Science* **305**, 1014–1032.

Wignall, P.B., Newton, R.J., Little, C.T.S., 2005b. The timing of

paleoenvironmental change and cause-and-effect relationships during the Early Jurassic mass extinction in Europe. *American Journal of Science* **305**, 1014–1032.

Wilkin, R.T., Barnes, H.L., 1997. Formation processes of framboidal pyrite. *Geochemica et Cosmochimica Acta* **61**, 323–339.

Williams, M., Benton, M.J., Ross, A., 2015. The Strawberry Bank Lagerstätte reveals insights into Early Jurassic life. *Journal of the Geological Society* 2014–144.

Wilson, D.D., Brett, C.E., 2013. Concretions as sources of exceptional preservation, and decay as a source of concretions: examples from the middle Devonian of New York. *Palaios* **28**, 305–316.

Winter, B.L., Knauth, L.P., 1992. Stable isotope geochemistry of early Protezozoic carbonate concretions in the Animikie group of the Lake Superior region: evidence for anaerobic bacterial processes. *Precambrian Research* **54**, 131–151.

Wolff, G.A., Rukin, N., Marshall, J.D., 1991. Geochemistry of an early diagenetic concretion from the Birchi Bed (L. Lias, W. Dorset, U.K.). *Organic Geochemistry* **19**, 431–444.

Woo, K.S., Khim, B.K., 2006. Stable oxygen and carbon isotopes of carbonate concretions of the Miocene Yeonil Group in the Pohang Basin, Korea: Types of concretions and formation condition. *Sedimentary Geology* **183**, 15–30.

Wraige, E.J., Belt, S.T., Lewis, C.A., Cooke, D.A., Robert, J., 1997. Variations in structures and distributions of C_{25} highly branched isoprenoid (HBI) alkenes in cultures of the diatom , Haslea ostrearia (Simonsen). *Organic Geochemistry* **27**, 497–505.

Yoshida, H., Ujihara, A., Minami, M., Asahara, Y., Katsuta, N., Yamamoto, K., Sirono, S., Maruyama, I., Nishimoto, S., 2015. Early post-mortem formation of carbonate concretions around tusk-shells over week-month timescales. *Scientific reports* 1–7.

Zatoń, M., Kremer, B., Marynowski, L., Wilson, M.A., Krawczyński, W., 2011.

Middle Jurassic (Bathonian) encrusted oncoids from the Polish Jura, southern Poland. *Facies* **58**, 57–77.

Zatoń, M., Marynowski, L., 2004. Konzentrat-Lagerstätte-type carbonate concretions from the uppermost Bajocian (Middle Jurassic) of the Częstochowa area , South-Cental Poland. *Geological Quarterly* **48**, 339–350.

Zhang, J., Quay, P.D., Wilbur, D.O., 1995. Carbon isotope fractionation during gas-water exchange and dissolution of CO_2. *Geochimica et Cosmochimica Acta* **59**, 107–114.

Zhou, Y., Grice, K., Stuart-williams, H., Farquhar, G.D., Hocart, C.H., Lu, H., Liu, W., 2010. Biosynthetic origin of the saw-toothed profile in $\delta^{13}C$ and $\delta^{2}H$ of *n*-alkanes and systematic isotopic differences between *n*-, *iso*-, and *anteiso*-alkanes in leaf waxes of land plants. *Phytochemistry* **71**, 388–403.

Ziegler, P.A., 2005. EUROPE : Permian to Recent Evolution: Jurassic, in: Selley, R.C., Cocks, L.R.M., Plimer, I.R. (Eds.), Encyclopedia of Geology. Elsevier, pp. 106–112.

Appendix

Following pages contain documents stating:

The rights, granted by Elsevier to the first author of the publication that forms **Chapter 2** of this thesis, to reproduce their articles in full or in part, for a wide range of scholarly, non-commercial purposes, including in a thesis (provided that this is not to be published commercially)

The rights, granted by Nature Publishing Group to the first author of the publication that forms **Chapter 3** of this thesis, to reproduce the contribution in any printed volume (book or thesis).

The rights, granted by Wiley to the first author of the publication that forms **Chapter 5** of this thesis to reuse my own article in a new publication (*e.g.* thesis).

ELSEVIER (/)

SEARCH MENU

Personal use

Authors can use their articles, in full or in part, for a wide range of scholarly, non-commercial purposes as outlined below:

- **Use by an author in the author's classroom teaching (including distribution of copies, paper or electronic)**
- **Distribution of copies (including through e-mail) to known research colleagues for their personal use (but not for Commercial Use)**
- **Inclusion in a thesis or dissertation (provided that this is not to be published commercially)**
- **Use in a subsequent compilation of the author's works**
- **Extending the Article to book-length form**
- **Preparation of other derivative works (but not for Commercial Use)**
- **Otherwise using or re-using portions or excerpts in other works**

These rights apply for all Elsevier authors who publish their article as either a subscription article or an open access article. In all cases we require that all Elsevier authors always include a full acknowledgement and, if appropriate, a link to the final published version hosted on Science Direct.

(http (http (http (http
s://w s://w s://tws://pl
ww.farwu.ll it- us.go
os- nkeditor.coogle.
book.ru.co m/El-com
com m se- /u/o/
/El- /co vier- +el-

Permission requests

On this page

Nature Publishing Group grants permission for authors, readers and third parties to reproduce material from its journals and online products as part of another publication or entity. This includes, for example, the use of a figure in a presentation, the posting of an abstract on a web site, or the reproduction of a full article within another journal. Certain permissions can be granted free of charge; others incur a fee.

For answers to frequently asked questions **click here**

Types of permission request

Permission can be obtained for re-use of portions of material - ranging from a single figure to a whole paper - in books, journals/magazines, newsletters, **thes**es/dissertations, classroom materials/academic course packs, academic conference materials, training materials (including continuing medical education), promotional materials, and web sites. Some permission requests can be granted free of charge, others carry a fee.

Nature Publishing Group rarely grants free permission for PDFs of full papers to be reproduced online, however e-print PDFs can be **purchased as commercial reprints**. If you wish to purchase multiple stand-alone copies of a Nature Publishing Group paper, which is then printed and shipped to you, please go to **commercial reprints**.

Permission request options

Permission requests from authors

The authors of articles published by Nature Publishing Group, or the authors' designated agents, do not usually need to seek permission for re-use of their material as long as the journal is credited with initial publication. For further information about the terms of re-use for authors please see below.

Author Requests

If you are the author of this content (or his/her designated agent) please read the following. Since 2003, ownership of copyright in in original research articles remains with the Authors*, and provided that, when reproducing the Contribution or extracts from it, the Authors acknowledge first and reference publication in the Journal, the Authors retain the following non-exclusive rights:

a. To reproduce the Contribution in whole or in part in any printed volume (book or **thes**is) of which they are the author(s).

b. They and any academic institution where they work at the time may reproduce the Contribution for the purpose of course teaching.

c. To reuse figures or tables created by them and contained in the Contribution in other works created by them.

d. To post a copy of the Contribution as accepted for publication after peer review (in Word or Tex format) on the Author's own web site, or the Author's institutional repository, or the Author's funding body's archive, six months after publication of the printed or online edition of the Journal, provided that they also link to the Journal article on NPG's web site (eg through the DOI).

NPG encourages the self-archiving of the accepted version of your manuscript in your funding agency's or institution's repository, six months after publication. This policy complements the recently announced policies of the US National Institutes of Health, Wellcome Trust and other research funding bodies around the world. NPG recognizes the efforts of funding bodies to increase access to the research they fund, and we strongly encourage authors to participate in such efforts.

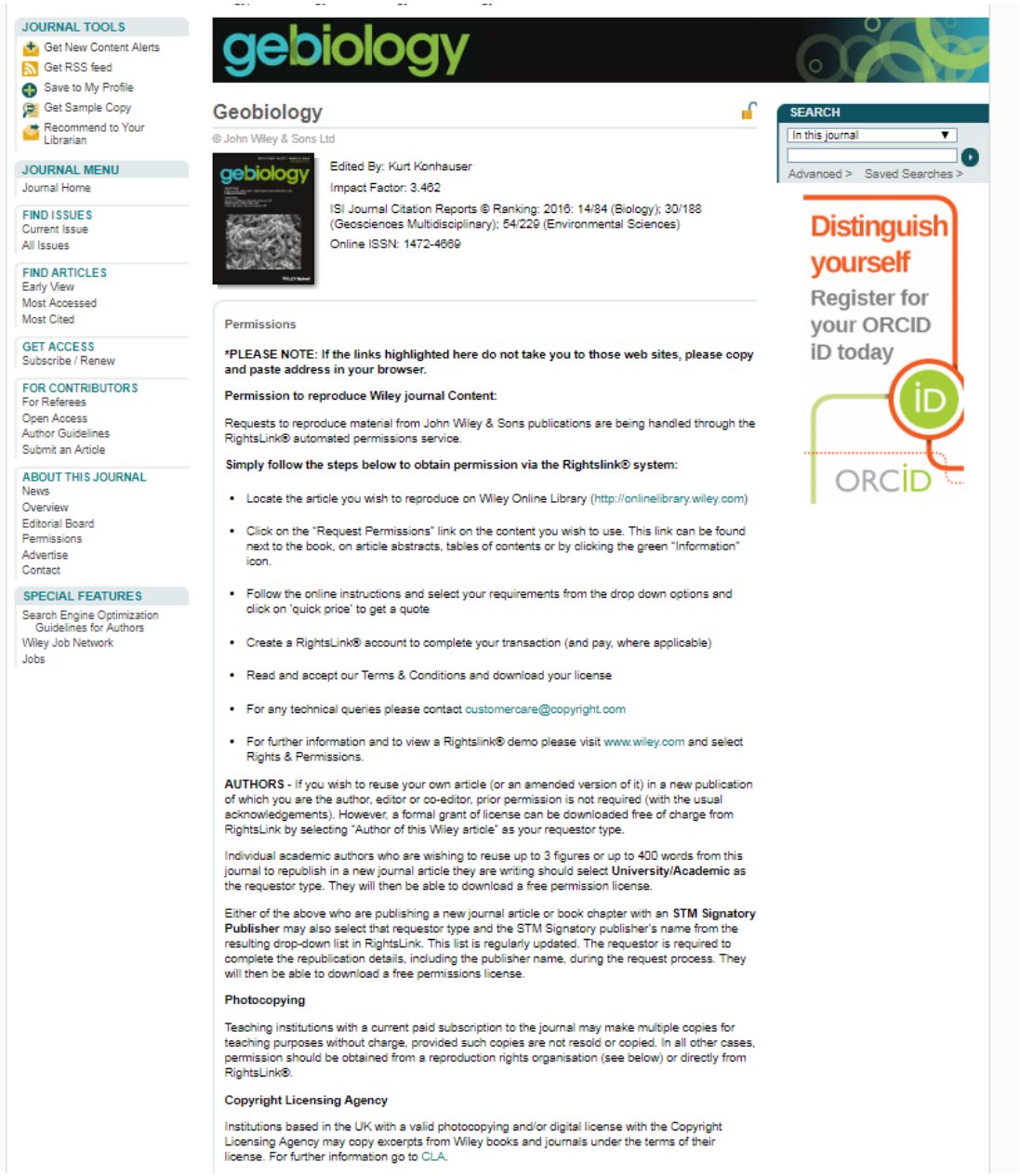

JOURNAL TOOLS
Get New Content Alerts
Get RSS feed
Save to My Profile
Get Sample Copy
Recommend to Your Librarian

JOURNAL MENU
Journal Home

FIND ISSUES
Current Issue
All Issues

FIND ARTICLES
Early View
Most Accessed
Most Cited

GET ACCESS
Subscribe / Renew

FOR CONTRIBUTORS
For Referees
Open Access
Author Guidelines
Submit an Article

ABOUT THIS JOURNAL
News
Overview
Editorial Board
Permissions
Advertise
Contact

SPECIAL FEATURES
Search Engine Optimization Guidelines for Authors
Wiley Job Network
Jobs

gebiology

Geobiology

Edited By: Kurt Konhauser

Impact Factor: 3.462

ISI Journal Citation Reports ® Ranking: 2016: 14/84 (Biology); 30/188 (Geosciences Multidisciplinary); 54/229 (Environmental Sciences)

Online ISSN: 1472-4669

SEARCH
In this journal
Advanced > Saved Searches >

Permissions

***PLEASE NOTE: If the links highlighted here do not take you to those web sites, please copy and paste address in your browser.**

Permission to reproduce Wiley journal Content:

Requests to reproduce material from John Wiley & Sons publications are being handled through the RightsLink® automated permissions service.

Simply follow the steps below to obtain permission via the Rightslink® system:

- Locate the article you wish to reproduce on Wiley Online Library (http://onlinelibrary.wiley.com)
- Click on the "Request Permissions" link on the content you wish to use. This link can be found next to the book, on article abstracts, tables of contents or by clicking the green "Information" icon.
- Follow the online instructions and select your requirements from the drop down options and click on 'quick price' to get a quote
- Create a RightsLink® account to complete your transaction (and pay, where applicable)
- Read and accept our Terms & Conditions and download your license
- For any technical queries please contact customercare@copyright.com
- For further information and to view a Rightslink® demo please visit www.wiley.com and select Rights & Permissions.

AUTHORS - If you wish to reuse your own article (or an amended version of it) in a new publication of which you are the author, editor or co-editor, prior permission is not required (with the usual acknowledgements). However, a formal grant of license can be downloaded free of charge from RightsLink by selecting "Author of this Wiley article" as your requestor type.

Individual academic authors who are wishing to reuse up to 3 figures or up to 400 words from this journal to republish in a new journal article they are writing should select **University/Academic** as the requestor type. They will then be able to download a free permission license.

Either of the above who are publishing a new journal article or book chapter with an **STM Signatory Publisher** may also select that requestor type and the STM Signatory publisher's name from the resulting drop-down list in RightsLink. This list is regularly updated. The requestor is required to complete the republication details, including the publisher name, during the request process. They will then be able to download a free permissions license.

Photocopying

Teaching institutions with a current paid subscription to the journal may make multiple copies for teaching purposes without charge, provided such copies are not resold or copied. In all other cases, permission should be obtained from a reproduction rights organisation (see below) or directly from RightsLink®.

Copyright Licensing Agency

Institutions based in the UK with a valid photocopying and/or digital license with the Copyright Licensing Agency may copy excerpts from Wiley books and journals under the terms of their license. For further information go to CLA.